Ph D Thesis

DESIGN AND SYNTHESIS OF CONJUGATED POLYMERS FOR PHOTOVOLTAIC AND CHEMOSENSOR APPLICATIONS

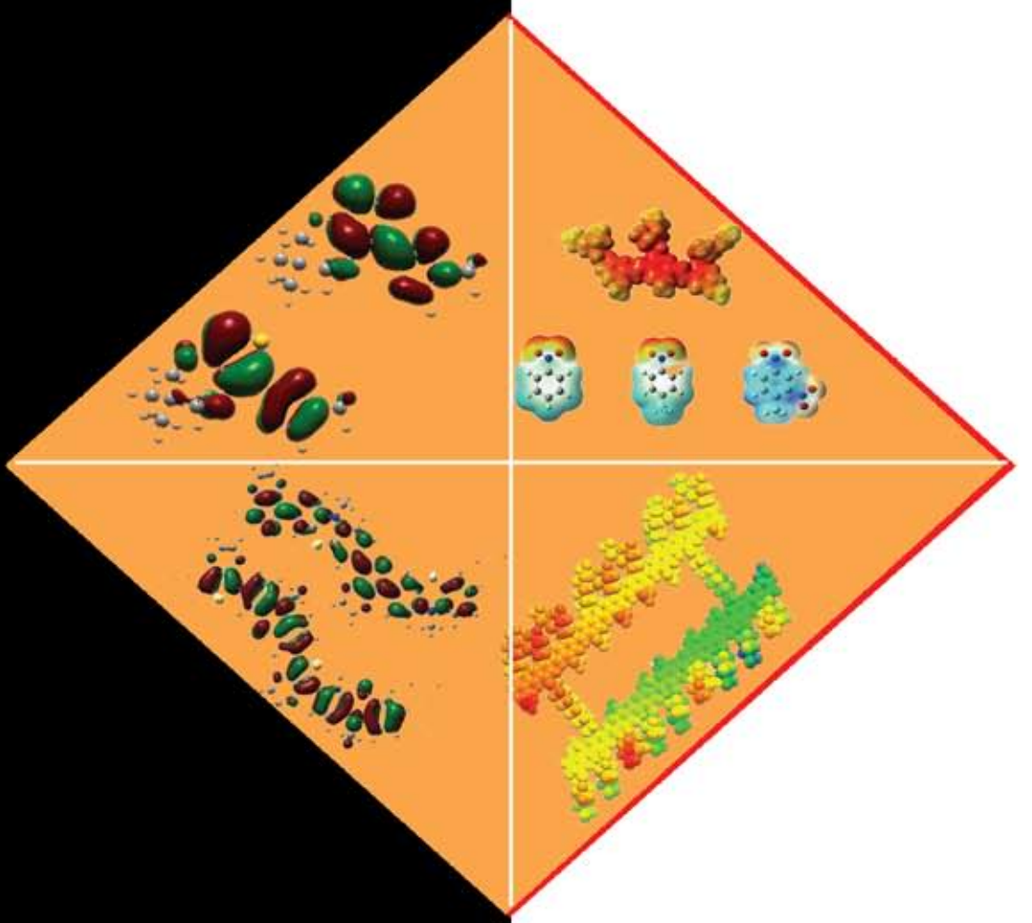

MAHESH KUMAR M. V.

DEPARTMENT OF APPLIED CHEMISTRY
COCHIN UNIVERSITY OF SCIENCE AND TECHNOLOGY
KOCHI-22

January 2012

DESIGN AND SYNTHESIS OF CONJUGATED POLYMERS FOR PHOTOVOLTAIC AND CHEMOSENSOR APPLICATIONS

Thesis submitted to the

Cochin University of Science and Technology

in partial fulfilment of the requirements for the award of the degree of

DOCTOR OF PHILOSOPHY IN CHEMISTRY

Under the Faculty of Science

By

Mahesh Kumar M. V.

DEPARTMENT OF APPLIED CHEMISTRY

COCHIN UNIVERSITY OF SCIENCE AND TECHNOLOGY

KOCHI-22

January 2012

Department of Applied Chemistry
Cochin University of Science and Technology
Kochi – 682 022, India

Dr. K. Sreekumar
Professor & Head

Phone: 0484-2862430
0484-2421530
Email: ksk@cusat.ac.in

Certificate

*This is to certify that the thesis entitled "**Design and Synthesis of Conjugated Polymers for Photovoltaic and Chemosensor Applications**" submitted for the award of the Degree of Doctor of Philosophy of the Cochin University of Science and Technology, is a record of original research work carried out by Mr. Mahesh Kumar M. V. under my supervision and guidance in the Department of Applied Chemistry, and further that it has not formed the part of any other thesis previously.*

Kochi-22
09/01/2012

Dr. K. Sreekumar
(Supervising Teacher)

Declaration

I hereby declare that the thesis entitled **"Design and Synthesis of Conjugated Polymers for Photovoltaic and Chemosensor Applications"** submitted for the award of Ph.D. Degree, is based on the original work done by me under the guidance of Dr. K. Sreekumar, Professor, Department of Applied Chemistry, Cochin University of Science and Technology and further that it has not previously formed the basis for the award of any other degree.

Kochi-22 **Mahesh Kumar M. V.**

09/01/2012

Acknowledgment

Dr. K. Sreekumar- My supervising guide, for the guidance, for the barrierless freedom offered during my research period

Dr. K. Girish Kumar- Former Head of the Department and doctoral committee member

Dr. M.R. Prathapachandra Kurup- Former Head of the Department

All the other faculty members, administrative staff, librarian-For the support

Dr. K. P. Vijayakumar and Dr. C. Sudha Kartha, Department of Physics, CUSAT-For photovoltaic device fabrication and testing

Dr. B. Kannan, Computer Applications, CUSAT-For solving mathematical problems

Dr. Kavitha Arora, AIRF, JNU.-For various analyses

Ms. Anu Singh, AIRF-For some cyclic voltammetric measurements

SAIF CUSAT-For NMR analysis

Center for Modeling Simulation and Design, University of Hyderabad, Hyderabad-For providing supercomputing facility

Prof. Arun Agarwal and Mr. E. Vinod kumar, CMSD-For helping the theoretical calculations

Dr. R. Ramesh, School of Chemistry, Bharathidasan University, Trichy: For Motivation and advice

NMR Research Centre IISc Bangalore-For NMR analysis

Ajai Kumar, Senior Technical Assistant, AIRF-For spectral analysis

DRDO, New Delhi-For financial assistance

Mr. M. R. Rajesh Menon-My co-worker

Friends of the Department of Applied Chemistry, Department of Physics and PSeLRT-For their love, tolerance and support

My dear labmates-For love and affection

My family members

Mahesh Kumar M. V.

PREFACE

Conjugated polymers have attracted much scientific and technological interest due to their potential use as semiconductors and electro-active materials in diverse applications such as transistors, photovoltaic devices, nonlinear optical devices, and polymer light-emitting diodes. The present work involves three objectives.

- Design of new conjugated polymers using tools of quantum chemistry and synthesis of the designed polymers by adopting suitable synthetic strategies.
- Explore the application of conjugated polymers as active layer in photovoltaic devices.
- Fabrication and testing of nitroaromatic detectors using fluorescent conjugated polymers

This thesis is comprised of nine chapters.

The first chapter is an introduction to the current scenario of research on conjugated polymers and their applications in photovoltaic devices and explosive detectors. This chapter also gives general introduction on the different types of theoretical calculations used in the present work.

In the second chapter, electronic structure calculation and synthesis by Suzuki polycondensation reaction of two phenothiazine/2,1,3-chalcogenadiazole polymers are described. In addition, suitability of the polymers for photovoltaic application is investigated by fabricating a linear heterojunction device using indium sulphide as the n-type material.

In the third chapter, the effect of structural changes of quinoxaline derivatives on the band gap of phenothiazine/quinoxaline copolymers are investigated by theoretical calculation and experimental methods like UV-Visible absorption spectroscopy and electrochemical methods. The photoactivity of the polymers are also discussed.

The fourth chapter discusses the electronic structure calculation and synthesis by direct arylation reaction of copolymers of phenothiazine with 3,4-dimethoxythiophene, 3,4-ethylenedioxythiophene and 3,4-propylenedioxythiophene. We have also demonstrated the superiority of the direct arylation reaction for synthesizing polymers over Suzuki and Stille polycondensation reaction. The

photovoltaic activity of the polymer is also tested using the ITO/In_2S_3/polymer/Ag heterojunction.

The fifth chapter includes the possibility of tuning the energy levels of the homopolymer, poly(ProDOT) by introducing the two 2,1,3-chalcogenadiazoles, 2,1,3-benzothiadiazole and benzoselenadiazole unit to the polymer chain. The design principle is verified by theoretical calculation and the polymers are synthesized through direct arylation reaction. The photoactivity of the polymers is also investigated.

In the sixth chapter, the copolymers of ProDOT with four quinoxalines-unsubstituted, acenaphthylene, phenyl and phenanthrene substituted are investigated by theoretical and experimental methods. The structural variations by different substituents on quinoxaline markedly affect the band gap of the polymers. The photovoltaic activity of all the polymers is tested using the ITO/In_2S_3/polymer/Ag heterojunction.

The seventh chapter presents the synthesis, characterization and photovoltaic applications of two novel 3.4-propylenedioxythiophene/1-alkyl-1,2,4-triazole copolymers with cross conjugated frame work structure. The theoretically determined frontier energy levels and energy gap were correlated with experimentally determined optical and electrochemical results. The stacking property of the polymers in thin film is also studied. The photoactivity of the polymers in the linear heterojunctions is investigated.

In the eighth chapter, we have investigated the optical and electrochemical properties of MEH PPV, MEH PPV with six and ten carbon alkyl spacer, and use of the polymers for detecting the presence of nitroaromatics. The MEH PPV with six carbon and ten carbon spacer showed recyclable sensitivity towards nitroaromatics like nitrobenzene, 4-nitrotoluene and 2,4-dinitrotoluene. The effects of interfering compounds are also studied.

The conclusions drawn from each part of the work and references are given to the end of each chapter. The summary and outlook of the work done are presented as the final chapter.

Contents

Chapter 1

AN INTRODUCTION TO π-CONJUGATED POLYMERS AND THEIR APPLICATIONS

Contents

1.1. Introduction

Most organic polymers are insulators and are used to isolate metallic conductors from other conducting materials. The research on conducting polymers began in 1970s, when films of polyacetylene were found to exhibit profound increase in electrical conductivity when exposed to halogen vapor[1]. In 2000, three scientists, Alan Heeger, Alan MacDiarmid, and Hideki Shirakawa, founders of the conjugated conducting polymer chemistry, won the Nobel Prize in chemistry for their discovery. After their pioneering work, serveral conjugated polymers were developed including polythiophene, polypyrrole, poly(paraphenylene), polyaniline, poly(phenylene vinylene), polyfluorene etc[2]. These initial discoveries have led to a modern class of organic materials with the conductivity of classical

inorganic systems. But they retain the interesting properties of the plastics like mechanical flexibility and low production costs.

This type of organic polymers are called synthetic metals[3,4]. They are semiconductors in their neutral state and exhibit increased conductivity upon oxidation or reduction. As a result, they have received considerable technological interest, leading to their current applications in sensors, organic field effect transistors (OFETs), organic photovoltaic (OPV) devices, electrochromic devices, and organic light emitting-diodes (OLEDs)[5-7]. In addition to this, organic polymers which are used as active layers in such electronic devices has led to the realistic promise of flexible electronics in the near future[8-12]. One advantage of utilizing conjugated polymers for technological applications is the ability to tune the material properties at the molecular level. This is typically accomplished through synthetic modification of the monomeric units, the combination of dissimilar units to make copolymeric systems. This thesis work envisages the two applications of conjugated polymers, in photovoltaic devices and in nitroaromatic detectors. In the first part of the present work, we have tried to design novel polymers for photovoltaic applications with the aid of quantum chemical tools. The design of polymers with appropriate properties before synthesis can eliminate the less effective materials before synthesis. This can in turn reduce the production cost. The second part of the thesis includes the design and synthesis of crosslinked MEH PPV for the detection of nitroaromatics.

This introductory chapter describes the fundamental concepts and terminology used in photovoltaic and chemosensor technology. This chapter includes four sections. The first section, illustrates the common photovoltaic architectures and superiority of inverted heterojunction devices. In the next section, strategies for engineering the polymers for

photovoltaic devices and common reaction pathways for obtaining the polymers are included. In the third section, the use of quantum chemical tools for designing the active layer polymers are described. Special emphasis is given to the use of Density Functional Theory. In the final section, the use of amplified quenching of fluorescence of polymers as a technique for transduction of signals in the detection of nitroaromatics and the associated molecular wire concept are explained.

1.2. Organic Photovoltaic Devices

1.2.1. History and importance of photovoltaic devices

Becquerel was the first to recognize photovoltaic effect in 1839, when he shined light onto an AgCl electrode in an electrolyte solution and a light induced voltage was observed[13]. Forty-four years later, Fritts created the first device made from Selenium wafers with a power conversion efficiency (PCE) of approximately 1%[14]. In 1954, Bell Laboratories improved the efficiency of a Si cell to 6%[15]. Today, standard solar panels based on multicrystalline silicon have power conversion efficiencies around 15%. However, the requirement for heavy investment in semiconductor processing technologies of the silicon-based solar cells has limited their popularization. Therefore, it became increasingly important to find a new technology which could utilize inexpensive materials as well as fabrication methods to collect solar energy. In 1986, the first organic thin-film solar cell with reasonable efficiency (approximately 1%) was created and reported by Tang[16]. Advantages of organic photovoltaic devices over conventional solar cells are

a. Organic materials can be easily made via various synthetic pathways.

b. Structure tuning by introducing different functionalizations, organic compounds can fulfill the requirements of an efficient photovoltaic device. For example, broad absorption spectra, suitable energy levels, and self-organization abilities facilitate efficient exciton and charge transport.

c. Most organic compounds can be dissolved in common organic solvents. They can be processed not only via vacuum evaporation/sublimation, but also by means of other low-cost manufacturing technologies, such as roll-to roll or inkjet printing, drop-casting, spin- or dip-coating, doctor-blading, and other solution casts.

d. In thin films, organic polymers have shown high absorption coefficients, which allow organic solar cells to be efficient in thin films and under low sunlight irradiation.

e. Solar cells based on organic materials are structurally flexible. Organic solar cells have a much larger application potential than conventional solar cells. They can be used not only as electricity providers on roof tops, like common inorganic solar cells, but can also be used for decoration in fashion windows, toys, and chargers for mobile phones or laptops.

1.2.2. Operating principles

The process of conversion of light into electricity by an organic solar cell can be schematically described by the following figure 1. For the working of a solar cell we need a donor and an acceptor joined together to form p-n junction as in the figure 1. In the first step, absorption of a photon leading to the formation of excitons (electron-hole pair) occur. In the

second step, excitons diffuse towards the donor-acceptor interface, where they get dissociated in to free charges. In the final step the free charges are transported towards the respective electrodes with the aid of internal electric field, which generates photocurrent and photovoltage.

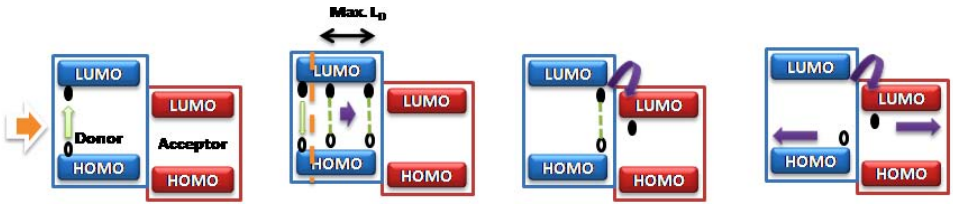

Figure 1: Working mechanism for donor-acceptor heterojunction solar cells

1.2.3. Characterization of a photovoltaic device

The current-voltage characteristics of a solar cell in the dark and under illumination are shown in figure 2. In the dark, there is no current flowing, until the contacts start to inject at forward bias for voltages larger than the open circuit voltage. In the fourth quadrant, the device generates power under light irradiation. At maximum power point (MPP), the product of current and voltage is the largest.

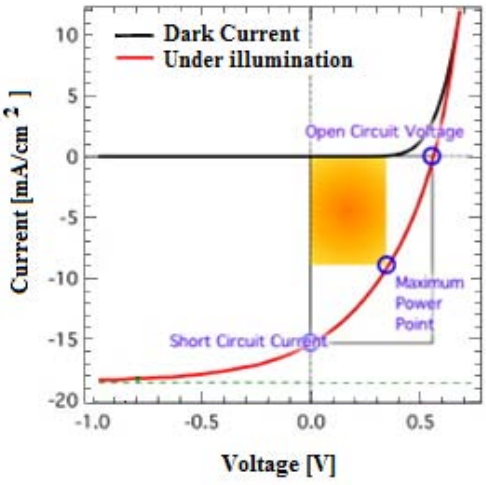

Figure 2: Current voltage characteristics of an organic solar cell

The photovoltaic power conversion efficiency of a solar cell is determined by the following formula[17]

$$\eta = \frac{V_{oc} * I_{sc} * FF}{P_{in}}$$

$$FF = \frac{V_{mpp} * I_{mpp}}{V_{oc} * I_{sc}}$$

Where V_{oc} is the open circuit voltage, I_{sc} is the short circuit current, FF is the fill factor, and P_{in} is the incident light power density. I_{mpp} and V_{mpp} are the current and voltage at the maximum power point.

1.2.3.1.Open circuit voltage

The maximum possible voltage across a photovoltaic cell is the voltage across the cell in sunlight when no current is flowing. In organic solar cells, the open circuit voltage is found to be linearly dependent on the highest occupied molecular orbital HOMO level of the donor (p-type semiconductor) and lowest unoccupied molecular orbital LUMO level of the acceptor[18,19]. Open circuit voltage is also affected by the nano morphology of the active layer in the polymer fullerene bulk heterojunction solar cells[20].

1.2.3.2.Short circuit current

This is the current that flows through an illuminated solar cell when there is no external resistance (i.e., when the electrodes are simply connected or short-circuited). The short-circuit current is the maximum current that a device is able to produce. Under an external load, the current will always be less than I_{sc}.

1.2.3.3.Maximum power point

The points, I_{mpp} and V_{mpp} on the I–V curve where the maximum power is produced is the MPP. Power (P) is the product of current and voltage (P = IV) and is illustrated in the figure 2 as the area of the rectangle formed between a point on the I–V curve and the axes. The maximum power point is the point on the I–V curve where the area of the resulting rectangle is largest.

1.2.3.4.Fill factor

The ratio of a photovoltaic cell's actual maximum power output to its theoretical power output if both current and voltage were at their maxima, I_{sc} and V_{oc}, respectively is the fill factor. This is a key quantity used to measure cell performance.

1.2.4. Common photovoltaic architectures

On the basis of device structures, organic polymer based photovoltaics (OPVs) can be divided into three main categories: bilayer heterojunction, bulk heterojunction, and inverted heterojunction devices.

1.2.4.1. Bilayer heterojunction devices

The device structure of bilayer heterojunction device is shown in figure 3. The device is fabricated in sandwich structure, in which the active layer is located between the ITO and the metal electrode. As shown in figure 3, the donor layer and acceptor layer are deposited on the ITO coated glass plate layer by layer. On the top of the active layer, the metal electrode (silver/aluminium) was coated by vacuum evaporation technique**.** When sunlight falls on the device, the donor and acceptor absorbs light and excitons are generated. These excited species move towards the donor-acceptor interface. At the interface, they get dissociated to free charges.

Finally, the free charges move towards the respective electrodes with the help of internal electric field. The separated layer structure of donor and acceptor has a small interfacial area limiting the amount of absorbers which can actually contribute to the photocurrent. The excitons are generated near the donor-acceptor interface which can be dissociated to the free charge carriers. The exciton diffusion length is generally much less than the optical absorption length, which limits the quantum efficiency of such devices. This technology was first used by Tang by using two-active-layer structure of perylenedibenzimidazole and copper phthalocyanine[16].

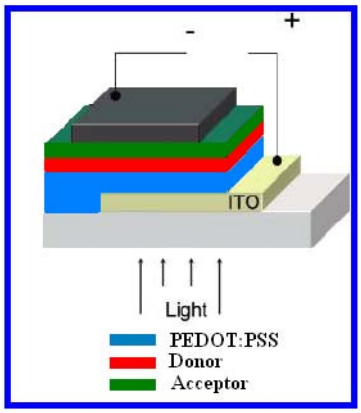

Figure 3: Schematic representation of bilayer heterojunction devices

1.2.4.2. Bulk heterojunction photovoltaic devices

To improve the efficiency of bilayer heterojunction devices, the concept of bulk heterojunction was introduced, in which the interfacial area between the donor and acceptor was increased. In this device, the donor and acceptor materials are mixed together and excitons can easily access the donor-acceptor interface and dissociate to free charge carriers[21,22] (figure 4). Replacing perylenedibenzimidazole in the bilayer device of Tang with C60, a power conversion efficiency of 5% was reported by Forrest et al. in 2005[23]. Such solar cells have efficiencies approaching 6-7%[24-26]. Even an efficency of 8.13% was reported by Solarmer Energy Inc.

at the end of 2010[27]. In these devices, the PEDOT: PSS layer provides an improved interface between the active layer and the electrode and improves the performance of the devices.

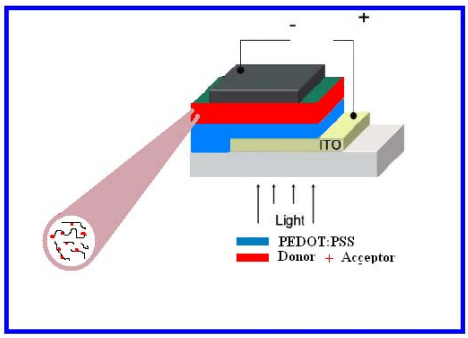

Figure 4: Schematic representation of a bulk heterojunction device

1.2.4.3. Inverted heterojunction photovoltaic devices

In both bilayer and bulk heterojunction devices, the electrons flow from acceptor to the metal electrode and holes flow from donor to the ITO. The ITO is capable of collecting both the holes and electrons, because the work function of ITO is 4.5 eV - 4.7 eV, in between the HOMO and LUMO of the conjugated polymers**.** The polarity of the ITO electrode depends mainly on the layer top to it. For hole extraction, ITO can be coated with a high-work-function layer (such as PEDOT:PSS) or covered by donor materials (such as polymers or metal phthalocyanine). If ITO electrode is coated by hole blocking materials such as ZnO, TiO_2, or In_2S_3,[28-35] an inverted solar cell can be processed and ITO can collect electrons. The advantage of inverted structure is the stability of the cell when compared to the normal structured cell[36].

1.3. Molecular Engineering of Conjugated Polymers for Photovoltaic Applications

The most critical challenge in developing ideal p-type materials is to design and synthesize a conjugated polymer that simultaneously possesses good film-forming properties, strong absorption ability, high hole mobility, and suitable HOMO-LUMO energy levels.

1.3.1. Conditions for good p-type material

The magnitude of the band gap and the positions of the HOMO and LUMO energy levels are the most important characteristics for determining the optical and electrical properties of a given conjugated polymer. These in turn greatly influence the ultimate photovoltaic performance. The first step in the photovoltaic mechanism which converts light energy to electrical energy in a device involves the absorption of sunlight by the photoactive material. The wavelength of the maximum photon flux density of the solar spectrum is located at approximately 700 nm, which corresponds to a low energy of 1.77 eV (figure 5)[37]. To fully exploit the endless source of solar energy, the absorption spectrum of a conjugated polymer needs to cover both the red and near infrared ranges to match the greater part of the terrestrial solar spectrum and hence harvest the maximum photon flux. It is highly desirable to develop conjugated polymers with broader absorptions through narrowing their optical band gap.

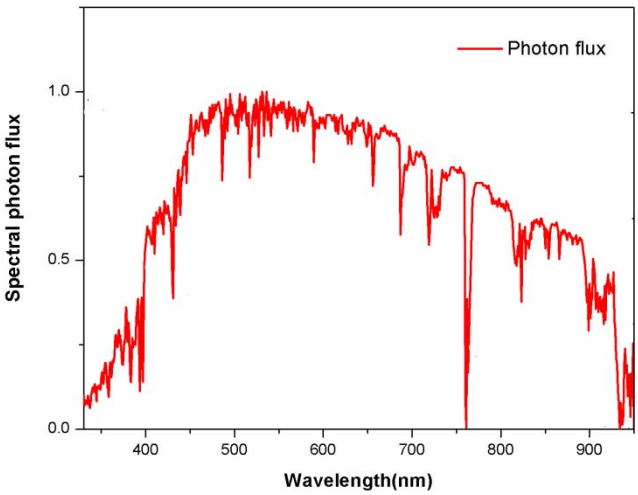

Figure 5: Solar photon flux spectra (AM1.5)

One way to reduce the band gap is by either raising the HOMO level or lowering the LUMO level of the polymer or by compressing the two levels closer together simultaneously. Unfortunately, the optical property associated with light harvesting is not the only one factor under consideration in designing new p-type polymers. Following photoexcitation, the generated exciton diffuses to the D-A interface to achieve charge separation. To obtain high efficiencies from polymer solar cells, the properties of the n-type material used should also be taken into account. It has been demonstrated that the open-circuit voltage in solar cells with ohmic contacts is linearly dependent on the magnitude of the built-in potential, defined as the difference between the HOMO level of a p-type polymer and the LUMO level of an n-type material. The donor with the lower HOMO level will better reach the theoretically attainable V_{oc}, whereas reduction in a polymer's band gap to broaden the absorption coverage by lifting up the HOMO level will inevitably result in a loss of V_{oc}. On the other hand, the LUMO level of p-type materials has to be at least 0.3 eV higher than that level of the acceptor to guarantee the formation of a downhill driving force for the energetically favorable electron transfer and overcome the binding energy of the intra-chain exciton[38-40]. Lowering the LUMO level of a conjugated polymer to achieve

a narrow band gap may result in the LUMO level eventually being lower than that of the acceptor, thus hampering the efficient electron transfer. A compromise is needed to balance the trade-off between the small band gap of the donor and the favorable energy HOMO-LUMO relationship between the donor and acceptor. As a result, the effort to find new p-type polymers for photovoltaic devices is not solely directed to pursuing low band gaps but also to controlling the band gap by modulating the HOMO-LUMO levels to their optimal values.

1.3.2. Tool box for band gap engineering

In order to fulfill the requisite condition of the polymer for photovoltaic devices, we have to follow some design strategies to fine tune the band gap and energy levels. This section deals with the important strategies used for the molecular engineering of conjugated polymers for photovoltaic applications and are illustrated in figure 6.

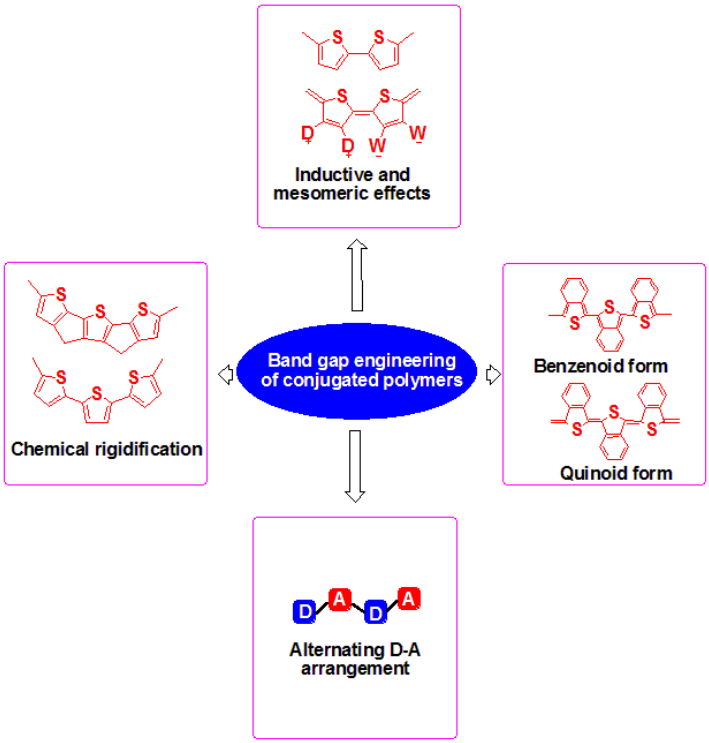

Figure 6: Band gap engineering strategies for conjugated polymers

There are two possible resonance structures for the polyaromatic conjugated polymers like polyphenylenene and poly(phenylene vinylene). The first is called the benzenoid form. In this, each phenyl unit maintains its aromaticity with confined π-electrons. Delocalization of the flowing π-electrons along the conjugated chain converts double bonds into single bonds and transforms single bonds into double bonds, leading to a resonance structure referred to as the quinoid form. Compared to the benzenoid form, the quinoid form is energetically less stable and hence has a smaller band gap, because, adopting a quinoid structure requires destruction of the aromaticity and a loss in the stabilization energy. The ratio of the aromatic to quinoid population in a polyaromatic conjugated system can be correlated and represented by a geometrical parameter, bond length alteration (BLA). This is defined as the average of the difference in length between adjacent carbon-carbon bonds in a polyene chain. The more the benzenoid form prevails in the ground state, the larger the BLA value obtained. As the quinoid contribution increases, the carbon-carbon single bonds between two adjacent rings adopt more double bond character and the BLA starts to decrease. The HOMO-LUMO band gap decreases linearly as a function of the increasing quinoid character with corresponding decreasing BLA value. A reduction in aromaticity of the aromatic units in the conjugated main chain allows a greater tendency to adopt the quinoid form through π-electron delocalization. Benzene rings with a high degree of aromaticity cause polyphenylene to have a high band gap of 3.2 eV. By inserting a double bond to dilute the effect of the benzene rings and reduce the aromaticity, the band gap of poly(phenylene vinylene) is reduced to 2.4 eV. Furthermore, thiophene has a lower aromaticity than benzene, so polythiophene is even more likely to adopt a quinoid form, and consequently, it has a lower band gap of 2.0 eV[41]. The most creative way to

effectively increase the quinoid character of polythiophene is represented by polyisothianaphthene (PITN). The main chain of PITN tends to favor the quinoid form to selectively maintain the benzene aromaticity, making PITN the first well-known conjugated polymer with a narrow band gap as low as 1 eV.[42,43]

Molecular modification used to impose steric or electronic effects on conjugated main chains affords various useful strategies for reducing the band gap. Planarization between adjacent aromatic units allows parallel π-orbital interactions to extend conjugation and facilitate delocalization. This in turn leads to a decrease in the BLA and reduction of the band gap. One way to control the rotational disorder due to steric hindrance is to tie and rigidify two adjacent aromatic units through covalent chemical bonding. This effect has been well demonstrated in a series of polymers by the work of Roncali *et al*[44]. For example, P1, where the bithiophene repeating unit is rigidified and bridged by the sp^3 carbon of a ketal group, exhibits a remarkably low band gap of 1.2 eV [45]. Extension of the bridged system from bithiophene to terthiophene for P2 further decreases the band gap to 1.1 eV[6].

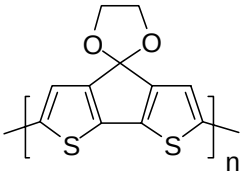

P1

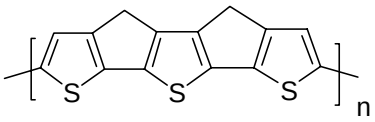

P2

Substituents directly attached to the aromatic unit in the main chain represent another effective way of perturbing the molecular orbitals through either inductive or mesomeric effects. In general, electron-donating groups raise the HOMO energy, while electron-withdrawing groups lower the

LUMO energy, resulting in a decreased band gap. For example, poly(3,4-ethylenedioxythiophene) (**P3**) with direct attachment of electron-donating alkoxy groups has a band gap of 1.5 eV, which is about 0.5 eV lower than that of the parent polythiophene.[46] For **P4,** the dual effects of electron-donating amino groups and electron-withdrawing nitro groups on the neighboring thiophene units results in a dramatically reduced band gap of 1.1 eV due to its high degree of zwitterionic and quinoid character[47].

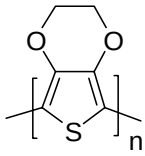

P3

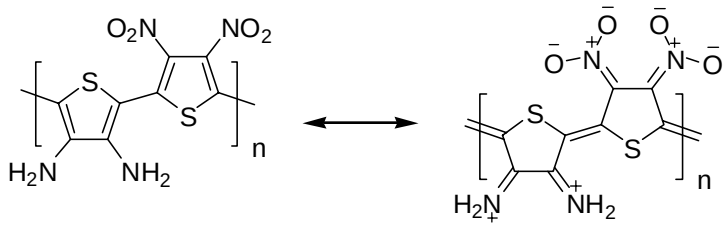

P4

A more powerful strategy in designing low band gap conjugated polymers is to alternate a conjugated electron rich donor (D) unit and an electron-deficient acceptor (A) unit in the same polymer backbone. The reduction in the band gap is illustrated in a simpler way by introducing the concept of hybridization of the molecular orbitals between the donor and acceptor in the D-A polymer. As shown in the figure 7, the HOMO of the donor segment will interact with the HOMO of the acceptor segment to yield two new HOMOs for the D-A polymer. Similarly, the LUMO of the donor will interact with that of the acceptor to produce two new LUMOs of the D-A polymer. After the electrons redistribute themselves from their original non interacting orbitals to the new hybridized orbitals of the

polymer, a higher lying HOMO and a lower lying LUMO are formed. This leads to a narrowing of the optical band gap.

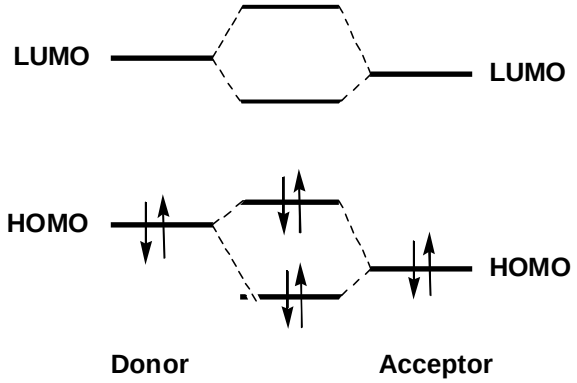

Figure 7: Orbital interactions of donor and acceptor units in a D-A conjugated polymer

The copolymer **P5** with alternating electron-rich thiophene and electron-deficient quinoxaline moieties exhibits a band gap of 1.7 eV[48]. The degree of band gap reduction is strongly dependent on the strength of donor and acceptor segments embedded in the conjugated polymer. A good choice of the donor-acceptor combination allows for tuning the band gap to the desired magnitude. With a stronger donor of pyrrole and a stronger acceptor of benzothiadiazole, copolymer **P6** shows a very low band gap of 1.1 eV in comparison with **P5**. Such a low band gap was also attributed to the presence of intramolecular hydrogen bonding, which results in conformational planarization assisted by supramolecular interaction[49].

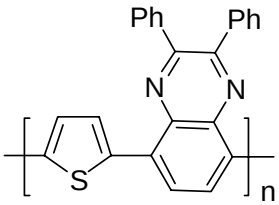

P5

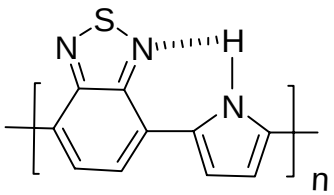

P6

In addition to this design strategies for tuning the energy levels and band gap, the polymer must possess solubility in common organic solvents. This is achieved by introducing alkyl side chains to the polymer backbone.

1.4. Routes for Synthesis of Conjugated Polymers

There are several synthetic strategies available for the formation of a single bond between two unsaturated carbons. In addition to electrochemical[50-52] or chemical oxidative polymerizations[53], transition-metal-catalyzed cross-coupling reactions provide a particularly powerful synthetic strategy for Csp^2-Csp^2 and Csp-Csp^2 bond formation[54]. The cross-coupling reaction involves a transition-metal-catalyzed oxidative addition reaction across the C-X bond of an electrophile followed by transmetalation with a main group organometallic nucleophile, which again is followed by a reductive elimination step leading to the carbon-carbon bond formation (figure 8). The most commonly employed transition-metal catalysts are nickel or palladium based complexes. The organometallic nucleophiles can be Grignard reagents (Kumada-Corriu)[55], stannyl (Stille)[56], boron reagents (Suzuki-Miyaura)[57] or copper (Sonogashira)[58]. Thus, conjugation lengths can be extended through consecutive transformations in the catalytic cycle. The application of these reactions in conjugated polymer chemistry is illustrated using some recent literature.

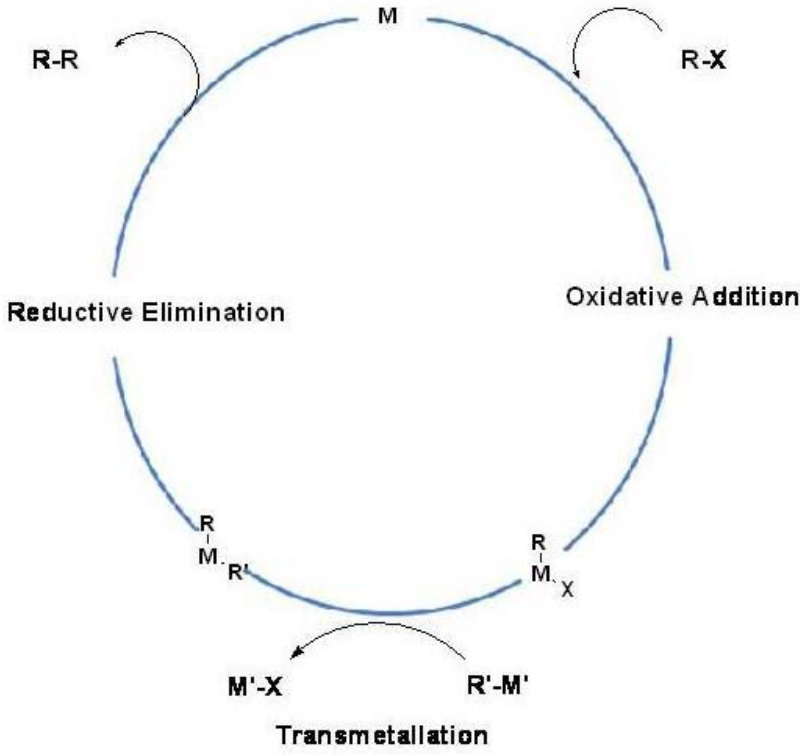

Figure 8: Catalytic cycle of transition-metal catalyzed reactions

1.4.1. Kumada-Corriu reaction

Ni or Pd catalyzed cross-coupling reaction of Grignard reagents with alkyl, vinyl or aryl halides is named Kumada cross-coupling reaction. McCullough used this reaction to synthesise head–tail regioregular poly(3-hexyl thiophene) as shown in Scheme 1 [59,60]. The regioregular polymerization of 3-alkylthiophene can be achieved by selective lithiation of 2-bromo-3-alkylthiophene with lithium diisopropylamide followed by transmetallation using magnesium bromide to yield the organomagnesium intermediate. The use of a Ni(dppp)Cl_2 catalyst for the polymerization of this intermediate gives the corresponding poly(3-alkylthiophene) with over 90% head-tail regioselectivity.

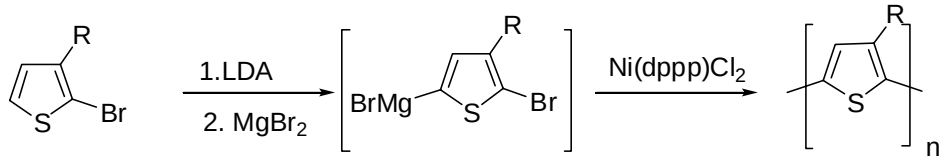

P7

Scheme 1: Synthesis of poly(3-hexylthiophene) by Kumada reaction

McCullough reported another method for the synthesis of regioregular poly(3-alkylthiophene)s by Grignard metathesis (GRIM). Treatment of 2,5-dibromo-3-hexylthiophene with a variety of alkyl Grignard reagents resulted in two metalated regioisomers. Introduction of a catalytic amount of $Ni(dppp)Cl_2$ to this isomeric mixture afforded poly(3-hexylthiophene), which contained greater than 95% regioregularity (scheme 2).[61,62]

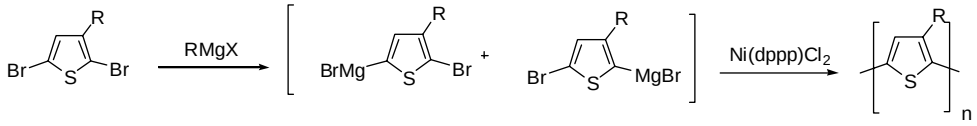

P8

Scheme 2: Synthesis of regioregular poly(3-hexylthiophene) by GRIM method

1.4.2. Stille cross-coupling reaction

Stille coupling is more suitable for thiophene-containing polymers using monomers with stannyl groups on the thiophene ring. For example, Li *et al* synthesized phenothaizine/thiophene copolymer by utilizing the Stille cross-coupling reaction. They used 3,7-dibromo-10-octylphenothiazine and distannyl derivative of thiophene as monomers and $Pd(PPh_3)_4$ as the catalyst (scheme 3)[63].

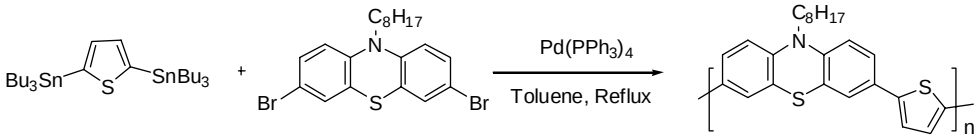

P9

Scheme 3: Synthesis of P9 by Stille reaction

Similar reaction was used by Hou *et al* to copolymerize ethylhexyl substituted 4*H*-cyclopenta[2,1-*b*:3,4-*b'*]dithiophene and 2,1,3-benzoselenadiazole (scheme 4)[64].

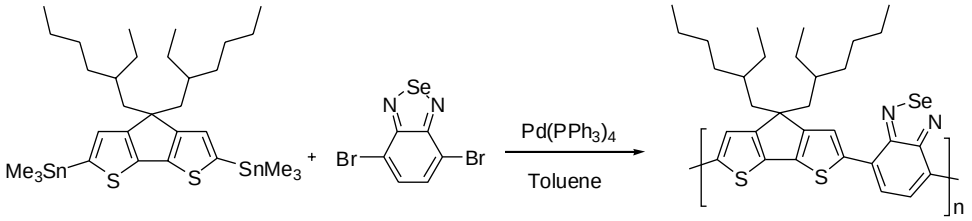

P10

Scheme 4: Synthesis of P10 by Stille reaction

1.4.3. Suzuki-Miyaura coupling reaction

Suzuki coupling is more widely used for preparing benzene-containing polymers with boronic groups on the benzene ring of the monomer. Cheng et al used this method to synthesize didecyloxyphenylene based alternating D-A copolymers with thienopyrazine, 2,1,3-benzothiadiazole, quinoxaline, pyridyl and 4,7-dithien-2-yl-2,1,3-benzothiadiazole as acceptors (scheme 5). Photovoltaic device was fabricated using a blend of these polymers and PCBM and showed 0.4-0.41% efficiency[65].

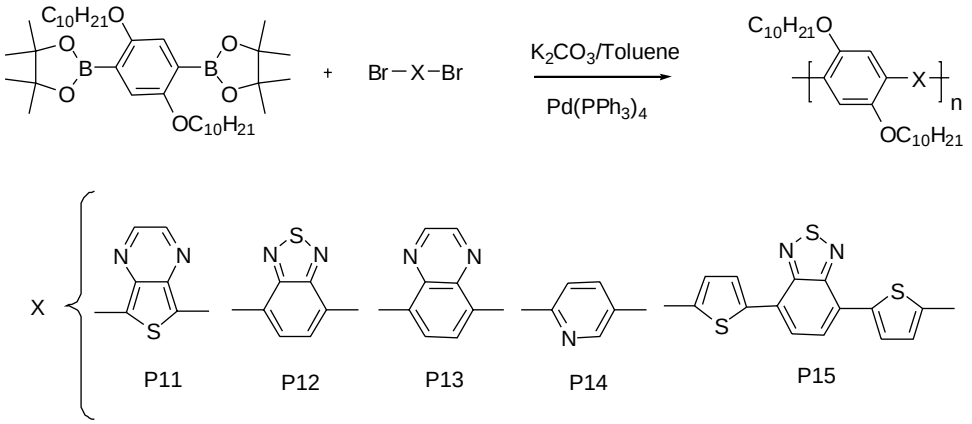

Scheme 5: Synthesis of dialkoxyphenylene based D-A copolymers by Suzuki reaction (P11-P15)

1.4.4. Sonogashira reaction

Raja *et al* synthesized two thienopyrazine based low-band gap poly(heteroarylene ethynylene)s for photovoltaic devices, by palladium catalysed Sonogashira reaction (scheme 6). The polymers showed about 2% efficiency under illumination[66].

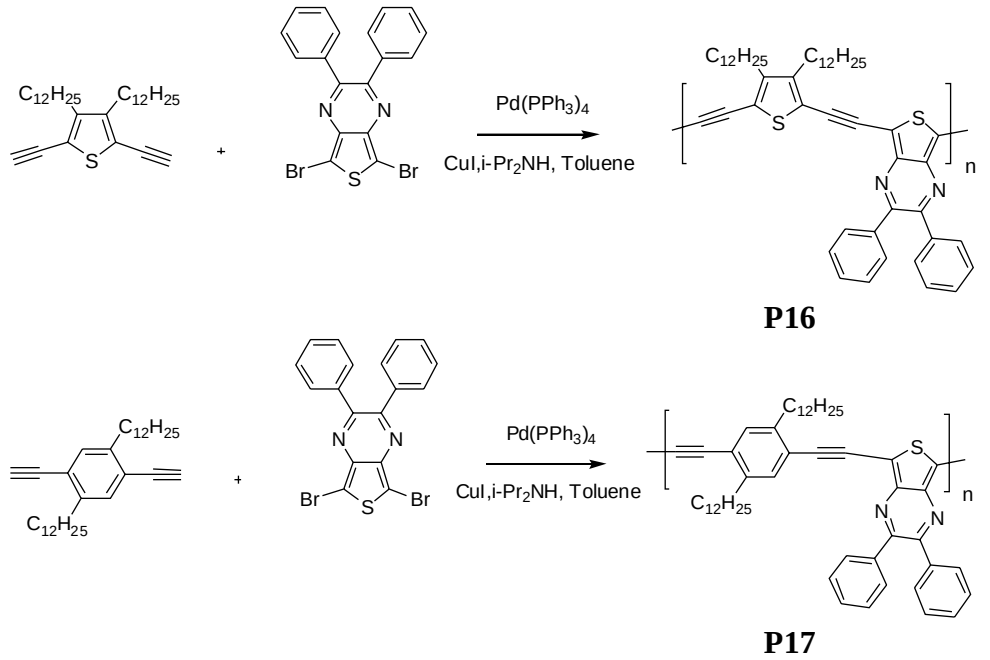

Scheme 6: Synthesis of poly(heteroarylene ethynylene) based copolymers by Sonogashira reaction

1.4.5. Heck reaction

Huo *et al* synthesized alternating copolymers of electron-rich arylamine/dialkoxyphenylene and electron-deficient 2,1,3-benzothiadiazole using palladium acetate as catalyst by Heck reaction. They studied the photovoltaic properties of the copolymers by fabricating the bulk heterojunction device[67].

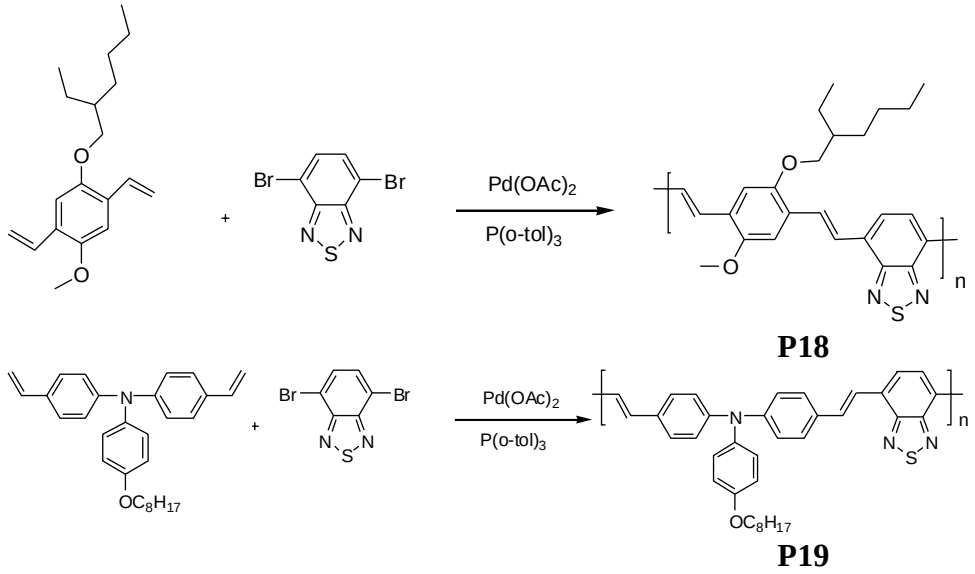

Scheme 7: Synthesis of P18 and P19 by Heck reaction

1.4.6. Yamamoto reaction

Nickel-mediated Yamamoto dehalogenation coupling reactions also provide a pathway for carrying out self-polymerizaiton of single monomers. Li *et al* in 2006 synthesized soluble polycarbazole by Yamamoto reaction using $Ni(COD)_2$ as the catalyst (scheme 8). They also studied the photovoltaic properties of the polycarbazole with PCBM as acceptor[68].

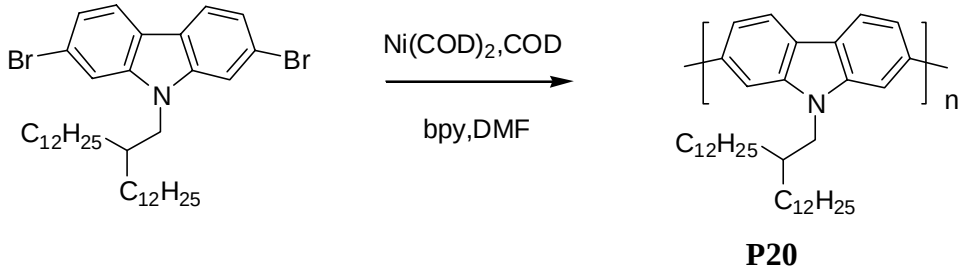

P20

Scheme 8: Synthesis of polycarbazole by Yamamoto reaction

1.4.7. Knoevenagel condensation

This reaction is useful in the synthesis of vinylene containing conjugated polymers via the carbon-carbon double bond formation between two respective monomers. Reynolds *et al*. reported the synthesis of a range of CN-PPV derivatives containing dioxythiophene moieties in the main chain (scheme 9)[69,70]. These donor-acceptor conjugated polymers possess narrow band gaps of about 1.5-1.8 eV and good solubilities in common organic solvents.

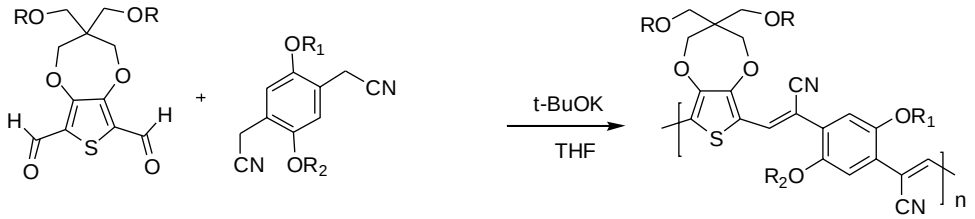

P21

Scheme 9: Synthesis of 3,4-propylenedioxythiophene/cynovinylene copolymer by Knoevenagel condensation

In addition to Knoevenagel condensation, Gilch polymerization route provides another way to synthesize vinylene containing polymers. This involves the reaction of α,α′-dihalo-*p*-xylene with excess of base to obtain conjugated PPV through a one-pot straight forward elimination-polymerization-elimination three step procedure (scheme 10)[71-73].

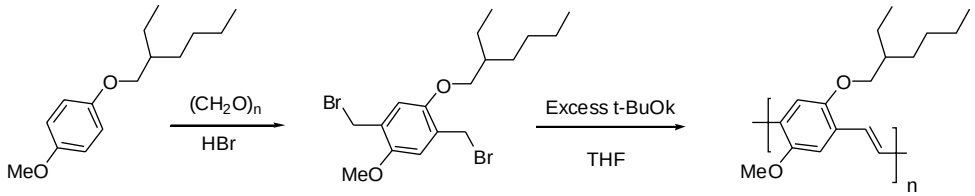

P22

Scheme 10: Synthesis of MEH PPV by Gilch polymerization route

The details of the Gilch polymerization mechanism can be seen in scheme 11. The first step of this mechanism involves the deprotonation of

the most acidic hydrogen by the basic oxygen of the tert-butoxide (t-BuOK). This creates a resonance-stabilized carbanion that then attacks the benzylic hydrogens of other monomer molecules in a SN_2 reaction, causing the bromine to leave and thus connecting the two molecules. The presence of excess base then causes an E_2 reaction to occur, forming the vinyl bonds present within the polymer backbone.

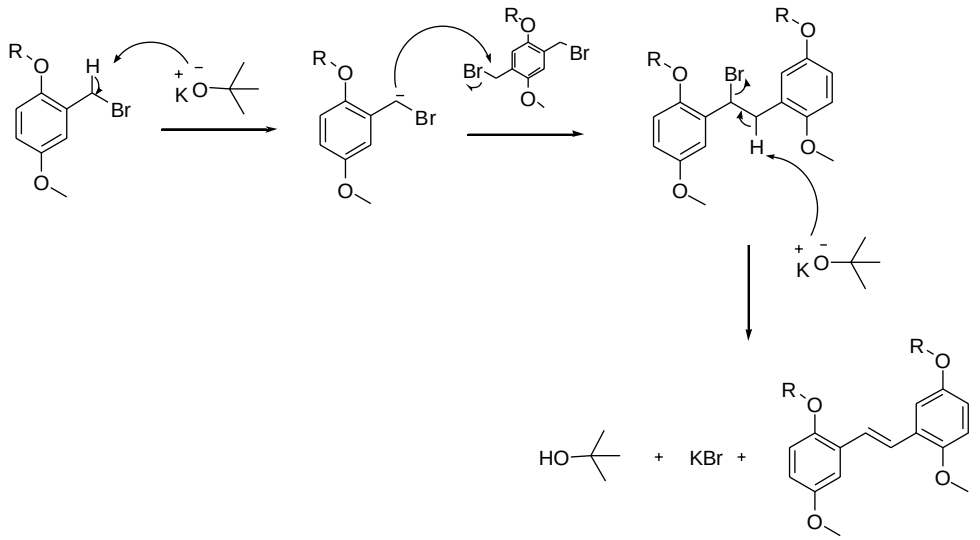

Scheme 11: Mechanism of Gilch polymerization route

1.5. Theoretical Calculation of Electronic Structure of Conjugated Polymers

The most important task of conjugated polymer research is to find a suitable member of a polymer group which possesses optimal property for the photovoltaic applications. Normally, polymers are synthesized and their properties are measured. On the basis of the results, polymers with appropriate properties only are used for fabricating devices. This procedure is obviously very expensive and it may happen that the polymer family does not consist of those polymers which have optimal properties for the prescribed purpose. A much less expensive and safe procedure is to

calculate the electronic structure with a good approximation using tools of quantum chemistry and eliminate unsuitable materials before synthesis. Though such calculations require large CPU time, they certainly are orders of magnitude cheaper than the conventional experimental approach. Theoretical studies will help to establish the relationships between the structure and the electronic properties of conjugated polymers. Hence it contributes to a better understanding of the structural variables and help to realize strategies for band gap control. This section provides the details of theoretical tools available for calculating the properties of the conjugated polymers.

There are two categories of theoretical approaches available to calculate the electronic and structural properties of conjugated polymers. The first approach is called the molecular or oligomer method. A number of researchers have used oligomers to extrapolate band gaps of conjugated polymers[74-77]. The key feature of this method is to investigate the physical properties of the oligomers as a function of gradually increasing size, until convergence is reached. The properties of polymers can be extrapolated.

The second approach is based on the standard solid state methods using Born–Karman periodic boundary condition, Bloch functions, and translational symmetry called periodic boundary condition approach (PBC). The PBC-DFT method was implemented in the Gaussian 03[78] and G 09[79] quantum chemical codes. The PBC model in the G 03 and G 09 package is based on Gaussian type orbitals (GTOs)[80,81]. Bloch functions[82] were employed to transform GTOs into "crystal orbitals" for calculating the periodic boundary condition systems[83-86]. Recently, Wang *et al*. have demonstrated the use of PBC-DFT method to generate the optimized geometry and electronic structure of single-walled carbon nano-tubes[87]. To get a better fit with experiments, hybrid exchange correlation functionals

are widely used in the PBC/DFT formalism. Widely used hybrid DFT methods include Becke's three parameter[88] hybrid functional using the Lee–Yang–Parr (LYP)[89] correlation functional (B3LYP). The good agreement between B3LYP and experimental band gaps for semiconducting polymers has also been demonstrated recently in the theoretical study of periodic organic polymers by Janesko[90]. Recently, electronic properties of vinylene-linked heterocyclic conducting polymers were calculated using density functional theory method in periodic boundary condition approach[91]. Recently introduced Heyd-Scuseria-Ernzerhof (HSE) functional[92] incorporates a screened Hartree-Fock interaction, more computationally efficient than traditional hybrid functionals like B3LYP. HSE06 computed band gaps are comparable to that calculated using B3LYP[91]. In the present work, we have used both B3LYP and HSE06 combined with 6-31G basis set to calculate the properties of the conjugated polymers.

1.6. Chemical Sensors Based on Amplified Quenching of Fluorescence

Conjugated polymer has emerged as one of the most important classes of transduction materials, which readily transform a chemical signal in to easily measurable electrical and optical events. This section of the chapter is concerned with fluorescence based methods of conjugated polymers as transduction medium. The interest in conjugated polymer as sensory material is due to their ability to produce signal gain in response to interaction with analytes and so they are called as amplifying fluorescent polymers. The amplification sensitivity of the conjugated polymer is due to its ability to transport the excitons. The utility of conjugated polymers for fluorescence based sensing was first demonstrated by Timothy Swager from MIT[93,94]. In this work, they have demonstrated the high sensitivity of conjugated polymer based sensor over single fluorophore sensor by introducing the concept of "molecular wire" (figure 9a). The signal is

amplified due to the fact that the polymer needs only a small fraction of receptor sites to be occupied to affect complete quenching. In the case of monomeric indicator, every receptor must be occupied for complete quenching (figure 9a). The origin of this result can be explained using the band diagram of the conjugated polymer (figure 9b).When the conjugated polymer absorbs light, excitons are generated and migrate along the polymer backbone. Analyte binding will produce trapping sites, whereby the excitation is deactivated by electron transfer quenching.

a. Traditional fluorescent chemosensor

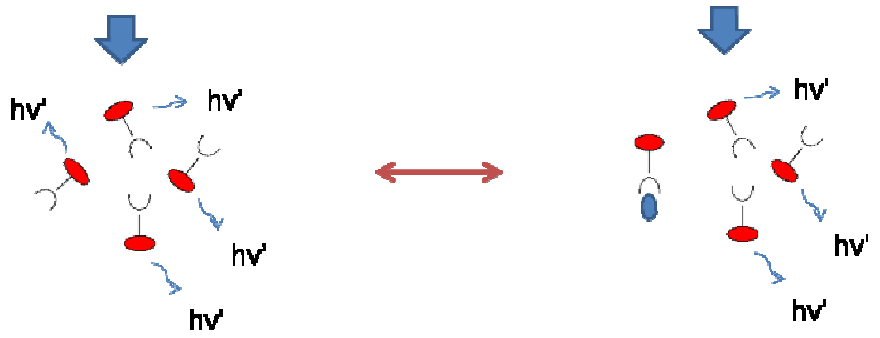

b. Receptors wired in series

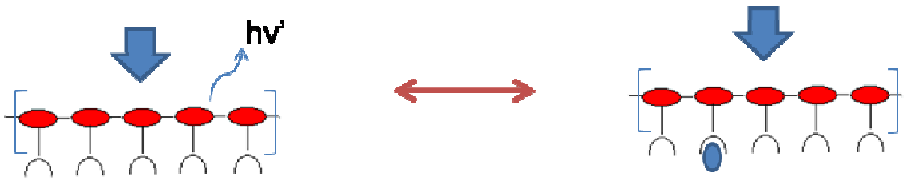

c. Molecular wire

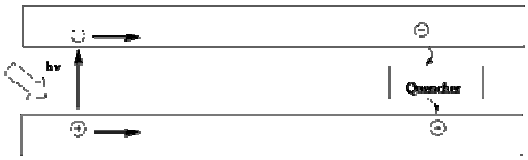

Figure 9: a. Comparison of fluorescence quenching for isolated chromophore with that of chromophore connected in series. c. Band diagram illustrating the mechanism by which the molecular wire receptor assembly produces an enhancement in fluorescence chemosensory response

The amplified quenching of fluorescence was used for the detection of explosives like 2,4,6-trinitrotoluene (TNT) and 2,4-dinitrotoluene (DNT) in 1998 by Yang and Swager[95,96]. To facilitate binding of TNT and DNT, as well as create a stable emissive thin film of a poly-(phenylene ethynylene), Yang and Swager developed a series of porous polymers utilizing a rigid, shape persistent iptycene group. The porous structure served to prevent direct interactions between the polymer backbones, which generally led to quenching, and to create a structure that behaved as a "sponge" for electron-poor π-electron accepting analytes. Harnessing this design principles, they had synthesized polymers P23-25 and iptycene free polymer P26 was also synthesized for comparison.

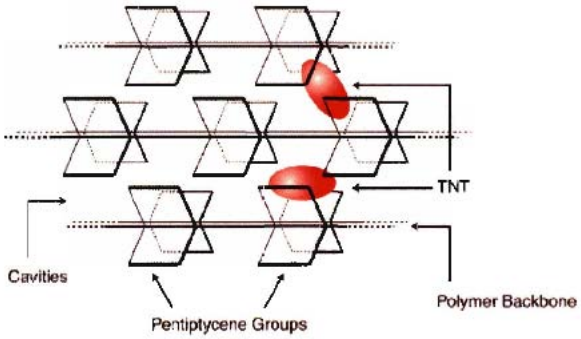

Figure 10: Conceptual drawing of rigid, shape-persistent iptycene containing polymers and resulting porous structure

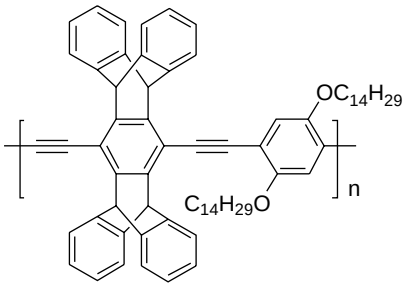

P23

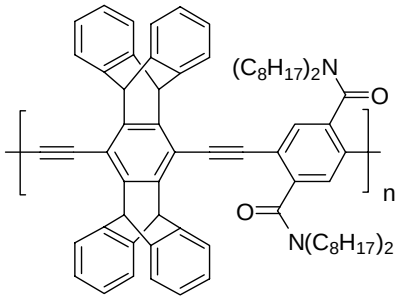

P24

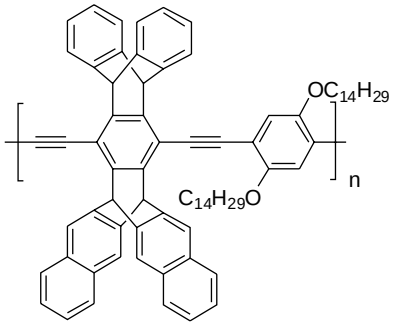

P25

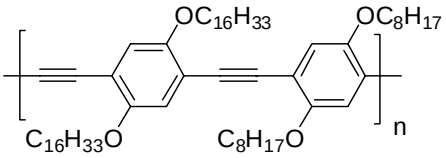

P26

Absorption and fluorescence emission spectra were recorded as films while exposed to equilibrium vapor pressures of various analytes. For polymer **P23**, it was observed that TNT and DNT significantly quenched the fluorescence by an electron-transfer mechanism. Thin films of **P23** displayed a sizeable quenching within seconds of exposure to 10 ppb of TNT vapor, thereby demonstrating the extraordinary sensitivity imparted by energy migration. Films of P23-P25 displayed selectivities towards electron-poor analytes that were consistent with their electronic structure and size-exclusion characteristics. They did systematic studies on a large number of analytes to demonstrate the extraordinary sensitivity imparted by energy migration.

Swager's group has reported several sensitivity-enhancing improvements to the TNT-sensing material. Amplification of quenching depends strongly on how many binding sites each exciton can visit. One potential way to improve this quantity is to increase the fluorescence lifetime of the sensing material. If each exciton has a longer time before it decays intrinsically to the ground state, excitons may be able to sample more locations within the polymer film. Swager reported a series of PPEs that incorporated triphenylene moieties into the backbone of a conjugated polymer, such as P27[97]. Relative to the more traditional phenylene based

PPEs, the authors found that the triphenylene-containing PPEs had longer excited-state lifetimes.

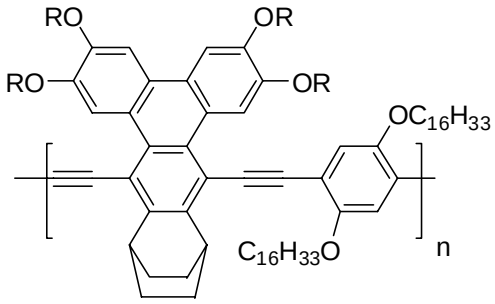

R=2-ethylhexyl

P27

Also in 2001, Yamaguchi and Swager reported dibenzochrysene based PPEs such as P28 that had excited-state lifetimes between 1 ns and 3 ns (corresponding phenylene-based materials have sub-nanosecond lifetimes)[98]. Sensing experiments with these polymers showed that they had higher sensitivity to TNT than polymers such as P23 and P27.

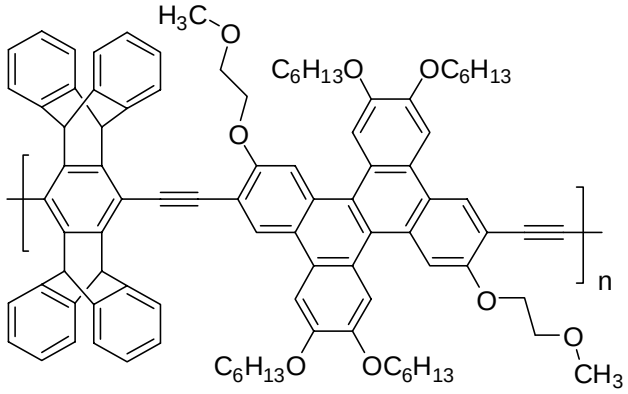

P28

Trogler studied the possibility of using poly(metalloles) like P29 for sensing the explosives. They observed that thin films were sensitive to TNT concentrations as low as 50 ppb after 60 s exposure[99]. The structural control

over polymetallole structures led to the tunable fluorescence quenching by specific nitroaromatics[100]. Polysilole, polygermole, and metallole–silane copolymers were tested in toluene solution with picric acid, TNT, DNT, and NB. Varied polymer compositions led to tunable interactions between quenchers and polymetalloles, with a unique aggregate response for each quencher. This result suggested the organization of these polymers into a sensor array for the identification of specific nitroaromatics.

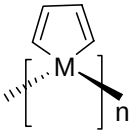

M=Ge, Si

P29

In 2011, Nie *et al* synthesized a novel fluorescent poly(2,7-carbazole) with a 4-[tris-(4-octyloxyphenyl) methyl]phenyl side chain to detect the explosive compounds, TNT and DNT[101]. It showed high recycled fluorescence quenching sensitivity, which was due to its strong electron donating ability and weaker interaction between the polymer chains caused by the bulky side chain.

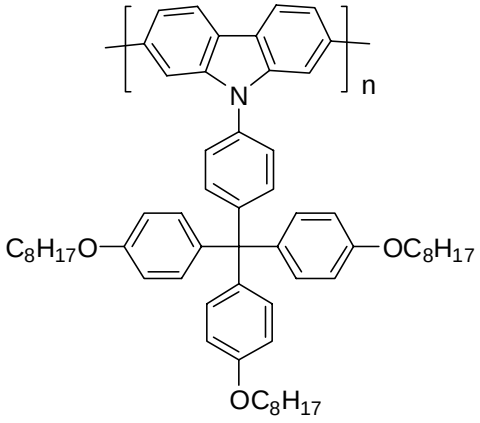

P30

Zhang *et al* synthesized fluorescent nanoscale zinc(II)-carboxylate coordination polymers for explosive sensing[102]. They demonstrated the sensing of TNT and DNT with the polymer and sensitivity of this polymer was due to large surface area to volume ratio and strong binding affinity to explosive molecules.

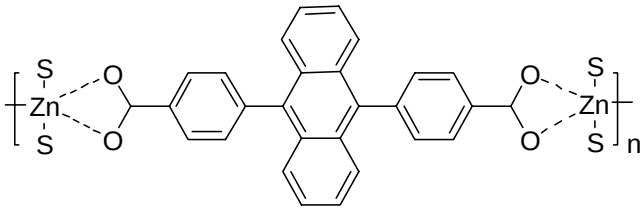

P31

Venkataraman *et al* synthesized two thiophene based polymers containing 1,2,3-triazole (P32 and P33) [103]. The dipolar 1,2,3-triazole moiety can enhance the interaction of DNT and TNT with the polymer in thin films and bulky side chains can decrease the chain packing in thin films resulting in enhanced analyte diffusion.

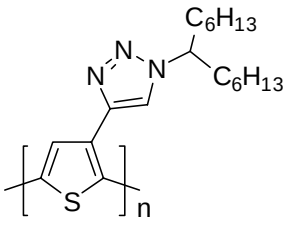

P32

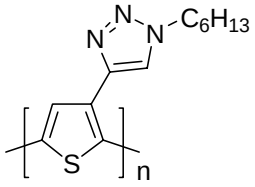

P33

1.7.Scope of the thesis

- Design of novel conjugated polymers for photovoltaic application using Density Functional Theory in the Periodic Boundary Condition (PBC) formalism.
- Synthesis of the polymers adopting appropriate synthetic strategies.

- Explore the application of the synthesized polymers as active layer in the inverted bilayer heterojunction device using In_2S_3 as the n-type material.
- Design and synthesis of fluorescent conjugated polymers for nitroaromatic detection.
- Explore the application of the fluorescent conjugated polymers for nitroaromatic detection.

1.8.Materials and methods

All the chemicals were purchased from various chemical manufactures and used as received unless otherwise stated. All the solvents were purified according to standard procedures prior to use. NMR spectra were recorded on a Bruker 400MHz spectrometer with TMS as internal standard using $CDCl_3$ solvent (SAIF, CUSAT; NMR Research Center, IISc, Bangalore; AIRF, JNU, New Delhi). Infra red spectra were recorded by the KBr pellet method on a JASCO 4100 spectrometer in the range 400-4000 cm^{-1}. UV-Visible spectra were recorded on Labomed 3650 instrument. Fluorescence spectra were recorded on Horiba Jobin Yon Fluoro Max instrument (Department of Physics, CUSAT)**.** TG/DTA was recorded on a Perkin Elmer Pyris Diamond 6 TG/DTA instrument at a heating rate of 10^0C/min under nitrogen atmosphere using platinum crucible. The X-ray diffraction pattern of the polymers were obtained by using a Rigaku D MAX III VC Ni-filtered Cu K alpha radiation (λ=1.5404A^0 at a scan rate 4^0/min) (SAIF, CUSAT). I-V measurement was done using a Keithley Source Measure Unit (SMU, K236). The GPC analysis was done on Waters Empower instrument calibrated with polystyrene using toluene and THF as solvent (PS&RT, CUSAT; SCTIMST, Thiruvananthapuram).

1.9. References

1. Shirakawa, H.; Louis, E. J.; MacDiarmid, A. G.; Chiang C. K.; Heeger, A. J. *J. Chem. Soc. Chem. Commun*., **1977**, 474, 578.
2. Skotheim, T. A.; Reynolds, J. R. Eds.; *Handbook of Conducting Polymers*, 3rd ed., CRC Press: Boca Raton, FL, **2007.**
3. MacDiarmid, A. G. *Angew. Chem. Int. Ed*., **2001**, 40, 2581.
4. MacDiarmid, A. G.; Epstein, A. J. *Mat. Res. Soc. Symp. Proc.*, **1994**, 328, 133.
5. Perepichka, I. F.; Perepichka, D. F. Eds *Handbook of Thiophene-based Materials*, John Wiley & Sons: Hoboken, NJ, **2009**.
6. Roncali, J. *Chem. Rev*., **1992**, 92, 711.
7. Monk, P.; Mortimer, R.; Rosseinsky, D. *Electrochromism and Electrochromic Devices*, Cambridge University Press, **2007.**
8. Logothetidisa, S.; Laskarakis, A. *Eur. Phys. J. Appl. Phys*., **2009**, 46, 12502.
9. Sekitani, T.; Someya, T. *Adv. Mater*., **2010**, 22, 2228.
10. de Leeuw, D. M.; Cantatore, E. *Mat. Sci. Semicond. Process*., **2008**, 11, 199.
11. Allen, K. J. *Proc. IEEE*., **2005**, 93, 1394.
12. Rasmussen, S. C.; Ogawa, K.; Rothstein, S. D, *Handbook of Organic Electronics and Photonics*, H. S. Nalwa, Ed.; American Scientific Publishers: Stevenson Ranch, CA, **2008.**
13. Becquerel, A. E. *Comptes Rendus*, **1839**, 9, 561.
14. http://en.wikipedia.org/wiki/Charles_Fritts.
15. Chapin, D. M.; Fuller, C. S.; Pearson, G. L. *J. Appl. Phys.*, **1954**, 25,676.
16. Tang, C. W. *Appl. Phys. Lett.*, **1986**, 48, 183.

17. Hoppe, H.; Sariciftci, N. S. *J. Mater. Chem.*, **2004**, 19, 1924.
18. Brabec, C. J.; Cravino, A.; Meissner, D.; Sariciftci, N. S.; Fromherz, T.; Minse, M.; Sanchez, L.; Hummelen, J. C. *Adv. Funct. Mater.*, **2001**, 11, 374.
19. Mallairas, G. G.; Salem, J. R.; Brock, P. J.; Scott, J. C. *J. Appl. Phys.*, **1998**, 84, 1583.
20. Liu, L.; Shi, Y.; Yang, Y. *Adv. Funct. Mater.*, **2001**, 11, 420.
21. Hiramoto, M.; Fujiwara, H.; Yokoyama, M. *J. Appl. Phys.*, **1992**, 72, 3781.
22. Taima, T.; Chikamatsu, M.; Yoshida, Y.; Saito, K.; Yase, K. *Appl. Phys. Lett.*, **2004**, 85, 6412.
23. Xue, J.; Rand, B. P.; Uchida, S.; Forrest, S. R. *J. Appl. Phys.*, **2005**, 98, 124903.
24. Park, S. H.; Roy, A.; Beaupre, S.; Cho, S.; Coates, N.; Moon, J. S.; Moses, D.; Leclerc, M.; Lee, K.; Heeger, A. J. *Nature Photon.*, **2009**, 3, 297.
25. Liang, Y.; Feng, D.; Wu, Y.; Tsai, S. T.; Li, G.; Ray, C.; Yu, L. *J. Am. Chem. Soc.*, **2009**, 131, 7792.
26. Chen, H.-Y.; Hou, J.; Zhang, S.; Liang, Y.; Yang, G.; Yang, Y.; Yu, L.; Wu, Y.; Li, G. *Nature Photon.*, **2009**, 3, 649.
27. http://www.solarmer.com/newsevents.php
28. Chen, L. M.; Hong, Z.; Li, G.; Yang, Y. *Adv. Mater.*, **2009**, 21, 1434.
29. Long, Y. *Appl. Phys. Lett.*, **2009**, 95, 193301.
30. Ng, T. W.; Lo, M. F.; Liu, Z. T.; Wong, F. L.; Lai, S. L.; Fung, M. K.; Lee, C. S.; Lee, S. T. *J. Appl. Phys.*, **2009**, 106, 114501.
31. Niggemann, M.; Gombert, A. *Org. Photovoltaics*, **2008**, 441.

32. Xu, Z.; Chen, L.-M.; Yang, G.; Huang, C. H.; Hou, J.; Wu, Y.; LiG.; Hsu, C.-S.; Yang, Y. *Adv. Funct. Mater.*, **2009**, 19, 1227.
33. Zhao, D. W.; Liu, P.; Sun, X. W.; Tan, S. T.; Ke, L.; Kyaw, A. K. K. *Appl. Phys. Lett.*, **2009**, 95, 153304.
34. Rajesh Menon, M. R.; Maheshkumar, M. V.; Sreekumar, K.; Sudha Kartha, C.; Vijayakumar, K. P. *physica status solidi*, **2012**, 209, 199.
35. Rajesh Menon, M. R.; Maheshkumar, M. V.; Sreekumar, K.; Sudha Kartha, C. ; Vijayakumar, K. P. *Solar Energy Materials and Solar Cells*, **2010**, 94, l2212.
36. Krebs, F. C.; Gevorgyan, S. A.; Alstrup, J. *J. Mater. Chem.*, **2009**, 19, 5442.
37. The data of Solar Spectral Irradiance (air mass 1.5) was obtained from the Web site http://rredc.nrel.gov/solar/spectra/am1.5/
38. Brabec, C. J.; Winder, C.; Sariciftic, N. S.; Hummelen, J. C.; Dhanabalan, A.; van Hal, P. A.; Janssen, R. A. J. *Adv. Funct. Mater.*, **2002**, 12, 709.
39. Halls, J. J. M.; Cornil, J.; dos Santos, D. A.; Silbey, R.; Hwang, D. H.; Holmes, A. B.; Bredas, J. L.; Friend, R. H. *Phys. Rev. B.*, **1999**, 60, 5721.
40. Koster, L. J. A.; Mihailetchi, V. D.; Blom, P. W. M. *Appl. Phys. Lett.*, **2006**, 88, 093511.
41. Roncali, J. *Chem. Rev.*, **1997**, 97, 173.
42. Bredas, J. L.; Heeger, A. J.; Wudl, F. *J. Phys. Chem.*, **1986**, 85, 4673.
43. Hoogmartens, I.; Adriaensens, P.; Vanderzande, D.; Gelan, J.;Quattrocchi, C.; Lazzaroni, R.; Bredas, J. L. *Macromolecules*, **1992**, 25, 7347.

44. Brisset, H.; Thobie-Gautier, C.; Gorgues, A.; Jubault, M.; Roncali, J. *J. Chem. Soc., Chem. Commum.,* **1994**, 1305.
45. Orti, E.; Sanchis, M. J.; Viruela, P. M.; Vituela, R. *Synth. Met.*, **1999**, 101, 602.
46. Pei, Q.; Zuccarello, G.; Ahlskog, M.; Inganas, O. *Polymer*, **1994**, 35, 1347.
47. Zhang, Q. T.; Tour, J. M. *J. Am. Chem. Soc.*, **1998**, 120, 5355.
48. Yamamoto, T.; Zhou, Z.-H.; Kanbara, T.; Shimura, M.; Kizu, K.; Maruyama, T.; Nakamura, Y.; Fukuda, T.; Lee, B.-L.; Ooba, N.; Tomaru, S.; Kurihara, T.; Kaino, T.; Kubota, K.; Sasaki, S. *J. Am.Chem. Soc.*, **1996**, 118, 10389.
49. van Mullekom, H. A. M.; Vekemans, J. A. J. M.; Meijer, E. W. *Chem. Commun.,* **1996**, 2163.
50. Sadki, S.; Schottland, P.; Brodie, N.; Sabouraud, G. *Chem. Soc. Rev.*, **2000**, 29, 283.
51. Sotzing, G. A.; Reynolds, J. R.; Steel, P. J. *Adv Mater*., **2004**, 9, 795.
52. Waltman, R. J.; Bargon, J. *Can. J. Chem.*, **1986**, 64, 76.
53. Toshima, N.; Hara, S. *Prog. Polym. Sci.*, **1995**, 20, 155.
54. Cheng, Y. J.; Luh, T. Y. *J. Organomet. Chem.*, **2004**, 689, 4137.
55. Tamao, K.; Sumitani, K.; Kumada, M. *J. Am. Chem. Soc.*, **1972**, 94, 4374.
56. Stille, J. K. *Angew. Chem., Int. Ed.,* **1986**, 25, 508.
57. Miyaura, N.; Suzuki, A. *Chem. Rev.,* **1995**, 95, 2457.
58. Sonogashira, K. *J. Organomet. Chem.*, **2002**, 653, 46.
59. McCullough, R. D.; Lowe, R. D. *J. Chem. Soc., Chem. Commun.,* **1992**, 70.
60. McCullough, R. D.; Lowe, R. D.; Jayaraman, M.; Anderson, D. L. *J. Org. Chem.*, **1993**, 58, 904.

61. Loewe, R. S.; Khersonsky, S. M.; McCullough, R. D. *Adv. Mater.*, **1999**, 3, 250.
62. Loewe, R. S.; Ewbank, P. C.; Liu, J.; Zhai, L.; McCullough, R. D. *Macromolecules,* **2001**, 34, 4324.
63. Sang, G.; Zou, Y.; Li, Y. *J. Phys. Chem. C*, **2008**, 112, 12058.
64. Hou, J.; Chen, T. L.; Zhang, S.; Chen, H.-Y.; Yang, Y. *J. Phys. Chem. C.*, **2009**, 113, 1601.
65. Liu, C. L.; Tsai, J. H.; Lee, W. Y.; Chen, W. C.; Jenekhe, S. A. *Macromolecules,* **2008**, 41, 6952.
66. Ashraf, R. S.; Shahid, M.; Klemm, E.; Al-Ibrahim, M.; Sensfuss, S. *Macromol. Rapid Commun.*, **2006**, 27, 1454.
67. Huo, L.; He, C.; Han, M.; Zhou, E.; Li, Y. *J. Polym. Sci. Part A: Poly. Chem.*, **2007**, 45, 3861.
68. Li, J.; Dierschke, F.; Wu, J.; Grimsdale, A. C.; Mullen, K. *J. Mater. Chem.*, **2006**, 16, 96.
69. Thompson, B. C.; Kim, Y. G.; Reynolds, J. R. *Macromolecules,* **2005**, 38, 5359.
70. Thompson, B. C.; Kim, Y. G.; McCarley, T. D.; Reynolds, J. R. *J. Am. Chem. Soc.*, **2006**, 128, 12714
71. Gilch, H. G.; Wheelwright, W. L. *J. Polym. Sci., Part A: Polym. Chem.*, **1966**, 4, 1337.
72. Wan, W. C.; Antoniadis, H.; Choong, V. E.; Razafitrimo, H.; Gao,Y.; Feld, W. A.; Hsieh, B. R. *Macromolecules,* **1997**, 30, 6567.
73. Neef, C. J.; Ferraris, J. P. *Macromolecules,* **2000**, 33, 231.
74. Zade, S. S.; Zamoshchik, N.; Bendikov, M. *Acc. Chem. Res.*, **2011**, 44, 14.

75. Zhang, L.; Zhang, Q.; Ren, H.; Yan, H.; Zhang, J.; Zhang, H.; Gu, J. *Solar Energy Materials and Solar Cells*, **2008**, 92, 581.
76. Ra, C. S.; Yim, S.; Park, G. *Bull. Korean Chem. Soc*., **2008**, 29, 891.
77. Salzner, U.; Lagowski, J. B.; Pickup, P. G.; Poirier, R. A. *Synth. Met*., **1998**, 96, 177.
78. Frisch, M. J.; Trucks, G. W.; Schlegel, H. B.; Scuseria, G. E.; Robb, M. A.; Cheeseman, J. R.; Montgomery, J. A.; Vreven, Jr., T.; Kudin, K. N.; Burant, J. C.; Millam, J. M.; S.Iyengar, S.; Tomasi, J.; Barone, V.; Mennucci, B.; Cossi, M.; Scalmani, G.; Rega, N.; Petersson, G. A.; Nakatsuji, H.; Hada, M.; Ehara, M.; Toyota, K.; Fukuda, R.; Hasegawa, J.; Ishida, M.; Nakajima, T.; Honda, Y.; Kitao, O.; Nakai, H.; Klene, M.; Li, X.; Knox, J. E.; Hratchian, H. P.; Cross, J. B.; Bakken, V.; Adamo, C.; Jaramillo, J.; Gomperts, R.; Stratmann, R. E.; Yazyev, O.; Austin, A. J.; Cammi, R.; Pomelli, C.; Ochterski, J. W.; Ayala, P. Y.; Morokuma, K.; Voth, G. A.; Salvador, P.;. Dannenberg, J. J.; Zakrzewski, V. G.; Dapprich, S.; Daniels, A. D.; Strain, M. C.; Farkas, O.; Malick, D. K.; Rabuck, A. D.; Raghavachari, K.; Foresman, J. B.; Ortiz, J. V.; Cui, Q.; Baboul, A. G.; Clifford, S.; Cioslowski, J.; Stefanov, B. B.; Liu, G.; Liashenko, A.; Piskorz, P.; Komaromi, I.; Martin, R. L.; Fox, D. J.; Keith, T.; Al-Laham, M. A.; Peng, C. Y.; Nanayakkara, A.; Challacombe, M.; Gill, P. M. W.; Johnson, B.; Chen, W.; Wong, M. W.; Gonzalez, C.; Pople, J. A.; Gaussian 03, Revision C.02, Gaussian, Inc., Wallingford CT, **2004**.
79. Gaussian 09, Revision B02, Frisch, M. J.; Trucks, G. W.; Schlegel, H. B.; Scuseria, G. E.; Robb, M. A.; Cheeseman, J. R.; Scalmani,

G.; Barone, V.; Mennucci, B.; Petersson, G. A.; Nakatsuji, H.; Caricato, M.; Li, X.; Hratchian, H. P.; Izmaylov, A. F.; Bloino, J.; Zheng, G.; Sonnenberg, J. L.; Hada, M.; Ehara, M.; Toyota, K.; Fukuda, R.; Hasegawa, J.; Ishida, M.; Nakajima, T.; Honda, Y.; Kitao, O.; Nakai, H.; Vreven, T.; Montgomery, Jr., J. A.; Peralta, J. E.; Ogliaro, F.; Bearpark, M.; Heyd, J. J.; Brothers, E.; Kudin, K. N.; Staroverov, V. N.; Kobayashi, R.; Normand, J.; Raghavachari, K.; Rendell, A.; Burant, J. C.; Iyengar, S. S.; Tomasi, J.; Cossi, M.; Rega, N.; Millam, N. J.; Klene, M.; Knox, J. E.; Cross, J. B.; Bakken, V.; Adamo, C.; Jaramillo, J.; Gomperts, R.; Stratmann, R. E.; Yazyev, O.; Austin, A. J.; Cammi, R.; Pomelli, C.; Ochterski, J. W.; Martin, R. L.; Morokuma, K.; Zakrzewski, V. G.; Voth, G. A.; Salvador, P.; Dannenberg, J. J.; Dapprich, S.; Daniels, A. D.; Farkas, Ö.; Foresman, J. B.; Ortiz, J. V.; Cioslowski, J.; Fox, D. J. Gaussian, Inc., Wallingford CT, **2009**.

80. Cao, H.; Ma, J.; Zhang, G.; Jiang, Y. *Macromolecules*, **2005,** 38, 1123.
81. Kudin, K. N.; Scuseria, G. E. *Phys. Rev*. B., **2000**, 61, 16440.
82. Pisani, C.Ed. *Lecture Notes in Chemistry*, Springer-Verlag, Heidelberg, **1996,** Vol. 67.
83. Feibelman, P. J. *Phys. Rev. B*., **1987**, 35, 2626.
84. Jaffe, J. E.; Hess, A. C. *J. Chem. Phys*., **1996**, 105, 10983.
85. Hirata, S.; Iwata, S. *J. Chem. Phys*., **1997**, 107, 10075.
86. Sun, J. Q.; Bartlett, R. J. *J. Chem. Phys*., **1998**, 109, 4209.
87. Wang, H. W.; Wang, B.C.; Chen, W. H.; Hayashi, M. *J. Phys. Chem. A*., **2008**, 112, 1783.
88. Lee, C.; Yang, W.; Parr, R. G. *Phys. Rev. B*., **1988**, 37, 785.

89. Burke, K.; Perdew, J. P.; Wang, Y.; Dobson, J. F.; Vignale, G.; Das, M. P. (Eds.), *Electronic Density Functional Theory: Recent Progress and New Directions*, Plenum Press, New York, **1998**.
90. Janesko, B. G. *J. Chem. Phys*., **2011**, 134, 184105.
91. Wong, B. M.; Cordaro, J. G. *J. Phys. Chem. C*.**, 2011**, 115, 18333.
92. Heyd, J.; Scuseria, G. E.; Ernzerhof, M. *J. Chem. Phys*., **2006**, 124, 219906.
93. Zhou, Q.; Swager, T. M. *J. Am. Chem. Soc*., **1995**, 117, 7017.
94. Zhou, Q.; Swager, T. M. *J. Am. Chem. Soc*., **1995**, 117, 12593.
95. Yang, J. S.; Swager, T. M. *J. Am. Chem. Soc.*, **1998**, 120, 5321.
96. Yang, J. S.; Swager, T. M. *J. Am. Chem. Soc*., **1998**, 120, 11864.
97. Rose, A.; Lugmair, C. G.; Swager, T. M. *J. Am. Chem. Soc*., **2001**,123, 11298.
98. Yamaguchi, S.; Swager, T. M. *J. Am. Chem. Soc.*, **2001**, 123, 12087.
99. Sohn, H.; Calhoun, R. M.; Sailor, M.J.; Trogler, W. C. *Angew. Chem., Int. Ed.*, **2001**, 40, 2104.
100. Sohn, H.; Sailor, M. J.; Magde, D.; Trogler, W. C. *J. Am. Chem. Soc*., **2003**, 125, 3821.
101. Nie, H.; Zhao, Y.; Zhang,M.; Ma,Y.; Baumgartenb, M.; Mullen, K. *Chem. Commun*., **2011**, 47, 1234.
102. Zhang, C.; Che, Y.; Zhang, Z.; Yang, X.; Zang, L. *Chem. Commun.*, **2011**, 47, 2336.
103. Nagarjuna, G.; Kumar, A.; Kokil, A.; Jadhav, K. G.; Yurt, S.; Kumar, J.; Venkataraman, D. *J. Mater. Chem.*, **2011**, 21, 16597.

Chapter 2

DONOR-ACCEPTOR TYPE COPOLYMERS OF PHENOTHIAZINE AND 2,1,3-CHALCOGENADIAZOLES: SYNTHESIS, CHARACTERIZATION AND PHOTOVOLTAIC APPLICATIONS

Contents

The band structure and Density of States of two phenothiazine based polymers, poly(N-octylphenothiazine-alt-2,1,3-benzothiadiazole) (PPHENO-BTZ) and poly(N-octyl phenothiazine-alt-2,1,3-benzoselenadiazole) (PPHENO-BSE) copolymers were calculated by employing Density Functional Theory in the Periodic Boundary Condition formalism. Both the polymers were synthesized using palladium catalysed Suzuki polycondensation reaction in good yields. The polymers were characterized using ^{1}H NMR, UV-Visible spectroscopy, Cyclic Voltammetry, and GPC etc. The theoretically calculated values were in good agreement with experimental results. The polymers showed good solubility in common organic solvents like chloroform, tetrahydrofuran etc. Linear heterojunction photovoltaic devices were fabricated using these polymers with a device structure ITO/In_2S_3/polymer/Ag. The heterojunctions of PPHENO-BTZ and PPHENO-BSE showed efficiencies of 0.035% and 0.037% respectively.

2.1. Introduction

The π-conjugated polymer with donor-acceptor architectures have wide interest in organic solar cells because of the built in intramolecular

charge transfer which can manipulate the energy levels of the materials, leading to a small band gap polymer with enhanced optical properties[1-4]. Phenothiazine is a well-known heterocyclic compound with electron-rich sulfur and nitrogen heteroatoms. Recently, polymers and oligomers containing phenothiazine units have wide research interest due to their unique electro-optic properties. As a result, these materials are potential candidates for light emitting diodes[5], photovoltaic devices[6] and chemiluminescence applications[7,8]. Alternating copolymer of phenothiazine and divinyl benzene or divinyl thiophene in the main chain were well studied for the electrochromic devices[9-10]. Large number of donor-acceptor copolymers of phenothiazine with cynovinylene[11],and quinoline[12,13], were reported. Jenekhe et al. have synthesized an alternating copolymer of phenothiazine and fluorene by the Suzuki coupling reaction and characterized their properties.[14]

In this chapter, we have investigated the theoretical electronic structure properties of two copolymers composed of phenothiazine donor and 2,1,3-benzothiadiazole and 2,1,3-benzoselenadiazole acceptors. Their synthesis, electrochemistry, optical, thermal and photovoltaic properties are discussed.

Although, benzothiadiazole is an electron accepting heterocycle that has been utilized for the synthesis of n-type materials, benzothiadiazole is also used as acceptor moiety in low band gap polymers. Broad sunlight absorption band could be achieved for the D-A type 2,1,3-benzothiadiazole containing polymers. These types of donor-acceptor polymers have been studied extensively and have showed outstanding photovoltaic performance[15-19].

In addition to this, we have explored the photovoltaic property of a bilayer heterojunction ITO/In_2S_3/polymer/Ag. In most polymer solar cells, the front electrode is a transparent conducting oxide, such as indium-tin oxide (ITO), which functions as a high work function electrode for hole collection. For the efficient operation of the device, the back electrode must be a low work function metal such as calcium, which facilitates smooth collection of electrons[20]. However, these metals are reactive and get easily oxidized in air. This issue is normally addressed by capping the reactive metal with a less reactive one and by encapsulating the device to protect it from environmental effects during operation. On the other hand, the devices can be made more stable by avoiding the need for a reactive low work function top electrode. This can be accomplished by inverting the device geometry such that the holes and electrons generated in the active layer exit the device in the direction opposite to that in a normal device[21]. In this reversed geometry, a hole blocking layer, usually, an inorganic n-type semiconductor is inserted between the ITO and the active layer so that only electrons are collected by the ITO, where as the back electrode becomes the hole collecting positive electrode, which can be made from a high work function metal that is more stable in air. In this work, we have used indium sulfide (In_2S_3) as the electron selective layer. In_2S_3 being an n-type compound semiconductor with high electron affinity, wide band gap and excellent photosensitivity, should function as efficient electron acceptor/hole blocking layer in polymer photovoltaics. Its potential as buffer layer material in inorganic solar cells has already been demonstrated in literature.[22]

2.2. Results and discussion

2.2.1. Theoretical calculation

2.2.1.1. Theoretical methodology

The ground state geometries of oligomers were optimized by means of the hybrid density functional theory (DFT) [23] at the B3LYP [24-26] (Becke, three-parameter, Lee-Yang-Parr) level of theory using double zeta basis set LanL2DZ (Los Alamos ECP plus DZ)[27]. LanL2DZ basis set describes core electrons of the heavier elements by means of an effective core potential. This permits the study of Se containing compounds with less computational time. The harmonic vibrational frequencies obtained with B3LYP/ LanL2DZ were used to characterize the stationary points as local minima. Although the oligomer approach can be used to study the properties of conjugated polymers, periodic boundary condition (PBC) calculation is more computationally cost effective, because, in PBC calculation, polymer molecule of infinite chain length is optimized using translational symmetry. In addition to this, PBC allows the calculation of band structure in the positive region of the first Brillouin zone (between k=0 and k=π/a). The starting unit cell geometries for the periodic boundary condition (PBC/DFT) calculation were taken from the central portion of the optimized oligomer and optimized inside a given lattice length on the constraints of periodic boundary condition by assuming that the unit cell is repeated identically an infinite number of times along the translation vector. Band structures in the positive region of the first Brillouin zone (between k=0 and k=π/a) were calculated along the k-vector of these one-dimensional polymers with 30 k-points after the optimization using the B3LYP/LanL2DZ level of theory. The lowest 4 unoccupied and highest 4 occupied bands in the positive region of the first Brillouin zone were plotted.

All the calculations described here were carried out using G 03 suite of codes[28]. Density of state (DOS) is generated with GAUSSSUM 2.2[29].

2.2.1.2. Optimized geometries and electronic properties of model compounds

Since the electronic properties of the polymers depend on their constituent monomers, we have started with studying the properties of constituents, phenothiazine (PT), 2,1,3-benzothiadiazole (BTZ), 2,1,3-benzoselenadiazole (BSE), phenothiazine/ 2,1,3- benzothiadiazole (PT-BTZ) and phenothiazine/2,1,3-benzoselenadiazole (PT-BSE) (figure 1). The intramolecular charge transfer from phenothiazine to 2,1,3-chalcogenadiazole was calculated by taking the summation of Mulliken charge distribution on phenothiazine unit and was found to be 0.034e and 0.06e respectively for PT-BTZ and PT-BSE. It is noted from energy levels of model compounds that LUMO levels of BTZ and BSE are found to be -2.35 eV and -2.44 eV respectively (figure 2). The lower the LUMO energy level, the higher the acceptor strength. The energy gap of the PT-BTZ and PT-BSE is calculated to be 2.74 eV and 2.61 eV respectively. The lower energy gap of PT-BSE is presumably due to the slightly higher acceptor strength of the BSE unit. Hence, the trend of the intramolecular charge transfer is similar to that of the acceptor strength. The charge transfer from donor to acceptor is also rationalized by analyzing the frontier energy levels of PT-BTZ and PT-BSE. It is observed that, in the both the molecules, HOMO is localized on phenothiazine unit, while LUMO is strongly confined to the acceptor 2,1,3-chalcogenadiazole unit (figure 3).

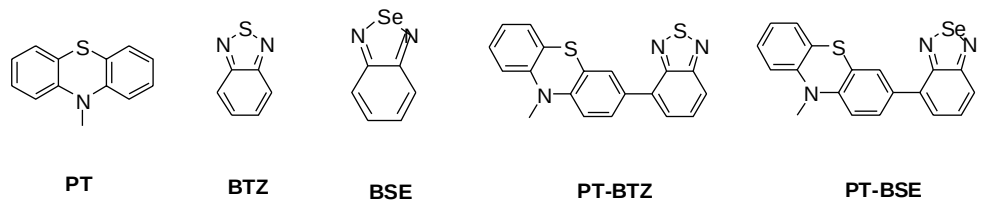

Figure 1: Structure of model compounds

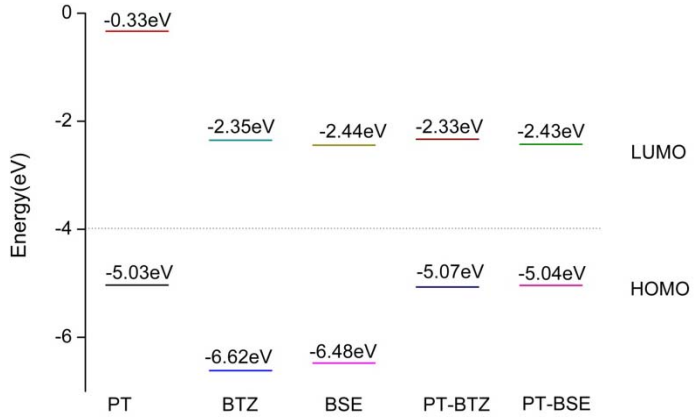

Figure 2: Energy levels of PT, BTZ, BSE, PT-BTZ and PT-BSE

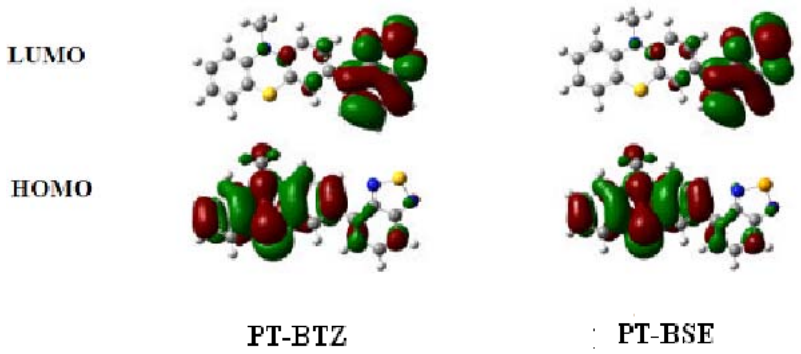

Figure 3: Frontier molecular orbital distribution of monomeric unit of PT-BTZ and PT-BSE

2.2.1.3. Band structure of the polymers

The optimized repeating unit for the periodic boundary calculation is given in figure 4. Horizontal lines represent the translational vector which is equal to the one dimensional cell size. For both the polymers, length of the vector is ~25.2 A^0. It can be seen from figure 5 that lowest band gap occur at Γ point (k=0), suggesting that both the polymers are direct band gap polymers. The values of HOCO (highest occupied crystal orbital) and LUCO (lowest unoccupied crystal orbital) correspond to experimental HOMO and LUMO respectively. The energy levels of the HOMO and LUMO were determined from the maximum point of the highest occupied

molecular orbital and the minimum point of the lowest unoccupied molecular orbitals, respectively. The band gap was obtained from the minimum difference between the HOMO and LUMO energy levels at a constant k. Comparing the band structure of PPHENO-BTZ and PPHENO-BSE with band structure of poly(phenothiazine), we can find the influence of 2,1,3-chalcogenadiazole unit on the energy gap of the polymer. From the band structures, we can see that, by the introduction of acceptor unit, energy of HOCO level of poly(PHENO) is decreased by a factor of 0.237 eV and 0.14 eV while LUCO level is decreased by a factor of 1.62 eV and 1.53 eV and we get PPHENO-BTZ and PPHENO-BSE with a reduced band gap of 1.98 eV and 1.96 eV respectively (table 1).

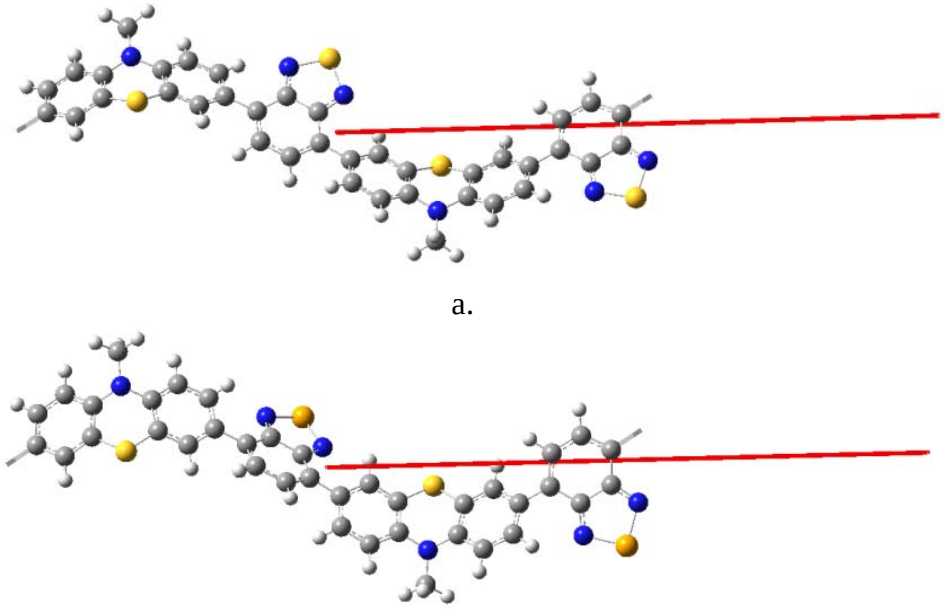

a.

b.

Figure 4: Unit cell of (a). PPHENO-BTZ and (b). PPHENO-BSE for the PBC/B3LYP/LANL2DZ calculation. The red line represents the translational vector

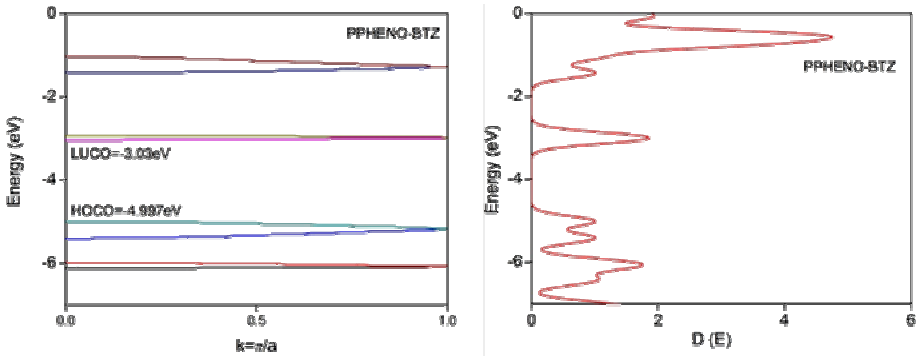

a.

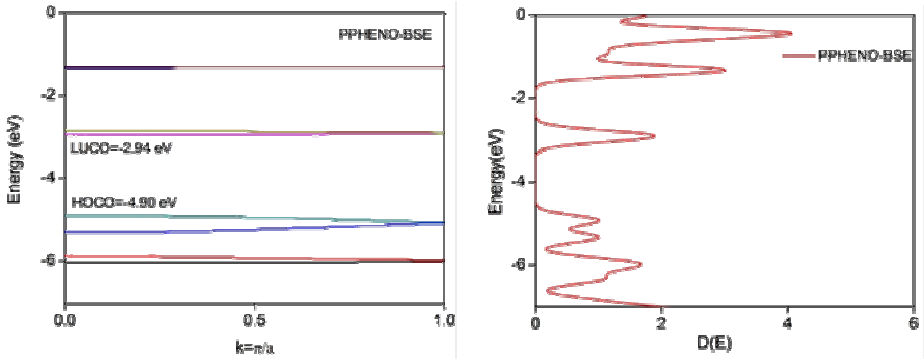

b.

Figure 5: Band structure and density of states of (a). PPHENO-BTZ (b). PPHENO-BSE

Table 1: Band structure data of poly(PHENO), PPHENO-BTZ and PPHENO-BSE

Polymer	HOCO (eV)	LUCO (eV)	E_g (eV)
Poly(PHENO)	-4.76	-1.41	3.35
PPHENO-BTZ	-4.997	-3.03	1.98
PPHENO-BSE	-4.90	-2.94	1.96

2.2.2. Synthesis of monomers and polymers

2.2.2.1. Monomer synthesis

Scheme 1 summarizes the synthesis of key monomers. Starting from 2,1,3-benzothiadiazole, 4,7-dibromo-2,1,3-benzothiadiazole was prepared by bromination of 2,1,3-benzothiadiazole in 47% HBr. To obtain 4,7-dibromo-2,1,3-benzoselenadiazole, 4,7-dibromo-2,1,3-benzothiadiazole was reduced by $NaBH_4$ in absolute ethanol to give 2,3-diamino-1,4-dibromobenzene. 2,3-diamino-1,4-dibromobenzene was reacted with selenium dioxide to give 4,7-dibromo-2,1,3-benzoselenadiazole in 73% yield. The precursor monomer 3,7-dibromo-10-octylphenothiazine was synthesized in two steps starting from phenothiazine. It was converted to 3,7-bis(4,4,5,5-tetramethyldioxaborolan)-10H-phenothiazine by reaction with n-butyl lithium followed by 2-isopropoxy-4,4,5,5-tetramethyl-1,3,2-dioxaborolane at -78^0C. The ^{1}H NMR and ^{13}C NMR of 3,7-bis (4,4,5,5-tetramethyldioxaborolan)-10H-phenothiazine is depicted in figure 6. The ^{1}H NMR spectrum of 3,7-bis(4,4,5,5-tetramethyldioxaborolan)-10H-phenothiazine showed multiplets at δ 0.78-2.4 due to alkyl protons and a triplet at δ 3.75 due to $-NCH_2-$ protons. It showed multiplets at δ 6.71-7.4 due to aromatic protons.

2.2.2.2. Polymer synthesis

Standard Suzuki polycondensation reaction was used to synthesise both the polymers (scheme 2). The resulting polymers were collected by adding to polymerization solution to cold methanol followed by filtration. The crude polymer was purified by soxhlet extraction using methanol. The polymer was dissolved in small amounts of toluene and reprecipitated from methanol and dried under vacuum to offer the pure polymer. Both polymers

are readily soluble in common organic solvents such as chloroform, THF, and toluene and can be easily processed in to thin films. The polymers were characterized using ^{1}H NMR (figure 7). The ^{1}H NMR spectrum of PPHENO-BTZ and PPHENO-BSE showed multiplets at δ 0.8-2 region due to alkyl protons. The peaks corresponding to –NCH_2- protons are observed at δ 3.8-3.9 as triplet. The peaks corresponding to aromatic protons are observed at 6.9-7.8 as multiplets. The isolated yield and molecular weight of both the polymers are summarized in table 2. The molecular weight of polymers were determined by gel permeation chromatography in toluene referring to polystyrene standards.

The thermal properties of the polymers were determined by thermogravimetric analysis (Table 2). Both the polymers were found to exhibit good thermal stability, losing less than 5% of their weight on heating to 265°C in TGA runs under nitrogen.

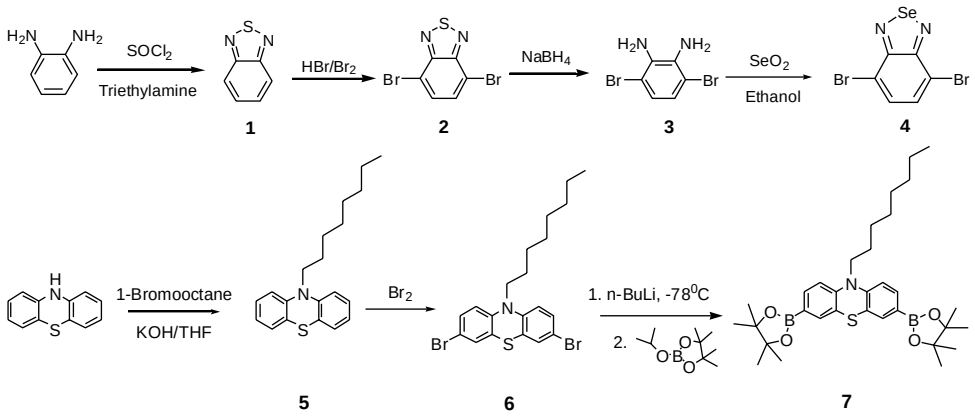

Scheme 1. Synthesis of monomers

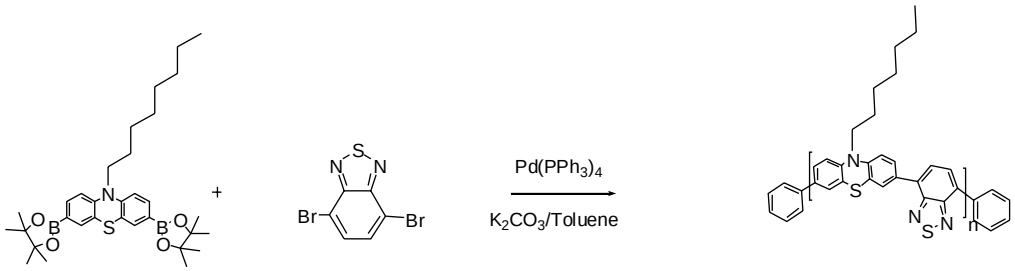

PPHENO-BTZ

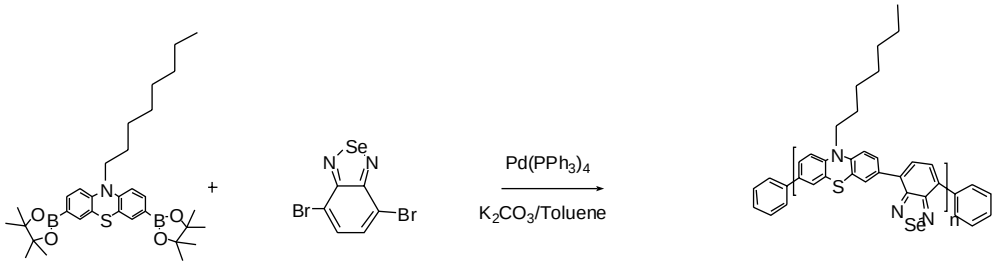

PPHENO-BSE

Scheme 2: Synthesis of PPHENO-BTZ and PPHENO-BSE

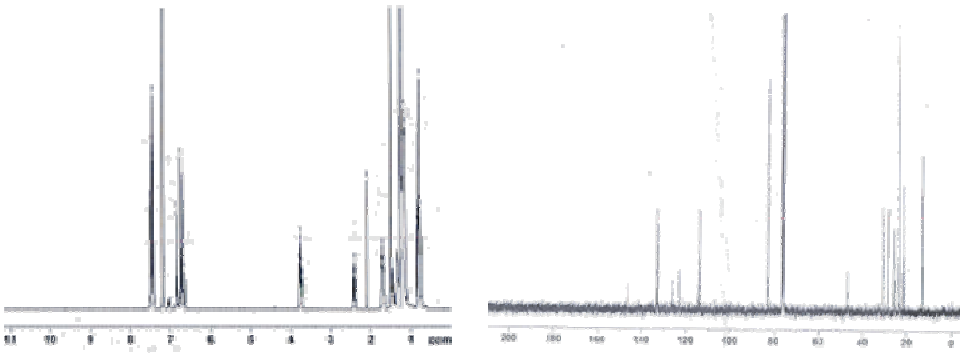

Figure 6: ^{1}H and ^{13}C NMR spectra of 10-octyl-3,7-bis(4,4,5,5 tetramethyl[1,3,2] dioxaborolan-2-yl)-10H-phenothiazine

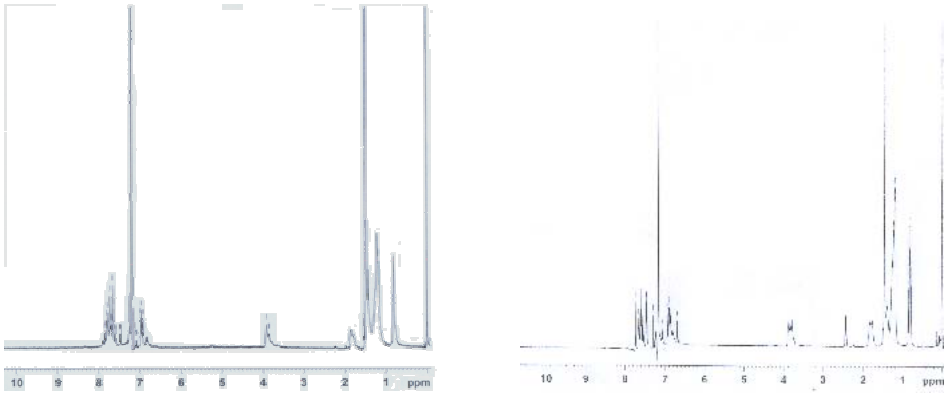

Figure 7: ^{1}H NMR spectra of PPHENO-BTZ and PPHENO-BSE

Table 2: Results of polymerization and thermal stability of polymers

Polymer	Yield (%)	M_n[a]	M_w[a]	PDI	Td(^{0}C)[b]
PPHENO-BTZ	59	15532	42834	2.7	267
PPHENO-BSE	42	5800	16847	2.9	287

a. Determined by GPC in toluene based on polystyrene standards.
b. Onset decomposition temperature measured by TGA under nitrogen.

2.2.3. Optical and photoluminescence properties

Figure 8 shows the absorption spectra of the polymers in chloroform. PPHENO-BTZ shows absorption peak at 470 nm in dilute chloroform solution, while in thin film form the absorption peak is located at 494 nm and absorption onset at 606 nm, which corresponds to an optical gap of 2.05 eV. PPHENO-BSE exhibits peaks at 493 nm and 523 nm in solution and in thin film form respectively and absorption onset is at 643 nm. The optical band gap of PPHENO-BSE is calculated to be 1.93 eV. The reduced gap of PPHENO-BSE is due to the greater acceptor strength of 2,1,3-benzoselenadiazole than the 2,1,3-benzothiadiazole, which was revealed by the theoretical calculation on the model compounds and polymers. As seen from the figure, a red shift in solid state absorption of both the polymers is observed compared with that of the absorption in

solution, which may be due to the pronounced interchain interaction in the solid state. The optical properties of the polymers are listed in table 3.

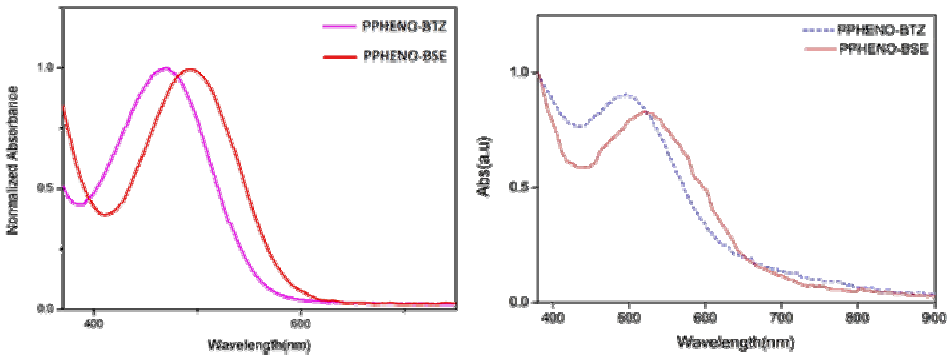

Figure 8: UV-Visible spectra of the polymer in chloroform solution and in thin film from. The polymer films were spun coated from 5 mg/mL chlorobenzene solution on to glass substrate.

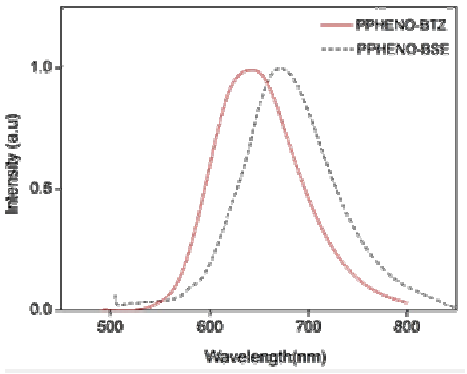

Figure 9: PL spectra of the polymer in chloroform solution

Figure 9 shows the emission spectra of PPHENO-BTZ and PPHENO-BSE in chloroform. The maximum emission of PPHENO-BTZ appears at 642 nm. The PL emission spectrum of the PPHENO-BSE was red shifted from that of the PPHENO-BTZ and exhibited peak emission at about 672 nm.

Table 3: Optical properties of the polymers

Polymer	UV-Visible Absorption λ_{max} (nm)		Emission λ_{max} (nm)	UV-Visible Absorption onset(film) (λ_{onset})	E_g^{opt} (eV)
	Solution	Film			
PPHENO-BTZ	470	494	642	606	2.05
PPHENO-BSE	493	523	672	643	1.93

2.2.4. Electrochemical properties

The electronic states of the conjugated polymers, which are important for the construction of photovoltaic devices, are investigated using cyclic voltammetry (CV). Figure 10 shows the cyclic voltammetric curve of PPHENO-BTZ and PPHENO-BSE film on Pt electrode in 0.1 M Bu_4NPF_6 solution in acetonitrile at a scan rate of 100 mV/sec. The electrochemical data are summarized in table 4. From the onset of oxidation, the HOMO levels of PPHENO-BTZ and PPHENO-BSE are estimated to be -5.15 eV and -5.12 eV respectively based on the equation, HOMO=-(4.4+E_{ox}^{onset}). The SCE energy level of -4.4 eV below the vacuum level is used. The HOMO level of poly(10-hexyl phenothiazine) reported by Jeneke *et al* under the same condition was -5.0 eV[30]. This indicates that HOMO levels of PPHENO-BTZ and PPHENO-BSE are predominantly contributed by phenothiazine moiety. Thus, one can use phenothiazine moiety for building air stable donor-acceptor copolymers with low lying HOMO level. As shown in figure 10, PPHENO-BTZ shows peaks at 1.57 V, 0.96 V and shoulder peak at 0.81 V. Similarly, PPHENO-BSE shows peaks at 1.49 V, 0.86 V and 0.78 V. This multiple oxidation peaks in the CV of both the polymers are analogous to poly(10-hexyl phenothiazine) and oligo phenothiazine[30,31].

PPHENO-BTZ and PPHENO-BSE show one reversible reduction peak at -1.637 V and -1.414 V respectively and onset of reduction is at -1.41 V and -1.3 V respectively. The LUMO levels estimated using the equation LUMO=-(4.4+E_{red}^{onset}) are -2.99 eV and -3.1 eV respectively. The band gap is calculated to be 2.16 eV and 2.02 eV respectively and is in well agreement with the theoretically calculated values. The lower band gap of PPHENO-BSE is due to the higher acceptor strength of BSE unit, which enhances charge transfer from donor to the acceptor.

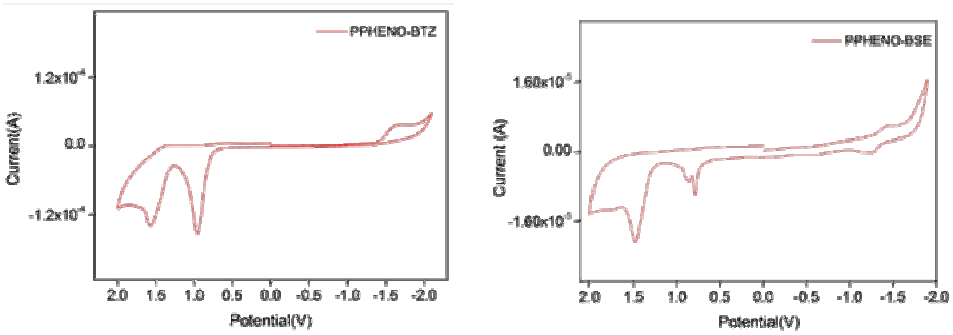

Figure 10: CV curves of PPHENO-BTZ and PPHENO-BSE film on Pt electrode in 0.1 M Bu_4NPF_6 solution in acetonitrile at a scan rate of 100 mV/sec

Table 4: Redox properties of the polymers

Polymer	E_{red} (V)	E_{ox} (V)	HOMO (eV)	LUMO (eV)	E_g (eV)
PPHENO-BTZ	-1.41	0.750	-5.15	-2.99	2.16
PPHENO-BSE	-1.30	0.716	-5.12	-3.1	2.02

2.2.5. Photovoltaic device

From the theoretical as well as experimental data, it was found that the polymers PPHENO-BTZ and PPHENO-BSE have low band gaps which are very much suitable for photovoltaic application. This was verified by fabricating a heterojunction device using both the polymers and the semiconductor In_2S_3. Figure 11 shows the current density-voltage (J-V)

characteristics of the heterojunction under illumination and in the dark. As could be seen, the device clearly exhibits rectifying behaviour in the dark which may be due to the barrier formed at the In_2S_3/ polymer interface. Under white light illumination (50 mW/cm^2), the device exhibits a short circuit current density (J_{sc}) of 79.8 µA/cm^2 and an open circuit voltage (V_{oc}) of 629.09 mV for PPHENO-BTZ and 91.1 µA/cm^2 and 608.47 mV respectively for PPHENO-BSE. The fill factor (FF) and power conversion efficiency were calculated to be 35.17% and 33.46% and 0.035% and 0.037% respectively for PPHENO-BTZ and PPHENO-BSE. Photovoltaic characteristics of bilayer heterojunction devices of PPHENO-BTZ and PPHENO-BSE are summarized in table 5.

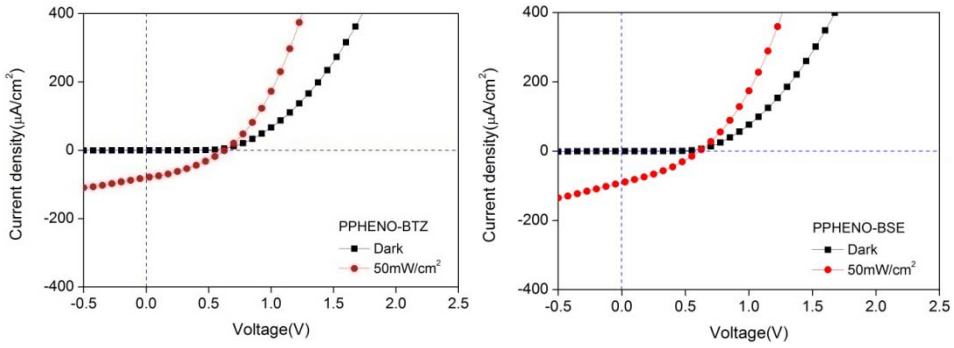

Figure 11: J-V characteristics of ITO/In_2S_3/polymer/Ag heterojunction

Table 5: Photovoltaic characteristics of bilayer heterojunction devices of PPHENO-BTZ and PPHENO-BSE

Polymer	V_{oc} (mV)	J_{sc} (µA/cm^2)	Efficiency (%)	Fill factor (%)
PPHENO-BTZ	629.09	79.8	0.035	35.17
PPHENO-BSE	608.47	91.1	0.037	33.46

A schematic energy diagram for an In_2S_3/polymer device with Ag and ITO electrodes, before the materials are placed in contact, is shown in figure 12. The energies of the conduction band (CB) and valence band

(VB) edges for In_2S_3 are -3.9 eV and -6.4 eV respectively, whereas the LUMO and HOMO levels of PPHENO-BTZ are -2.99 eV, -5.15 eV respectively. The work functions of Ag and ITO electrodes are taken to be about -4.26 eV and -4.7 eV, respectively. The device principle can be explained as follows: the excitons photogenerated in polymer gets diffused to the In_2S_3/PPHENO-BTZ interface. Since the LUMO of PPHENO-BTZ lies above the CB edge of In_2S_3, the excitons are expected to efficiently dissociate by electron transfer to In_2S_3. In the same manner, a photoinduced hole transfer from In_2S_3 to PPHENO-BTZ is expected. Furthermore, since electrons are carried to one contact by In_2S_3, and holes are transported by the PPHENO-BTZ layer to the opposite contact, the paths of oppositely charged carriers are separated and recombination should be suppressed. A similar observation can be made with In_2S_3/PPHENO-BSE heterojunction.

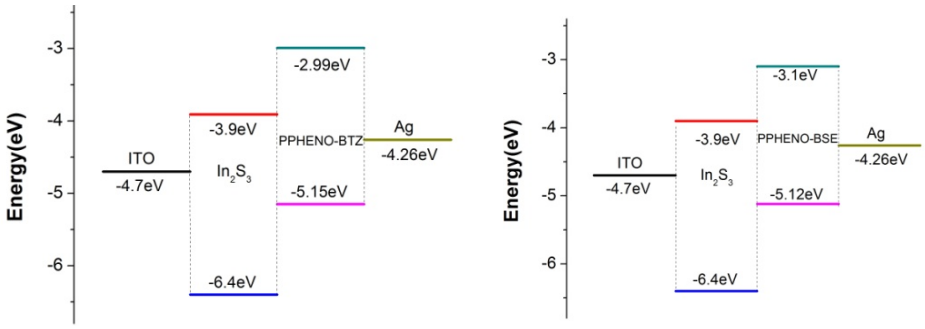

Figure 12: Energy level diagram of ITO/In_2S_3/PPHENO-BTZ/Ag and ITO/In_2S_3/PPHENO-BSE/Ag photovoltaic devices

2.3. Conclusion and perspectives

In conclusion, it was shown theoretically that the introduction of 2,1,3-chalcogenadiazole unit to the phenothiazine unit effectively reduced the band gap of the conjugated polymers in accordance with the donor-acceptor concept. The band gap reduction depends on the acceptor strength of the 2,1,3-chalcogenadiazole which facilitates the charge transfer from

phenothaizine unit to the 2,1,3-chalcogenadiazole. Both the polymers were synthesized by Suzuki polycondensation reaction and characterized by electrochemical and photophysical methods. The experimental results are in good agreement with the theoretically calculated values. Thus the theoretical calculation prior to synthesis is advantageous from the point of view of screening out the less effective material. A linear heterojunction device was fabricated using indium sulfide as n-type layer and showed photoactivity under illumination due to the electron transfer from donor polymer to acceptor indium sulfide layer. A further improvement may be achieved by designing a bulk heterojunction device by considering the energy levels of polymer and acceptor.

2.4. Experimental Section

2.4.1. Benzothiadiazole[32] (1):1,2-phenylenediamine(5.42 g, 50 mmol), triethylamine (30 mL) and dichloromethane (150 mL) were stirred under nitrogen with drop wise addition of thionyl chloride (9.5 mL) in dichloromethane (30 mL). After the addition was complete, the reaction was heated at reflux for 15 min. The mixture was filtered; the solid residue was washed with dichloromethane and discarded. The filtrate was evaporated under vacuum to give a black residue. The residue was recrystallized from hexane to give 2,1,3-benzothiadiazole as yellow needles.

Yield: 54% (3.7 g). M.P.: 43-45^{o}C.

2.4.2. 4,7-Dibromo-2,1,3-benzothiadiazole[33](2): A mixture of 6.8 g (0.5 mol) of 2,1,3-benzothiadiazole in 15 mL of 47% hydrobromic acid was heated under reflux with stirring while 24 g (0.15 mol, 15.3 mL) of bromine was added slowly. After completion of the bromine addition, the

reaction mixture became a suspension of solid in hydrobromic acid and 7.5 mL of hydrobromic acid was added, and the mixture was heated under reflux for another 2.5 h. The mixture was filtered, washed well with water, recrystallized from chloroform, and dried to give white needle crystals.

Yield	:	93% (13.65 g)
M. P.	:	187-188°C.
^{1}H NMR (400 MHz, $CDCl_3$)	:	δ 7.73 (s, 2H).
^{13}C NMR (100 MHz, $CDCl_3$)	:	δ 153.3, 132.7, 114.3
GC-MS	:	m/z=293.8

2.4.3. 3,6-dibromo-1,2-phenylenediamine[33] (3): To a suspension of 4,7-dibromo-2,1,3-benzothiadiazole (5.88 g, 0.02 mol) in ethanol (190 mL), sodium borohydride (14 g, 0.37 mol) was added in three portions at 0°C, and the mixture was stirred for 20 h at room temperature. After evaporation of the solvent, 200 mL of water was added, and the mixture was extracted with ether. The extract was washed with brine and dried over anhydrous sodium sulfate. Evaporation of the solvent gave 3,6-dibromo-1,2-phenylenediamine as a pale yellow solid.

Yield	:	85% (4.52 g)
^{1}H NMR (400 MHz, $CDCl_3$)	:	δ 3.90 (s, 4 H), 6.85 (s, 2H).
^{13}C NMR (100 MHz, $CDCl_3$)	:	δ 133.7, 123.4, 109.7
GC-MS	:	m/z=265.9

2.4.4. 4,7-Dibromo-2,1,3-benzoselenadiazole[33](4): To a solution of **3** (2.7 g, 10 mmol) in refluxing ethanol (55 mL), was added a solution of selenium dioxide (1.17 g, 10.5mmol) in hot water (22 mL). The mixture was heated under reflux for 2 h. Filtration of the yellow precipitate and

recrystallization from ethyl acetate gave 4,7-dibromo-2,1,3-benzoselenadiazole (**4**) as golden yellow needles.

Yield	:	73% (2.5 g)
M. P.	:	285-287 °C
^{1}H NMR (400 MHz, $CDCl_3$)	:	δ 7.63 (s, 2H).
^{13}C NMR (100 MHz, $CDCl_3$)	:	δ 157.2, 132.1, 116.5.
GC MS	:	m/z=341.8

2.4.5. 10-*n*-Octylphenothiazine[34] (5): Phenothiazine (10 g, 50 mmol), potassium hydroxide (20.0 g, 500 mmol), and DMSO (100 mL) were placed in a 250 mL two-necked flask. The mixture was stirred for half an hour. Octyl bromide (7.7 mL, 55 mmol) was added dropwise to the reaction mixture in 20 min, and this mixture was stirred for 24 h at room temperature. The reaction mixture was poured into water, extracted with methylene chloride, and dried with $MgSO_4$. The resulting liquid was purified by column chromatography using petroleum ether as eluent which gave colourless liquid.

Yield	:	93% (13.2 g)
^{1}H NMR 400MHz, $CDCl_3$)	:	δ 0.87 (t, *J*=6.8 Hz, 3H), 1.24-1.43 (m, 10H), 1.77 (m, 2H), 3.80-3.84 (t, *J*=7.2 Hz, 2H), 6.83-6.91 (m, 4H), 7.11-7.15 (m, 4H).
GC-MS	:	m/z=311.17

2.4.6. 3,7-Dibromo-10-(octyl)-phenothiazine (6):

10-n-Octylphenothiazine (7.5 g, 0.024 mol) was dissolved in 50 mL of dichloromethane, and bromine (8.0 g, 0.05 mol) was injected into the solution using a syringe and stirred for 4 h at room temperature. Dilute aqueous sodium hydroxide (20 mL) was added to the reaction mixture and kept for 30 min. The reaction mixture was extracted three times using dichloromethane and brine, and the organic layer was separated and concentrated. The crude product was purified using column chromatography using hexane as the eluent which gave yellow oil.

Yield	:	79% (9.0 g)
^{1}H-NMR (400MHz, $CDCl_3$)	:	δ 0.86 (t, *J*=6.4 Hz, 3H), 1.14-1.51 (m, 10 H), 1.74 (m, 2H), 3.72 (t, *J*=7.2 Hz, 2H), 6.66 (d, *J*=8.4 Hz, 2H), 7.18–7.20 (dd, J_1=8 Hz, J_2=2.4 Hz, 2H), 7.24 (d, *J*=8 Hz, 2H).
GC-MS	:	m/z=469.99

2.4.7. 10-octyl-3,7-bis(4,4,5,5-tetramethyldioxaborolan-2-yl)-10H-phenothiazine (7):

To a solution of 3,7-Dibromo-10-(octyl)-phenothiazine (2 g, 4.262 mmol) in THF (35 mL) at -78^{o}C was added by syringe (5.59mL, 8.95 mmol) of n-butyl lithium (1.6 M in hexane). The mixture was stirred at -78^{o}C, warmed to 0^{o}C for 15 min and cooled again to -78^{o}C for 15 min. 2-Isopropoxy-4,4,5,5,-tetramethyl-1,3,2-dioxaborolane (1.86 g,10 mmol) was added rapidly to the solution and the resulting mixture was warmed to room temperature and stirred for 24 h. The mixture was poured into water and

extracted with ether. The organic extract was washed with brine and dried over $MgSO_4$. The solvent was removed and the residue was purified by several reprecipitations from methanol/acetone mixture to provide the product as a slight yellow solid.

Yield	:	51% (1.22 g)
M. P.	:	87^{o}C
^{1}H NMR (400 MHz, $CDCl_3$)	:	δ 0.78 (t, *J*=6.3 Hz, 3 H), 1.49-1.71 (m, 34 H), 2.4 (m, 2 H), 3.75 (t, *J*=7.2 Hz 2 H), 6.71 (m, 2 H), 7.48 (m, 2 H), 7.4 (m, 2H).
^{13}C NMR (100 MHz, $CDCl_3$)	:	δ 12.91, 13.07, 21.22, 21.59, 23.80, 25.66, 25.78, 25.89, 28.13, 28.15, 28.17, 30.7, 46.46, 82.6, 113.64, 122.9, 125.97, 132.70, 132.95, 146.21.
GC-MS	:	m/z=563.34

2.4.8. General procedure for polymerization through Suzuki Coupling

Under nitrogen atmosphere, the dibromo monomers (2&4) (0.18 mmol), 10-octyl-3,7-bis(4,4,5,5-tetramethyl[1,3,2]dioxaborolan-2-yl)-10H-phenothiazine (7) (0.18 mmol) were mixed together with 10 mol% (0.018 mmol) of $Pd(PPh_3)_4$ in a 50 mL R.B flask. Degassed aqueous solution of potassium carbonate (10 mL) (2.0 M) and toluene (20 mL) (1:2, volume ratio) were added to the flask. The mixture was stirred vigorously at 80-

90°C for 72 h under nitrogen atmosphere. The resulting solution was added dropwise into stirring methanol to precipitate the polymer. The fibrous solid was collected by filtration and washed with methanol and water. The material was washed continuously with methanol and acetone for 2 days in a Soxhlet extractor to remove the oligomers and catalyst residues. The product was dried under reduced pressure.

2.4.8.1. Synthesis of PPHENO-BTZ

10-octyl-3,7-bis(4,4,5,5-tetramethyl[1,3,2]dioxaborolan-2-yl)-10H-phenothiazine (0.1 g, 0.18 mmol), 4,7-dibromobenzothiadiazole (0.052 g, 0.18 mmol), $Pd(PPh_3)_4$ (0.02 g, 0.018 mmol), 2 M Na_2CO_3 (10 mL) and toluene (20 mL) were used.

Yield	:	59% (0.046 g)
UV-Visible (λmax, Chloroform)	:	470 nm
GPC	:	M_n=15532, PDI=2.7
^{1}H NMR (400 MHz, $CDCl_3$)	:	δ 0.88 (m, ~3H, -CH_3), 1.19-1.29 (m, ~12H, aliphatic-H), 3.83-3.9 (t, ~2H, -NCH_2-), 6.9-7.8 (m, Ar-H of phenothiazine and benzothiadiazole)

2.4.8.2. Synthesis of PPHENO-BSE

10-octyl-3,7-bis(4,4,5,5-tetramethyl[1,3,2]dioxaborolan-2-yl)-10H-phenothiazine (0.1 g, 0.18 mmol), 4,7-dibromo-2,1,3-benzoselenadiazole (0.060 g, 0.18 mmol), $Pd(PPh_3)_4$ (0.02 g, 0.018 mmol), 2 M Na_2CO_3 in 20 mL toluene.

Yield	:	42% (0.036 g)

UV-Visible (λmax, Chloroform) :		494 nm
GPC	:	M_n=5800, PDI=2.9
^{1}H NMR (400 MHz, $CDCl_3$)	:	δ 0.81(m, ~3H, -CH_3), 1.21-1.84 (m, ~12H, aliphatic-H), 3.8-3.9 (t, 2H, -NCH_2), 6.7-7.76 (m, Ar-H of phenothiazine and benzoselenadiazole)

2.5. Photovoltaic device fabrication

Heterojunction photovoltaic device was fabricated using the two polymers as the electron donor and the compound semiconductor In_2S_3 as the electron acceptor. In_2S_3 is an n-type semiconductor having high electron affinity and is a potentially good acceptor material like CdS and TiO_2 for polymer solar cells. Indium sulfide (In_2S_3) thin films were deposited on ITO coated glass substrates by spraying aqueous solutions of indium chloride ($InCl_3$), and thiourea ($CS(NH_2)_2$), keeping the substrate at 350±5 ^oC with a spray rate of 2 ml/min. The thickness of the film was 200 nm. Heterojunctions were prepared by spin coating a solution of polymers in chlorobenzene, on top of the In_2S_3 layer. The layer thickness was approximately 100 nm as obtained from Stylus profilometer measurements. Silver electrodes were vacuum deposited (at a pressure of ~6×10^{-6} Torr) on top of the polymer layer and served as the end contact. The schematic diagram is shown in figure13. Dark and illuminated J-V characteristics of the cell were measured using a Keithley Source Measure Unit (SMU, K236) and Metric's Interactive Characterization Software (ICS).

The cell was illuminated using a tungsten halogen lamp, with an intensity of 50mW/cm^2, on the substrate surface. An infrared filter, along with a water jacket, was used to ensure that there was no heating of the cell during the measurement.

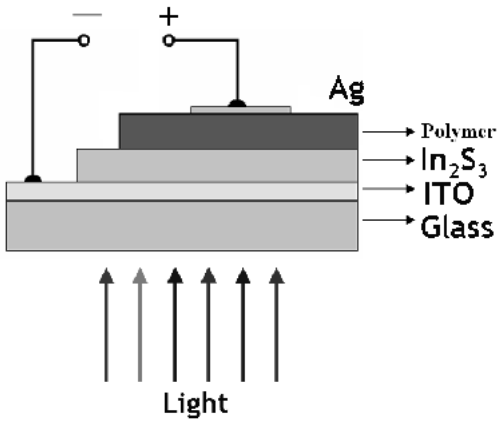

Figure 13: Schematic diagram of In_2S_3/Polymer heterojunction

2.6. References

1. Steckler, T. T.; Zhang, X.; Hwang, J.; Honeyager, R.; Ohira, S.; Zhang, X.-H.; Grant, A.; Ellinger, S.; Odom, S. A.; Sweat, D.; Tanner, D. B.; Rinzler, A. G.; Barlow, S.; Bredas, J. L.; Kippelen, B.; Marder, S. R.; Reynolds, J. R. *J. Am. Chem. Soc*., **2009**, 131, 2824.
2. Beaujuge, P. M.; Ellinger, S.; Reynolds, J. R. *Nature Mater*., **2008**, 7, 795.
3. Jhong, S. W.; Yen, J. C.; Martin, D.; Chao, H. H.; Chin, Y. C.; Chain, S. H.; *Chem. Commun*., **2010**, 46, 3259.
4. Merve, C.; Melek, P.; Fatih, A.; Ahmet, M. O.; Atilla, C., *Chem. Mater*., **2010**, 22, 4034.
5. Hwang, D. H.; Kim, S. K.; Park, M.J.; Lee, J.H.; Koo, B.W.; Kang, I. N.; Kim, S. H.; Zyung, T., *Chem. Mater*., **2004**, 16, 1298.
6. Cho, N. S.; Park, J. H.; Lee, S. K.; Lee, J.; Shim, H. K.; Park, M. J.; Hwang, D. H.; Jung, B. J., *Macromolecules*, **2006**, 39, 177.
7. Lai, R. Y.; Kong, X.; Jenekhe, S. A.; Bard, A. J., *J. Am. Chem. Soc.*, **2003**, 125, 12631.

8. Sun, D.; Rosokha, S. V.; Koich, J. K., *J. Am. Chem. Soc.*, **2004**, 126, 1388.

9. Wu, T. Y.; Chen, Y., *J. Polym. Sci. A: Polym. Chem.*, **2002**, 40, 4452.

10. Kim, S. K.; Lee, J. H.; Hwang, D. H., *Synth. Met.*, **2005**, 152, 201.

11. Moo, J. P.; Jonghee, L.; Jong, H. P.; Sang, K. L.; Jeong, I. L.; Hye, Y. C.; Do, H. H.; Hong, K. S., *Macromolecules*, **2008**, 41, 3063.

12. Fernando, F.; Samson, A. J.; Allen, J. B., *Chem. Mater*., **2003**, 15, 1264.

13. Samson, A. J.; Liangde. Lu.; Maksudul M. A., *Macromolecules*, **2001**, 34, 7315.

14. Kong, X.; Kulkarni, A. P.; Jenekhe, S. A. *Macromolecules*, **2003**, 36, 8992.

15. Brabec, C. J.; Winder, C.; Sariciftci, N. S.; Hummelen, J. C.; Dhanabalan, A.; van Hal, P. A.; Janssen, R. A. J., *Adv. Funct. Mater*., **2002**, 12, 709.

16. Zhou, Q.; Hou, Q.; Zheng, L.; Deng, X.; Yu, G.; Cao, Y., *Appl. Phys. Lett*., **2004**, 84, 1653.

17. Wang, E.; Wang, L.; lan, L.; Luo, C.; Zhuang, W.; Peng, J.; Cao, Y., *Appl. Phys. Lett*., **2008**, 92, 033307.

18. Lu, J.; Liang, F.; Drolet, N.; Ding, J.; Tao, Y.; Movileanu, R. *Chem. Commun*., **2008**, 5315.

19. Muhlbacher, D.; Scharber, M.; Morana, M.; Zhu, Z.; Waller, D.; Gaudiana, R.; Brabec, C., *Adv. Mater.*, **2006**, 18, 2884.

20. Lai, S. L.; Chan, M. Y.; Lee, C. S.; Lee, S. T., *J. Appl. Phys*., **2003**, 94, 7297.

21. Frederik C. K.; Suren, A. G.; Jan, A., *J. Mater. Chem*., **2009**, 19, 5442.

22. Teny, T. J.; Meril M. C.; Kartha, C. S.; Vijayakumar, K. P.; Abe, T.; Kashiwaba, Y., *Sol. Energy Mater. Sol. Cells*, **2005**, 89, 27.

23. Parr, R. G.; Yang, W., *Density-Functional Theory of Atoms and Molecules;* Oxford University Press, **1989**, New York.

24. Becke, A. D., *J. Chem. Phys.*, **1993**, 98, 5648.

25. Lee, Yang, W.; Parr, R. G., *Phys. Rev. B.*, **1994**, 37, 785.

26. Stephens, P. J.; Devlin, F. J.; Chabalowski, C. F.; Frisch, M. J., *J. Phys. Chem.*, **1994**, 98, 11623.

27. Hay P. J.; Wadt, W. R. *J. Chem. Phys.*, **1985**, 82, 270.

28. Frisch, M. J.; Trucks, G. W.; Schlegel, H. B.; Scuseria, G. E.; Robb, M. A.; Cheeseman, JR, *et al.*, Gaussian 03, revision E.01. Pittsburgh, PA: Gaussian, Inc, **2003**.

29. Noel O'Boyle M, Vos Johannes G. GAUSSSUM 2.2. Dublin City University, **2010**. Available from: <http://gausssum.sourceforge.net>.

30. Xiangxing Kong, Abhishek, P. K.; and Samson, A. J., *Macromolecules*, **2003**, 36, 8992.

31. Kramer, C. S.; Zeitler, K.; Muller, T. J. J., *Tetrahedron Lett.*, **2001**, 42, 8619.

32. Pilgram, K.; Zupan, M.; Skiles, R. *J. Heterocycl. Chem.*, **1970**, 7, 629.

33. Isao, Y.; Choi, B.J.; Koizumi, T.; Kubota, K.; Yamamoto, T., *Macromolecules*, **2007**, 40, 438.

34. Guangyi, S.; Yingping, Z.; Yongfang, L., *J. Phys. Chem. C.*, **2008**, 112, 12058.

Chapter 3

EFFECT OF STRUCTURAL CHANGES OF QUINOXALINE DERIVATIVES ON THE BAND GAP OF PHENOTHIAZINE/ QUINOXALINE COPOLYMERS

Contents

In this chapter, the effects of structural changes of the quinoxaline derivatives on the band gap of phenothiazine/quinoxaline polymers are discussed. The electronic structure of three phenothiazine/quinoxaline copolymers with acenaphthylene, phenyl and phenanthrene substituted quinoxalines were investigated. Theoretical calculations showed that the band gap varied with the acceptor strength of quinoxaline part. The band gap varied in the order PPHENO-DBDP< PPHENO-DDQ< PPHENO-DDACE. The three polymers were synthesized through Suzuki polycondensation reaction using Pd(0) catalyst. The polymers were characterized using ^1H NMR, GPC, cyclic voltammtery etc. The experimental results support the theoretical prediction. The photovoltaic activity of the polymer was also tested using the ITO/In_2S_3/polymer/Ag heterojunction. The heterojunctions with PPHENO-DDACE, PPHENO-DDQ and PPHENO-DBDP showed efficiencies of 0.02%, 0.01%, and 0.02% respectively.

3.1. Introduction

Quinoxaline is an n-type building block in semiconducting polymers and this N-heterocycle has been utilized to construct large number of donor-acceptor polymers in photovoltaic devices, with typical donor-acceptor structure. The π-conjugated heterocyclic polymers of

poly(quinoxaline) derivatives has been explored as electron transporting or electron accepting materials because of their high electron affinity due to the two symmetric unsaturated nitrogen atoms in quinoxaline[1-5]. Quinoxaline-containing segments were shown to be promising acceptors when combined with fluorene or thiophene forming D-A polymers[6-8]. The impressive performance of quinoxaline-based polymers has shown its obvious potential for achieving high performance in PSCs[9-11].

In this chapter, we discuss the effect of structural change in the quinoxaline unit on the band gap and energy levels of alternating copolymer of phenothiazine with acenaphthylene, phenyl and phenanthrene substituted quinoxalines. The electronic properties are calculated using density functional theory to get more insight into the structure-property correlation. Synthesis, optical and electrochemical properties of the copolymers were also studied. Suitability of the polymers for photovoltaic application was explored by fabricating a linear hetrojunction device using In_2S_3 as n-type material.

3.2. Results and Discussion

3.2.1. Theoretical Calculation

3.2.1.1. Theoretical Methodology

The ground state geometries of oligomers were optimized by means of the hybrid density functional theory (DFT)[12] at the HSEh1PBE referred to as HSE06 in the literature (full Heyd-Scuseria-Ernzerhof functional)[13,14], level of theory using 6-31G basis set. The harmonic vibrational frequencies obtained with HSE06/6-31G were used to characterize the stationary points as local minima. The band structure was calculated using HSE06/6-31G theory using the unit cell taken from the central portion of the optimized

tetramer. The calculation described in this chapter was done using G09 suite of codes[15] on IBM power servers.

3.2.1.2. Model compounds

In order to investigate the effect of structural change of the quinoxaline derivatives on the band gap of phenothiazine/quinoxaline copolymers, we start the calculation from model compounds (figure 1). The HOMO and LUMO levels are calculated using HSE06/6-31G method. From the energy level diagram, it is noted that the LUMO level of DDACE, DDQ and DBDP occurs at -2.26 eV, -2.36 eV and -2.56 eV. Thus, the acceptor strength is in the order DDACE< DDQ< DBDP. As expected, the energy gap of the model compounds PT-DDACE, PT-DDQ and PT-DBDP are in the order, PT-DDACE> PT-DDQ> PT-DBDP, as a function of acceptor strength (figure 2). The reduction in the energy gap of the D-A monomer is due to the charge transfer from donor phenothiazine unit to the acceptor quinoxaline. This can be visualized from the frontier orbital distribution of the model compounds (figure 3).

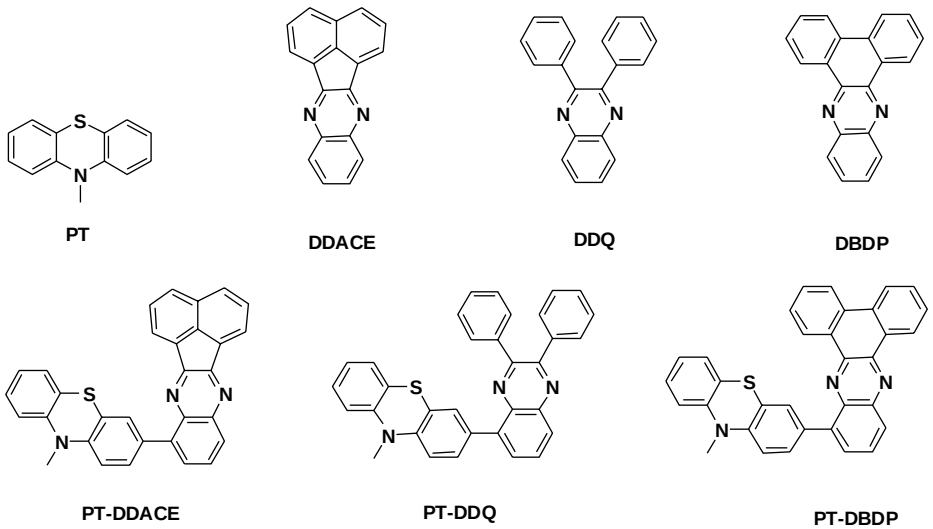

Figure 1: Structure of model compounds

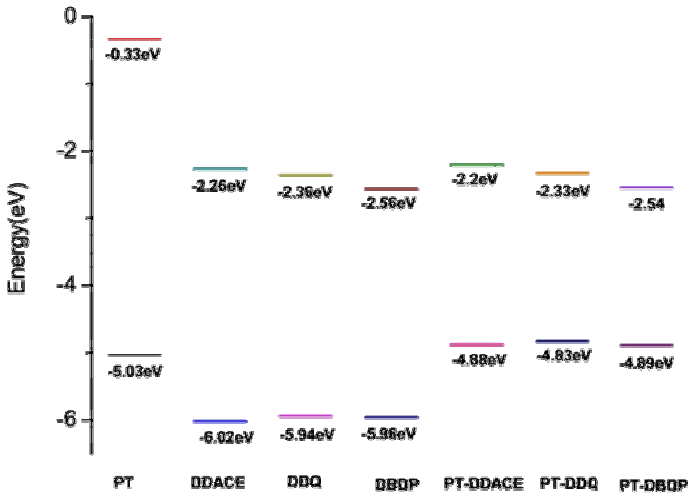

Figure 2: Energy levels of PT, DDACE, DDQ, DBDP, PT-DDACE, PT-DDQ and PT-DBDP

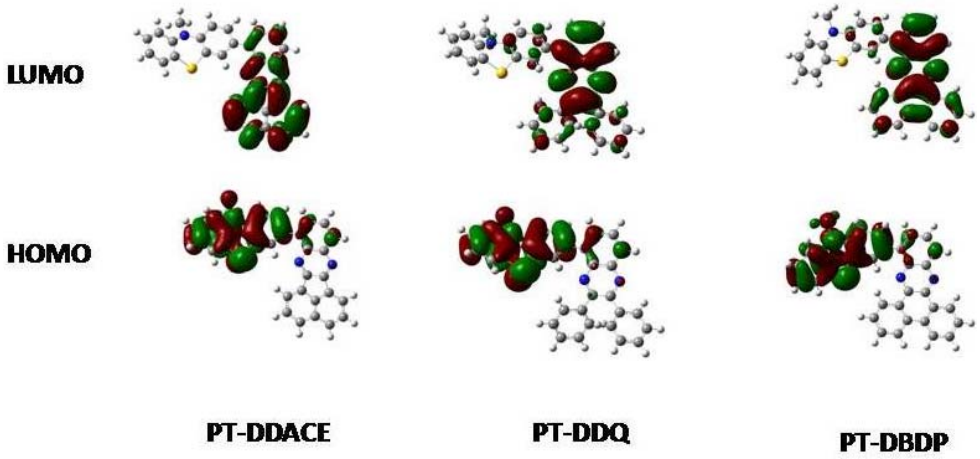

Figure 3: Frontier molecular orbital distribution plots of model compounds

3.2.1.3. Band structure of polymers

Optimized unit cells for the periodic boundary calculation are shown in figure 4. The length of the translational vector is 25 A^0. The band structure of the polymers PPHENO-DADCE, PPHENO-DDQ and PPHENO-DBDP is shown in figure 5. It can be noted from the band structure that all the polymers are direct band gap polymers, because the lowest band gap occurs at k=0. It could be seen from the band structure that LUMO level of the

poly(phenothiazine) is reduced by 0.84 eV, 0.97 eV and 1.32 eV respectively by introducing DDACE, DDQ and DBDP units to the phenothiazine chain. The band gaps of PPHENO-DDACE, PPHENO-DDQ and PPHENO-DBDP are 2.38 eV, 2.3 eV and 2.0 eV respectively. The band structure data of the polymers are summarized in table 1.

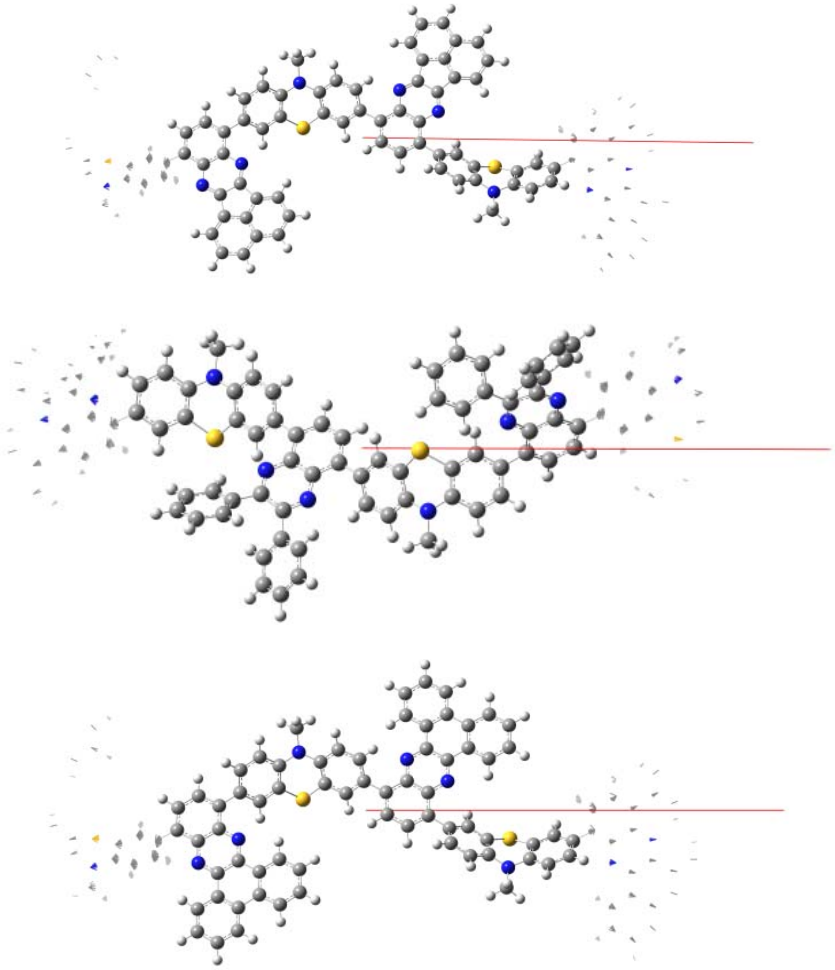

Figure 4: Unit cell for the band structure calculation of PPHENO-DDACE, PPHENO-DDQ, and PPHENO-DBDP

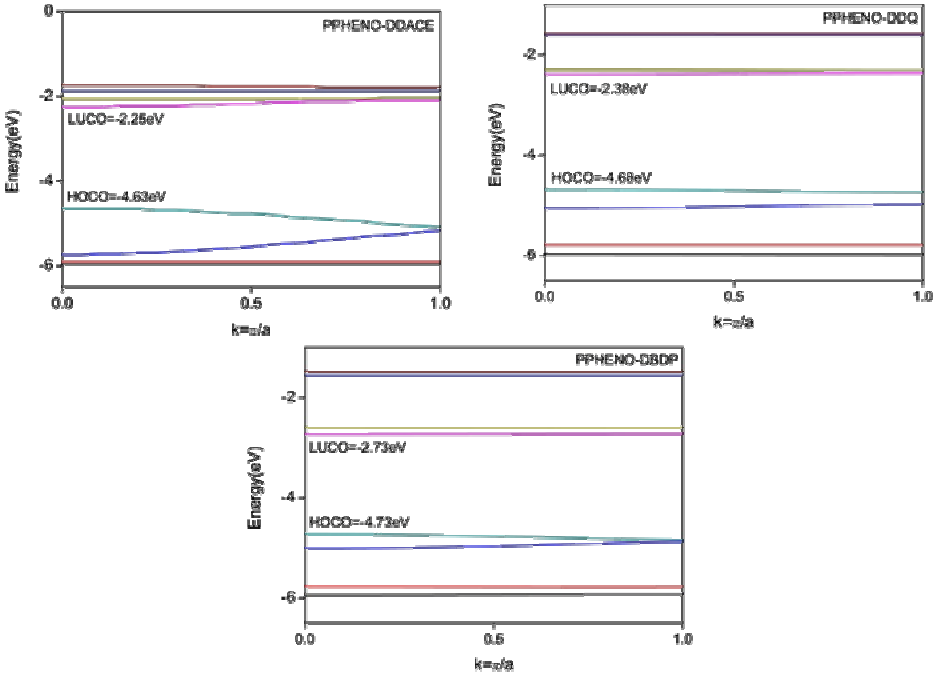

Figure 5: Band structure of PPHENO-DDACE, PPHENO-DDQ, and PPHENO-DBDP

Table 1: Band structure data# of PPHENO-DDACE, PPHENO-DDQ, PPHENO-DBDP

Polymer	HOCO (eV)	LUCO (eV)	E_g (eV)
PPHENO	-4.76	-1.41	3.36
PPHENO-DDACE	-4.63	-2.25	2.38
PPHENO-DDQ	-4.68	-2.38	2.3
PPHENO-DBDP	-4.73	-2.73	2.0

Method HSE06/6-31G

3.2.2. Synthesis and characterization of monomers and polymers

3.2.2.1. Monomer synthesis

The scheme for the synthesis of diboronate ester of phenothiazine has been depicted in chapter II. The synthetic route for the preparation of acenaphthylene, phenyl and phenanthrene substituted quinoxalines are shown in scheme 1. 5,8-Dibromo-acenaphthyl quinoxaline (DDACE), 5,8-

dibromo-2,3-diphenylquinoxaline (DDQ) , 10,13 -dibromodibenzo[a,c] phenazine (DBDP) were synthesized through condensation reaction[16] of 1,2-dibromo-3,4-phenylenediamine with 1,2-acenaphthaquinone, benzil and 9,10-phenanthrenequinone in ethanol/acetic acid, in 79%, 70% and 80% yields. The compounds were characterized using ^{1}H NMR, and ^{13}C NMR spectroscopy and melting point measurement.

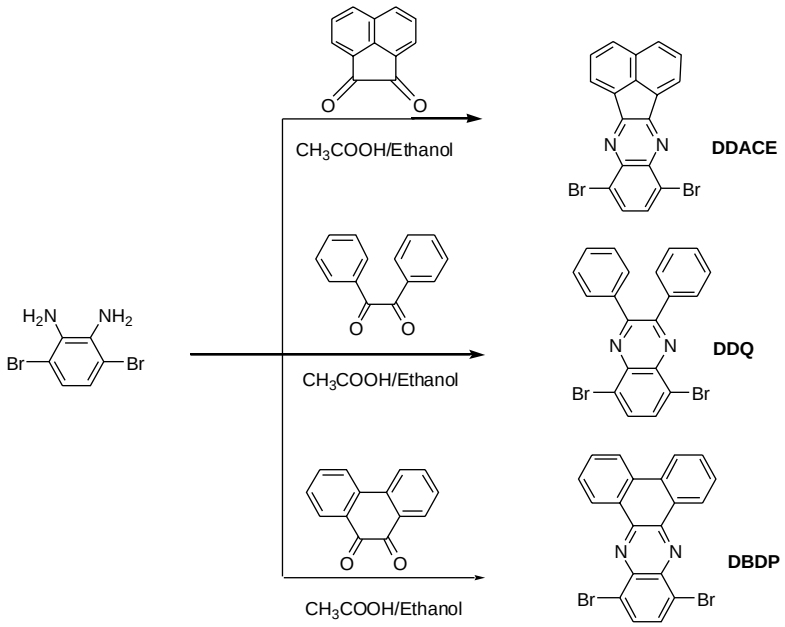

Scheme 1: Synthesis of monomers DDACE, DDQ and DBDP

3.2.2.2. Polymer synthesis

The polymers were synthesized through typical Suzuki polycondensation reaction between diboronate ester of phenothiazine and DDACE, DDQ and DBDP, which gave PPHENO-DDACE, PPHENO-DDQ and PPHENO-DBDP in 37%, 51% and 46% yields (scheme 2). The polymers are endcapped with phenyl group by quenching the reaction with phenyl boronic acid and bromobenzene. All the polymers are soluble in THF, chloroform, chlorobenzene, toluene etc. The polymerization results and molecular weight data of the polymers are summarized in table 2. All

the polymers were characterized using UV-Visible spectroscopy, ^{1}H NMR, cyclic voltammetry etc. The thermal properties of the polymers were investigated by thermogravimetric analysis. All the polymers showed thermal decomposition under nitrogen in the range of 250-295^{o}C (table 2). The ^{1}H NMR spectra of the polymers are shown in figure 6. It could be seen that aromatic region is highly populated and all the polymers showed triplet in the region δ 3.8-3.9 due to –NCH_2- protons. PPHENO-DDACE and PPHENO-DBDP show peaks in the region δ 2-2.2, which may be due incomplete capping of the polymers using phenyl boronic acid and bromobenzene.

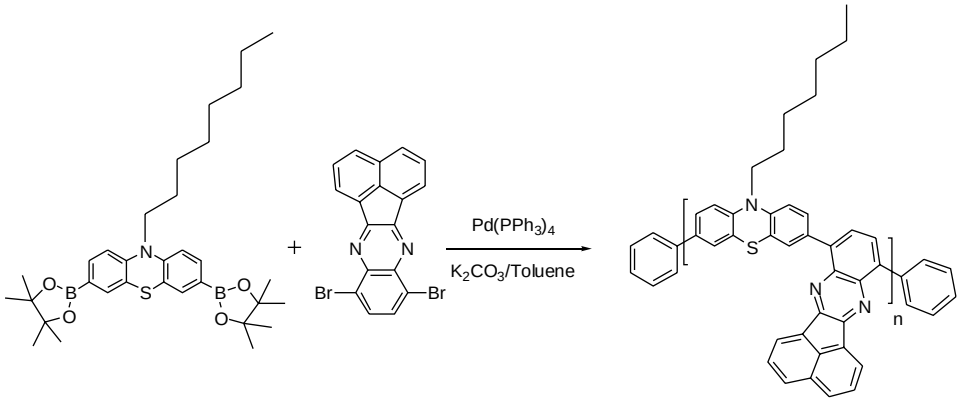

DDACE **PPHENO-DDACE**

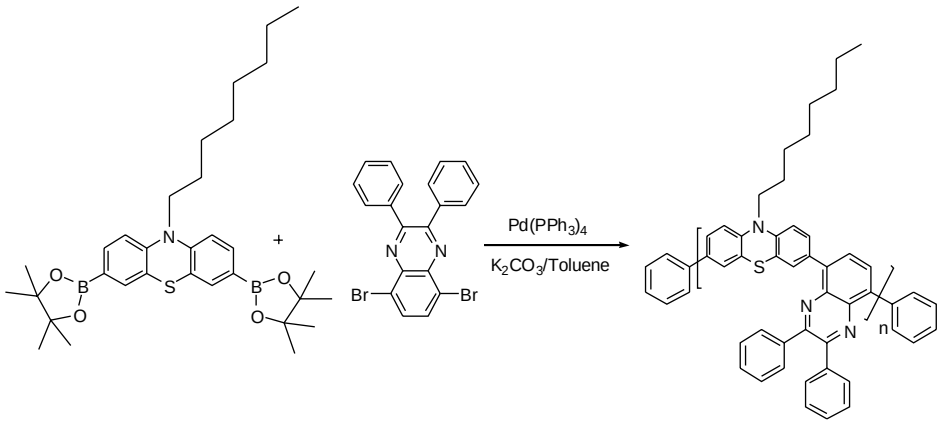

DDQ **PPHENO-DDQ**

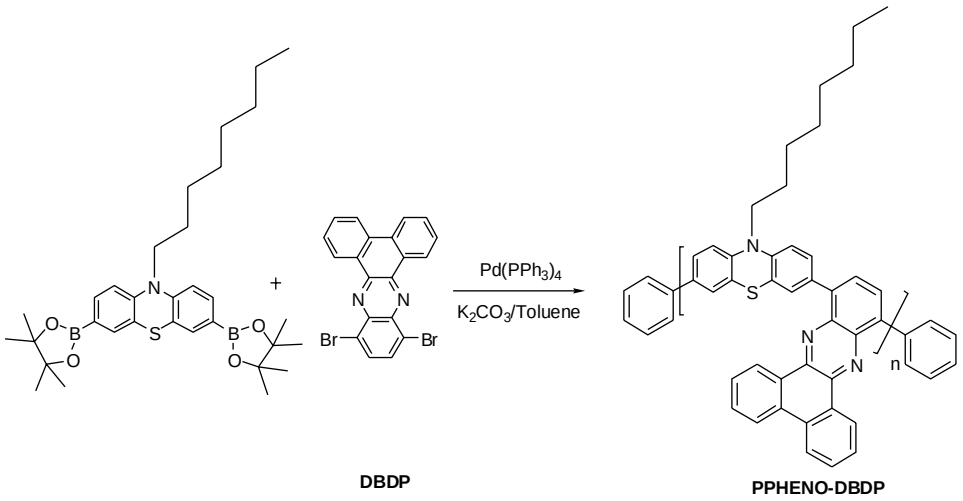

Scheme 2: Synthesis of polymers PPHENO-DDACE, PPHENO-DDQ and PPHENO-DBDP

Table 2: Results of polymerization and thermal stability of polymers

Polymer	M_n[a]	M_w[a]	PDI	Yield (%)	T_d (^{0}C)[b]
PPHENO-DDACE	4248	7541	1.77	37	257
PPHENO-DDQ	9578	18427	1.92	51	270
PPHENO-DBDP	5905	7078	1.19	46	295

a. Determined using GPC in toluene based on polystyrene standard. b. Onset of decomposition measured by TGA under nitrogen

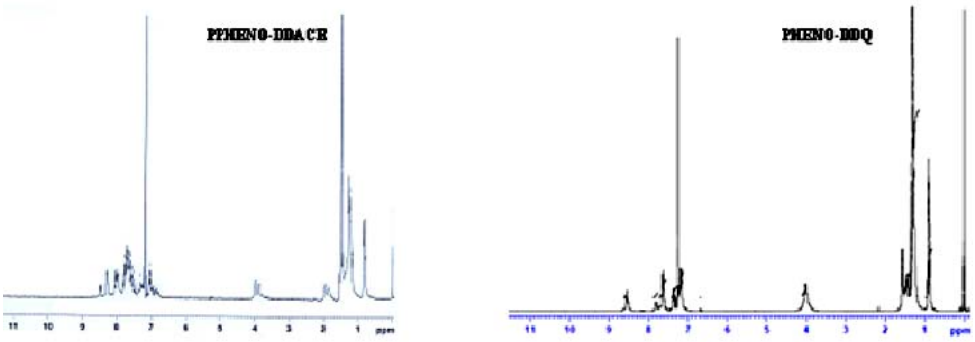

a. b.

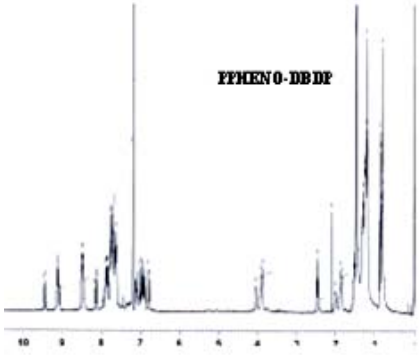

c.

Figure 6: ^{1}H NMR spectrum of a. PPHENO-DDACE, b. PPHENO-DDQ, and c. PPHENO-DBDP

3.2.3. Optical properties

Figure 7a shows the absorption spectrum of polymers in chloroform as the solvent along with the photograph of polymer solution. It can be seen that with polymers based on the strong acceptor, ie DBDP, brown colour is achieved due to the red shifted absorbance in solution. The absorption maximum of PPHENO-DDACE, PPHENO-DDQ and PPHENO-DBDP occur at 439 nm, 450 nm and 477 nm. To optically evaluate the magnitude of the band gap, the thin film absorbance is measured as shown in figure 7b for spin cast film from chlorobenzene solution on to glass substrates. The absorption maximum in thin film is slightly red shifted than in solution. This may be due to the slight increase in the coplanarity of the polymer chain in the solid state. It is observed that the band gap ranges from 1.92-2.24 eV. The band gap is less than the band gap of the homopolymer poly(phenothiazine). This is due to the orbital mixing of phenothiazine donor unit and quinoxaline acceptor unit. The variation in the band gap is in the order PPHENO-DDACE> PPHENO-DDQ> PPHENO-DBDP. As expected, the optical band gap varies as the function of the electron withdrawing property of the comonomers. It is assumed that greater the acceptor strength of the quinoxaline, greater will be the donor –

acceptor interaction, which leads to greater reduction in the band gap. The reduction in the band gap is induced by the charge transfer from phenothiazine unit to the quinoxaline unit. This is visualized by analyzing the wave functions of the HOCO and LUCO of the polymers. The wave functions of HOCO and LUCO are localized on the phenothiazine and quinoxaline unit respectively.

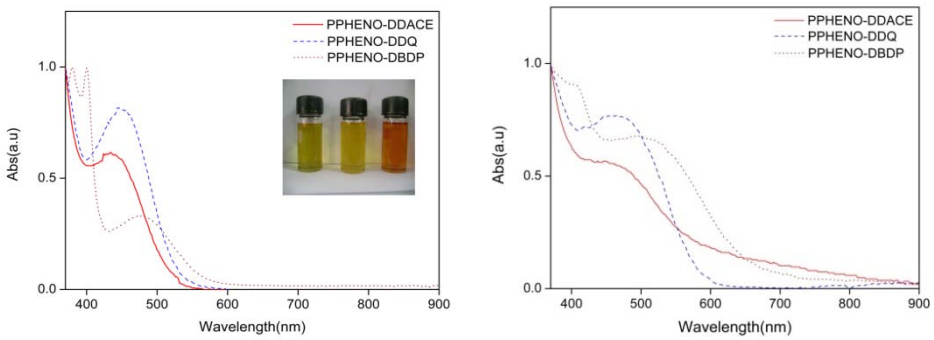

Figure 7: UV-Visible absorption spectrum of polymers in (a). chloroform (b) thin film on glass substrate cast from chlorobenzene solution

The photoluminescence spectrum of the polymers is shown in figure 8. The wavelength corresponding to the absorption maximum of each polymer is used as excitation wavelength. The emission maximum of the PPHENO-DDACE, PPHENO-DDQ and PPHENO-DBDP occur at 657 nm, 652 nm and 687 nm respectively.

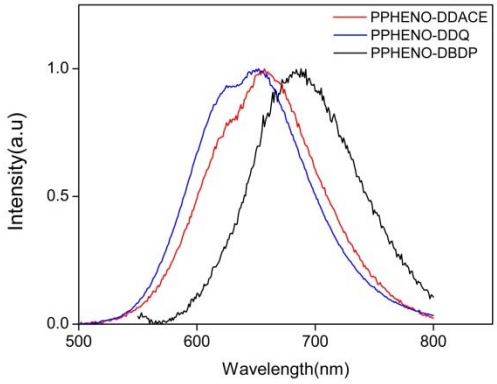

Figure 8: PL spectra of polymers in chloroform solution

Table 3: Optical properties of the polymers in solution and in thin film on glass substrate

Polymer	UV-Visible Absorption λ_{max}(nm)		Emission λ_{max} (nm) (solution)	UV-Visible Absorption Onset (film)	E_g^{opt} (eV)
	Solution	Film			
PHENO-DDACE	439	454	657	555	2.24
PHENO-DDQ	450	467	652	590	2.11
PHENO-DBDP	477	500	687	646	1.92

3.2.4. Electrochemical properties

To determine the highest occupied molecular orbital (HOMO) and lowest unoccupied molecular orbital (LUMO) level of the three polymers, cyclic voltammetry was carried out for the three polymer films on Pt electrode in 0.1M Bu_4NPF_6 solution in acetonitrile. The cyclic voltammograms of the polymers are shown in figure 9. All the three polymers showed a couple of irreversible oxidation peaks in the positive potential region and a reversible reduction peak in the negative potential. The HOMO and LUMO were estimated from the onset of oxidation and reduction potential according to the equation proposed by Bredas[17]. The onset of oxidation and reduction potentials for the three polymers obtained from cyclic voltammetry are summarized in Table 4. The HOMO energy of PPHENO-DDACE, PPHENO-DDQ, and PPHENO-DBDP possess almost the same value of -5.08 eV, while the LUMO value varied in proportion to the acceptor strength of the quinoxaline. The acceptor strength of the quinoxaline calculated theoretically varied in the order DBDP> DDQ> DDACE. So the energy gap of the polymers varies in the order PPHENO-DBDP< PPHENO-DDQ< PPHENO-DDACE. The same observation was also ascertained by the periodic boundary calculation on the polymers using HSE06/6-31G method.

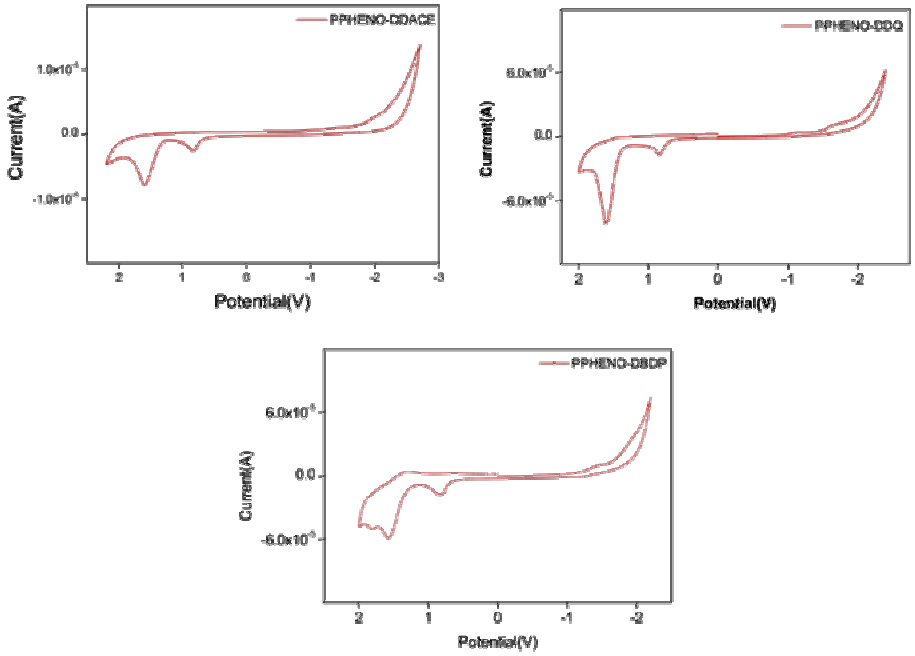

Figure 9: CV curves of PHENO-BTZ and PHENO-BSE film on Pt electrode in 0.1M Bu_4NPF_6 solution in acetonitrile at a scan rate of 100 mV/sec

Table 4: Electrochemical properties of the polymers

Polymer	E_{ox} (V)	E_{red} (V)	HOMO (eV)	LUMO (eV)	E_g (eV)
PPHENO-DDACE	0.682	-1.846	-5.082	-2.55	2.53
PPHENO-DDQ	0.687	-1.495	-5.087	-2.905	2.18
PPHENO-DBDP	0.689	-1.256	-5.089	-3.144	1.95

3.2.5. Photovoltaic device

The suitability of the polymers for photovoltaic applications was verified by fabricating a heterojunction device using the polymers as active layer and the semiconductor In_2S_3 as n-type material. Figure 10 shows the current density-voltage (J-V) characteristics of the heterojunction under illumination and in the dark. As could be seen, the device clearly exhibits rectifying behaviour in the dark which may be due to the barrier formed at the In_2S_3/ polymer interface. Under white light illumination (50 mW/cm^2), the device of PPHENO-DDACE, PPHENO-DDQ, and PPHNEO-DBDP

exhibits a short circuit current density (J_{sc}) of 54.1 µA/cm^2, 80.4 µA/cm^2, 61.7 µA/cm^2 and open circuit voltage (V_{oc}) of 477.42 mV, 169.93mV, and 610.51 mV respectively. The fill factor (FF) /efficiency were calculated to be 19.95%/0.02%, 28.19%/0.01and 28.27%/0.02% respectively for PPHENO-DDACE, PPHENO-DDQ, and PPHNEO-DBDP. Photovoltaic characteristics of bilayer heterojunction devices of the polymers are summarized in table 5.

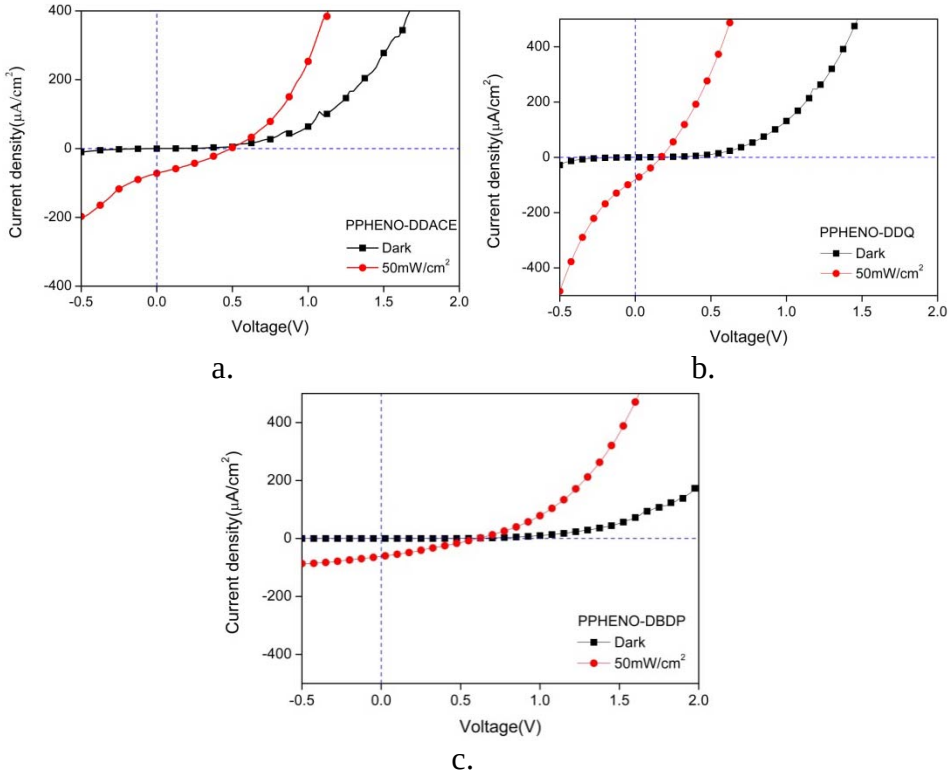

Figure 10: J-V characteristics of ITO/In_2S_3/polymer/Ag heterojunctions of PPHENO-DDACE, b. PPHENO-DDQ, and c. PPHENO-DBDP

Table 5: J-V characteristics of ITO/In_2S_3/polymer/Ag heterojunctions

Polymer	V_{oc} (mV)	J_{sc} (μA/cm^2)	Efficiency (%)	Fill factor (%)
PPHENO-DDACE	477.42	54.1	0.02	19.95
PPHENO-DDQ	169.93	80.4	0.01	28.19
PPHENO-DBDP	610.51	61.7	0.02	28.27

3.3. Conclusion and perspectives

Theoretical calculation predicted that structural modification of quinoxaline unit allowed successful tuning of the band gap and energy level of the phenothiazine copolymer over a broad range from 2.38 eV to 1.93 eV. The reduction in the energy level is the function of the acceptor strength of the quinoxaline unit. The lower band gap of phenothiazine/quinoxaline copolymers compared to homopolymer poly(phenothiazine) may be due to the charge transfer from donor phenothiazine unit to the acceptor quinoxaline unit. The designed polymers are synthesized through Suzuki polycondensation reaction. Theoretically predicted values are in good agreement with the optically and electrochemically determined band gap. We have explored the photoactivity of all the polymers by fabricating a heterojunction with a device structure of ITO/In_2S_3/polymer/Ag. A further improvement in the device can be achieved by optimizing the device parameters.

3.4. Experimental methods

3.4.1. Synthesis of 5,8-dibromoacenaphthyl quinoxaline (DDACE):

A solution of 3,6-dibromo-1, 2-phenylenediamine (0.15 g, 0.56 mmol) and acenaphthenequinone (0.10 g, 0.55 mmol) in ethanol (20 mL) and few drops of glacial acetic acid was heated to reflux for 1h, and cooled to 0^{o}C. The precipitate formed was separated by filtration and washed with ethanol to afford 5,8-dibromoacenaphthyl quinoxaline as light yellow solid.

Yield : 79% (0.183 g)

^{1}H NMR (400MHz, $CDCl_3$) : δ 8.54 (d, *J*=7.2 Hz, 2H), 8.15 (d, *J*=8.4 Hz, 2H), 7.92 (s, 2H), 7.89-7.86 (m, 2H)

3.4.2. Synthesis of 5,8-Dibromo-2,3-diphenyl quinoxaline (DDQ):

A solution of 3,6-dibromo-1, 2-phenylenediamine (1.0 g, 3.8 mmol) and benzil (0.80 g, 3.8 mmol) in ethanol (40 mL) and few drops of glacial acetic acid was heated to reflux for 1h, and cooled to 0^{o}C. The

precipitate formed was isolated by filtration and washed with ethanol to afford 5,8-dibromo-2,3-diphenyl quinoxaline as light yellow solid.

Yield	:	1.16 g (70%)
M. P.	:	221^{o}C.
^{1}H NMR (400MHz, $CDCl_3$)	:	δ 7.92 (s, 2H), 7.64 (m, 4H), 7.37 (m, 6 H).
^{13}C NMR (100MHz, $CDCl_3$)	:	δ 123.7, 128.4, 129.6, 130.2, 133.1, 137.9, 139.4, 154.14
GC-MS	:	m/z=439.9

3.4.3. Synthesis of 10,13-dibromodibenzo[a,c]phenazine (DBDP):

A solution of 3,**6**-dibromo-1,2-phenylenediamine (1.03 g, 3.9 mmol) and phenanthrene-9,10-dione (0.81 g, 3.9 mmol) in 42 mL ethanol/ acetic acid (20:1) was heated to reflux for 2 h, and cooled to 0^{o}C. The precipitate formed was isolated by filtration and washed with ethanol to afford 10,13-dibromodibenzo[a,c]phenazine as yellow solid.

Yield	:	1.37 g (80%).
M.P. (^{0}C)	:	317
^{1}H NMR (400 MHz, $CDCl_3$)	:	δ 9.48 (dd, J_1=8 Hz, J_2=1.2 Hz, 2 H), 8.57 (dd, J_1=8 Hz, J_2=0.8 Hz, 2 H), 8.04 (s, 2H), 7.87-7.83 (dt, J_1=15.2 Hz, J_2=1.6 Hz, 2 H), 7.81-7.77 (dt, J_1=13.2 Hz, J_2=1.2 Hz, 2 H).
^{13}C NMR (100MHz, $CDCl_3$)	:	δ123.1, 124.2, 127.3, 128.4, 129.6, 131.3, 132.7, 132.9, 143.5.
GC-MS	:	m/z=437.9

3.4.4. General Procedure for Polymerization through Suzuki Coupling

Under nitrogen atmosphere, dibromo monomers (0.18 mmol), 10-octyl-3,7-bis(4,4,5,5-tetramethyl[1,3,2]dioxaborolan-2-yl)-10H-phenothiazine (0.18 mmol) were mixed together with 10 mol% of $Pd(PPh_3)_4$ (0.018 mmol) in a small R. B. flask. Degassed aqueous solution of 2.0 M potassium carbonate (10 mL) and toluene (20 mL) (1:2, volume ratio) were added to the flask. The mixture was stirred vigorously at 80-90°C for 72 h under nitrogen atmosphere. The resulting solution was added drop wise into stirring methanol to precipitate the polymer. The fibrous solid was collected by filtration and washed with methanol and water. The product was washed continuously with methanol and acetone for 2 days in a Soxhlet extractor to remove the oligomers and catalyst residues. The product was dried under reduced pressure.

3.4.4.1. Synthesis of PPHENO-DDACE

10-octyl-3,7-bis(4,4,5,5-tetramethyl[1,3,2]dioxaborolan-2-yl)-10H phenothiazine (0.1 g, 0.18 mmol), 5,8-dibromoacenaphthyl quinoxaline (0.078 g, 0.18 mmol), $Pd(PPh_3)_4$ (0.02 g, 0.018 mmol) were used. Red coloured solid.

Yield	:	37% (36.8 mg)
UV/Vis ($CHCl_3$) λ_{max}	:	439 nm
T_d (^0C)	:	257
^1H NMR (400 MHz, $CDCl_3$)	:	8.4-7.55 (m, ~8H of quinoxaline part), 7.38-7.3 (m, 2H of phenothiazine), 7.13-7.08 (m, 2H of phenothiazine), 6.96-6.8 (m, 2H of phenothiazine), 3.89 (t, ~2H, -NCH_2-), 1.8-1.1-1.9 (m, ~12H, aliphatic-H), 1.6-0.9 (m, ~3H, -CH_3)

GPC : M_n =4248, PDI=1.77

3.4.4.2. Synthesis of PPHENO-DDQ

10-octyl-3,7-bis(4,4,5,5-tetramethyl[1,3,2]dioxaborolan -2-yl) -10H-phenothiazine (0.1 g, 0.18 mmol), 5,8-Dibromo-2,3-diphenyl quinoxaline (0.079 g, 0.18 mmol), $Pd(PPh_3)_4$ (0.02 g, 0.018 mmol) were used. Red coloured solid.

Yield : 51 % (53.5 mg)

UV/Vis ($CHCl_3$) λ_{max} : 450 nm

T_d (^{0}C) : 270

^{1}H NMR (400 MHz, $CDCl_3$) : δ 8.03-7.52 (m, ~10H of quinoxaline part), 7.31-6.71 (m, ~6H of phenothiazine), 3.84 (t, 2H, -NCH_2-), 1.9-1.1 (m, ~12H, aliphatic-H), 0.86-0.8 (t, ~3H, -CH_3).

^{13}C NMR (100MHz, $CDCl_3$) : δ 137.49, 132.07, 131.98, 129.19, 129.1, 128.26, 127.34, 30.75, 28.21, 26.07, 25.94, 21.61, 13.08.

GPC : M_n=9578, PDI=1.92

3.4.4.3. Synthesis of PPHENO-DBDP:

10-octyl-3,7-bis(4,4,5,5-tetramethyl[1,3,2]dioxaborolan-2-yl)-10H-phenothiazine (0.1 g, 0.18 mmol), 10,13-Dibromodibenzo[a,c]phenazine (0.078 g, 0.18 mmol), $Pd(PPh_3)_4$ (0.02g, 0.018 mmol) were used. Red coloured solid.

Yield : 46% (47.8 mg)

UV/Vis ($CHCl_3$) λ_{max} : 477 nm

T_d (^{o}C) : 295

^{1}H NMR (400 MHz, $CDCl_3$)	:	δ 9.46- 7.76 (m, ~10H of quinoxaline part), 7.4-6.77 (m, ~6H of phenothiazine), 3.9 (t, 2H, -NCH_2-), 1.18-2.1 (m, ~12 H, aliphatic-H), 0.86-0.79 (m, ~3H, -CH_3).
GPC	:	M_n =5905, PDI=1.19

3.5. References

1. Yamamoto, T.; Zhou, Z. H.; Kanbara, T.; Shimura, M.; Kizu, K.; Maruyama, T.; Nakamura, Y.; Fukuda, T.; Kaino, T.; Kubota, K.; Sasaki, S. *J. Am. Chem. Soc.*, **1996**, 118, 10389.
2. Aldakov, D.; Palacios, M. A. Jr. *Chem. Mater*., **2005**, 17, 5238.
3. Tsami, A.; Bunnagel, T. W.; Farrell, T.; Scharber, M.; Choulis, S. A.; Brabec, C. J.; Scherf, U. *J. Mater. Chem.*, **2007**, 17, 1353.
4. Mammo, W.; Admassie, S.; Gadisa, A.; Zhang, F. L.; Inganas, O.; Andersson, M. R. *Solar Energy Materials Solar Cells*, **2007**, 91, 1010.
5. Huo, L. J.; Tan, Z. A.; Zhou, Y.; Zhou, E. J.; Han, M. F.; Li, Y. F. *Macromol. Chem. Phys.*, **2007**, 208, 1294.
6. Gadisa, A.; Mammo, W.; Andersson, L. M.; Admassie, S.; Zhang, F.; Andersson, M. R.; Ingan, O. *Adv. Funct. Mater*., **2007**, 17, 3836.
7. Lindgren, L. J.; Zhang, F. L.; Andersson, M.; Barrau, S.; Hellstrom, S.; Mammo, W.; Perzon, E.; Ingan€as, O.; Andersson, M. R. *Chem. Mater*., **2009**, 21, 3491.
8. Wang, E. G.; Hou, L. T.; Wang, Z. Q.; Hellstrom, S.; Zhang, F. L.; Inganas, O.; Andersson, M. R. *Adv. Mater*., **2010**, 22, 5240.
9. Zhang, F. L.; Bijleveld, J.; Perzon, E.; Tvingstedt, K.; Barrau,S.; Inganas, O.; Andersson, M. R. *J. Mater. Chem*., **2008**, 18, 5468.
10. Zhou, E. J.; Cong, J. Z.; Tajima, K.; Hashimoto, K. *Chem. Mater*., **2010**, 22, 4890.

11. Kitazawa, D.; Watanabe, N.; Yamamoto, S.; Tsukamoto, *J. Appl. Phys. Lett*., **2009**, 95, 053701.
12. Parr, R. G.; Yang, W., *Density-Functional Theory of Atoms and Molecules;* Oxford University Press, **1989**, New York.
13. Heyd, J.; Scuseria, G. E.; Ernzerhof, M. *J. Chem. Phys.*, **2003**, 118, 8207.
14. Krukau, A. V.; Vydrov, O. A.; Izmaylov, A. F.; Scuseria, G. E. *J. Chem. Phys.*, **2006**, 125, 224106.
15. Gaussian 09, Revision B02, Frisch, M. J.; Trucks, G. W.; Schlegel, H. B.; Scuseria, G. E.; Robb, M. A.; Cheeseman, J. R.; Scalmani, G.; Barone, V.; Mennucci, B.; Petersson, G. A.; Nakatsuji, H.; Caricato, M.; Li, X.; Hratchian, H. P.; Izmaylov, A. F.; Bloino, J.; Zheng, G.; Sonnenberg, J. L.; Hada, M.; Ehara, M.; Toyota, K.; Fukuda, R.; Hasegawa, J.; Ishida, M.; Nakajima, T.; Honda, Y.; Kitao, O.; Nakai, H.; Vreven, T.; Montgomery, Jr., J. A.; Peralta, J. E.; Ogliaro, F.; Bearpark, M.; Heyd, J. J.; Brothers, E.; Kudin, K. N.; Staroverov, V. N.; Kobayashi, R.; Normand, J.; Raghavachari, K.; Rendell, A.; Burant, J. C.; Iyengar, S. S.; Tomasi, J.; Cossi, M.; Rega, N.; Millam, N. J.; Klene, M.; Knox, J. E.; Cross, J. B.; Bakken, V.; Adamo, C.; Jaramillo, J.; Gomperts, R.; Stratmann, R. E.; Yazyev, O.; Austin, A. J.; Cammi, R.; Pomelli, C.; Ochterski, J. W.; Martin, R. L.; Morokuma, K.; Zakrzewski, V. G.; Voth, G. A.; Salvador, P.; Dannenberg, J. J.; Dapprich, S.; Daniels, A. D.; Farkas, Ö.; Foresman, J. B.; Ortiz, J. V.; Cioslowski, J.; Fox, D. J. Gaussian, Inc., Wallingford CT, **2009**.
16. Younus, M.; Kohler, A. D.; Cron, S.;Chawdary, N.; Al Mandhary, M. R. A.; Khan, M.S.; Lewis, J.; Long, N. J.; Friend, R. H.; Raithby, P. R. *Angrew. Chem. Int. Ed.*, **1998**, 37, 3036.
17. Bredas, J. L.; Silbey, R.; Boudreux, D. X.; Chance, R. R., *J. Am. Chem. Soc*., **1983**, 105, 6555.

Chapter 4

SYNTHESIS OF 3,4-ALKYLENEDIOXYTHIOPHENE/PHENOTHIAZINE COPOLYMERS BY DIRECT ARYLATION REACTION: THEORY, CHARACTERIZATION AND PHOTOVOLTAIC APPLICATIONS

Contents

In this chapter, electronic structure calculation and synthesis of three copolymers of phenothiazine with 3,4-dimethoxythiophene, 3,4-ethylenedioxythiophene and 3,4-propylenedioxythiophene are described. The polymers were synthesized through direct arylation reaction. The superiority of direct arylation reaction over conventional Stille, Suzuki and Kumada reactions are also discussed. The polymers were characterized using ^1H NMR, GPC, cyclic voltammetry, differential pulse voltammetry etc. The experimental results could reproduce the theoretical energy gap of the polymers. The photovoltaic activity of the polymers was also tested using the ITO/In_2S_3/polymer/Ag heterojunction. The heterojunctions of PDMT-PHENO, PEDT-PHENO and PPRO-PHENO showed efficiency of 0.022%, 0.054% and 0.01% respectively.

4.1. Introduction

Conventionally, most of the π-conjugated polymers were synthesized by transition-metal catalyzed cross-coupling reactions such as Suzuki coupling[1-3], Stille coupling[4-6], Kumada reaction[7-10] etc. One limitation or inefficiency of the metal mediated cross-coupling reaction is the requirement for activating groups on both the arene partners. This pre-activation of both partners is inherently wasteful, since several steps can be

required for the installation of these activating groups. Although these methods are effective for the synthesis of large number of π-conjugated polymers, they require the tedious synthesis of bifunctional organoboron /organotin compounds/organo magenesium as monomers (scheme 1). Therefore, the development of a convenient, environmentally friendly and industrially accessable method for synthesizing π-conjugated polymers is highly desirable. In this direction, we have come across two reports on direct arylation of electron rich thiophenes[11,12]. Homopolymer of functionalized ProDOT prepared by direct arylation reaction catalysed by palladium acetate was reported recently[13]. In terms of the prior preparation of organometallic monomers and the treatment of toxic byproduct, polycondensation by direct arylation is superior to conventional methods based on a cross-coupling reaction (figure 1).

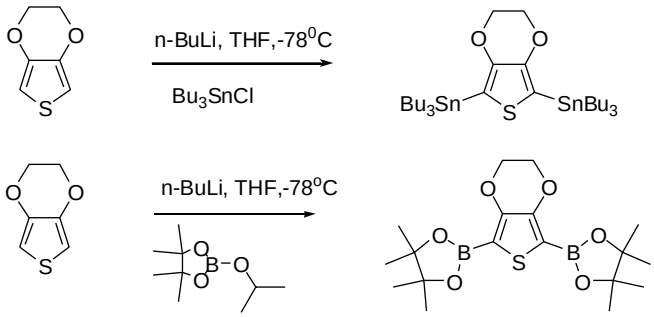

Scheme 1: Synthesis of distannane and diboronate esters of 3,4-ethylenedioxythiophene

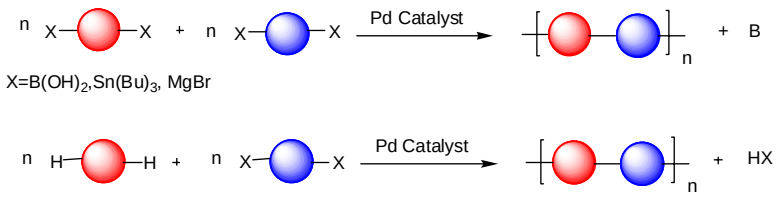

Figure 1: Schematic representation of polycondensation using conventional cross-coupling and direct arylation reaction

In this chapter, we have tried to calculate the electronic properties of the alternating copolymers of phenothiazine with 3,4-dimethoxythiophene, 3,4-ethylenedioxythiophene and 3,4-propylenedioxythiophene. The alkoxy group in the 3 and 4 position of the thiophene activates the C-H bond and is susceptible for direct arylation reaction with arylhalide. The synthesis of polymers through direct arylation reaction, optical and electrochemical properties of the polymers are investigated. We have also tried to explore the application of these polymers as active layer in photovoltaic devices.

4.2. Results and discussion

4.2.1. Theoretical calculation

The ground state geometries of oligomers were optimized by means of the hybrid density functional theory (DFT)[14] at the HSEh1PBE referred to as HSE06 in the literature (full Heyd-Scuseria-Ernzerhof functional)[15,16], level of theory using 6-31G basis set. The harmonic vibrational frequencies obtained with HSE06/6-31G were used to characterize the stationary points as local minima. The band structure is calculated using HSE06/6-31G theory using the unit cell taken from the central portion of the optimized tetramer. The calculation described in this chapter was done using G09 suite of codes[17] on IBM power servers.

The optimized geometry of the unit cell for the PBC/HSE06 calculation is given in figure 2. The length of the translational vector is optimized to be $23.6A^0$. The calculated band structure is shown in figure 3. It is noted from the figure that, in all the polymers, the lowest band gap occur at k=0 suggesting that all the polymers are direct band gap polymers. All the polymers show almost the same band gap of 2.5 eV, indicating that bridging and increasing the alkyl side chain have little effect on the band

gap. On examination of the HOCO and LUCO of the polymers, we can see that HOCO and LUCO wave function is distributed both in the phenothiazine and thiophene. This facilitates the overlap between the levels and enhanced absorption occur for the lowest optical transition. The band structure data of PDMT-PHENO, PEDT-PHENO and PPRO-PHENO are given in table 1.

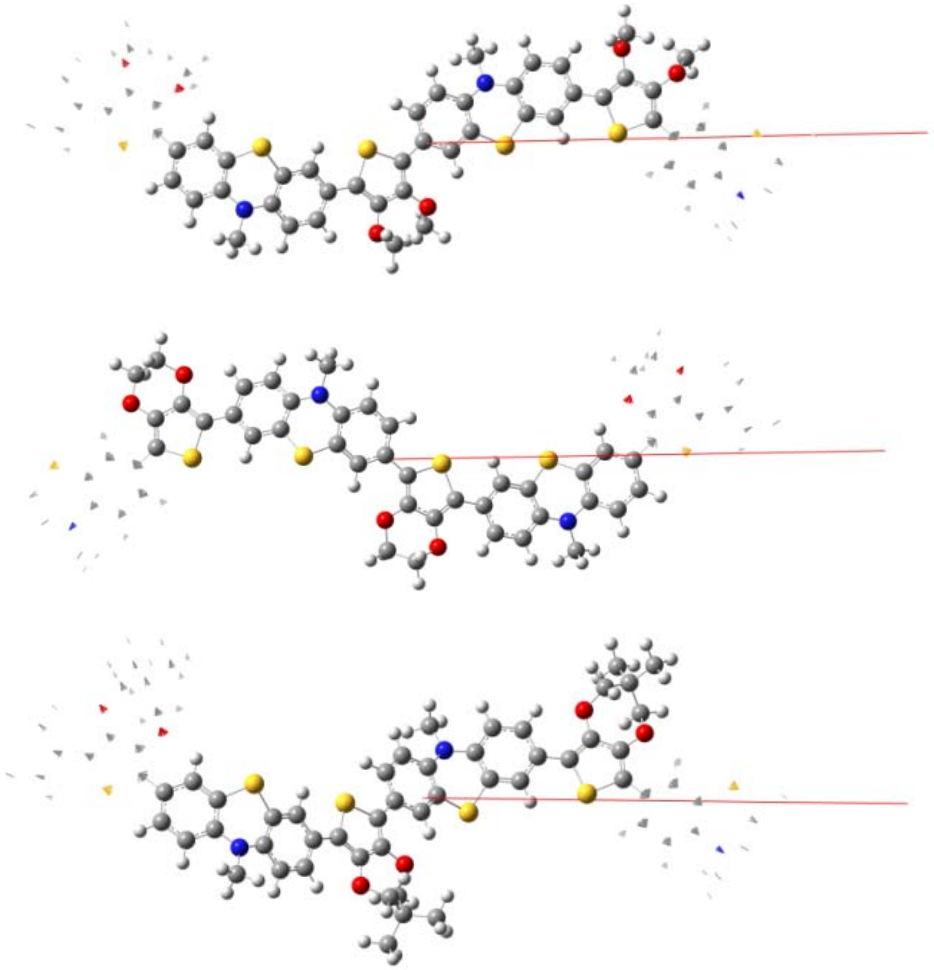

Figure 2: Optimized unit cell for the PBC/HSE06 calculation of PDMT-PHENO, PEDT-PHENO and PPRO-PHENO

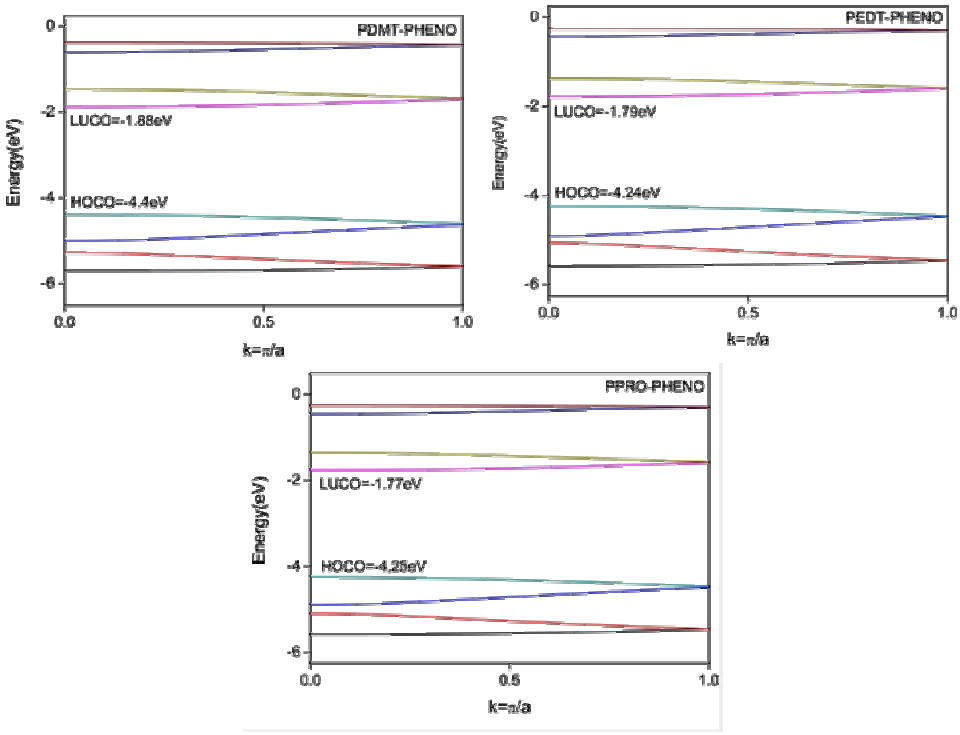

Figure 3: Band structure of PDMT-PHENO, PEDT-PHENO and PPRO-PHENO

Table 1: Band structure data[#] of PDMT-PHENO, PEDT-PHENO and PPRO-PHENO

Polymer	HOCO (eV)	LUCO (eV)	E_g (eV)
PDMT-PHENO	-4.4	-1.88	2.52
PEDT-PHENO	-4.24	-1.79	2.45
PPRO-PHENO	-4.25	-1.77	2.48

PBC/HSE06/6-31G

4.2.2. Synthesis and characterization of monomers and polymers

Synthetic route for the synthesis of 3,4-propylenedioxythiophene is outlined in scheme 2 and scheme 3. The 3,4-dimethoxythiophene[18,19] (scheme 2) and 2,2-dioctyldiethyl malonate[20] (Scheme 3) are prepared through reported procedures. 3,3-dioctyl-3,4-dihydro-2H-thieno[3,4-*b*][1,4]-dioxepine (here in ProDOT) is synthesized through the

transetherification of 3,4-dimethoxythiophene and 2,2-dioctylpropanediol in the presence of p-toluene sulphonic acid to give ProDOT in 53% yield (scheme 3). 2,2-dioctylpropanediol is synthesized starting from diethyl malonate, alkylating it with 1-bromooctane and reducing the resultant compound with $LiAlH_4$ (scheme 3). Three polymers carrying 3,4-dimethoxythiophene, 3,4-ethylenedioxythiophene and 3,4-propylenedioxythiophene with 10-octyl phenothiazine is synthesized through direct arylation using palladium acetate as catalyst (scheme 4). This gave PDMT-PHENO, PEDT-PHENO and PPRO-PHENO in 45%, 33% and 58% yields respectively. All the polymers were characterized using ^{1}H NMR, UV-Visible spectroscopy, GPC, Cyclic voltammetry, Differential pulse voltammetry, TGA etc. The ^{1}H NMR spectra of the polymers are shown in figure 4. PDMT-PHENO shows two peaks at δ 3.93, which corresponds to two –O-CH_3 groups which may be due to the slightly twisted geometry of phenothiazine unit. There is a triplet at δ 3.8 corresponding to –N-CH_2- group. PEDT-PHENO showed a multiplet corresponding to the -O-CH_2- group of ethylenedioxythiophene and is due to the restricted rotation of -O-CH_2- group by the ethylene bridge. PEDT-PHENO also showed a triplet corresponding to –N-CH_2- group. A similar observation can be made with ^{1}H NMR spectrum of PPRO-PHENO. The ^{1}H NMR spectra of the polymers contain a small peak in the aromatic region corresponding to the end group. The polymerization results including the molecular weight data of the polymers are summarized in table 2.

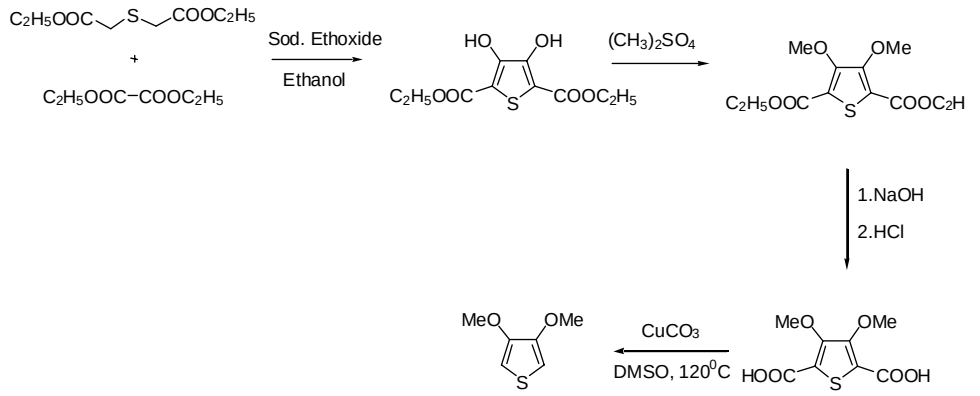

Scheme 2: Synthesis of 3,4-dimethoxythiophene

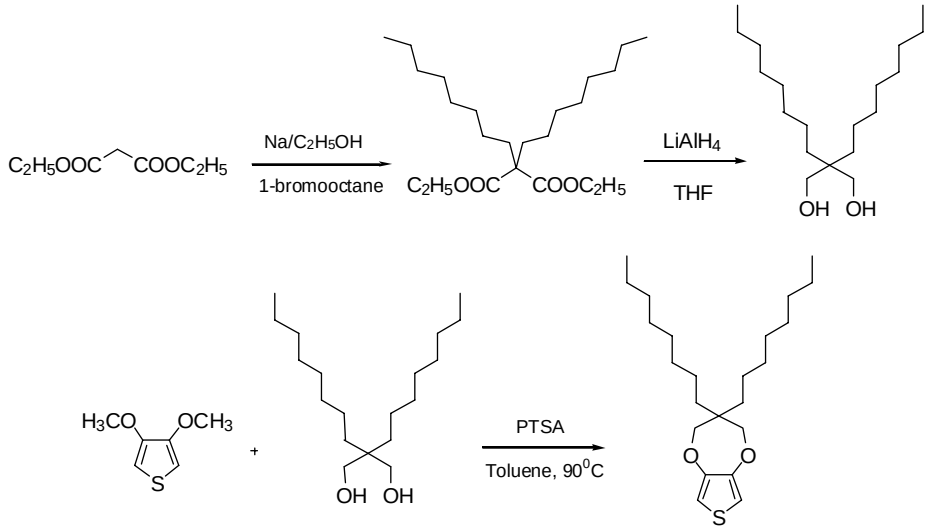

Scheme 3: Synthesis of 3,4-propylenedioxythiophene

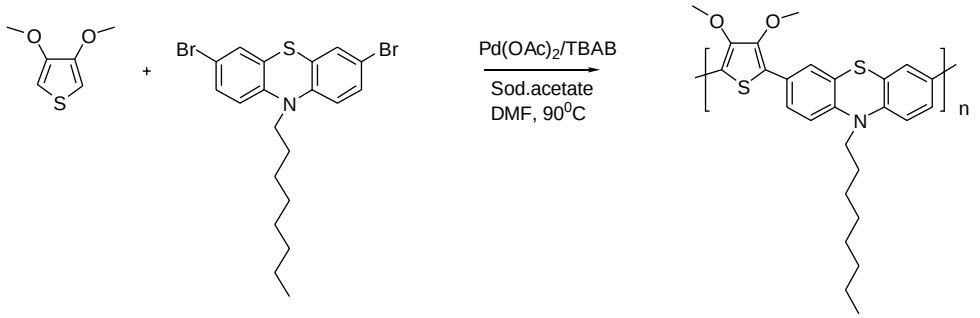

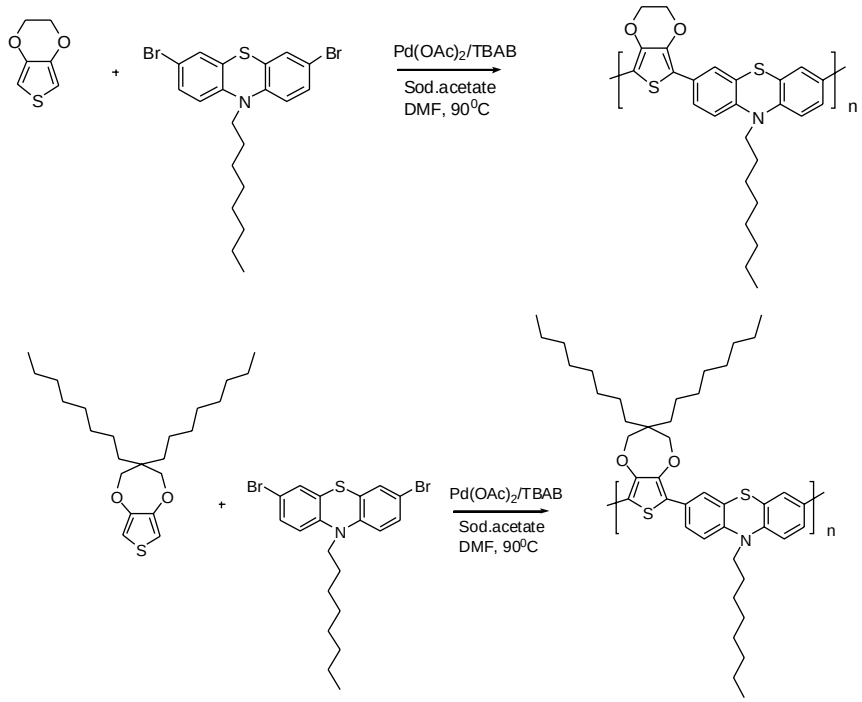

Scheme 4: Synthesis of PDMT-PHENO, PEDT-PHENO and PPRO-PHENO

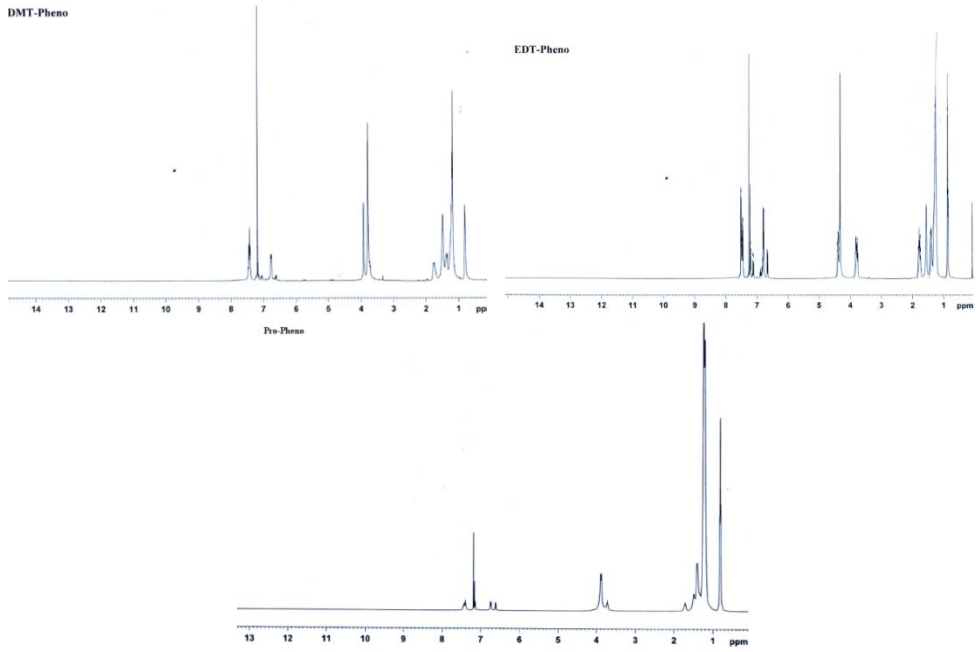

Figure 4: ^{1}H NMR spectra of PDMT-PHENO, PEDT-PHENO and PPRO-PHENO

Table 2: Polymerization results and thermal stability of the polymers

Polymers	M_n[a]	M_w[a]	PDI	Yield (%)	T_d (^{0}C)[b]
PDMT-PHENO	2517	7025	2.7	45	249
PEDT-PHENO	3705	5739	1.54	33	330
PPRO-PHENO	4500	7115	1.58	58	288

a. Determined using GPC in toluene using polystyrene standards.
b. Onset of decomposition measured by TGA analysis

4.2.3. Optical properties

The optical properties of the polymers were investigated in chloroform solution and in thin film. The absorption spectrum of polymers in chloroform solution and in thin film cast from chlorobenzene on to glass substrate is shown in figure 5a and 5b. The PDMT-PHENO, PEDT-PHENO and PPRO-PHENO showed absorption maximum at 425 nm, 435 nm and 438 nm respectively. In thin film, the absorption maximum was red shifted slightly by 4 nm to 12 nm. This result suggests that polymers have low ordered structure in solid state. The absorption onset of PDMT-PHENO, PEDT-PHENO and PPRO-PHENO in thin film occurs at 555 nm, 550 nm, and 590 nm respectively. The optical band gap calculated was found to be 2.24 eV, 2.26 eV and 2.1 eV respectively. The strong absorption of the polymer in the visible region is attributed to the enhanced HOMO-LUMO overlap, resulting from the delocalized molecular orbital density for both HOCO and LUCO wave functions of the polymers. The delocalized structures of HOCO and LUCO are depicted in figure 6.

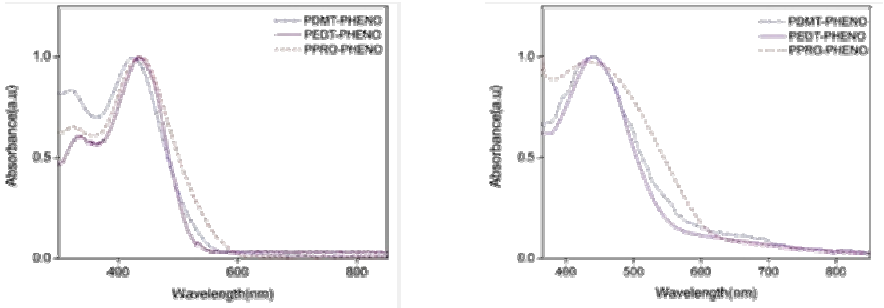

Figure 5: Absorption spectrum of polymers a. in chloroform solution and b. in thin film on glass substrate

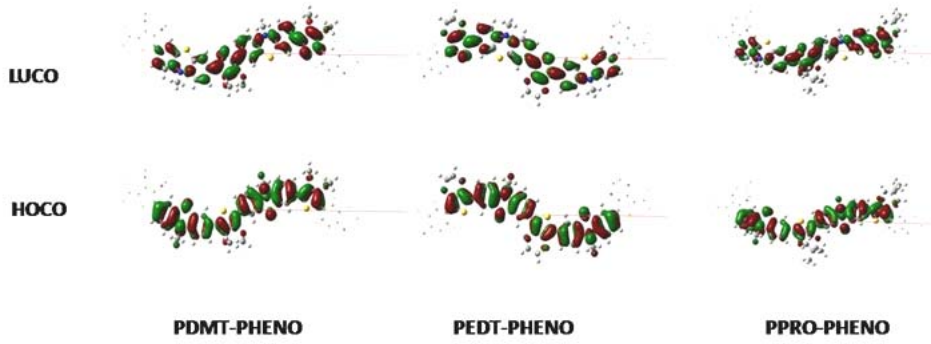

Figure 6: Distribution of HOCO and LUCO of PDMT-PHENO, PEDT-PHENO and PPRO-PHENO

The photoluminescence spectra of the polymers are shown in figure 7. The wavelength corresponding to the absorption maximum is used as the excitation wavelength. The PDMT-PHENO, PEDT-PHENO, PPRO-PHENO showed emission maximum at 523 nm, 519 nm, and 524 nm**.**

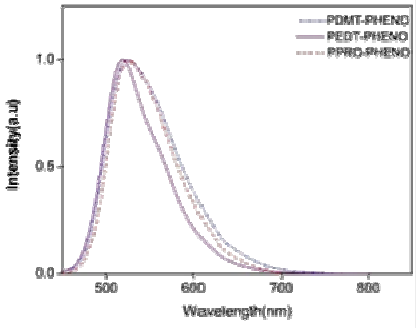

Figure 7: Photoluminescence spectra of polymers in chloroform solution

Table 3: Optical properties of polymers in chloroform solution and in thin film on glass substrate

Polymer	Absorption λ_{max} (nm)		Emission λ_{max} (nm) (Solution)	Absorption onset (film) λ_{onset}	E_g^{opt} (eV)
	Solution	Film			
PDMT-PHENO	424	436	523	555	2.24
PEDT-PHENO	435	441	519	550	2.26
PPRO-PHENO	438	442	524	590	2.1

4.2.4. Electrochemical properties

Cyclic voltammetry is used to assess the HOMO and LUMO levels of the polymers. The onset of first oxidation process of PDMT-PHENO, PEDT-PHENO and PPRO-PHENO occurs at 0.65 V, 0.58 V and 0.64 V respectively, corresponding to HOMO of -5.05 eV, -4.98 eV,-5.04 eV. Similarly, onset of first reduction process occurs at 2.05 V, 2.06 V and 2.06 V, corresponding to LUMO values of -2.35 eV, -2.34 eV, -2.34 eV for PDMT-PHENO, PEDT-PHENO and PPRO-PHENO, respectively. All the polymers showed good reversibility towards the oxidation and reduction processes, pointing out good chemical stability of the polymers. The band gap of the polymers are calculated to be 2.7 eV, 2.64 eV and 2.7 eV respectively for PDMT-PHENO, PEDT-PHENO and PPRO-PHENO. From the electrochemical studies it is assumed that bridging the two alkoxy group have little effect on the band gap of the 3,4-dialkoxythiophene/phenothiazine copolymers. The electrochemical band gap showed deviations of the order of 0.4-0.6 eV from the optical band gap. This may be due to the difference in the mechanism of optical excitation and electrochemical oxidation and reduction processes. In the former process excitation creates excitons (bound electrons and hole pair) and the latter process creates ions. The low energy of excitons compared to the ions and solvation of the ions in the electrochemical experiment were reflected in the observed electrochemical band gap.

The redox properties of the polymers were also investigated by differential pulse voltammetry. The band gaps of PDMT-PHENO, PEDT-PHENO and PPRO-PHENO are 2.60 eV, 2.45 eV and 2.62 eV respectively. The DPV estimated band gaps were found to be smaller than those determined by CV. This may be due to minimization of charging background current in DPV and sharper redox onset compared to the CV. DPV

determined band gap differ by 0.3 eV-0.5 eV from the optical band gap. The electrochemical properties of the polymers are presented in table 4.

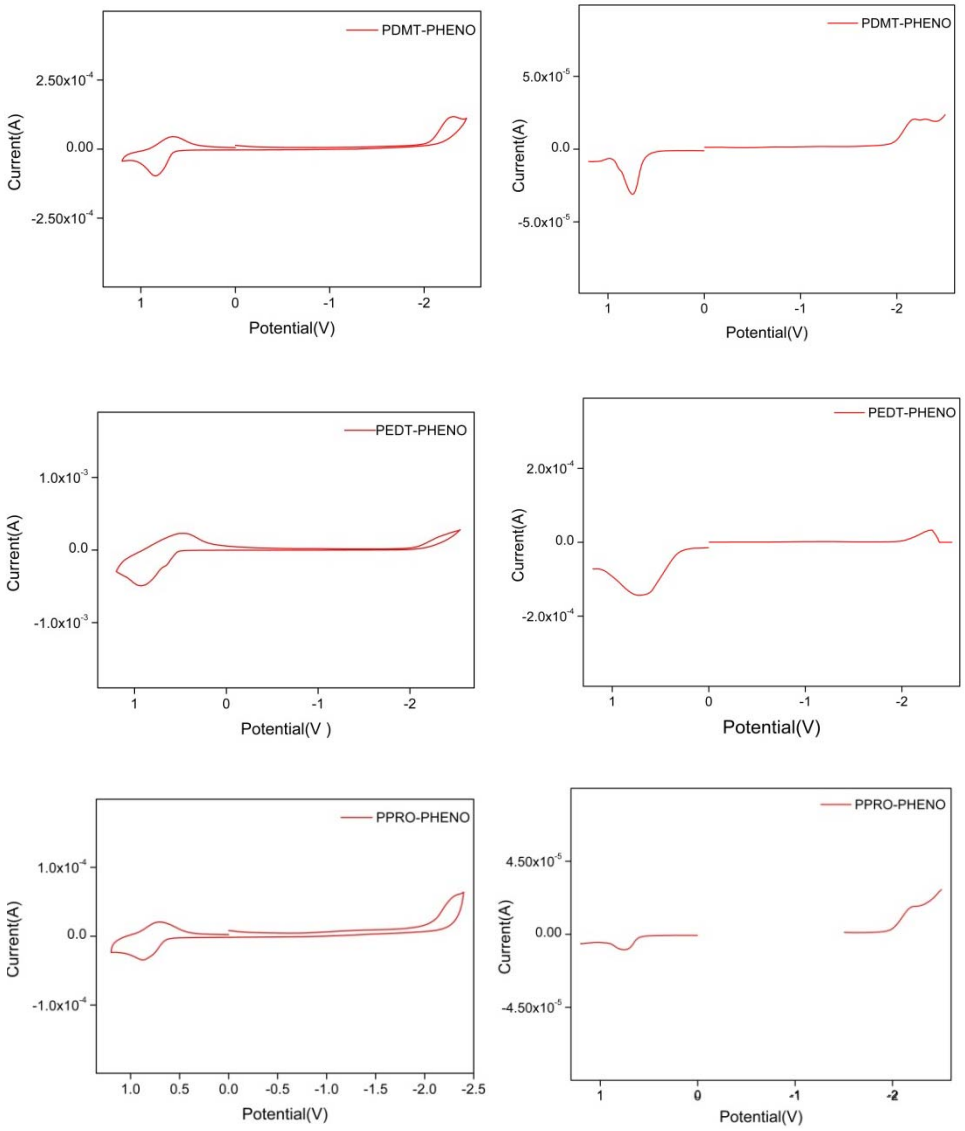

Figure 8: Cyclic voltammograms (scan rate 100mV/s) and differential pulse voltammograms (step time of 0.1 s) of PDMT-PHENO, PEDT-PHENO and PPRO-PHENO films cast on a platinum electrode in Bu_4NPF_6/acetonitrile

Table 4: Electrochemical data of PDMT-PHENO, PEDT-PHENO and PPRO-PHENO

Polymer	Cyclic Voltammetry					Differential Pulse Voltammetry				
	E_{ox} (V)	E_{red} (V)	HOMO (eV)	LUMO (eV)	E_g (eV)	E_{ox} (V)	E_{red} (V)	HOMO (eV)	LUMO (eV)	E_g (eV)
PDMT-PHENO	0.65	-2.05	-5.05	-2.35	2.7	0.62	-1.98	-5.02	-2.42	2.60
PEDT-PHENO	0.58	-2.06	-4.98	-2.34	2.64	0.42	-2.03	-4.82	-2.37	2.45
PPRO-PHENO	0.64	-2.06	-5.04	-2.34	2.7	0.61	-2.01	-5.01	-2.39	2.62

4.2.5. Photovoltaic device characteristics

The suitability of the polymer for active layer in photovoltaic device was verified by fabricating a heterojunction device using the polymers and the semiconductor In_2S_3. Figure 9 shows the current density-voltage (J-V) characteristics of the heterojunctions under illumination and in the dark. As could be seen, the devices clearly exhibited rectifying behaviour in the dark which may be due to the barrier formed at the In_2S_3/ polymer interface. Under white light illumination (50 mW/cm^2), the devices, ITO/In_2S_3/polymer/Ag heterojunction of PDMT-PHENO, PEDT-PHENO and PPRO-PHENO exhibited efficiencies of 0.022%, 0.054% and 0.01% respectively. The important photovoltaic characteristics of bilayer heterojunction devices of the polymers are summarized in table 5.

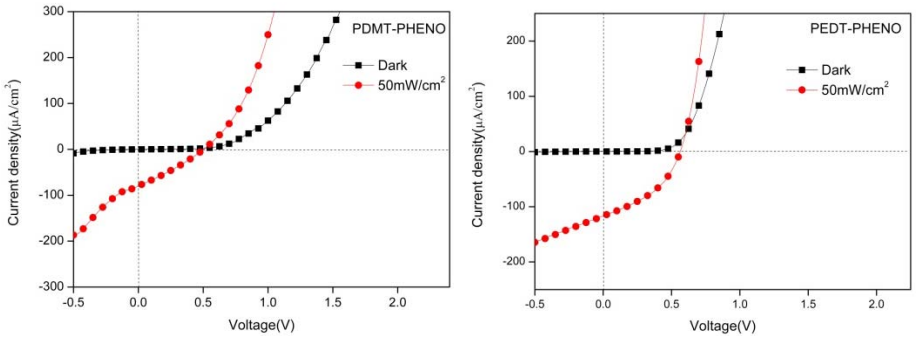

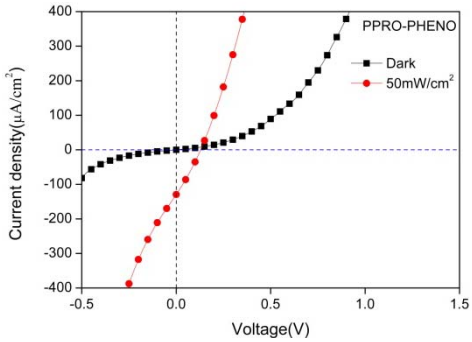

Figure 9: J-V characteristics of ITO/In_2S_3/polymer/Ag heterojunctions of PDMT-PHENO, PEDT-PHENO and PPRO-PHENO

Table 5: J-V characteristics of ITO/In_2S_3/polymer/Ag heterojunctions

Polymer	V_{oc} (mV)	J_{sc} ($\mu A/cm^2$)	Efficiency (%)	Fill factor (%)
PDMT-PHENO	489.22	72.0	0.022	30.88
PEDT-PHENO	564.00	117.0	0.054	40.76
PPRO-PHENO	129.58	129.0	0.01	27.79

4.3. Conclusions and perspectives

The electronic structure of three copolymers of phenothiazine with 3,4-dimethoxythiophene, 3,4-ethylenedioxythiophene and 3,4-propylenedioxythiophene were calculated using HSE06/6-31G method. The designed polymers were synthesized through cost effective direct arylation reaction using palladium acetate as catalyst. The direct arylation reaction is superior to the conventional cross-coupling reactions like Suzuki, Stille and Kumada polycondensation reactions by considering the easy reaction conditions. The reaction can be carried out in wet solvents. One problem associated with low molecular weight of the polymer may be due to the precipitation of the polymer in DMF. It can be overcome by using proper choice of solvent system. The band gap of the polymers are experimentally determined using optical and electrochemical methods and are in good

agreement with the theoretical results. All the three polymers showed photoactivity under illumination in the heterojunction ITO/In_2S_3/polymer/Ag heterojunction. The device performance can be improved by the optimizing the device parameters.

4.4. Experimental methods

The 3,4-dimethoxythiophene[18,19] and 2,2-dioctyldiethylmalonate[20] are prepared through reported procedures.

4.4.1. Synthesis of 2,2-dioctyl-1,3-propanediol:

To a solution of the 2,2-dioctyldiethylmalonate (1) (10.0 g, 25.9 mmol) in dry THF was added $LiAlH_4$ (2.8 g, 73.4 mmol) at 0 °C. The reaction mixture was stirred for 24 h at room temperature, and water was carefully added. The reaction mixture was stirred for 1 h and allowed to stand to settle the salts. A clear THF layer was carefully decanted, and the combined layers were dried over $MgSO_4$. Purification of the crude product by column chromatography on silica gel using hexane/ethyl acetate (2:1) as eluent afforded the diol as clear oil.

Yield	:	83% (6.5 g)
^{1}H NMR (400 MHz, $CDCl_3$)	:	δ 3.56 (s, 4H,-OCH_2-), 2.50 (s, 2H, -OH), 1.40-1.15 (m, 28H, aliphatic H), 0.88 (t, *J*=6.72 Hz, 6H).

4.4.2. Synthesis of 3,3-dioctyl-3,4-dihydro-2*H*-thieno[3,4-*b*][1,4]-dioxepine (ProDOT):

2,2-dioctylpropane-1,3-diol (1.08 g, 0.036 mol), 3,4-dimethoxythiophene (0.5 g, 0.0346 mol), and *p*-toluene sulfonic acid monohydrate (0.04 g, 0.21mmol) in 20 mL of toluene was refluxed for 48 h. The reaction mixture was

washed with water and concentrated to give a dark oil. The oil was purified by column chromatography using dichloromethane/hexane (1:4, volume ratio) as eluent to yield ProDOT as clear oil.

Yield	:	53% (0.7 g)
^{1}H NMR (400 MHz, $CDCl_3$)	:	δ 6.4 (s, 2H, Ar-H), 3.83 (s, 4H, -OCH_2), 1.35-1.27 (m, 28H, aliphatic-H) , 0.88-0.86 (t, *J*=5.6 Hz 6H, -CH_3)
^{13}C NMR (100 MHz, $CDCl_3$)	:	δ 149, 104.6, 77.5, 77.3, 77, 76.7, 43.7, 31.9, 31.8, 30.5, 29.5, 29.3, 22.8, 22.7, 14.1
GC MS	:	m/z =380.32

4.4.3. General procedure for the polymerization

To a stirred solution of dialkoxythiophene (0.53 mmol) in 10 mL DMF was added tetrabutylammonium bromide (0.53 mmol) and sodium acetate (2.1 mmol). The reaction mixture was stirred at room temperature for 15 min followed by addition of 3,7-dibromo-10-octylphenothiazine (0.53 mmol) and 10 mol% palladium acetate. The reaction was cooled to room temperature and poured in to methanol. The precipitate was filtered and washed with methanol. The polymer was purified by soxhlet extraction using acetone and methanol for 24 h. The residue was dissolved in minimum amount of toluene and precipitated from methanol and dried in vacuum.

4.4.3.1. Synthesis of PDMT-PHENO

3,4-dimethoxythiophene (0.076 g, 0.53 mmol), 3,7-dibromo-10-octylphenothiazine (0.25 g, 0.53 mmol), tetrabutylammonium bromide (0.171 g, 0.53 mmol), sodium acetate (0.29 g, 2.12 mmol), palladium acetate (0.012 g, 0.053 mmol), DMF (10 mL) were used. Yellow solid

Yield	:	45% (108 mg)
UV-Visible (Chloroform) λ_{max}	:	424 nm
GPC	:	Mn=2517, PDI=2.7
Td (^{0}C)	:	249
^{1}H NMR (400 MHz, $CDCl_3$)	:	δ 7.41-6.76 (m, ~6H of phenothiazine), 3.92 (d, ~6H of DMT), 3.79 (t, 2H, -NCH_2-), 1.77-1.18 (m, ~12H, aliphatic-H), 0.8 (t, ~3H, -CH_3)

4.4.3.2. Synthesis of PEDOT-PHENO

3,4-ethylenedioxythiophene (0.075 g, 0.53 mmol), 3,7-dibromo-10-octylphenothiazine (0.25 g, 0.53 mmol), tetrabutylammonium bromide (0.171 g, 0.53 mmol), sodium acetate (0.29 g, 2.12 mmol), palladium acetate (0.012 g, 0.053 mmol), DMF (10 mL) were used.

Yield	:	33% (70 mg)
UV-Visible (Chloroform) λ_{max}	:	435 nm
GPC	:	Mn=3705, PDI=1.54
T_d (^{0}C)	:	330
^{1}H NMR (400 MHz, $CDCl_3$)	:	δ 7.52-6.66 (m, ~6H of phenothiazine), 4.32-4.41 (m, ~4H, OCH_2), 3.78 (t, 2H, -NCH_2-), 1.82-1.25 (m, ~12H, aliphatic-H), 0.88 (m, ~3H, -CH_3)

4.4.3.3. Synthesis of PPRO-PHENO

ProDOT (0.202 g, 0.53 mmol), 3,7-dibromo-10-octylphenothiazine (0.25 g, 0.53 mmol), tetrabutylammonium bromide (0.171 g, 0.53 mmol),

sodium acetate (0.29 g, 2.12 mmol), palladium acetate (0.012 g, 0.053 mmol), DMF (10 mL) were used.

Yield	:	58% (0.21 g)
UV-Visible (Chloroform) λ_{max}	:	438 nm
GPC	:	Mn=4500, PDI=1.58
Td (^{0}C)	:	288
^{1}H NMR (400 MHz, $CDCl_3$)	:	δ 7.5-6.6 (m, ~6H of phenothiazine), 3.9-3.88 (d, ~4H, -OCH_2- of ProDOT), 3.72 (t, 2H, -NCH_2-), 1.73-1.21 (m, ~40H, aliphatic-H), 0.82-0.79 (m, ~9H, -CH_3)

4.5. References

1. Cheng, L. L.; Jung, H. T.; Wen, Y. L.; Wen, C. C.; Samson, A. J. *Macromolecules*, **2008**, 41, 6952.
2. Moo, J. P.; Jonghee, L.; Jong, H. P.; Sang, K. L.; Jeong, I. L.; Hye, Y. C.; Do, H. H.; Hong, K. S. *Macromolecules*, **2008**, 41, 3063.
3. Jean, B.; Swager, T. M. *Macromolecules*, **2008**, 41, 5559.
4. Guangyi, Sang.; Yingping, Z.; Yongfang, Li. *J. Phys. Chem. C.*, **2008**, 112, 12058.
5. Pierre, M. B.; Jegadesan, S.; Kaushik, R. C.; Stefan, E.; Tracy, D. M.; Franky, S.; Reynolds, J. R. *Chem. Mater*., **2010**, 22, 2093.
6. Bernd, T.; Rabindranath, A. R.; Kai, Z.; Yu, Z. *Beilstein J. Org. Chem.*, **2010**, 6, 830.

7. Lowe R. D.; Khersonsky, S. M.; McCullough, R. D. *Adv. Mater.*, **1999**, 11, 250.
8. McCullough, R. D.; Lowe, R. D.; Jayaraman, M.; Anderson, D. L. *J. Org. Chem.*, **1993**, 58, 904.
9. Miyakoshi, R.; Yokoyama, A.; Yokozawa, T. *Macromol. Rapid Commun.*, **2004**, 25, 1663.
10. Sheina, E. E.; Liu, J. S.; Iovu, M. C.; Laird, D. W.; McCullough, R. D. *Macromolecules*, **2004**, 37, 3526.
11. Mohanakrishnan, A. K.; Amaladass, P.; Clement, J. A., *Tetrahedron Lett.*, **2007,** 48, 539,.
12. Borghese, A.: Geldhof, G.: Antoine, L. *Tetrahedron Lett*., **2006**, 47, 9249.
13. Anshu, K.; Kumar, A., *Polym. Chem*., **2010,** 1, 286.
14. Parr, R. G.; Yang, W., *Density-Functional Theory of Atoms and Molecules;* Oxford University Press, **1989**, New York.
15. Heyd, J.; Scuseria, G. E.; Ernzerhof, M. *J. Chem. Phys*. **2003**, 118, 8207.
16. Krukau, A. V.; Vydrov, O. A.; Izmaylov, A. F.; Scuseria, G. E. *J. Chem. Phys.*, **2006**, 125, 224106.
17. Gaussian 09, Revision B02, Frisch, M. J.; Trucks, G. W.; Schlegel, H. B.; Scuseria, G. E.; Robb, M. A.; Cheeseman, J. R.; Scalmani, G.; Barone, V.; Mennucci, B.; Petersson, G. A.; Nakatsuji, H.; Caricato, M.; Li, X.; Hratchian, H. P.; Izmaylov, A. F.; Bloino, J.; Zheng, G.; Sonnenberg, J. L.; Hada, M.; Ehara, M.; Toyota, K.; Fukuda, R.; Hasegawa, J.; Ishida, M.; Nakajima, T.; Honda, Y.; Kitao, O.; Nakai, H.; Vreven, T.; Montgomery, Jr., J. A.; Peralta, J. E.; Ogliaro, F.; Bearpark, M.; Heyd, J. J.; Brothers, E.; Kudin, K.

N.; Staroverov, V. N.; Kobayashi, R.; Normand, J.; Raghavachari, K.; Rendell, A.; Burant, J. C.; Iyengar, S. S.; Tomasi, J.; Cossi, M.; Rega, N.; Millam, N. J.; Klene, M.; Knox, J. E.; Cross, J. B.; Bakken, V.; Adamo, C.; Jaramillo, J.; Gomperts, R.; Stratmann, R. E.; Yazyev, O.; Austin, A. J.; Cammi, R.; Pomelli, C.; Ochterski, J. W.; Martin, R. L.; Morokuma, K.; Zakrzewski, V. G.; Voth, G. A.; Salvador, P.; Dannenberg, J. J.; Dapprich, S.; Daniels, A. D.; Farkas, Ö.; Foresman, J. B.; Ortiz, J. V.; Cioslowski, J.; Fox, D. J. Gaussian, Inc., Wallingford CT, **2009**.

18. Fager, W. *J. Am. Chem. Soc*., **1945**, 67, 2217.

19. Quintero, D. C.; Bäuerle, P. *Chem. Commun*., **2002**, 22, 2690.

20. Christian, B. N.; Thomas, B., *Macromolecules*, **2005**, 38, 10379.

Chapter 5

SYNTHESIS, CHARACTERIZATION AND PHOTOVOLTAIC APPLICATIONS OF LOW BAND GAP ProDOT/2,1,3-CHALCOGENADIAZOLE COPOLYMERS

Contents

In this chapter, we have investigated the effect of introduction of two chalcogenadiazoles 2,1,3-benzothiadiazole and 2,1,3-benzoselenadiazole in to the poly(ProDOT) chain. On introduction of chalcogenadiazole unit, the HOMO and LUMO of the poly(ProDOT) was decreased by about 1eV and we get polymers with almost the same band gap as that of the homopolymer poly(ProDOT). So we have achieved tuning the energy level of homopolymer by introducing acceptors, without affecting the band gap. Both the polymers are synthesized through direct arylation reaction. Polymers are characterized using optical and electrochemical methods. Experimental results support the theoretical prediction. Polymers PPRO-BTZ and PPRO-BSE possess theoretical band gap of 1.8 eV and 1.79 eV and optical band gap of 1.52 eV and 1.51 eV. The photovoltaic activity of the polymer was also tested using the ITO/In_2S_3/polymer/Ag heterojunction. The heterojunctions of PPRO-BTZ and PPRO-BSE showed efficiency of 0.014% and 0.006% respectively.

5.1. Introduction

The 3,4-propylenedioxythiophene (ProDOT), is one of the symmetrical members of 3,4-alkylenedioxythiophene family like 3,4-ethylenedioxythiophene (EDOT). The main advantage of ProDOT over EDOT is that, we can graft solubilizing side chains to the polymer without disrupting the regiosymmetry of the polymers[1-5]. The application of 3,4-propylenedioxythiophene in electrochromic devices[6-10], photovoltaic devices[11-13], light emitting diodes[14] and non linear optical devices[15] are well reviewed in the literature.

In this chapter, we describe the electronic structure calculation, synthesis by direct arylation reaction, characterization and photovoltaic properties of two alternating copolymers of 3,4-propylenedioxythiophene with 2,1,3-benzothiadiazole and 2,1,3-benzoselenadiazole. The aim was to tune the energy levels of the poly(ProDOT), make them suitable for photovoltaic application and increase the air stability of the poly(ProDOT). This was prompted by the encouraging result that incorporation of the acceptor, cyanovinylene to Poly(ProDOT) decreased both the HOMO and LUMO levels of poly(ProDOT) and polymers with the same band gap as that of the homopolymer was obtained[12]. The photovoltaic properties of the 3,4-propylenedioxythiophene/cyanovinylene copolymers with PCBM acceptor was studied in detail[12]. Similarly, 3,4-propylenedioxythiophene and 2,1,3-benzothiadiazole copolymer was synthesized through Stille reaction[16]. The main problem associated with this method is that the synthesis of tributyltin compound of 3,4-propylenedioxythiophene was very difficult. They used stannane compound without purification. This might have led to the formation of side products and resulted in low molecular weight polymers. One way to overcome this problem is to avoid the use of stannane derivatives. So direct

arylation reaction is the right choice for the cost effective method for polymerizing 3,4-propylenedioxythiophene and 2,1,3-benzothiadiazole. 3,4-propylenedioxythiophene/2,1,3-benzoselenadiazole was also synthesized, keeping in mind the higher acceptor strength of the 2,1,3-benzoselenadiazole unit than the 2,1,3-benzothiadiazole.

5.2. Results and discussion

5.2.1. Band structure calculation

The ground state geometries of oligomers were optimized by means of the hybrid density functional theory (DFT)[17] at the B3LYP [18,19] (Becke, three-parameter, Lee-Yang-Parr) level of theory using double zeta basis set LANL2DZ (Los Alamos ECP plus DZ) [20]. LANL2DZ basis set describes core electrons of the heavier elements by means of an effective core potential. This permits the study of Se containing compounds with less computational time. The harmonic vibrational frequencies obtained with B3LYP/LANL2DZ were used to characterize the stationary points as local minima. All the calculations described here were carried out using Gaussian 03 suite of codes[21].

The optimized unit cell for the periodic boundary calculation on poly(ProDOT), PPRO-BTZ and PPRO-BSE are shown in figure 1. The length of the translational vector of poly(ProDOT) is $7.9A^0$ and for PPRO-BTZ and PPRO-BSE, it is $16.6A^0$. The calculated band structures and density of states are depicted in figure 2 and figure 3. It could be seen from the band structure that all the polymers are direct band gap polymers.

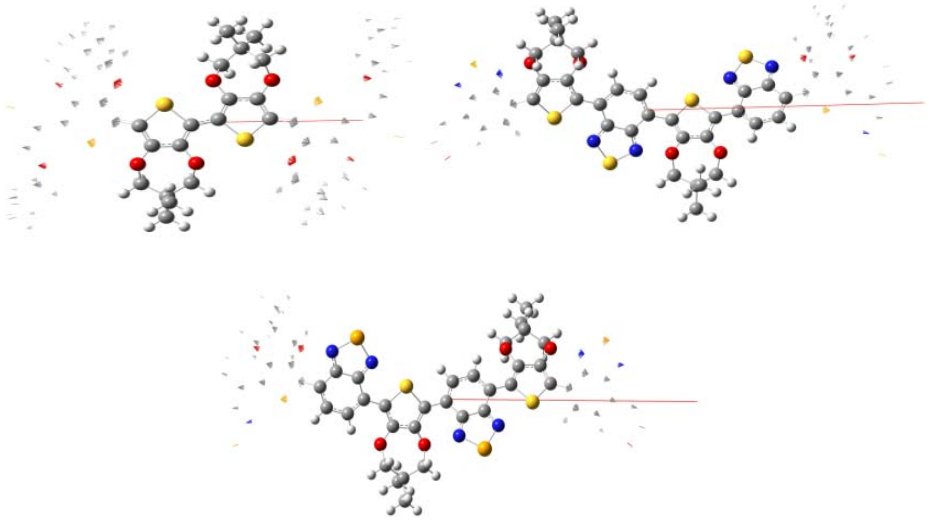

Figure 1: Unit cell for the PBC/B3LYP/LANL2DZ calculation of poly(ProDOT), PPRO-BTZ and PPRO-BSE

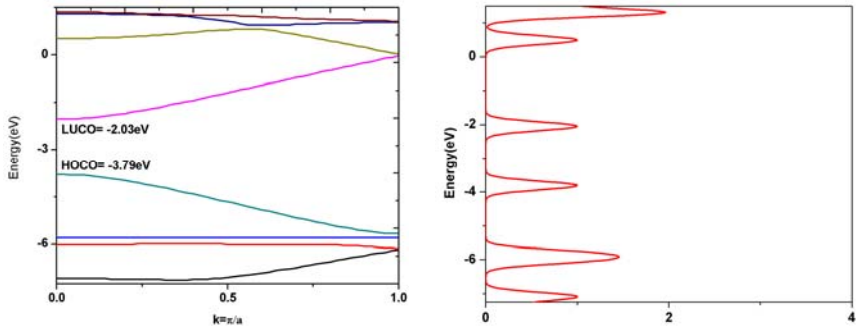

Figure 2: Band structure and density of states of poly(ProDOT)

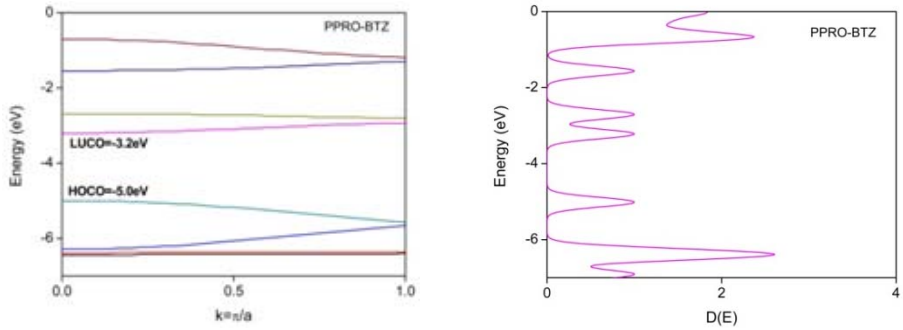

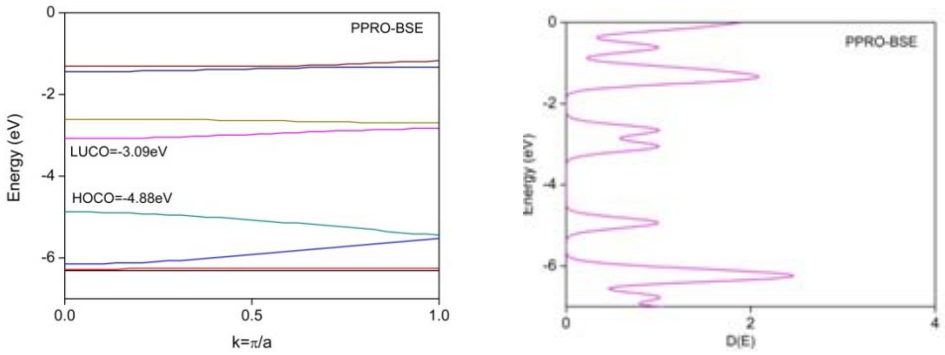

Figure 3: Band structure and Density of States of PPRO-BTZ and PPRO-BSE

The band structure data of the polymers are summarized in table 1. On comparing the band structure of copolymers with homopolymer poly(ProDOT), we can see that HOCO was decreased by 1.21 eV and 1.09 eV for PPRO-BTZ and PPRO-BSE respectively. Similarly LUCO was decreased by 1.17 eV and 1.06 eV respectively. The band gap of PPRO-BTZ and PPRO-BSE are calculated to be 1.8 eV and 1.79 eV. There is no considerable decrease in the band gap on the introduction of 2,1,3-benzoselenadiazole unit instead of 2,1,3-benzothiadiazole. This may be due to the slight increase in the dihedral angle between the adjacent ProDOT and BSE than the BTZ unit. Also we can observe that, on introduction of 2,1,3-benzoselenadiazole and 2,1,3-benzothiadiazole, band gap of the homopolymer poly(ProDOT) is not affected much. We have tuned the energy levels of the homopolymer by introducing acceptors and have made them suitable for photovoltaic application by matching the levels with acceptor In_2S_3.

Table 1: Band structure[#] data of poly (ProDOT), PPRO-BTZ and PPRO BSE

Polymer	HOCO (eV)	LUCO (eV)	Eg (eV)
Poly(ProDOT)	-3.79	-2.03	1.76
PPRO-BTZ	-5.0	-3.2	1.8
PPRO-BSE	-4.88	-3.09	1.79

#Method: PBC/B3LYP/LANL2DZ

5.2.2. Synthesis of monomers and polymers

The synthetic routes towards the key monomers are depicted in chapter II and chapter IV. The polymers are synthesized through direct arylation reaction between ProDOT and 4,7-dibromo-2,1,3-benzothiadiazole or 4,7-dibromo-2,1,3-benzoselenadiazole using palladium acetate as catalyst (Scheme 1). As benefitted from the side chain of ProDOT, both the polymers are readily soluble in THF, chlorobenzene, toluene, chloroform and can be easily processed as thin film. The polymers are characterized using UV-Visible spectroscopy, Cyclic voltammetry, ^{1}H NMR etc. The ^{1}H NMR spectra of the polymers are shown in figure 4. The polymers show only one broad peak in the aromatic region due to protons in the BTZ and BSE and one broad peak in the δ 4-4.1 region due to -OCH_2- proton of ProDOT. The isolated yield and molecular weight of both the polymers are summarized in table 2.

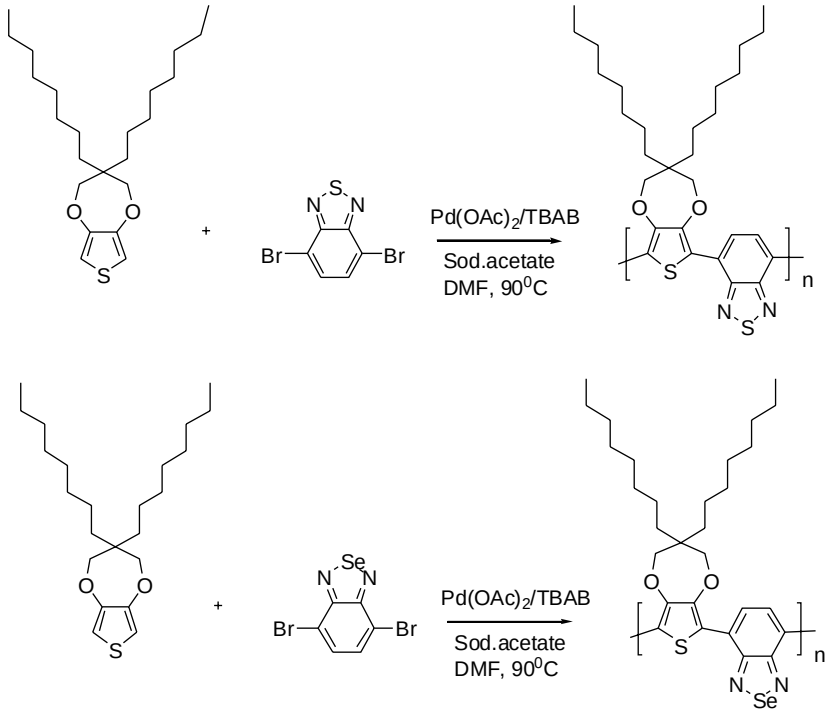

Scheme 1: Synthesis of 3,4-propylenedioxythiophene/2,1,3-chalcogenadiazole copolymer

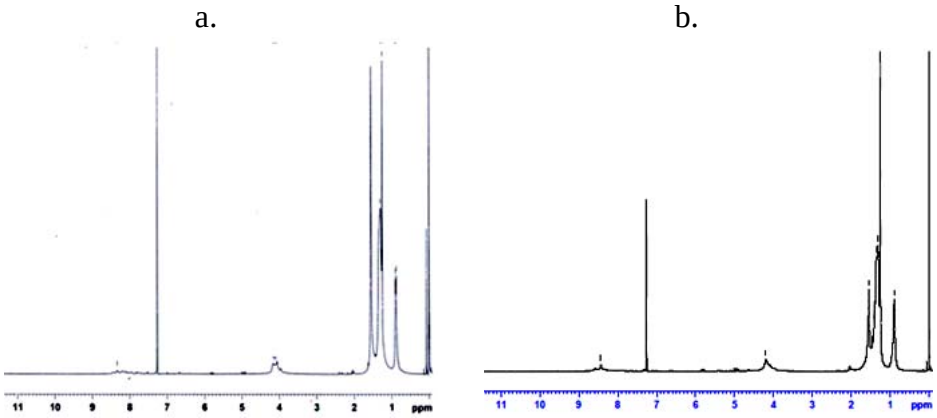

Figure 4: ^{1}H NMR spectrum of a. PPRO-BTZ and PPRO-BSE

Table 2: Polymerization results and thermal stability of polymers

Polymers	M_n[a]	M_w[a]	PDI	Yield (%)	T_d (^{0}C)[b]
PPRO-BTZ	4795	12207	2.54	61	285
PPRO-BSE	3805	10883	2.86	46	354

a. Determined by GPC in toluene based on polystyrene standards.
b. Onset decomposition temperature measured by TGA under nitrogen

5.2.3. Optical and photoluminescence properties

Absorption spectrum of the polymers are measured both in chloroform solution (figure 5a) and as thin film on glass sildes (figure 5b). PPRO-BTZ shows absorption maximum at 604 nm while PPRO-BSE shows maximum at 607 nm. Absorption maximum of PPRO-BTZ and PPRO-BSE in chloroform solution is red shifted by 68 nm and 37 nm in solid state and absorption maximum occurs at 672 nm and 644 nm respectively. This may be due to the inter chain interaction leading to the increase in coplanarity of the polymer chain in thin films. The onset of absorption is used to calculate the optical band gap of the polymers. For PPRO-BTZ and PPRO-BSE the onset of absorption occurs at 814 nm and 818 nm, corresponding to the band gap of 1.52 eV and 1.51 eV. Both the polymers possess almost the same band gap, as predicted by theoretical

calculation. The lowest energy transition is assigned as charge transfer band. This fact is supported theoretically by analyzing the HOCO and LUCO energy levels of the polymers. The HOCO and LUCO are localized on ProDOT and 2,1,3-chalcogenadiazoles respectively.

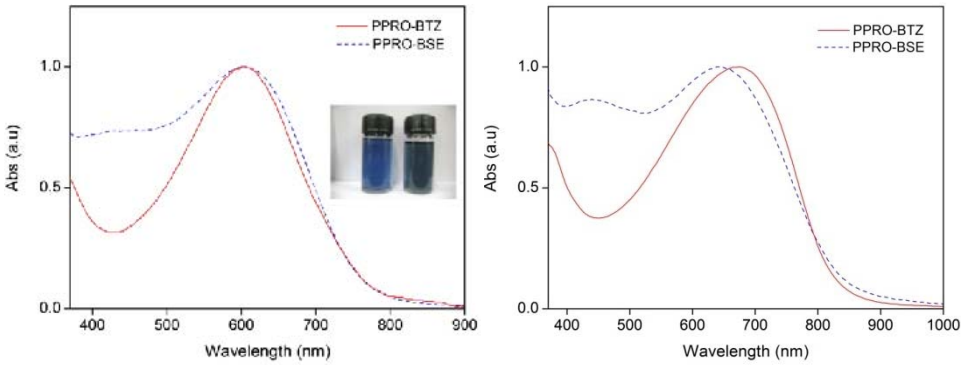

Figure 5: UV-Visible spectra of the polymers a. in chloroform solution and b. in thin film form. The polymer films were spun coated from 5mg/mL chlorobenzene solution on to glass substrate

The photoluminescence spectra of PPRO-BTZ and PPRO-BSE in chloroform solution are presented in figure 6. The wavelengths corresponding to the absorption maxima of the polymers are used as the excitation wavelength. The PPRO-BTZ shows emission maximum at 694 nm and PPRO-BSE and exhibited peak emission at about 745 nm.

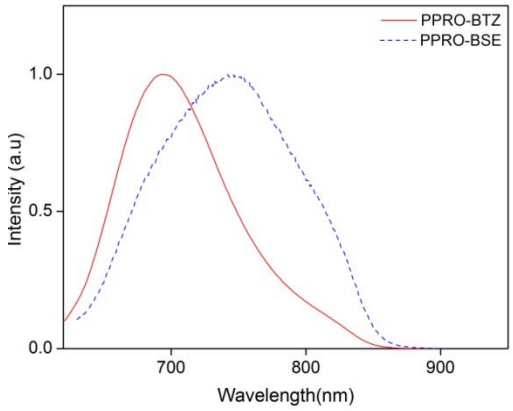

Figure 6: PL of PRO-BSE and PRO-BTZ in chloroform solution

Table: Optical properties of the polymers

Polymer	Absorption λ_{max} (nm)		Emission λ_{max}(nm)	Absorption onset (film) λ_{onset}	E_g^{opt}(eV)[a]
	Solution	Film			
PPRO-BTZ	604	672	694	814	1.52
PPRO-BSE	607	644	745	818	1.51

[a] Calculated from the onset of absorption

5.2.4. Electrochemical properties

Investigations on the electrochemical properties of the polymers are done using polymer film on platinum electrode in 0.1 M Bu_4NPF_6/acetonitrile electrolyte solution. Both the polymers possess one reduction peak and one oxidation peak. The HOMO and LUMO values are calculated from the onset of oxidation and reduction. The band gap of the PPRO-BTZ and PPRO-BSE are calculated to be 1.85 eV and 1.94 eV respectively. This band gap values do not correlate with the theoretical and optical band gap. A possible explanation for these differences can be found in the fact that, in the optical experiment the electrons and holes formed are bound, forming an exciton, whereas in the electrochemical experiment, ions are created. Apart from the exciton binding energy (which lowers the energy of the exciton, relative to that of the free charges), the solvation energy of the ions created in the electrochemical experiment has also an influence on the observed electrochemical band gap[22, 23].

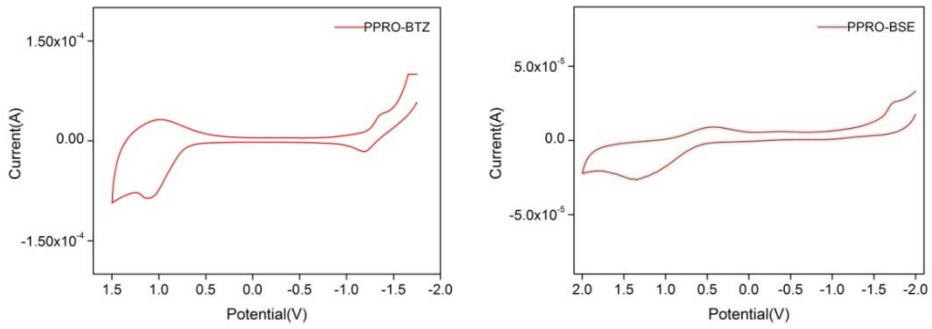

Figure 7: Cyclic voltammograms (scan rate of 100 mV/s) of polymer drop-cast onto a platinum electrode (0.02 cm^2) in 0.1M Bu_4NPF_6/Acetonitrile electrolyte solution

Table 4: Electrochemical properties of the polymers

Polymer	E_{ox} (V)	E_{red} (V)	HOMO (eV)	LUMO (eV)	E_g (eV)
PPRO-BTZ	0.629	-1.22	-5.03	-3.18	1.85
PPRO-BSE	0.511	-1.43	-4.91	-2.97	1.94

5.2.5. Photovoltaic device

The applicability of polymers for photovoltaic device was verified by fabricating a bilayer heterojunction device with the structure ITO/ In_2S_3/Polymer/Ag. Figure 8 shows the current density-volatge characteristics of the hetrojunctions under illumination and dark. Under white light illumination (50mW/cm^2), the device exhibits a short circuit current density (J_{sc}) of 51.4 µA/cm^2 and an open circuit voltage (V_{oc}) of 547.47 mV for PPRO-BTZ and 31.4 µA/cm^2 and 340.86 mV respectively for PPRO-BSE. The fill factor (FF) and efficiency were calculated to be 24.0 % and 26.2% and 0.014% and 0.006% respectively for PPRO-BTZ and PPRO-BSE. Photovoltaic characteristics of bilayer heterojunction devices of PPRO-BTZ and PPRO-BSE are summarized in table 5.

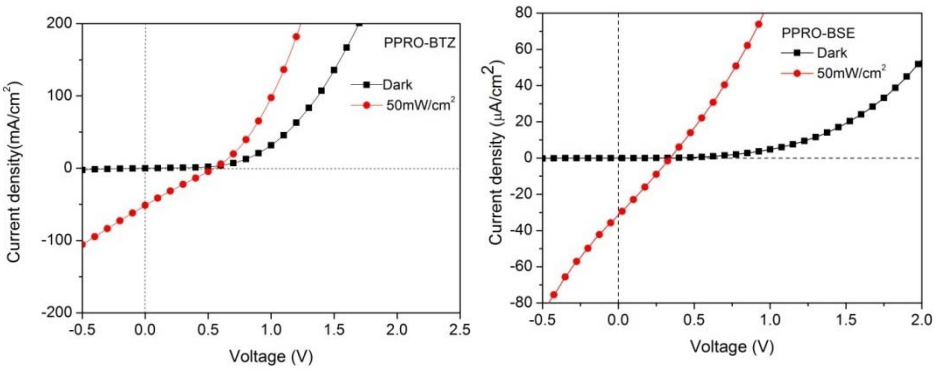

Figure 8: J-V Characteristics of ITO/ In_2S_3/Polymer/Ag heterojunctions of PPRO-BTZ and PPRO-BSE

Table 5: Photovoltaic characteristics of bilayer heterojunction devices of polymers

Polymer	V_{oc} (mV)	J_{sc} ($\mu A/cm^2$)	Fill Factor (%)	Efficiency (%)
PPRO-BTZ	547.47	51.4	24.0	0.014
PPRO-BSE	340.86	31.4	26.2	0.006

5.3. Conclusion and Perspectives

Electronic properties of two low band gap polymers based on 3,4-propylenedioxythiophene and 2,1,3-chalcogenadiazole was calculated using density functional theory in periodic boundary condiction formalism. According to theoretical calculation the energy levels are changed by introducing 2,1,3-benzothiadiazole and 2,1,3-benzoselenadiazole unit to ProDOT chain without affecting the band gap. The polymers are synthesized through cost effective palladium acetate catalysed direct arylation reaction in good yield. The band gap and energy levels of the polymers are determined using both optical and electrochemical methods, and showed agreement with the theoretical results. Both the polymers showed photo activity in the linear heterojunction ITO/In_2S_3/polymer/Ag. The device performance can be

improved by designing a bulk heterojunction using an acceptor, which have matching energy levels with the In_2S_3 and polymer.

5.4. Experimental section

The synthetic path towards the ProDOT**,** 4,7-Dibromo-2,1,3-benzothiadiazole and 4,7-Dibromo-2,1,3-benzoselenadiazole are depicted in chapter II and chapter IV.

5.4.1. Synthesis of PPRO-BTZ

To a solution of ProDOT (0.132 g, 0.347 mmol) in 20 ml of DMF, tetrabutylammonium bromide (0.112 g, 0.347 mmol), and sodium acetate (0.188 g, 1.38 mmol) were added. The solution was stirred at room temperature for 15 min followed by addition of 4,7-dibromo-2,1,3-benzothiadiazole (0.102 g, 0.347 mmol) and palladium acetate (10 mol%). The reaction mixture was stirred for 3 days at 90^0C and cooled to room temperature. It was precipitated into methanol (200 mL). The precipitate was filtered and purified via Soxhlet extraction with methanol and acetone successively to remove oligomers and catalyst residues. The polymer was dissolved in toluene and filtered. The filtrate was concentrated by evaporation, precipitated in methanol (200 mL), and collected as a dark blue solid.

Yield	:	61% (0.11 g)
GPC	:	M_n=4795, PDI=2.54
T_d (^{0}C)	:	285
UV-Visible λ_{max} (nm)	:	604

^{1}H NMR (400 MHz, $CDCl_3$)	:	δ 8.43 (b, Ar-H of benzothiadiazole), 4.05-4.16 (b, ~4H of ProDOT), 1.61-1.25 (m, ~28H, aliphatic-H), 0.88 (m, ~6H, -CH_3)

5.4.2. Synthesis of PPRO-BSE

To a solution of ProDOT (0.132 g, 0.347 mmol) in 20 ml of DMF, tetrabutylammonium bromide (0.112 g, 0.347 mmol), and sodium acetate (0.188 g, 1.38 mmol) was added. The solution was stirred at room temperature for 15 min followed by addition of 4,7-dibromo-2,1,3-benzoselenadiazole (0.118 g, 0.347 mmol) and palladium acetate (10 mol%). The reaction mixture was stirred for 3 days at 90^0C and cooled to room temperature. It was precipitated into methanol (200 mL). The precipitate was filtered and purified via Soxhlet extraction with methanol and acetone successively to remove oligomers and catalyst residues. The polymer was dissolved in toluene and filtered. The filtrate was concentrated by evaporation, precipitated in methanol (200 mL), and collected as a dark blue solid.

Yield	:	46% (89.2 mg)
GPC	:	M_n=3805, PDI=2.86
T_d (^{0}C)	:	354
UV-Visible λ_{max} (nm)	:	607
^{1}H NMR (400 MHz, $CDCl_3$)	:	δ 8.34 (b, Ar-H of benzoselenadiazole), 4.05-4.16 (b, ~4H of ProDOT), 1.55-1.29 (m, ~28H, aliphatic-H), 0.88 (m, ~6H, -CH_3)

5.5. References

1. Heywang, G.; Jonas, F. *Adv. Mater.*, **1992**, 4, 116.
2. Groenendaal, L.; Jonas, F.; Freitag, D.; Pielartzik, H.; Reynolds, J. R. *Adv. Mater.*, **2000**, 12, 481.
3. Reeves, B. D.; Grenier, C. R. G.; Argun, A. A.; Cirpan, A.; McCarley, T. D.; Reynolds, J. R. *Macromolecules*, **2004**, 37, 7559.
4. Welsh, D. M.; Kloeppner, L. J.; Madrigal, L.; Pinto, M. R.; Thompson, B. C.; Schanze, K. S.; Abboud, K. A.; Powell, D.; Reynolds, J. R. *Macromolecules*, **2002**, 35, 6517.
5. Kumar, A.; Welsh, D. M.; Morvant, M. C.; Piroux, F.; Abboud, K. A.; Reynolds, J. R. *Chem. Mater.*, **1998**, 10, 896.
6. Nielsen, C. B.; Bjrnholm, T.; *Macromolecules*, **2005**, 38, 25, 10379.
7. Emilie, M. G.; Kim, Y. G.; Mwaura, J. K.; Jones, A. G.; McCarley, T. D.; Shrotriya, V.; Reynolds, J. R. *Macromolecules*, **2006**, 39, 9132.
8. Cirpan, A.; Argun, A. A.; Grenier, R. G.; Reeves, B. D.; Reynolds, J. R. *J. Mater. Chem.*, **2003**, 13, 2422.
9. Mishra,S. P.; Sahoo, R.; Ambade, A. V.; Contractor A. Q.; Kumar, A. *J. Mater. Chem.*, **2004**, 14, 1896.
10. Grenier, R. G.; George,S. J.; Joncheray, T. J.; Meijer, E. W.; Reynolds, J. R. *J. Am. Chem. Soc.*, **2007**, 129, 35, 10694.
11. Thompson, B. C.; Kim, Y. G.; Reynolds, J. R. *Macromolecules*, **2005**, 38, 5359.
12. Thompson, B. C.; Kim, Y. G.; McCarley, T. D.; Reynolds, J. R. *J. Am. Chem. Soc.*, **2006**, 128, 12714.

13. Shin, W. S.; Kim, S. C.; Lee, S. J.; Jeon, H. S.; Kim, M. K.; Naidu, B. V. K.; Jin, S. H.;Lee, J. K.; Lee, J. W.; Gal, Y. S. *J. Polym. Sci.: Part A: Polym. Chem*., **2007**, 45, 1394.

14. Reeves, B. D.; Unur, E.; Ananthakrishnan, N.; Reynolds, J. R. *Macromolecule,* **2007**, 40, 5344.

15. Hammond, S. R.; Clot, O.; Firestone, K. A.; Bale,D. H.; Lao, D.; Haller, M.; Phelan, G. D.; Carlson, B.; Jen, A. K. Y.; Reid, P. J.; Dalton, L. R. *Chem. Mater*., **2008**, 20, 3425.

16. Amb, C. M.; Beaujuge, P. M.; Reynolds, J. R., *U. S. Patent*, **2011**, 0003967.

17. Parr, R.G.; Yang, W., *Density-Functional Theory of Atoms and Molecules;* Oxford University Press, New York, **1989**.

18. Becke, A. D., *J. Chem. Phys.*, **1993**, 98, 5648,.

19. Chengteh, L.; Weitao, Y.; Robert, G. P., *Phys. Rev. B,* **1988**, 37, 785.

20. Hay, P. J.; Wadt, W. R. *J. Chem. Phys*., **1985**, 82, 270.

21. Frisch, M. J.; Trucks, G. W.; Schlegel, H. B.; Scuseria, G. E.; Robb, M. A.; Cheeseman, JR, et al. Gaussian 03, revision A.1. Pittsburgh, PA: Gaussian, Inc; **2003.**

22. Wu, P. T.; Kim, F. S.; Champion, R. D.; Jenekhe, S. A. *Macromolecules,* **2008**, 41, 7021.

23. Sariciftci, N. S. *Primary Photoexcitations in Conjugated Polymers: Molecular Excitons* vs *Semiconductor Band Model*; World Scientific: Singapore, **1997**.

Chapter 6

SYNTHESIS, CHARACTERIZATION AND PHOTOVOLTAIC APPLICATIONS OF ProDOT/QUINOXALINE COPOLYMERS

Contents

In this chapter, a series of low band gap copolymers of 3,4-propylenedioxythiophene and quinoxaline were synthesized through direct arylation reaction using palladium acetate as catalyst. The band structures of the four polymers were calculated by employing density functional theory in the periodic boundary condition using HSE06 exchange correlation functional and 6-31G basis set. The polymers were characterized using ^{1}H NMR, UV-Vis, cyclic voltammetry and differenetial pulse voltammetry. The four polymers have energy gap below 2.0 eV and have broad absorption in the visible region. The electrochemical band gap showed deviation from theoretical and optical gap. This may be due to the difference in the mechanism of photo excitation and electrochemical redox processes or may be due to the swelling of the polymers in solution. The photovoltaic activity of the polymers was also tested using the ITO/In_2S_3/polymer/Ag heterojunction. The heterojunctions with PPRO-DQX, PPRO-DDACE, PPRO-DDQ and PPRO-DBDP showed efficiencies of 0.01%, 0.001%, 0.02% and 0.002% respectively.

6.1. Introduction

To achieve high efficiencies in organic polymer based solar cells, the active layer of polymer solar cells must have good absorption of sunlight. Since 54.3% of the sunlight energy is distributed in the visible region from 380 to 800 nm, an ideal active layer for a polymer solar cell should have a broad and strong absorption spectrum in this range[1]. ProDOT is proved to be an excellent donor unit in dye sensitized[2] solar cells and bulk hterojunction photovoltaic devices[3,4].

Quinoxaline has been widely implemented as an electron deficient comonomer of low-band gap polymers in photovoltaic devices. Quinoxaline containing segments were shown to be promising acceptors when combined with fluorene or thiophene forming D-A polymers[5-7]. The impressive performance of quinoxaline-based polymers has shown its obvious potential for achieving high performance in photovoltaic devices[5,6, 8-10]. In all the cases, the polymers are synthesized either through Stille or Suzuki polycondensation reaction, which make the synthesis tedious and costly. So we have tried to synthesize quinoxaline based polymers through direct arylation reaction. This process avoids the synthesis of distannane and diboronate esters, make the synthesis of polymer easier and cost effective. The theoretical calculation on polymers prior to synthesis gives more insight to the electronic structure of the polymers.

In this chapter, we discuss the electronic structure, synthesis, optical and electrochemical properties of four ProDOT/quinoxaline copolymers and have demonstrated the applicability of the polymers as active layer in photovoltaic devices. The structure-property relationship in these polymers are also discussed in detail.

6.2. Results and Discussion

6.2.1. Band structure calculation

The ground state geometries of oligomers were optimized by means of the hybrid density functional theory (DFT)[11] at the HSEh1PBE referred to as HSE06 in the literature (full Heyd-Scuseria-Ernzerhof functional)[12,13], level of theory using 6-31G basis set. The harmonic vibrational frequencies obtained with HSE06/6-31G were used to characterize the stationary points as local minima. The band structure was calculated using HSE06/6-31G theory using the unit cell taken from the central portion of the optimized tetramer. The calculation described in this chapter was done using G09 suite of codes[14] on IBM power servers.

The unit cell for the PBC/6-31G calculation is given in figure 1. The length of the unit cell is 16 A^o. The calculated band structure is shown in figure 2. It can be seen from the band structure that all the polymers are direct band gap polymers. The band gap of PPRO-DQX, PPRO-DDACE, PPRO-DDQ and PPRO-DBDP are 1.93 eV, 1.96 eV, 1.85 eV, and 1.74 eV respectively. The band gap of the polymer depends on the acceptor strength of the quinoxaline part. The acceptor strength of the quinoxaline part is in the order DQX< DDACE< DDQ< DBDP. PPRO-DQX and PPRO-DDACE show almost the same band gap due to the higher dihedral angle in PPRO-DDACE than the PPRO-DQX. In PPRO-DQX, the dihedral angle between the ProDOT and quinoxaline part is 30^0 while in PPRO-DDACE it is 48^0. So the steric hindrance to attain planarity plays a major role in determining the band gap of the polymers.

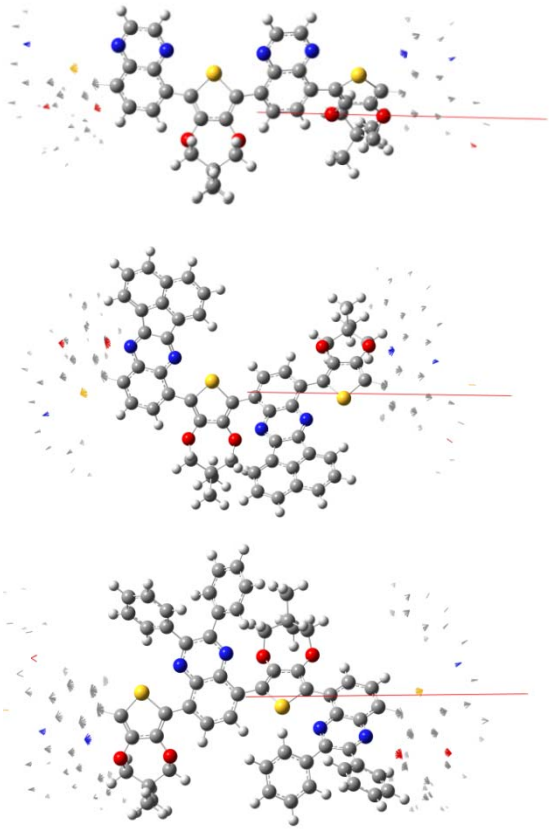

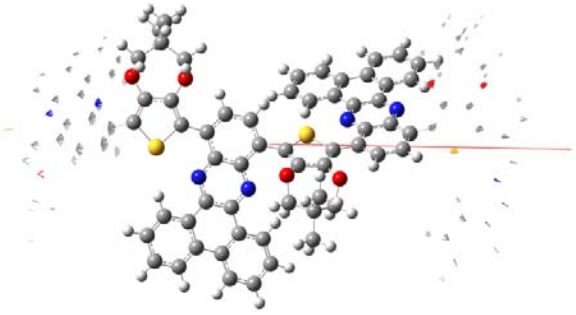

Figure 1: Unit cell for the PBC/HSE06/6-31G calculation of a. PPRO-DQX b. PPRO-DDACE, c. PPRO-DDQ and d. PPRO-DBDP

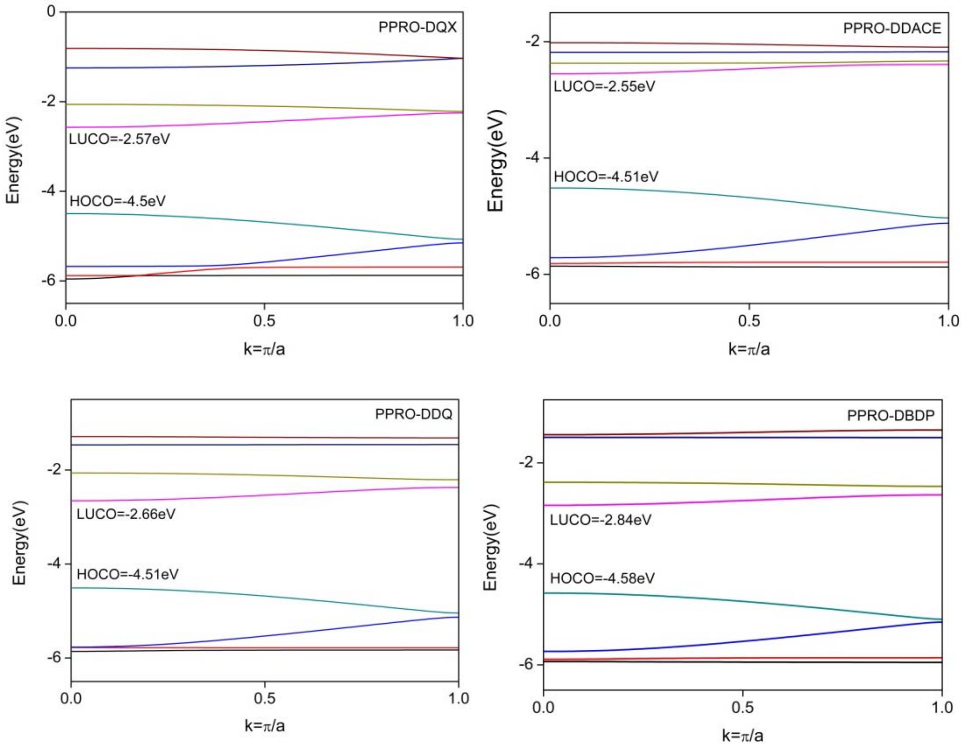

Figure 2: Band structures of a. PPRO-DQX, b. PPRO-DDACE, c. PPRO-DDQ and d. PPRO-DBDP

Table 1: Band structure data of polymers PPRO-DQX, PPRO-DDACE, PPRO-DDQ and PPRO-DBDP #

Polymer	HOCO(eV)	LUCO(eV)	Eg(eV)
PPRO-DQX	-4.5	-2.57	1.93
PPRO-DDACE	-4.51	-2.55	1.96
PPRO-DDQ	-4.51	-2.66	1.85
PPRO-DBDP	-4.58	-2.84	1.74

#Method PBC/HSE06/6-31G

6.2.2. Synthesis of monomers and polymers

The synthetic path towards DDACE, DDQ and DBDP are depicted in chapter III. The 5,8-dibromoquinoxaline (DQX) was synthesized from 3,6-dibromo-1,2-diaminobenzene and glyoxal in triethylamine/ethanol solution (scheme 1)[15]. The polymers, PPRO-DQX, PPRO-DDACE, PPRO-DDQ and PPRO-DBDP were synthesized through direct arylation reaction of ProDOT with DQX, DDACE, DDQ and DBDP respectively using palladium acetate as catalyst in DMF at 90^0C (scheme 2). PPRO-DQX, PPRO-DDACE, PPRO-DDQ and PPRO-DBDP were obtained in 44%, 57%, 36%, and 39% yield. The monomers and polymers were characterized using ^{1}H NMR, UV-Visible and fluorescence spectroscopy, cyclic voltammetry and differential pulse voltammetry. The thermal stability of the polymers was analysed using thermogravimetric analysis. It was found that, the polymers were stable up to 330^0C by TG/DTA analysis. The thermal stability of the polymers are adequate enough to fabricate photovoltaic cells. The number average and weight averge molecular weights of the polymers were determined using GPC in toluene using polystyrene as calibration standard. The weight average molecular weight of the polymers ranged from 4000-16900 Da. The M_n, M_w and PDI of polymers along with their thermal stability are tabulated in table 2. ^{1}H NMR spectrum of the polymers showed broad peak at δ 3.9-4.2 due to –O-

CH_2- protons except in the case of PPRO-DDQ which showed two peaks in that region. The singlet in this region confirms the alternating D-A type geometry of the polymers. In the case of PPRO-DDQ the two peaks may be due to the different chemical environment of the four $-OCH_2$ protons by the free rotation about the bonds with phenyl groups on the quinoxaline ring system. In the case of PPRO-DQX, one broad peak at δ 8.92 due to the aromatic protons of the quinoxaline was observed, which also confirmed the alternating nature of the polymers. The ^1H NMR spectra of the polymers are shown in figure 3.

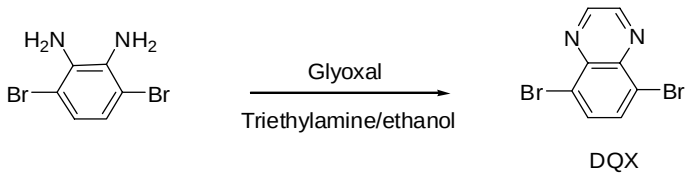

Scheme 1: Synthesis of 5,8-dibromoquinoxaline

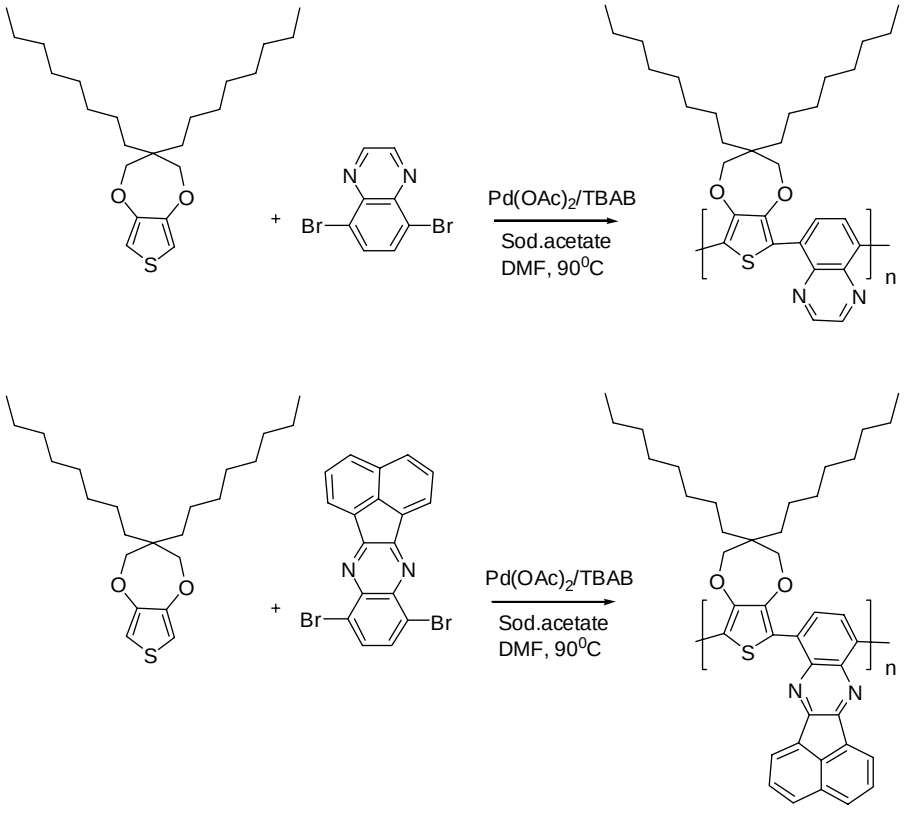

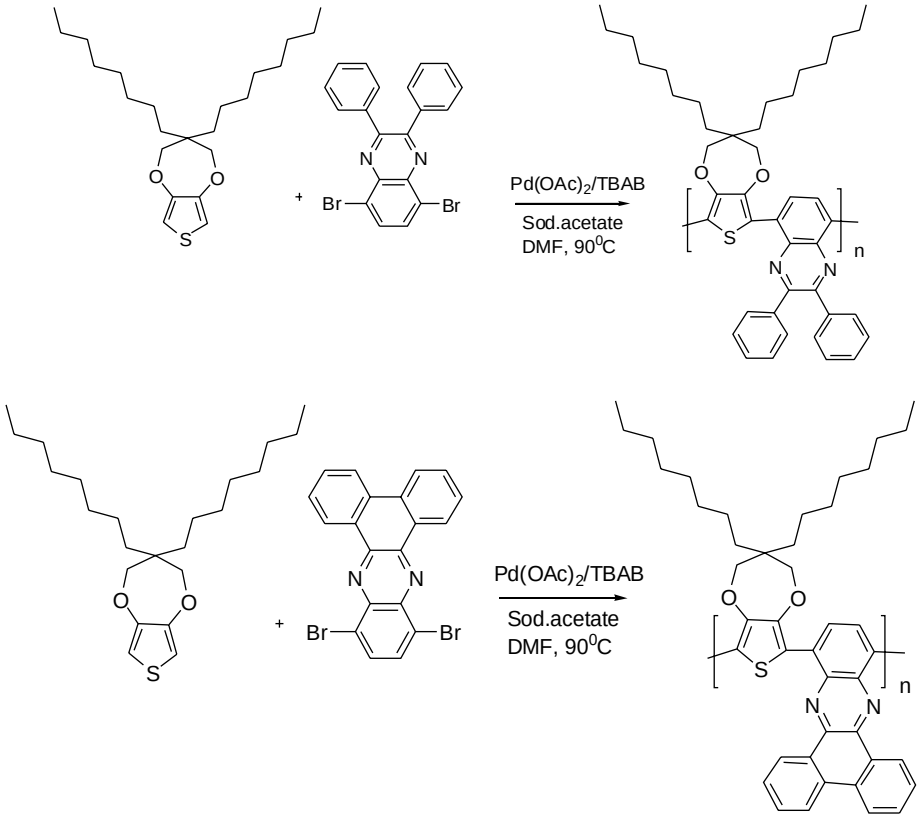

Scheme 2: Synthesis of PPRO-DQX, PPRO-DDACE, PPRO-DDQ and PPRO-DBDP

Table 2: Polymerization results and thermal stability of polymers

Polymer	M_n[a]	M_w[a]	PDI	Yield (%)	T_d (^{0}C)
PPRO-DQX	5954	16835	2.82	44	338
PPRO-DDACE	3419	4719	1.38	57	332
PPRO-DDQ	3248	3996	1.23	36	346
PPRO-DBDP	5512	8593	1.55	39	364

a. Determined using GPC in toluene using polystyrene as standard
b. Decomposition temperature determined TGA under nitrogen

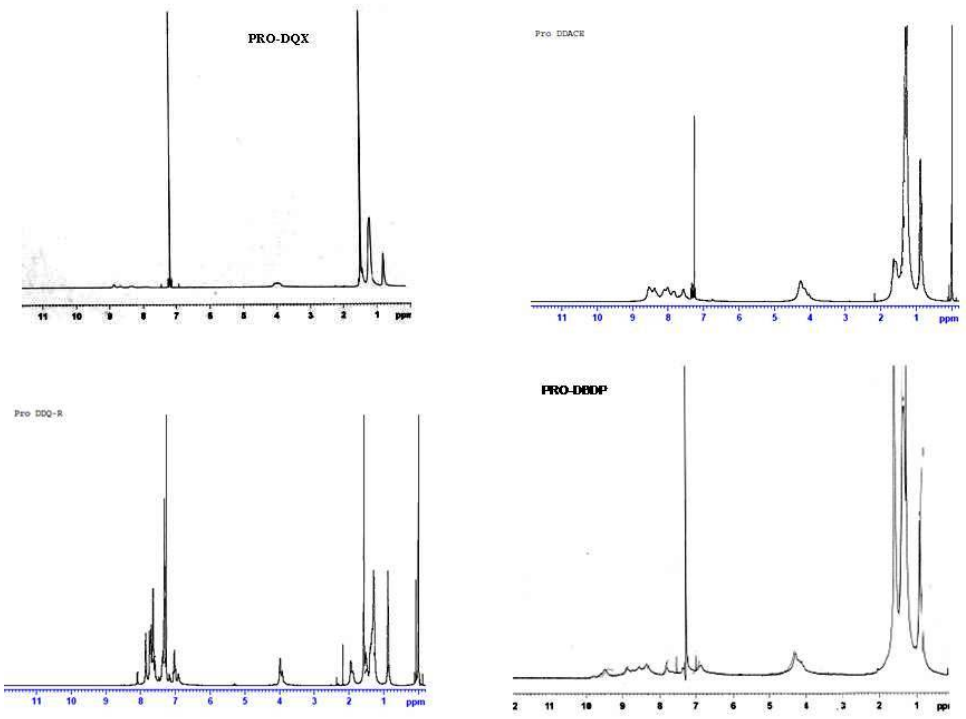

Figure 3: ^{1}H NMR spectrum of PPRO-DQX, PPRO-DDACE, PPRO-DDQ and PPRO-DBDP

6.2.3. Optical properties

The absorption spectrum of the polymers in chloroform solution is given in figure 4. The absorption maxima of the polymers PPRO-DQX, PPRO-DDACE, PPRO-DDQ and PPRO-DBDP occur at 525 nm, 538 nm, 567 nm, and 598 nm respectively. In thin film on glass plate, absorption maxima were red shifted by about 17 nm, 25 nm, 5 nm, and 20 nm respectively compared to that of polymers in solution. The shift is greater for PPRO-DDACE and PPRO-DBDP. This may be due to the π-π interaction between the polymer chains, which induce planarity for the polymer in solid state. The shift is less for PPRO-DDQ. This may be due to the puckered orientation of the phenyl rings in the quinoxaline. From this, we assume that, by linking the two phenyl rings in quinoxaline induces

ordering of the polymer chain which facilitates the charge transport and enhances the photovoltaic properties. The onset of absorption was used to calculate the optical band gap of the polymers. The onset of absorption of PPRO-DQX, PPRO-DDACE, PPRO-DDQ and PPRO-DBDP occur at 720 nm, 730 nm, 742 nm, and 768 nm which correspond to the band gap of 1.73 eV, 1.70 eV, 1.67 eV and 1.62 eV respectively. The optical band gap of the polymers are in agreement with the order predicted theoretically using the acceptor strength of the quinoxaline part. The order of band gap of PPRO-DQX and PPRO-DDACE deviate from those predicted by the theoretical calculation. This is because, theoretical calculations were done on infinite isolated polymer chains in the gas phase, while the optical measurements are done in condensed phase. Moreover, the conformations and inter polymer chain interactions of the polymers in the solid state were ignored in the periodic boundary condition calculation. The nature of the end groups of the polymers also affect the optical properties of the polymers, which is also ignored in the theoretical calculation.

The photoluminescence spectra of the polymers are recorded in chloroform solution using the absorption maximum of each polymer as the excitation wavelength and is shown in figure 5. The emission maxima of the polymers occur at 670 nm, 661 nm, 674 nm, and 714 nm respectively. The optical properties of the polymers are summarized in table 3.

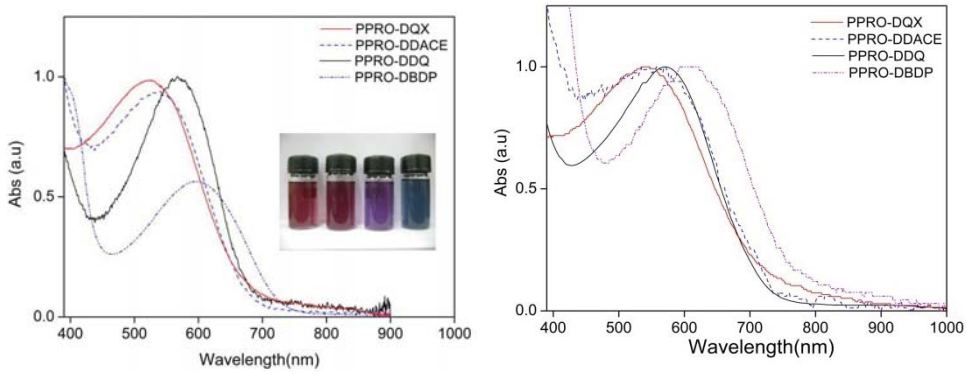

Figure 4: Absorption spectra of the polymers a. in chloroform solution and in film on glass plate.

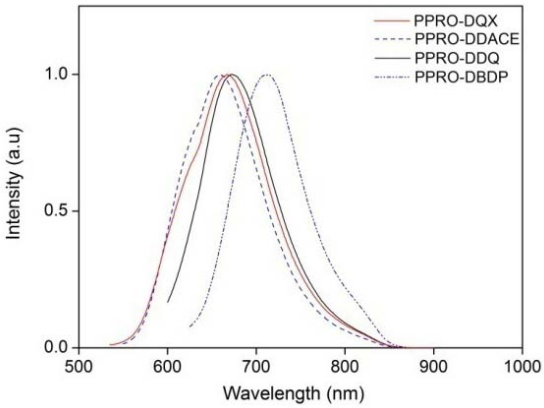

Figure 5: PL spectra of the polymer in chloroform solution

Table 3: Optical properties of the polymers

Polymer	Absorption λ_{max}(nm)		Emission λ_{max} (nm)	Absorption Onset (nm)	E_g^{opt} (eV)
	Solution	Film			
PPRO-DQX	525	543	670	720	1.73
PPRO-DDACE	538	563	661	730	1.70
PPRO-DDQ	567	572	674	742	1.67
PPRO-DBDP	598	618	714	768	1.62

6.2.4. Electrochemical properties

The electrochemical properties of the polymers were investigated using cyclic voltammetry on polymer films on a platinum electrode in 0.1 M Bu_4NPF_6/acetonitrile solution. The cyclic voltammogram of the polymers are shown in figure 6. It could be seen that all the polymers showed one reduction peak and one oxidation peak. The electrochemical band gap of the polymers are calculated using the formula proposed by Bredas[16]. The band gap of the polymers PPRO-DQX, PPRO-DDACE, PPRO-DDQ and PPRO-DBDP are 2.09 eV, 2.41 eV, 2.22 eV, and 2.02 eV respectively. The band gap order does not correlate with neither the theoretical values nor the optical band gap. The electrochemically determined values are verified by running the same experiment for several times to eliminate the experimental defects. But the values are unchanged for all the measurements. In order to verify this, we have also done the differential pulse voltammetry on the polymer films on platinum electrode in 0.1 M Bu_4NPF_6/acetonitrile solution. The DPV measured band gap of PPRO-DQX, PPRO-DDACE, PPRO-DDQ and PPRODBDP are 1.9 eV, 2.19 eV, 2.18 eV, and 1.66 eV. These values also do not support the theoretical and optical band gap values. In order to correlate this with the optical and theoretical values, we need to calculate the excitonic binding energy and solvation energy of the polymers. The electrochemical properties of the polymers are summarized in table 4.

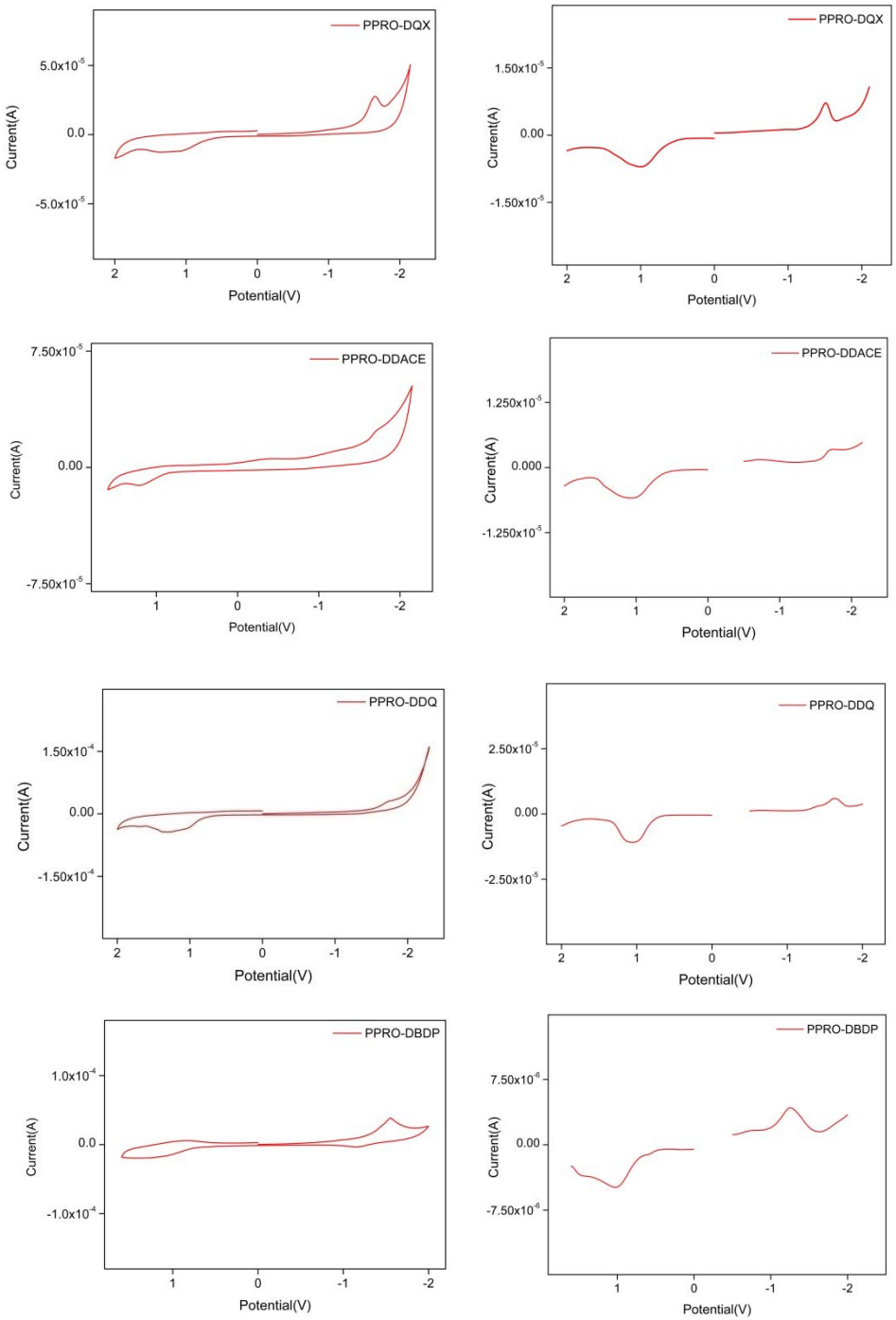

Figure 6: Cyclic voltammograms and differential pulse voltammograms of PPRO-DQX, PPRO-DDACE, PPRO-DDQ and PPRO-DBDP films cast on a platinum electrode in Bu_4NPF_6/acetonitrile

Table 4: Electrochemical data of the polymers

Polymer	Cyclic Voltammetry					Differential Pulse Voltammetry				
	E_{red} (V)	E_{ox} (V)	HOMO (eV)	LUMO (eV)	E_g (eV)	E_{red} (V)	E_{ox} (V)	HOMO (eV)	LUMO (eV)	E_g (eV)
PRO-DQX	-1.438	0.649	-5.05	-2.96	2.09	-1.271	0.627	-5.03	-3.13	1.9
PRO-DDACE	-1.558	0.845	-5.25	-2.84	2.41	-1.577	0.611	-5.01	-2.82	2.19
PRO-DDQ	-1.547	0.668	-5.07	-2.85	2.22	-1.44	0.741	-5.14	-2.96	2.18
PRO-DBDP	-1.276	0.743	-5.14	-3.12	2.02	-1.012	0.653	-5.05	-3.39	1.66

6.2.5. Photovoltaic devices

The suitability of the polymers as active layer in photovoltaic device was verified by fabricating a heterojunction device using the polymers and the semiconductor In_2S_3. Figure 9 shows the current density-voltage (J-V) characteristics of the heterojunctions under illumination and in the dark. As could be seen, the devices clearly exhibit rectifying behaviour in the dark which may be due to the barrier formed at the In_2S_3/ polymer interface. Under white light illumination (50mW/cm^2), the device ITO/In_2S_3/polymer/Ag heterojunction of PPRO-DQX, PPRO-DDACE, PPRO-DDQ and PPRO-DBDP exhibited efficiencies of 0.01%, 0.001%, 0.02%, 0.002% respectively. The important photovoltaic characteristics of bilayer heterojunction devices of polymers are summarized in table 5.

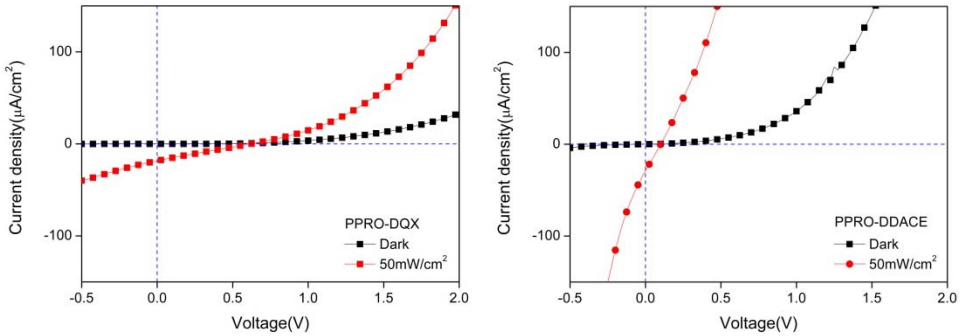

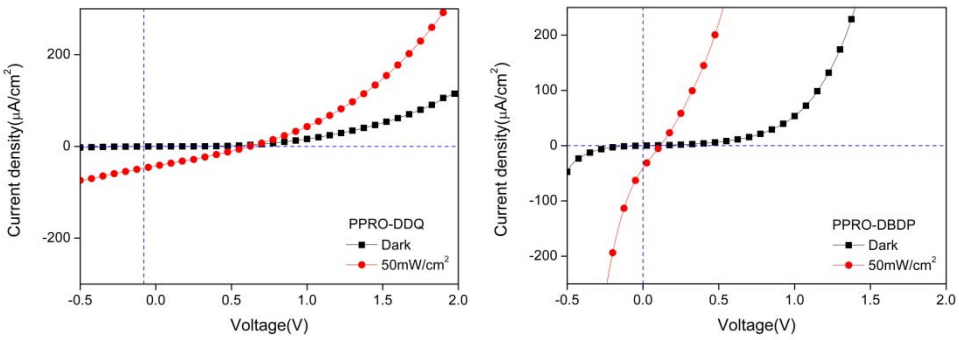

Figure 7: J-V characteristics of ITO/In_2S_3/polymer/Ag heterojunctions of PPRO-DQX, PPRO-DDACE, PPRO-DDQ and PPRO-DBDP

Table 5: J-V characteristics of ITO/In_2S_3/polymer/Ag heterojunctions

Polymer	V_{oc} (mV)	J_{sc} (μA/cm^2)	Efficiency (%)	Fill Factor (%)
PPRO-DQX	620.76	18.4	0.01	24.10
PPRO-DDACE	110.95	28.9	0.001	22.90
PPRO-DDQ	622.08	42.6	0.02	28.41
PPRO-DBDP	113.25	40.4	0.002	24.58

6.3. Conclusions and perspectives

In conclusion, we have designed theoretically a series of polymers containing ProDOT and quinoxaline as core units. The polymers are synthesized through cost effective direct arylation reaction. Direct arylation reaction was found to be convenient method for synthesizing the donor-acceptor polymers. Optical properties were correlated with the theoretical values. But the electrochemical band gap deviated from both the optical and theoretical values. This may be due to the difference in the mechanism of optical and electrochemical processes. In order to correlate the electrochemical measurement with the others, we have to calculate the solvation energy and exciton binding energy of the polymers. The feasibility of the polymers for photovoltaic application was demonstrated by fabricating a bilayer heterojunction device with a device structure ITO/In_2S_3/polymer/Ag and showed photoactivity under illumination.

Further improvement in the efficiency of the device can be achieved by optimizing the device parameters.

6.4. Experimental methods

The synthetic route towards DDACE, DDQ, DBDP, and ProDOT have been depicted in chapter III and chapter IV.

6.4.1. 5,8-Dibromoquinoxaline (DQX)

2,3-Diamino-1,4-dibromobenzene (2.45 g, 0.39 mmol) was dissolved in ethanol (30 mL). Glyoxal (1.5 mL, 40 wt. % solution in water) and few drops of dry triethylamine were added. The mixture was stirred at room temperature overnight. The white crystals that had formed were filtered off and recrystallized from ethanol to give white solid. Yield : 0.76 g (76%).

^{1}H-NMR (400 MHz, $CDCl_3$) : δ 9.01 (s, 2H), 8.00 (s, 2H).

^{13}C-NMR (100 MHz, $CDCl_3$) : δ 146, 141.56, 133.72, 123.97.

M. P. : 199^{0}C (literature 203^{0}C)

6.4.2. General procedure for direct arylation reaction

ProDOT, (0.17 mmol), tetrabutylammonium bromide (0.17 mmol), sodium acetate (0.69 mmol) and DMF (10 mL) were stirred at room temperature for 15 min. of dibromo derivative of quinoxaline (0.17 mmol) and palladium acetate (10 mol%) were added. The reaction mixture was stirred at 90^{0}C for 48 h. The reaction mixture was cooled and poured in to cold methanol. The precipitate was filtered. The polymer was purified by soxhlet extraction by successively using methanol and acetone as solvent. The polymer was dissolved in minimum amount of chloroform and precipitated in methanol. The precipitate was filtered and dried in vacuum for 24 h.

6.4.2.1. Synthesis of PPRO-DQX

ProDOT (0.066 g, 0.17 mmol), DQX (0.050 g, 0.17 mmol), Palladium acetate (0.0038 g, 0.017 mmol), Sodium acetate (0.094 g, 0.69

mmol), tetrabutylammonium bromide (0.056 g, 0.17 mmol), DMF (10 mL) were used. Brown solid.

Yield	:	44% (38 mg)
T_d (^{0}C)	:	338
UV-Visible λ_{max} (chloroform)	:	525 nm
IR (cm^{-1})	:	3435.56, 2923.56, 2855.1, 1633.41, 1462.74, 1424.17, 1375, 1318.11, 1049.09, 857.20
^{1}H NMR (400 MHz, $CDCl_3$)	:	δ 8.94 (b, ~2H of quinoxaline), 8.32 (b, ~2H of quinoxaline), 4.09-3.98 (b, ~4H, -OCH_2 of ProDOT), 1.7-1.22 (m, ~28H, aliphatic-H), 0.82 (b, ~6H, -CH_3)
GPC	:	M_n=5954, PDI= 2.82

6.4.2.2. Synthesis of PPRO-DDACE

ProDOT (0.066 g, 0.17 mmol), DDACE (0.071 g, 0.17 mmol), Palladium acetate (0.0038 g, 0.017 mmol), Sodium acetate (0.094 g, 0.69 mmol), tetrabutylammonium bromide (0.056 g, 0.17 mmol), DMF (10 mL) were used: Brown solid

Yield	:	56.8% (60.8 mg)
T_d (^{0}C)	:	332
UV-Visible λ_{max} (chloroform)	:	538 nm
IR	:	3434, 2922.59, 2850, 1635.34, 1566.88, 1464.67, 1419.35, 1373, 1300.75, 1083.8, 1032.69, 775.24
^{1}HNMR (400 MHz, $CDCl_3$)	:	8.91- 7.6 (m, ~8H of quinoxaline part), 4.2 (bs, ~4H, -OCH_2- of

ProDOT), 1.8-0.9 (m, ~28H, aliphatic-H), 0.88 (b, ~6H, $-CH_3$)

GPC : M_n=3419, PDI=1.38

6.4.2.3. Synthesis of PPRO-DDQ

ProDOT (0.066 g, 0.17 mmol), DDQ (0.075 g, 0.17 mmol), Palladium acetate (0.0038 g, 0.03 mmol), Sodium acetate (0.094 g, 0.69 mmol), tetrabutylammonium bromide (0.056 g, 0.17mmol), DMF (10 mL) were used. Violet solid

Yield : 36% (40.4 mg)

T_d (^{0}C) : 346

UV-Visible λ_{max} (chloroform) : 567 nm

IR (cm^{-1}) : 3436.53, 2923.56, 2852.2, 1605.45, 1566.88, 1416.46, 1382.71, 1331.61, 1228.43, 1057.76, 1026.91, 782.95, 760.78, 696.18

^{1}HNMR (400 MHz, $CDCl_3$) : δ 7.88-7.2 (m, ~12H of quinoxaline part), 3.99-3.87 (m, ~4H, $-OCH_2-$), 2.17-1.09 (m, ~28H, aliphatic-H), 0.84 (m, 6H, $-CH_3$)

^{13}C NMR (100 MHz, $CDCl_3$) : 130.12, 128.22, 77.29, 77.04, 76.78, 31.84, 29.31, 22.68, 14.16

GPC : M_n =3248, PDI= 1.23

6.4.2.4. Synthesis of PPRO-DBDP

ProDOT (0.066 g, 0.17 mmol), DBDP (0.074 g, 0.17 mmol), Palladium acetate (0.0038 g, 0.03 mmol), Sodium acetate (0.094 g, 0.69 mmol), tetrabutylammonium bromide (0.056 g, 0.17 mmol), DMF (10 mL) were used. Blue solid

Yield : 38.9% (43.6 mg)

T_d (^{0}C)	:	364
UV-Visible λ_{max} (chloroform)	:	598 nm
^{1}HNMR (400 MHz, $CDCl_3$)	:	δ 9.48-7.52 (m, ~10H of quinoxaline part), 4.3 (bs, ~4H, -OCH_2- of ProDOT), 1.8- 1.25 (m, ~28H, aliphatic-H), 0.9 (b, ~6H, -CH_3)
GPC	:	M_n=5512, PDI=1.55

6.5. References

1. Hou, J.; Chen H. Y.; Zhang, S.; Li, G.; Yang, Y. *J. Am. Chem. Soc.*, **2008**, 130,16144.
2. Liang, Y.; Peng, B.; Liang, J.; Tao, Z.; Chen, J. *Org. Lett.*, **2010**, 12, 1204.
3. Shin, W. S.; Kim, S. C.; Lee, S. J.; Jeon, H. S.; Kim, M. K.; Naidu, B. V. K.; Jin, S. H.; Lee, J. K.; Lee, J. W.; Gal, Y. S, *J. Polym. Sci.: Part A: Polym. Chem.*, **2007**, 45, 1394.
4. Thompson, B. C.; Kim, Y.-G.; Mccarley, T. D.; Reynolds, J. R., *J. Am. Chem. Soc*., **2006**, 128, 12714.
5. Gadisa, A.; Mammo, W.; Andersson, L. M.; Admassie, S.; Zhang, F. L.; Andersson, M. R.; Inganas, O. *Adv. Funct. Mater*., **2007**, 17, 3836.
6. Lindgren, L. J.; Zhang, F. L.; Andersson, M.; Barrau, S.; Hellstrom, S.; Mammo, W.; Perzon, E.; Inganas, O.; Andersson, M. R. *Chem. Mater*., **2009**, 21, 3491.
7. Wang, E. G.; Hou, L. T.; Wang, Z. Q.; Hellstrom, S.; Zhang, F. L.; Inganas, O.; Andersson, M. R. *Adv. Mater*., **2010**, 22, 5240.

8. Zhang, F. L.; Bijleveld, J.; Perzon, E.; Tvingstedt, K.; Barrau, S.; Inganas, O.; Andersson, M. R. *J. Mater. Chem.*, **2008**, 18, 5468.
9. Zhou, E. J.; Cong, J. Z.; Tajima, K.; Hashimoto, K. *Chem.Mater.*, **2010**, 22, 4890.
10. Kitazawa, D.; Watanabe, N.; Yamamoto, S.; Tsukamoto, *J. Appl. Phys. Lett.*, **2009**, 95, 053701.
11. Parr, R. G.; Yang, W., *Density-Functional Theory of Atoms and Molecules;* Oxford University Press, **1989**, New York.
12. Heyd, J.; Scuseria, G. E.; Ernzerhof, M. *J. Chem. Phys.*, **2003**, 118, 8207.
13. Krukau, A. V.; Vydrov, O. A.; Izmaylov, A. F.; Scuseria, G. E. *J. Chem. Phys.*, **2006**, 125, 224106.
14. Gaussian 09, Revision B02, Frisch, M. J.; Trucks, G. W.; Schlegel, H. B.; Scuseria, G. E.; Robb, M. A.; Cheeseman, J. R.; Scalmani, G.; Barone, V.; Mennucci, B.; Petersson, G. A.; Nakatsuji, H.; Caricato, M.; Li, X.; Hratchian, H. P.; Izmaylov, A. F.; Bloino, J.; Zheng, G.; Sonnenberg, J. L.; Hada, M.; Ehara, M.; Toyota, K.; Fukuda, R.; Hasegawa, J.; Ishida, M.; Nakajima, T.; Honda, Y.; Kitao, O.; Nakai, H.; Vreven, T.; Montgomery, Jr., J. A.; Peralta, J. E.; Ogliaro, F.; Bearpark, M.; Heyd, J. J.; Brothers, E.; Kudin, K. N.; Staroverov, V. N.; Kobayashi, R.; Normand, J.; Raghavachari, K.; Rendell, A.; Burant, J. C.; Iyengar, S. S.; Tomasi, J.; Cossi, M.; Rega, N.; Millam, N. J.; Klene, M.; Knox, J. E.; Cross, J. B.; Bakken, V.; Adamo, C.; Jaramillo, J.; Gomperts, R.; Stratmann, R. E.; Yazyev, O.; Austin, A. J.; Cammi, R.; Pomelli, C.; Ochterski, J. W.; Martin, R. L.; Morokuma, K.; Zakrzewski, V. G.; Voth, G. A.; Salvador, P.; Dannenberg, J. J.; Dapprich, S.; Daniels, A. D.;

Farkas, Ö.; Foresman, J. B.; Ortiz, J. V.; Cioslowski, J.; Fox, D. J. Gaussian, Inc., Wallingford CT, **2009**.

15. Karsten, B. P.; Bijleveld, J. C.; Viani, L.; Cornil, J.; Gierschner , J.; Janssen, R. A. J. *J. Mater. Chem.*, **2009**, 19, 5343.
16. Bredas, J. L.; Silbey, R.; Boudreux, D. X.; Chance, R. R. *J. Am. Chem. Soc.*, **1983**, 105, 6555.

Chapter 7

SYNTHESIS, CHARACTERIZATION AND PHOTOVOLTAIC PROPERTIES OF ProDOT/1-ALKYL-1,2,4-TRIAZOLE COPOLYMERS WITH CROSS CONJUGATED FRAME WORK STRUCTURE

Contents

Two novel 3.4-propylenedioxythiophene/1-alkyl-1,2,4-triazole copolymers with decyl and ethylhexyl side chains were synthesized through direct arylation reaction. The band strcture of the polymers were calculated using density functional theory. The HOCO, LUCO and band gap were calculated to be -4.95 eV, -2.65 eV and 2.3 eV respectively. The frontier energy levels and energy gap were experimentally determined using cyclic voltammetery, differenetial pulse voltammtery and optical measurement. The theoretically calculated values were in reasonable agreement with experimental results. A photovoltaic device with a device structure ITO/In_2S_3/Polymer/Ag was fabricated which showed efficiencies of 0.06% and 0.08% for PPRO-TD2 and PPRO-TEH2 respectively.

7.1. Introduction

1,2,4-triazole has been used as electron transporting and hole blocking layer in organic LEDs[1], due to the electron accepting ability of the electron withdrawing imine -C=N- group in the unit[2]. Charge transfer type alternating conjugated polymers bearing thiophene and 4-alkyl-1,2,4-triazole was synthesized through Stille coupling reaction and its π-stacked structure in solid state was studied[3].

1-alkyl-1,2,4-triazole/ProDoT copolymers have short conjugated system than the 4-alkyl-1,2,4-triazole/ProDOT copolymer. For example, in figure 1, PRO-1TZ carries only 6-π conjugated electrons, while PRO-4TZ carries 8-π conjugated electrons. The π-conjugated system is broken by two consecutive single bonds (b-c and c-e bond). The main feature of these types of cross conjugated systems is that they are able to expand their π-electron system[4]. The extent of expansion is smaller than the fully conjugated system. The polymeric systems containing 1,2,4-triazole which has cross-conjugated π-framework is a subject of recent interest because of the small expansion of π-conjugation and electron withdrawing nature of the 1-alkyl-1,2,4-triazole unit[5]. So 1-alkyl-1,2,4-triazole unit can be used as a building block in tuning the electronic and optical properties of the π-conjugated polymers, to make them suitable for special purposes.

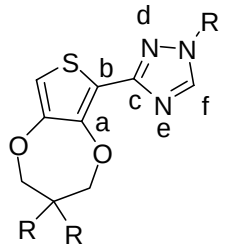

PRO-1TZ

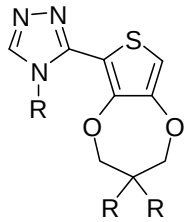

PRO-4TZ

Figure 1: Monomeric unit of ProDOT/1-alkyl-1,2,4-triazole and ProDOT/4-alkyl-1,2,4-triazole

This chapter deals with electronic property calculation, synthesis, characterization and photovoltaic properties of two new copolymers with cross conjugated structure, poly(dioctyl ProDOT/1-decyl-1,2,4-triazole)(PPRO-TD2) and poly(dioctyl ProDOT/1-ethyl hexyl-1,2,4-triazole) (PPRO-TEH2).

7.2. Results and Discussion

7.2.1. Theoretical studies

The ground state geometries of oligomers were optimized by means of the hybrid density functional theory (DFT)[6] at the HSEh1PBE (referred to as HSE06 in the literature) (Heyd-Scuseria-Ernzerhof functional)[7,8], level of theory using 6-31G basis set. The harmonic vibrational frequencies obtained with HSE06/6-31G were used to characterize the stationary points as local minima. The band structure was calculated using HSE06/6-31G theory using the unit cell taken from the central portion of the optimized tetramer. All the calculations were done using G09 software[9].

The optimized repeating unit for the periodic boundary calculation is given in figure 2. The long alkyl chain is replaced by methyl group to save the computational time. For both the polymers, length of the translational vector is ~13.98 A^0. It can be seen from figure 3 that, lowest band gap occur at Γ point (k=0), suggesting that both the polymers are direct band gap polymers. The HOCO occurs at -4.95 eV and LUCO occurs at -2.65 eV and we get a band gap of 2.3 eV. On comparing the band structure with poly(ProDOT), we can see that HOCO was decreased by a factor of 1.16 eV and LUCO was decreased by 0.6 eV. So 1-alkyl triazole is an effective candidate for lowering the HOMO and LUMO level of conjugated polymer, to make them suitable material for the fabrication of the photovoltaic devices. The band structure calculation data of poly(ProDOT) and poly(ProDOT/1-alkyl-1,2,4-triazole) are summarized in table 1. Based on this encouraging theoretical observation, the copolymers PPRO-TD2 and PPRO-TEH2 with decyl and 2-ethylhexyl side chain were synthesized through direct arylation reaction.

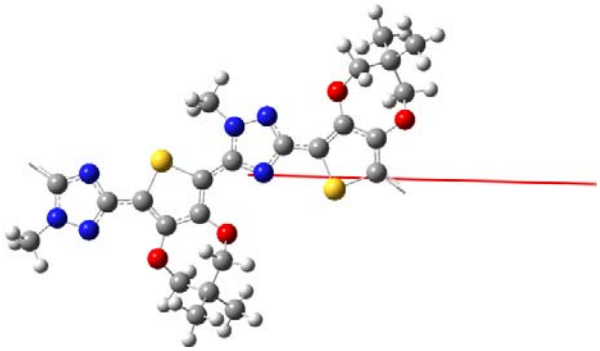

Figure 2: Unit cell for the HSE06 band structure calculation

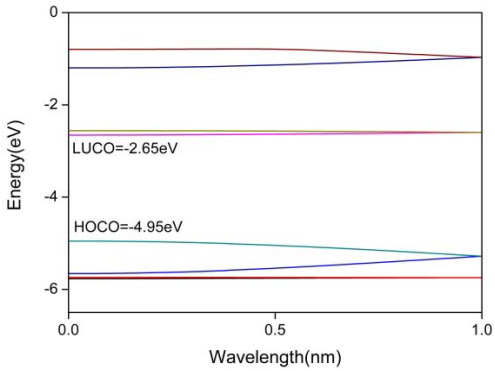

Figure 3: Band structure of ProDOT/1-alkyl-1,2,4-triazole copolymer

Table 1: Band structure data of ProDOT/1-alkyl-1,2,4-triazole copolymer[a]

Polymer	HOCO(eV)	LUCO(eV)	Eg(eV)
Poly(ProDOT)	-3.79	-2.03	1.76
Poly(ProDOT/1-alkyl triazole)	-4.95	-2.65	2.3

a. Calculated using PBC/HSE06/6-31G and PBC/B3LYP/6-31G method

7.2.2. Synthesis and characterization of monomers and polymers

7.2.2.1. Synthesis of Monomers

The synthetic routes towards ProDOT is depicted in chapter IV. The synthetic path towards the two 1-alkyl-3,5-dibromotriazole (TD2 and TEH2) is depicted in scheme 1. 1H-3,5-dibromotriazole was synthesized by bromination of 1H-1,2,4-triazole. This was alkylated with 1-bromodecane

and 1-bromo-2-ethylhexyl bromide to get TD2 and TEH2 in 82% and 77% yield respectively. There is no tautomeric migration of alkyl group from 1-position to 4-position as seen in 1H-1,2,4-triazole and 4H-1,2,4-triazole. This is confirmed by ^{1}H and ^{13}C NMR spectra of TD2 and TEH2 (figure 4 and figure 5). ^{13}C NMR spectra of TD2 and TEH2 show two distinct aromatic peaks at 129 and 140, while the 4-alkyl isomer shows only one peak above 130 ppm.

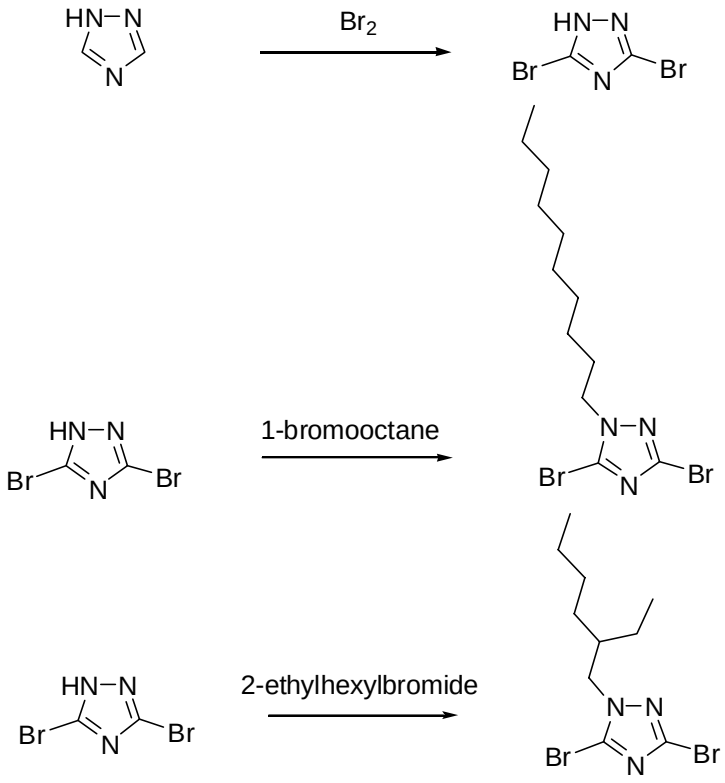

Scheme 1: Synthesis of monomers TD2 and TEH2

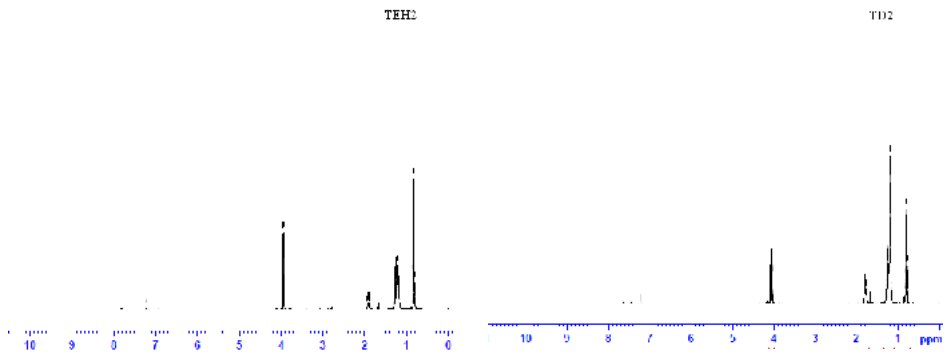

Figure 4: ^{1}H NMR spectra of TEH2 and TD2

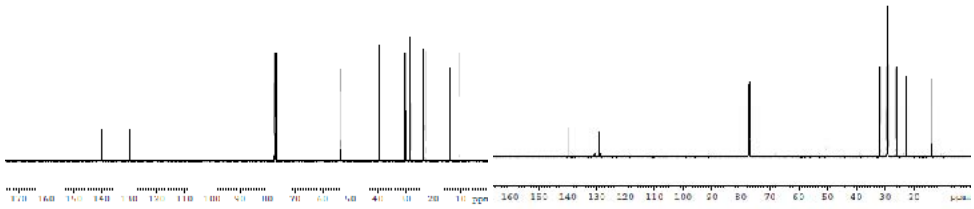

Figure 5: ^{13}C NMR spectra of TEH2 and TD2

7.2.2.2. Polymer synthesis

The polymers PPRO-TD2 and PPRO-TEH2 were synthesized by the reaction of 1-alkyl-3,5-dibromotriazole and dioctyl (3,4-propylenedioxythiophene) [ProDOT] based on direct arylation reaction using palladium acetate as catalyst (scheme 2). Both the polymers were soluble in common organic solvents such as chloroform, chlorobenzene, toluene, THF etc. Table 2 summarizes the polymerization results including molecular weight, PDI, and thermal stability of the copolymers. The low yield of the polymers may be due to the steric hindrance caused by the alkyl chain in the triazole unit. The polymers have weight average molecular weight of 8059 and 10434 with narrow polydispersity. The polymers are characterized using ^{1}H NMR, cyclic voltammetry, differential pulse voltammetry, XRD, UV-Visible spectroscopy, TGA etc. The ^{1}H NMR spectra of the polymers are shown in the figure 6. As shown in the figure, the signals corresponding to the end group are absent in the spectra of the polymers due to moderately good molecular weight of the polymer.

The non regularity of the polymers was confirmed by analyzing the signals in the region δ 4-4.3. The polymers showed multiplet in this region due–O-CH_2- protons. If the polymer is regioreguler we get only two peaks. The peak corresponding to the –NCH_2- protons appeared as triplet in the region δ 3.9. The thermal properties of the copolymers were determined by TGA measurements. The copolymers showed good thermal stability, with onset decomposition temperature (T_d, 5% weight loss) of 330°C under nitrogen (table 2).

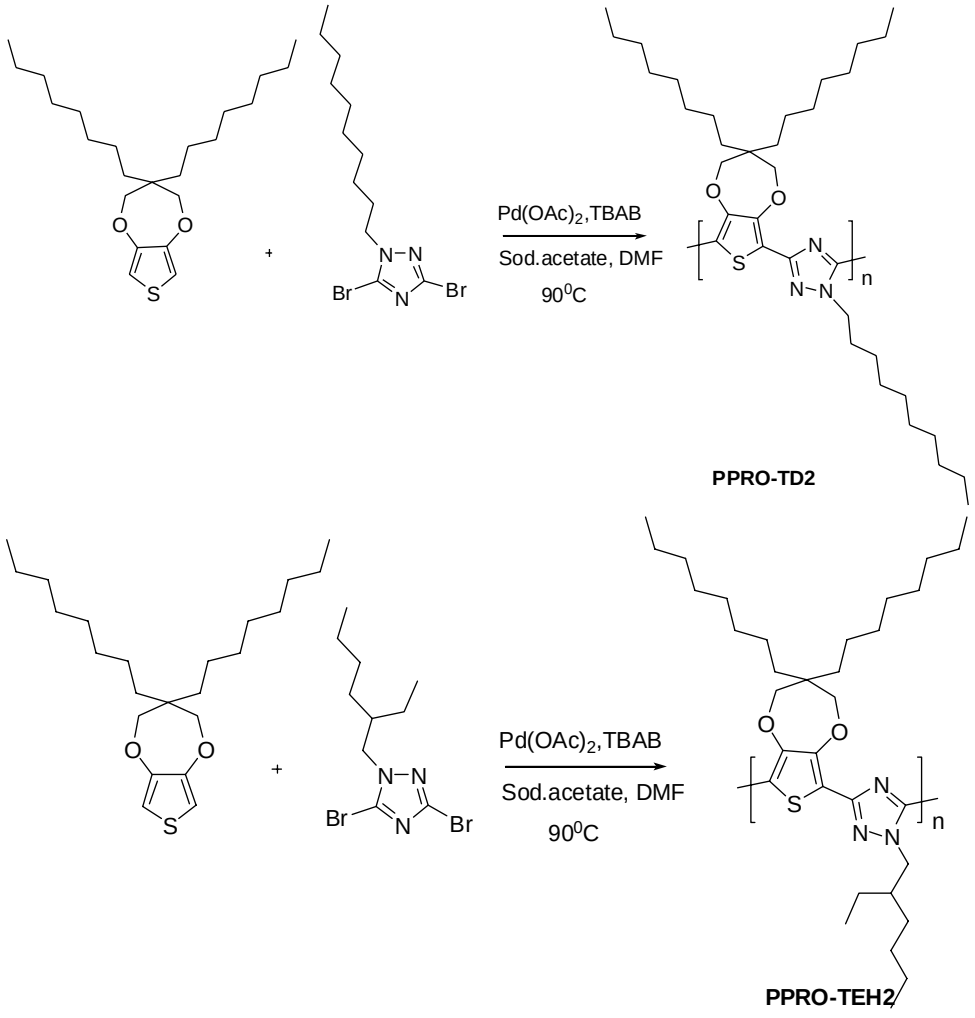

Scheme 2: Synthesis of polymers, PPRO-TD2 and PPRO-TEH2

Table 2: Polymerization results and thermal stability of polymers

Polymer	M_n	M_w	PDI	Yield (%)	T_d (^{0}C)
PPRO-TD2	5992	8059	1.34	21	334
PPRO-TEH2	6379	10434	1.63	27	339

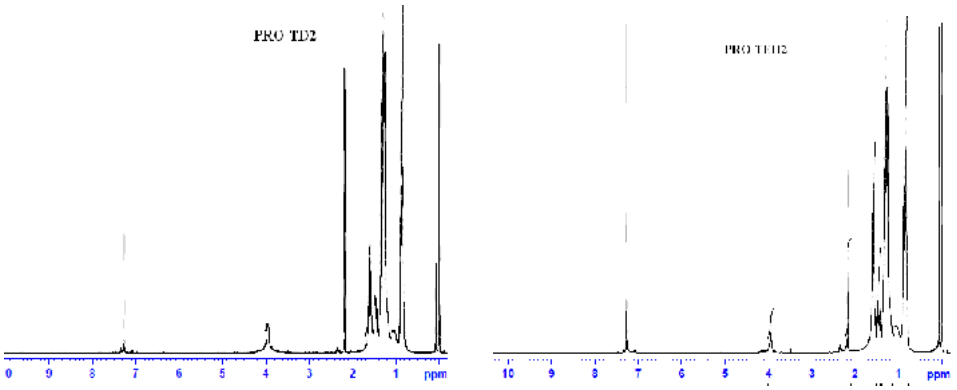

Figure 6: ^{1}H NMR spectra of PPRO-TD2 and PPRO-TEH2

7.2.3. Optical Properties

The electronic absorption spectra of the polymers in chloroform solution and as thin film on glass substrate are shown in figure 7. The absorption maxima of PPRO-TD2 and PPRO-TEH2 in dilute chloroform solution occur at 529 nm and 536 nm which are slightly red shifted in solid film to 543 nm and 550 nm respectively. This is expected to be due to slight increase in coplanarity of the polymer and occurrence of intermolecular electronic interactions between the polymer molecules in the thin fims. The strong absorption of the polymers was explained using the density functional theory calculation on model compound PRO-1TZ without alkyl chain. The frontier energy levels of the model compound is shown in figure 8. The HOMO and LUMO wave function of the model compound is delocalized over both the ProDOT and 1,2,4-triazole which is in contrast to donor-acceptor polymers described in chapters II and chapter III. This would favor HOMO-LUMO overlap and enhanced absorption for

the lowest optical transition. The solid state absorption spectrum of both the polymers showed a shoulder at 578 nm, and 588 nm respectively. The appearance of the new peak suggests formation of a π-stacked structure in the solid state. This type of shoulder peaks are shown by donor-acceptor polymers like benzotriazole/aryleneethylene copolymers[10].

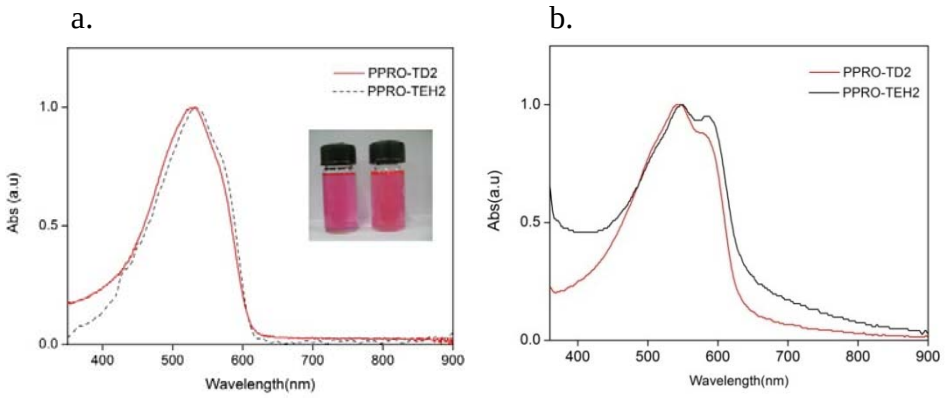

Figure 7: Absorption spectra of PPRO-TD2 and PPRO-TEH2. a. in chloroform solution and b. as thin film on glass plate

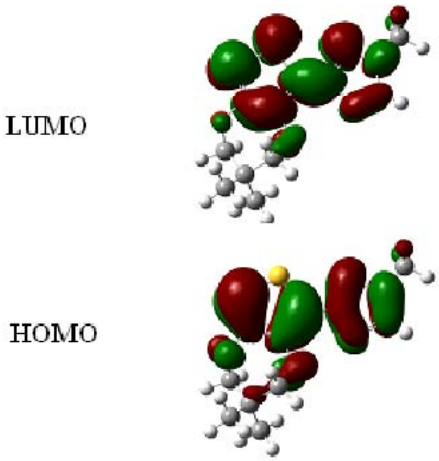

Figure 8: Frontier energy levels of PRO-1TZ

The π-stacking property of the polymers can be studied by observing solvent induced aggregation of polymers in solvent/non-solvent system. It is an attractive approach for the studies, since the isolation or aggregation

of polymer chains can be easily controlled by choosing the appropriate combination of a good solvent and a non-solvent. In a good solvent, the polymer chains exist as isolated chains, and addition of a poor solvent forces the polymer chains to enter in to an aggregate stage, which is similar to that in the film. The solvent induced aggregation studies were carried out in THF (good solvent) and methanol (poor solvent). The addition of methanol to polymer in THF has affected the absorption maxima of the polymer (figure 9). The colour of the polymer changes from red to violet with the addition of methanol. The transition point was noted at 30-40% methanol in THF. The absorption maximum of the polymers has shifted by 16 nm and a shoulder peak was observed at 580 nm and 587 nm for PPRO-TD2 and PPRO-TEH2, which were also found in polymers in thin film form.

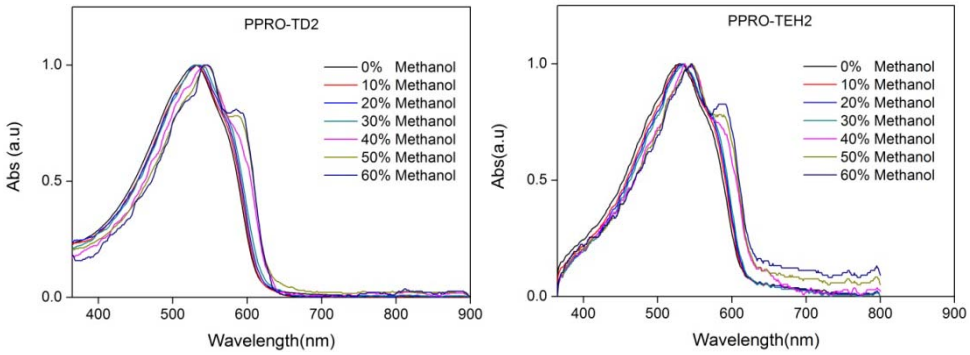

Figure 9: Absorption spectra of the polymers in THF/MeOH solvent mixture

Figure 10 shows the PL emission spectrum of PPRO-TD2 and PPRO-TEH2 in chloroform. The maximum PL of PPRO-TD2 and PPRO-TEH2 appear at 594 nm and 598 nm. The wavelength corresponding to the absorption maximum is used as the excitation wavelength. All the optical properties of the polymers are summarized in table 3.

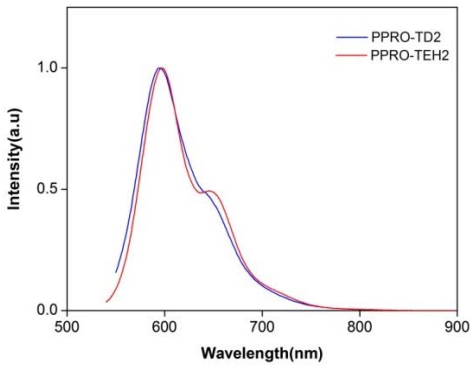

Figure 10: PL spectra of PPRO-TD2 and PPRO-TEH2

Table 2: Optical properties of PPRO-TD2 and PPRO-TEH2

Polymer	Absorption λ_{max} (nm) (Solution)	Absorption λ_{max} (nm) (film)	Emission λ_{max} (nm)	Abs. onset (nm) (film)	E_g (eV)
PPRO-TD2	529	543	594	625	1.99
PPRO-TEH2	536	550	598	631	1.96

7.2.4. Electrochemical properties

The cyclic voltammogram of PPRO-TD2 and PPRO-TEH2 recorded using Pt electrode in acetonitrile solution of 0.1M Bu_4NPF_6 is shown in figure 11. Both the polymers show one oxidation and reduction process. The oxidation peaks of PPRO-TD2 and PPRO-TEH2 occur at 0.376 V and 0.344 V respectively and reduction peaks occur at -1.96 V and -1.87 V respectively. The HOMO level of the PPRO-TD2 and PPRO-TEH2 calculated using the formula, HOMO=-(4.4+E^{onset}_{ox}) eV, are -4.78e V and -4.74 eV, while LUMO are -2.44 eV and -2.53 eV respectively. The band gaps of PPRO-TD2 and PPRO-TEH2 are calculated to be 2.34 eV and 2.21 eV respectively.

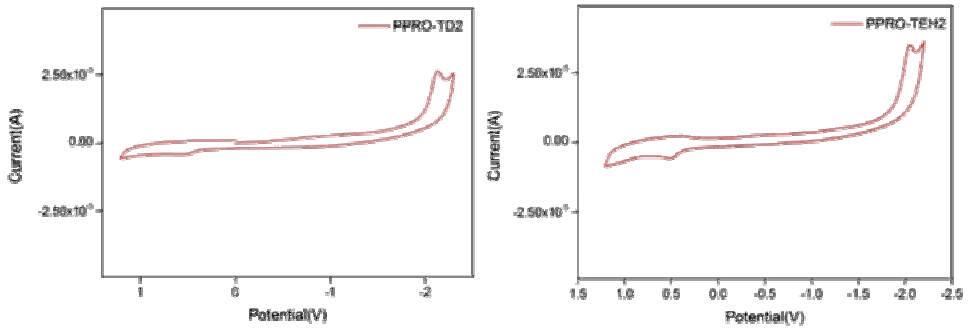

Figure 11: The cyclic voltammogram of PPRO-TD2 and PPRO-TEH2 thin films using Pt electrode in acetonitrile solution of 0.1M Bu_4NPF_6 supporting electrolyte.

In order to improve the accuracy of measuring the electrochemical band gap, differential pulse voltammetry (DPV) was performed (figure 12). Due to the increased sensitivity of DPV, the onset of the redox processes are sharper and allow for a more accurate determination. The onset of oxidation and reduction for PPRO-TD2 are at 0.311 V and -1.89 V, respectively. This leads to an electrochemical band gap of 2.2 eV. Similarly for PPRO-TEH2, the onset of oxidation, onset of reduction and band gap are estimated to be 0.309 V, -1.86 V and 2.16 eV respectively. The experimentally determined values are in good agreement with values obtained by PBC/HSE06/6-31G method. The electrochemical band gap is higher than the optical band gap. This is a common feature of the conjugated polymers and may be related to structural difference in the thin film due to swelling by the solvent, or due to the exciton binding energy for conjugated polymers [11,12].

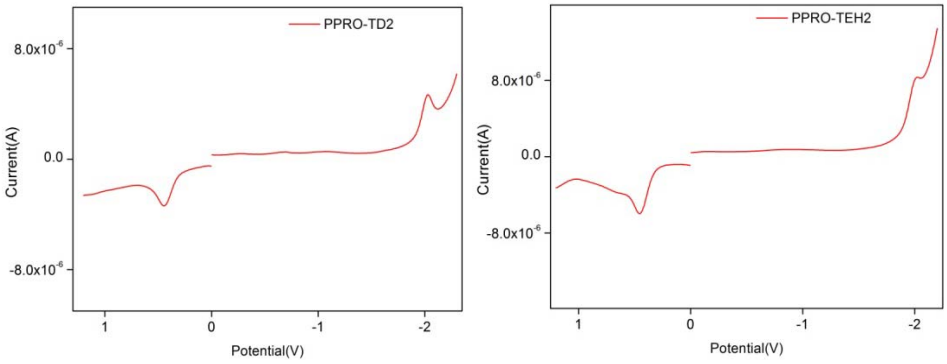

Figure 12: Differential pulse voltammogram (step time of 0.1 s) of drop cast film of PPRO-TD2 and PPRO-TEH2, on a platinum disk electrode in 0.1 M Bu_4NPF_6 supporting electrolyte

Table 3: Electrochemical data of PPRO-TD2 and PPRO-TEH2[a]

Polymer	Cyclic voltammetry (CV)					Differential pulse voltammetry (DPV)				
	E_{ox} (V)	E_{red} (V)	HOMO (eV)	LUMO (eV)	E_g (eV)	E_{ox} (V)	E_{red} (V)	HOMO (eV)	LUMO (eV)	E_g (eV)
PPRO-TD2	0.376	-1.96	-4.78	-2.44	2.34	0.311	-1.89	-4.71	-2.51	2.2
PPRO-TEH2	0.344	-1.87	-4.74	-2.53	2.21	0.309	-1.86	-4.70	-2.54	2.16

a. In acetonitrile with 0.1M Bu_4NPF_6 supporting electrolyte scanned at 100 mV/s for CV and step time of 0.1 s for DPV

7.2.5. X-ray diffraction data

The XRD patterns of the two polymers in thin film form are shown in figure 13. Even though the XRD peaks of PPRO-TD2 and PPRO-TEH2 are broad, the XRD data suggest that some portions of the polymers have ordered π-stacked structure in the solid state to give a distinct peak at d=3.3 A°. This peak was assigned to be the face-to-face packing distance between the stacked polymers. The schematic representation of the stacked structure of the polymer is shown in figure 14. The small peak observed in the low angle region (d=14.5) is assigned to be due to the distance between the conjugated main chains separated by the alkyl side chains. The shoulder peak at about 6.2 A^0 is assigned to a side-to-side distance between loosely packed alkyl chains[13].

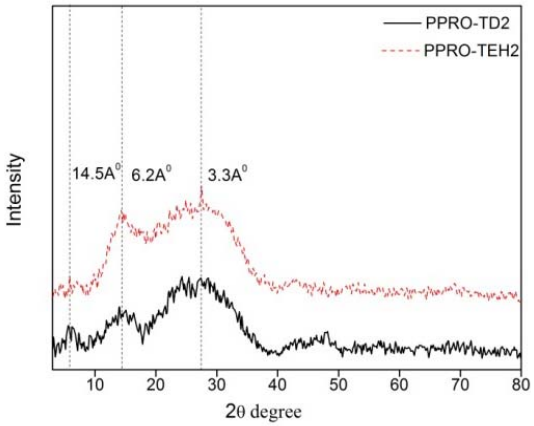

Figure 13: X-ray diffraction pattern of PPRO-TD2 and PPRO-TEH2

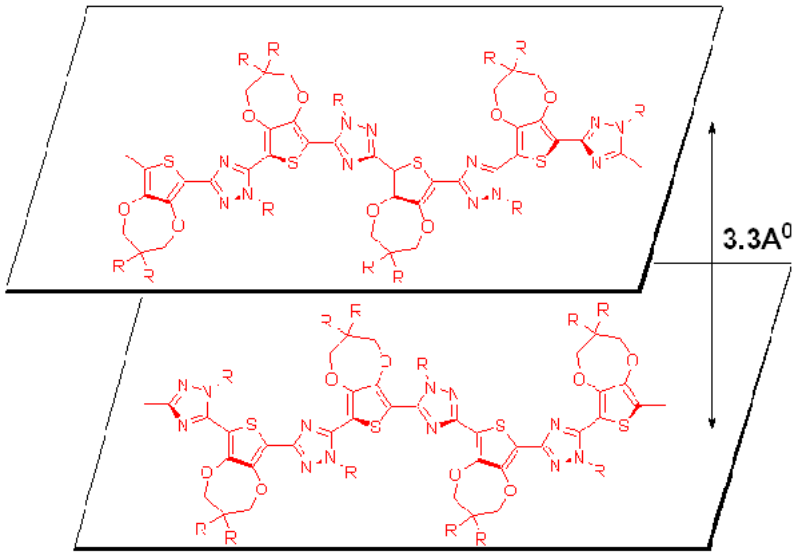

Figure 14: Schematic representation of π-stacked structure of the polymers

7.2.6. Photovoltaic device characteristics

The suitability of the polymer for active layer in photovoltaic device was verified by fabricating a heterojunction device using both the polymers and the semiconductor In_2S_3. Figure 15 shows the current density-voltage (J-V) characteristics of the heterojunctions under illumination and in the dark. As could be seen, both the devices exhibited rectifying behaviour in the dark which might be due to the barrier formed at the In_2S_3/ polymer

interface. Under white light illumination (50 mW/cm^2), the device ITO/In_2S_3/PPRO-TD2/Ag heterojunction exhibited a short circuit current density (J_{sc}) of 249 µA/cm^2 and an open circuit voltage (V_{oc}) of 424.83 mV. For the device ITO/In_2S_3/PPRO-TEH2/Ag, J_{sc} is 312 µA/cm^2 and 432.88 mV. The fill factor (FF) and efficiency were calculated to be 28.14% and 28.29% and 0.06% and 0.08% respectively for PPRO-TD2 and PPRO-TEH2. Photovoltaic characteristics of bilayer heterojunction devices of PPRO-TD2 and PPRO-TEH2 are summarized in table 4.

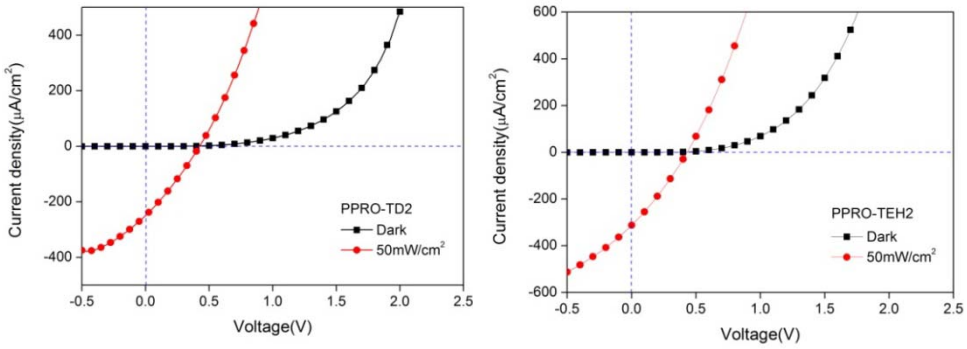

Figure 15: J-V curve of ITO/In_2S_3/polymer/Ag heterojunction

Table 4: J-V characteristics of ITO/In_2S_3/polymer/Ag heterojunction

Polymer	V_{oc} (mV)	J_{sc} (µA/cm^2)	Efficiency (%)	Fill factor (%)
PPRO-TD2	424.83	249	0.06	28.14
PPRO-TEH2	432.88	312	0.08	28.29

7.3. Conclusion and perspectives

In conclusion, incorporation of 1-alkyl-1,2,4-triazole unit to the poly(ProDOT) chain effectively reduces both the HOMO and LUMO levels of the polymer, which make them suitable for photovoltaic devices. This may be due to the partial expansion of the π-electrons in the π-conjugated system. This conclusion was supported by calculation using density functional theory on the model compound and polymers. The polymers are

synthesized through efficient direct arylation reaction using palladium acetate as catalyst. The polymers showed π-stacked structure in the solid state which may effectively increase the efficiency of the photovoltaic device. This was revealed by fabricating a bilayer heterojunaction device with device structure of ITO/In_2S_3/polymer/Ag.

7.4. Experimental section

The synthetic route towards the ProDOT was depicted in chapter IV.

7.4.1. Synthesis of 3,5-dibromo-1H-1,2,4-triazole

A mixture of 1,2,4-triazole (13.8g, 0.2 mol), distilled water (60 mL) and chloroform (25 mL) in a flask was stirred in an ice bath. Bromine (33.6 g, 0.21 mol) and an aqueous solution of NaOH (14 g, 0.35 mol) were simultaneously added slowly and the mixture was stirred overnight at room temperature. It was acidified with Conc HCl to obtain a white precipitate. The precipitate was separated by filtration, washed with water and dried under vacuum to give a white solid.

M. P: 208^{0}C (literature 210^{0}C)

7.4.2. Synthesis of 3,5-dibromo-1-(2-ethylhexyl)-1H-1,2,4-triazole (TEH2)

To a stirred mixture of 3,5-dibromotriazole (1.13 g, 5 mmol) and K_2CO_3 (1.11 g, 8 mmol) in DMF (40 mL), was added slowly 2-ethylhexyl bromide (5.5 mmol) at 10^{0}C. The mixture was stirred for 24 h at 70^{0}C and cooled to room temperature and poured to a large amount of water. The product was extracted with chloroform, washed with water and dried over anhydrous sodium sulphate. After filtration and evaporation, the product was dried under vacuum to give an yellow oil.

Yield	:	1.3 g (77%)
^{1}H NMR (400MHz, $CDCl_3$)	:	δ 3.93 (d, *J*=7.2 Hz, 2H, -NCH_2-), 1.9 (m, 1H, >CH-), 1.18-1.28 (m, 8H, aliphatic-H), 0.85-0.79 (m, 6H, -CH_3)
^{13}C NMR (100MHz, $CDCl_3$)	:	δ 10.4, 13.9, 22.8, 23.5, 28.3, 30.1, 39.5, 130, 140.

7.4.3. Synthesis of 3,5-dibromo-1-decyl-1H-1,2,4-triazole (TD2)

To a stirred mixture of 3,5-dibromotriazole (1.13 g, 5 mmol) and K_2CO_3 (1.11 g, 8 mmol) in DMF (40 mL), was added slowly 1-bromodecane (1.22 g, 5.5 mmol) at 10^0C. The mixture was stirred for 24 h at 70^0C and cooled to room temperature and poured in to large amount of water. The product was extracted with chloroform, washed with water and dried over anhydrous sodium sulphate. After filtration and evaporation, the product was dried under vacuum to give light yellow oil.

Yield	:	1.5 g (82%)
^{1}H NMR (400MHz, $CDCl_3$)	:	δ 4.03 (t, *J*=8 Hz, 2H, -NCH_2-), 1.78 (m, 2H), 1.24-1.1 (m, 14H, aliphatic-H), 0.8 (t, *J*=6.4 Hz, 3H, -CH_3)
^{13}C NMR (100MHz, $CDCl_3$)	:	δ 14.1, 22.6, 26.2, 28.9, 29.2, 29.3, 29.4, 31.8, 129, 140.

7.4.4. General procedure for the synthesis of copolymers

To a stirred solution of dioctyl ProDOT (0.17 mmol) in 10 mL DMF was added tetrabutylammonium bromide (0.17 mmol) and sodium acetate (0.68 mmol). The reaction mixture was stirred at room temperature for 15 min followed by addition of 3,5-dibromo-1-alkyl-1H-1,2,4-triazole (0.17 mmol) and 10% palladium acetate. The reaction mixture was stirred at

90^0C for 48 h. The reaction was cooled to room temperature and poured in to methanol. The precipitate was filtered and washed with methanol. The polymer was purified by soxhlet extraction using acetone and methanol for 24 h. The residue was dissolved in minimum amount of toluene and precipitated using methanol and dried under vacuum.

7.4.4.1. Synthesis of copolymer (PPRO-TD2)

ProDOT (0.066 g, 0.17 mmol), TD2 (0.63 g, 0.17 mmol), sodium acetate (0.93 g, 0.68 mmol), TBAB (0.56 g, 0.17 mmol), $Pd(OAc)_2$ (0.0038 g, 0.017 mmol), and DMF (10 mL) were used.

Yield	:	21 mg (21%)
Td	:	334^0C
^{1}H NMR (400MHz, $CDCl_3$)	:	δ 4.22-4.15 (m, -OCH_2- of ProDOT), 3.9 (t, ~2H, -NCH_2-), 2.17 (m, ~2H, -CH_2-), 1.6-0.95 (m, ~42H, aliphatic-H), 0.87-0.84 (m, ~9H, -CH_3)
UV-Visible λmax (nm)	:	529 nm
GPC	:	Mn=5992, PDI=1.34

7.4.4.2. Synthesis of copolymer (PPRO-TEH2)

ProDOT (0.066 g, 0.17 mmol), TEH2 (0.058 g, 0.17 mmol), sodium acetate (0.93 g, 0.68 mmol), TBAB (0.56 g, 1.74 mmol), $Pd(OAc)_2$ (0.0038 g, 0.017 mmol), and DMF (10 mL) were used.

Yield	:	26 mg (27%)
Td	:	339^0C

^{1}H NMR (400MHz, $CDCl_3$)	:	δ 4.15-4.19 (m, -OCH_2- of ProDOT), 3.9 (bs, ~2H, -NCH_2-), 2.17 (m, ~1H, >CH-), 1.9-0.96 (m, ~36H, aliphatic-H), 0.87-0.83 (m, ~12H, -CH_3)
UV-Visible λmax (nm)	:	536 nm
GPC	:	Mn=6379, PDI=1.63

7.5. References

1. Adachi, C.; Baldo, M. A.; Forrest, S. R.; Thompson, M. E., *Appl Phys Lett.*, **2000**, 77, 904.
2. Nenner, I.; Schulz, G. J., *J. Chem. Phys.*, **1975**, 62, 1747.
3. Takuma, Y.; Tatsuya, I.; Shintaro, S.; Takakazu, Y., *Macromolecules*, **2005**, 38, 1500.
4. Beny, J. P.; Dhawan,S. N.; Kagan, J.; Sundlass, S., *J. Org. Chem.*, **1982**, 47, 2201.
5. Takuma, Y.; Kimiyasu, N.; Takayuki, I.; Takakazu, Y., *Polymer.*, **2007**, 48, 4375.
6. Parr, R. G.; Yang, W., *Density-Functional Theory of Atoms and Molecules*; Oxford University Press, **1989**, New York.
7. Heyd, J.; Scuseria, G. E.; Ernzerhof, M. *J. Chem. Phys.*, **2003**, 118, 8207.
8. Krukau, A. V.; Vydrov, O. A.; Izmaylov, A. F.; Scuseria, G. E. *J. Chem. Phys.*, **2006,** 125, 224106.
9. Gaussian 09, Frisch, M. J.; Trucks, G. W.; Schlegel, H. B.; Scuseria, G. E.; Robb, M. A.; Cheeseman, J. R.; Scalmani, G.;

Barone, V.; Mennucci, B.; Petersson, G. A.; Nakatsuji, H.; Caricato, M.; Li, X.; Hratchian, H. P.; Izmaylov, A. F.; Bloino, J.; Zheng, G.; Sonnenberg, J. L.; Hada, M.; Ehara, M.; Toyota, K.; Fukuda, R.; Hasegawa, J.; Ishida, M.; Nakajima, T.; Honda, Y.; Kitao, O.; Nakai, H.; Vreven, T.; Montgomery, J. A.; Peralta, J. E.; Ogliaro, F.; Bearpark, M.; Heyd, J. J.; Brothers, E.; Kudin, K. N.; Staroverov, V. N.; Kobayashi, R.; Normand, J.; Raghavachari, K.; Rendell, A.; Burant, J. C.; Iyengar, S. S.; Tomasi, J.; Cossi, M.; Rega, N.;. Millam, J. M.; Klene, M.; Knox, J. E.; Cross, J. B.; Bakken, V.; Adamo, C.; Jaramillo, J.; Gomperts, R.; Stratmann, R. E.; Yazyev, O.; Austin, A. J.; Cammi, R.; Pomelli, C.; Ochterski, J. W.; Martin, R. L.; Morokuma, K.; Zakrzewski, V. G.; Voth, G. A.; Salvador, P.; Dannenberg, J. J.; Dapprich, S.; Daniels, A. D.; Farkas, Ö.; Foresman, J. B. ; Ortiz, J. V.; Cioslowski, J.; Fox, D. J.; Gaussian, Inc., Wallingford CT, **2009.**

10. Akitoshi, T.; Takakazu, Y., *Adv. Synth. Catal.*, **2004**, 346, 1818.
11. Heeney, M.; Zhang, W.; Crouch, D. J.; Chabinyc, M. L.; Gordyev, S.; Hamilton,.; Higgins, S. J.; McCulloch, I.; Skabara, P. J.; Sparrowe,, D.; Tierney, S. *Chem. Commun.*, **2007**, 5061.
12. Campbell, I. H.; Hagler, T. H.; Smith, D. J.; Ferraris, J. P. *Phys. Rev. Lett.*, **1996**, 76, 1900.
13. Swan, P. R., *J. Polym. Sci*., **1962**, 56, 403.

Chapter 8

DESIGN AND SYNTHESIS OF CONJUGATED POLYMERS FOR THE VAPOUR PHASE DETECTION OF NITROAROMATICS

Contents

In this chapter, we have investigated the optical and electrochemical properties of MEH PPV, MEH PPV with six (6PC) and ten carbon (10PC) alkyl spacer, and use of the polymers for probing the presence of nitroaromatics. Synthesis of crosslinked MEH PPV was carried out by Gilch polymerization route using potassium t-butoxide as base in dry THF at room temperature. The percentage of crosslinker was adjusted so as to get soluble and processable polymer. It was found that, more than 1 mol% of crosslinker resulted in an insoluble polymer/polymer gel. Amplified fluorescence quenching of MEH PPV and crosslinked MEH PPV was demonstrated using nitrobenzene, 4-nitrotoluene and 2,4-dinitrotoluene as analytes. The quenching efficiency of each analyte was correlated with vapour pressures. The ten carbon spacer MEH PPV showed greater sensitivity towards the analytes, which may be due to the high porosity when compared to MEH PPV and 6PC. The 6PC and 10PC showed recycled sensitivity towards all the analytes. The effect of interfering compounds were also studied.

8.1.Introduction

The poly (2-methoxy-5-ethyl hexyloxy)-1,4-phenylenevinylene (MEH-PPV) has attained wide interest because of its applications in optoelectronic devices such as light emitting diodes[1], photovoltaic cells[2-4], chemosensors[5] etc.

MEH PPV exhibits high solubility in common organic solvents due to the presence of branched alkoxy chain. The application of MEH PPV in optical and optoelectronic devices is limited due to its easy photo bleaching property. In the solid state, the conjugated polymer forms weakly emissive aggregates by aromatic π-π interaction. The control of π stack induced molecular aggregation in the polymer chain is the major task in the development of highly emissive conjugated polymers for fluorescence based chemosensors. Attempts have been made to control π-stacking in PPV derivatives by attaching cyclohexyl[6-8], adamantane[9], cholestanyl rings[10], phenyl[11], biphenyl[12], naphthyl[13] and tricyclodecane[14] to the polymer backbone. In this work, we have tried to control the π-stacking interaction of MEH PPV and make it photostable, by covalently separating the polymer chains by alkyl spacers of different lengths. We also hope that, crosslinking creates free volume inside the polymer matrix to accommodate the analyte to get better sensitivity towards nitroaromatics. Crosslinking the polymer chains is a well known method for producing porous polymers[15,16].

The detection of chemical explosives is crucial for military and civilian safety. It is estimated that 80% of the landmines contain TNT or mixture of explosives containing TNT. TNT for the explosives are manufactured by the nitration of toluene. During this process, some impurities like 2,4-dinitrotoluene (2,4-DNT), 2,6-dinitrotoluene etc will also be formed along with 2,4,6 -trinitrotoluene (TNT). Most of these fingerprinting compounds have higher vapour pressure than TNT and have room-temperature vapor pressure about 20 times that of the latter. It is found that, 2,4-DNT and 1,3-dinitrobenzene are the mostly detected chemical species over plastic coated TNT based landmines[17-19]. So we can use this chemical signature for the detection of explosives with low vapour

pressure. Therefore, the detection of nitroaromatic explosives is often achieved by detection of DNT.

Fluorescent conjugated polymers as sensory material are promising because of the extremely high signal amplification due to the conjugation cooperativity[20-23]. The observed amplification is due to the ability of the delocalized electronic structure of the conjugated polymers to facilitate efficient charge migration over large distance. The fluorescence quenching is due to energy migration along the polymer backbone to the receptor sites. In conjugated polymers signal amplification is due to the fact that the polymer chains need only a few occupied receptor sites to effect complete quenching. For monomeric indicators, all the receptor sites must be occupied to effect complete quenching.

The materials for chemosensory application need to satisfy some criteria like high photostability and thermal stability, ability to amplify the transduction event etc. The fluorescence quantum yield of thin films of conjugated polymers is decreased due to molecular aggregation induced by π-stacking. Another problem in the development of polymer based sensors is that, dense polymer films can prevent the rapid diffusion of analytes through the material. Swager's group at MIT has reported rigid three dimensional pentiptycene carrying polymers, to prevent the π-stacking[23].

In this chapter, we have investigated the synthesis and characterization of MEH PPV with six (6PC) and ten carbon (10PC) alkyl spacer, and use of these polymers for detecting nitroaromatiocs using nitrobenzene (NB), 4-nitrotoluene (NT) and 2,4-dinitrotoluene (DNT) as analytes. The photo stability and recycled usability of the polymers are studied in detail.

8.2. Results and Discussion

8.2.1. Monomer synthesis

The synthesis of monomers is outlined in Scheme 1. 1,4-bis(chloromethyl)-2-methoxy-5-(2'-ethylhexyloxy)benzene was synthesized by a two step procedure. It involves alkylation of 4-methoxy phenol with 2-ethyl hexyl bromide, followed by chloromethylation with formaldehyde and dry HCl gas.

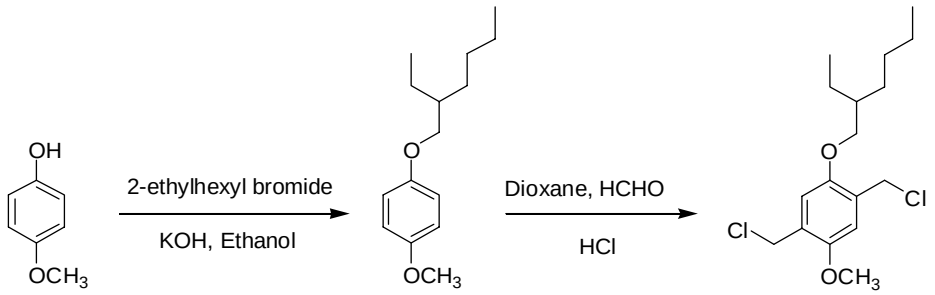

Scheme 1: Synthesis of 1,4- bis(chloromethyl)-2-methoxy-5-(2'-ethyl hexyloxy)benzene

Synthesis of the crosslinker was carried out by a four step synthetic procedure. In the first step, monoalkylation of hydroquinone was attained by KOH in ethanol at 70^0C. It was purified by column chromatography using DCM/hexane mixture (1:3 v/v) (scheme 2). Two mono alkylated hydroquinones were coupled by 1,10-dibromodecane in DMF at 80^0C using K_2CO_3 as base. It was purified by recrystallisation from hexane/methanol mixture (1:2 v/v). It was chloromethylated with formaldehyde/HCl to obtain the crosslinker with ten carbon spacer. It was purified by recrystallisation from hexane (scheme 4). We have also synthesized six carbon spacer crosslinker by the same method (scheme 3). All the compounds were characterized by IR, ^{1}H NMR, ^{13}C NMR etc. The ^{1}H

NMR and ^{13}C NMR spectra of the compounds are shown in figures 1, 2, 3 and 4.

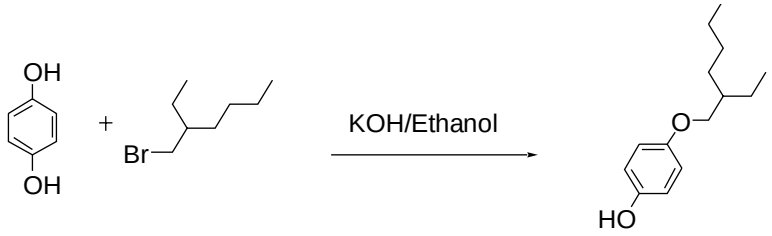

Scheme 2: Synthesis of 4-(2-ethyl hexyloxy)phenol (C1)

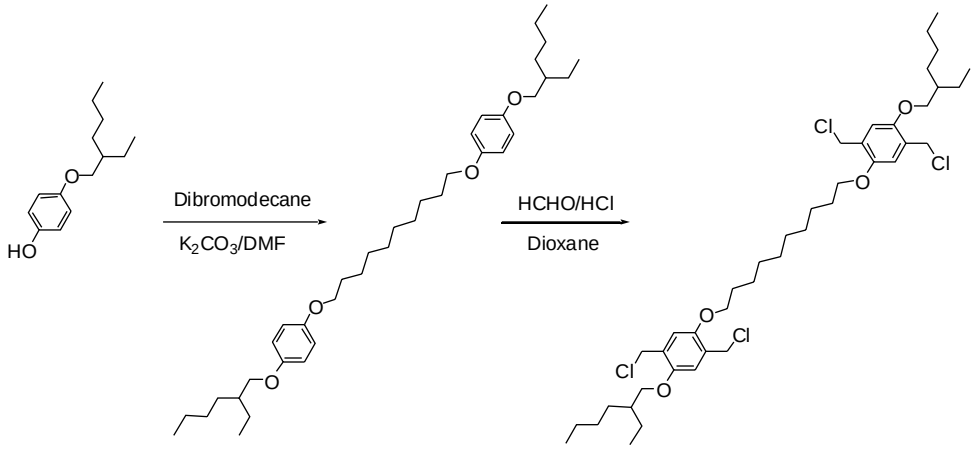

10C2 **10C3**

Scheme 3: Synthesis of crosslinker with ten carbon spacer

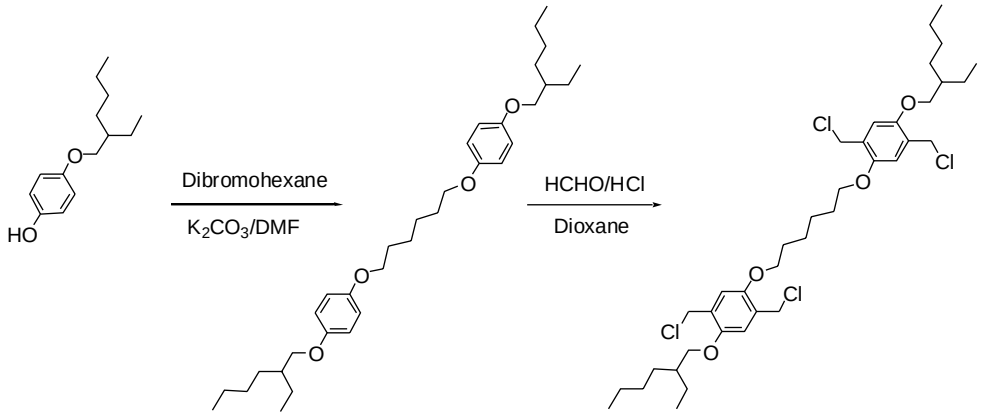

6C2 **6C3**

Scheme 4: Synthesis of crosslinker with six carbon spacer

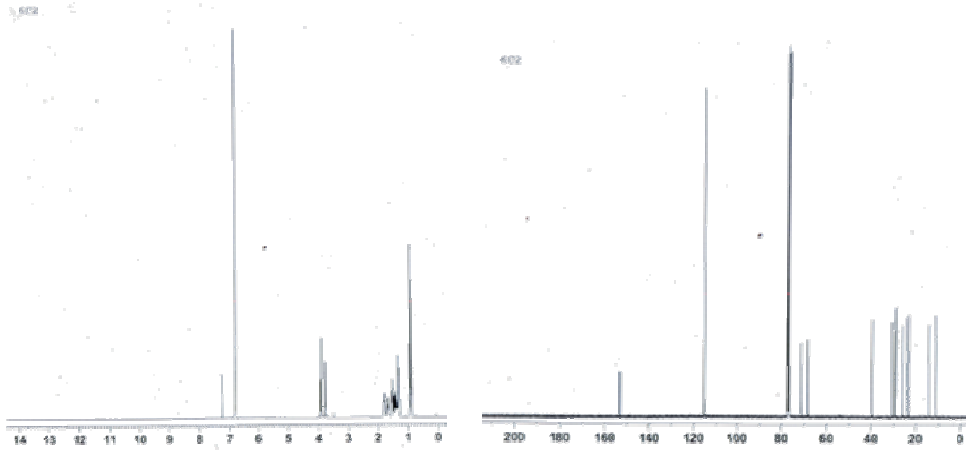

Figure 1: ^{1}H NMR and ^{13}C NMR spectra of 6C2

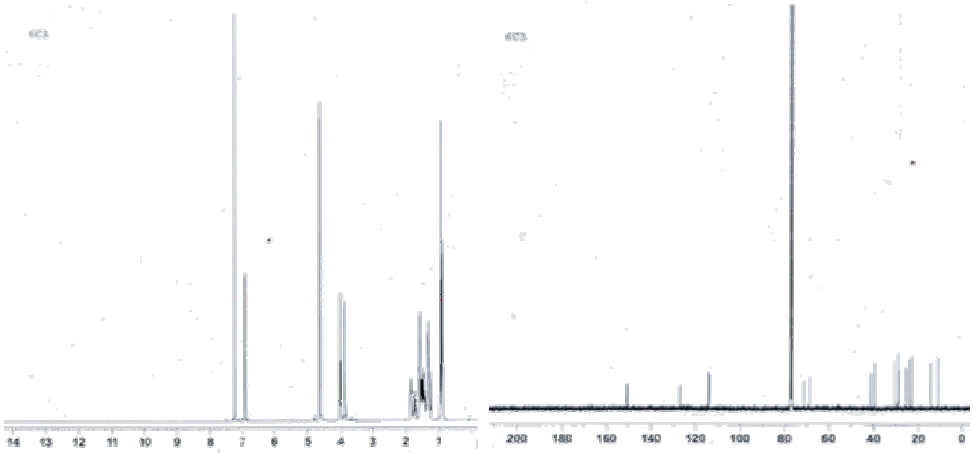

Figure 2: ^{1}H NMR and ^{13}C NMR spectra of 6C3

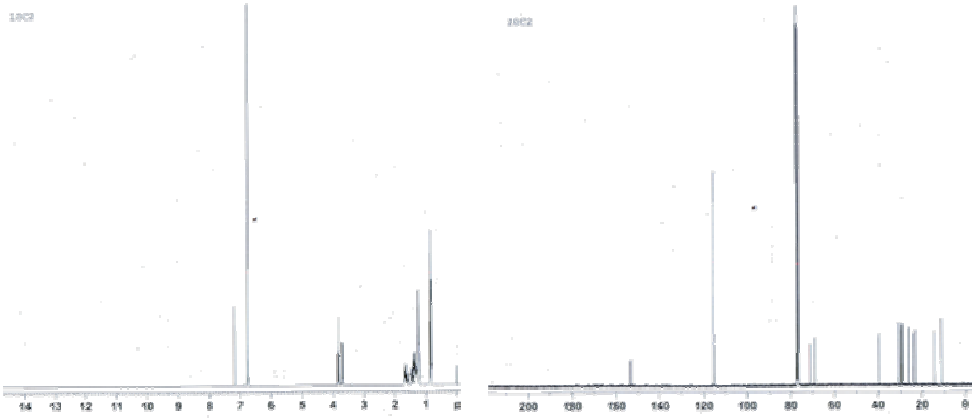

Figure 3: ^{1}H NMR and ^{13}C NMR spectra of 10C2

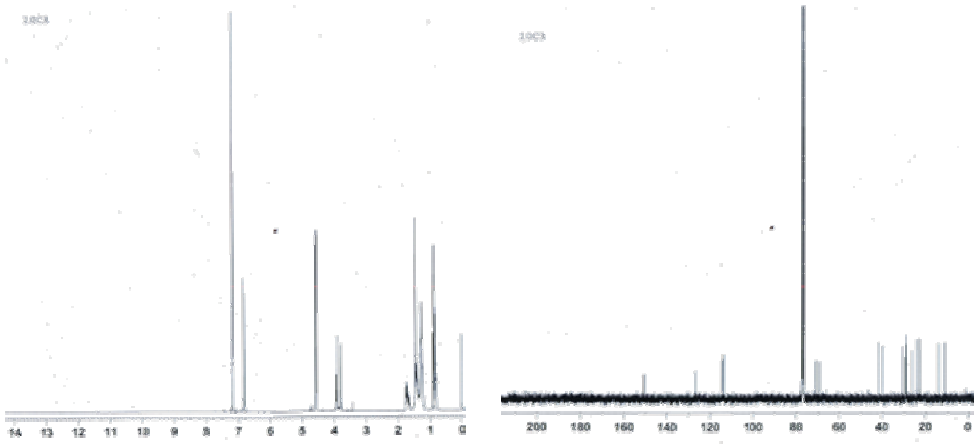

Figure 4: ^{1}H NMR and ^{13}C NMR spectra of 10C3

8.2.2. Polymer synthesis

Synthesis of crosslinked MEH PPV and MEH PPV are shown in scheme 5 and scheme 6. Two crosslinked MEH PPVs 6PC and 10PC were synthesized through copolymerisation of 1,4-bis(chloromethyl)-2-methoxy-5-(2'-ethyl hexyloxy)benzene and respective crosslinkers 6C3 and 10C3 by Gilch polymerization route using potassium t-butoxide as base in dry THF at room temperature. The percentage of crosslinker was adjusted to get the processable polymer. It was found that more than 1 mol% of crosslinker resulted in an insoluble polymer/polymer gel. A non crosslinked MEH PPV was also synthesized by using the same method (scheme 6). Polymers were characterized by IR, ^{1}H NMR, UV-Visible spectroscopy and fluorescence spectroscopy. The structural characterization of the crosslinked MEH PPV by ^{1}H NMR is ambiguous due to the difficulty in the identification of protons corresponding to the crosslinker to quantify the composition of the copolymer. The ^{1}H NMR spectra of the polymers are shown in figure 5. The number and weight-average molecular weights (M_n and M_w) and polydispersities of the polymers are summarized in table 1. The molecular weight of the crosslinked MEH PPVs and MEH PPV are higher than the

reported values[24-26], which confirmed that the experimental procedure adopted for the synthesis is adequate enough to produce high molecular weight polymers.

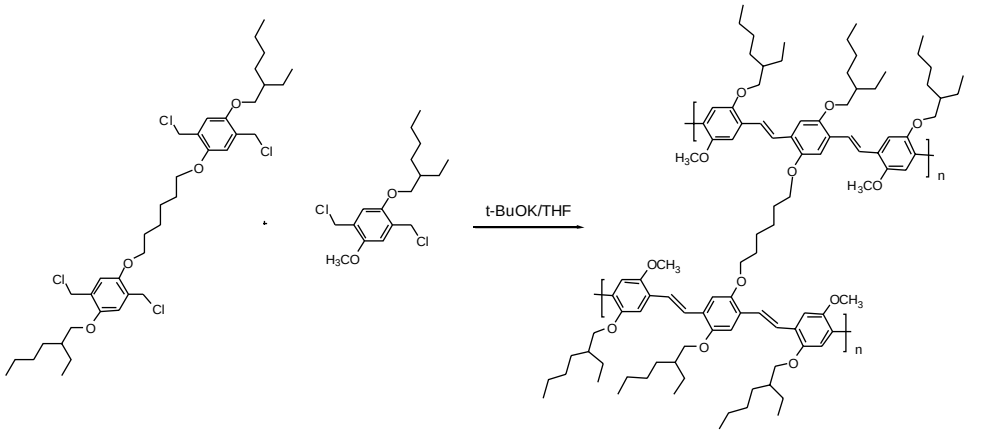

6PC

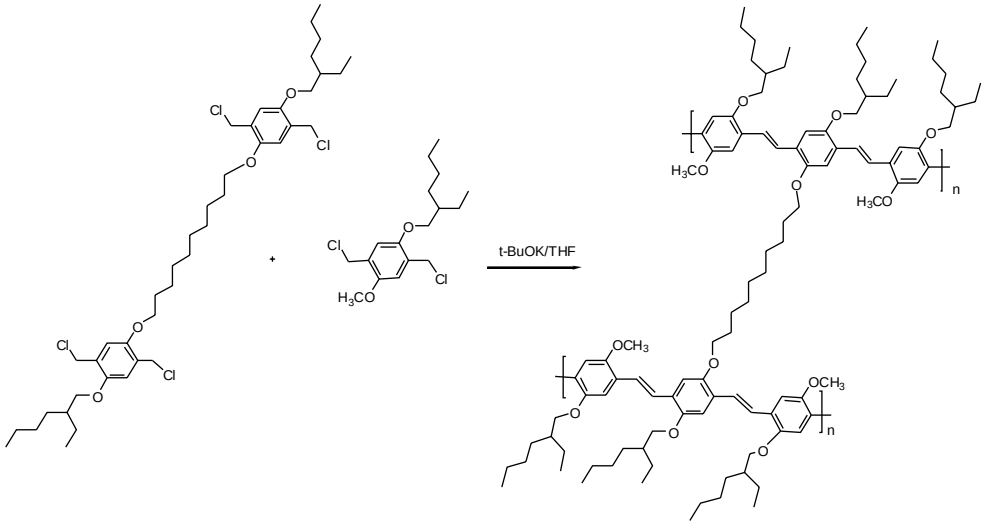

10PC

Scheme 5: Synthesis of crosslinked MEH PPV with six and ten carbon spacers

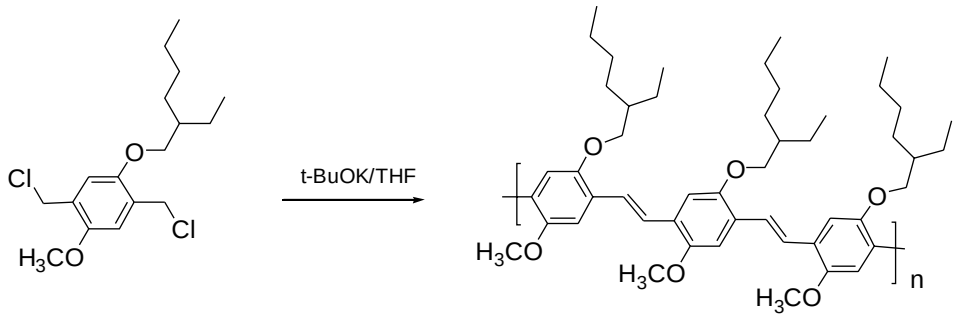

MEH PPV

Scheme 6: Synthesis of MEH PPV

Table 1: Polymerization results and thermal stability of polymers

Polymer	Yield (%)	M_n[a]	M_w[a]	PDI	T_d (^{0}C)
MEH PPV	45	251917	435652	1.73	395^{0}C
6PC	41	427633	649176	1.52	396^{0}C
10PC	37	223115	484662	2.17	395^{0}C

a. Determined using GPC in THF using polystyrene as standard for calibration
b. Decomposition temperature determined using TG under nitrogen.

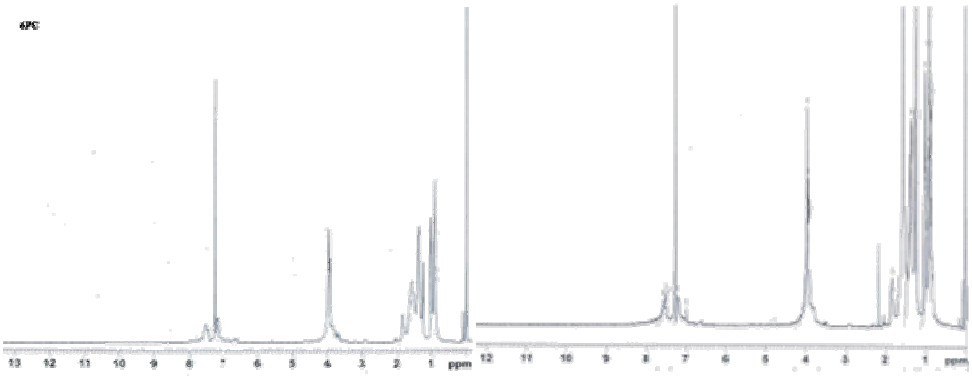

Figure 5: ^{1}H NMR spectra of 6PC and 10PC

8.2.3. Optical and electrochemical properties of the polymers

Absorption and fluorescence spectra of MEH PPV, 6PC and 10PC in chloroform solution are shown in figure 6. It could be seen that all the

polymers showed almost the same optical properties. Absorption maximum and emission maximum of the polymers occur at 499 nm and 563 nm.

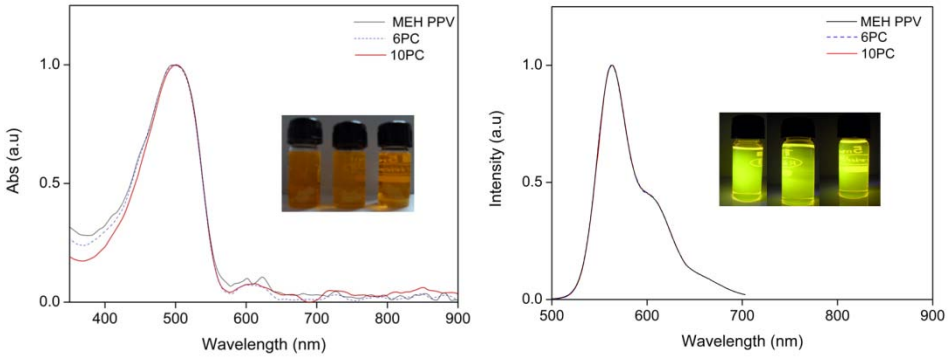

Figure 6: Absorption and emission spectra of MEH PPV, 6PC, and 10PC in chloroform

Absorption spectrum of the polymers as thin films showed λ_{max} at 515 nm, slightly red shifted than in solution (figure 7a). Excitation of the polymer film with blue LED light source (464 nm) led to the emission of an orange red colour with emission maximum at 585 nm (figure 7b). The optical properties of the polymers are presented in table 2.

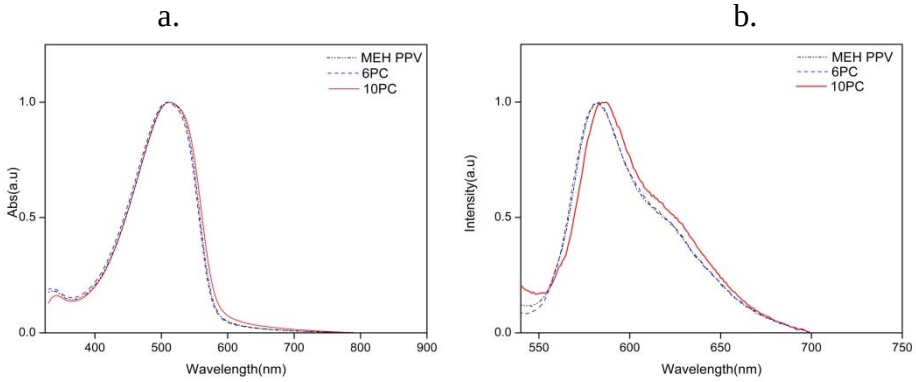

Figure 7: Absorption and PL of MEH PPV, 6PC and 10PC film on glass plate

Table 2: Optical properties of the polymers

Polymer	Abs. maximum λ_{max} (nm)		Emission maximum (nm)		Absorption Onset (nm)	E_g (eV)
	Solution	Film	Solution	Film		
MEH PPV	499	515	563	585	582	2.13
6PC	499	515	563	585	583	2.13
10PC	500	517	563	585	587	2.12

The energy levels of the polymers are investigated by cyclic voltammetry of polymer films on platinum electrode in 0.1M Bu_4NPF_6. The cyclic voltammogramms of the polymers are shown in figure 8. The polymers possessed one oxidation and reduction peak. It is an important factor determining the sensing ability of the polymers. The LUMO level of the polymer must be above the LUMO level of the acceptor for transferring the photo induced electron from the polymer to nitroaromatics. The two crosslinked polymers have the same level as the parent MEH PPV. The LUMO level of MEH PPV, 6PC and 10PC are -2.82 eV, -2.86 eV and -2.88 eV respectively. All the polymers have comparable levels with the nitroaromatics to assure the charge transfer. The electrochemical properties of the polymers are presented in table 3.

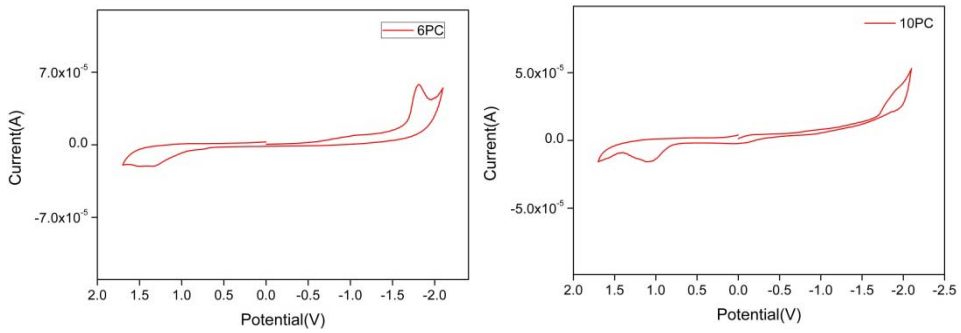

Figure 8: Cyclic voltammograms (scan rate 100mV/s) of 6PC and 10PC films cast on a platinum electrode in Bu_4NPF_6/acetonitrile

Table 3: Electrochemical properties of the polymers

Polymer	E_{ox} (V)	E_{red} (V)	HOMO (eV)	LUMO (eV)	E_g (eV)
MEH PPV	0.65	-1.58	-5.05	-2.82	2.23
6PC	0.62	-1.54	-5.02	-2.86	2.16
10PC	0.64	-1.52	-5.04	-2.88	2.16

8.2.4. Detection of nitroaromatics

Nitrobenzene (NB), 4-nitrotoluene (NT) and 2,4-dinitrotoluene (DNT) are used for fluorescence quenching studies. The analyte was taken in 3 mL glass vial and cotton gauge was placed above the vial to prevent direct contact between the analyte and the polymer film. The detection experiment was done by placing the polymer thin film over the vial at ambient temperature. The polymer film was prepared by spin coating the polymer solution in chlorobenzene (2 mg/mL). The fluorescence was measured using a seven fiber diode array system at 45 degree to the glass plate in every 500 msec using Ocean Optics SD2000 CCD array detector and OOBase32 software. The quenching studies of the polymers were done with excitation wavelength of 464 nm. The experimental set up for fluorescence quenching studies is shown in figure 9.

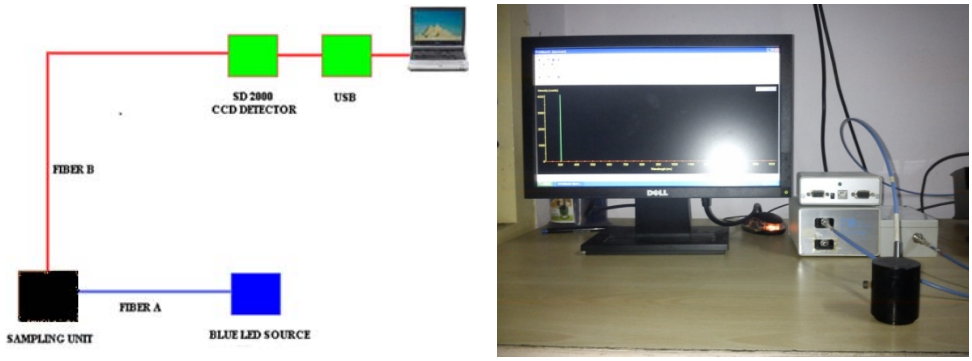

Figure 9: Experimental set up for the detection of nitroaromatics

The fluorescence quenching efficiency is defined as $(I_0\text{-}I)/I_0$ x100. Where I_0 and I are the fluorescence intensity prior to and after exposure to the analyte respectively. A rapid fluorescence quenching was observed for all three polymers up on exposure to NB, NT and DNT. The fluorescence quenching (%) of MEH PPV, 6PC and 10PC are summerized in table 4. All the polymers showed >90% quenching on exposure to nitrobenzene in 10 sec, which is due to the high vapour pressure of NB (figure 10a, figure 11a and figure 12a).

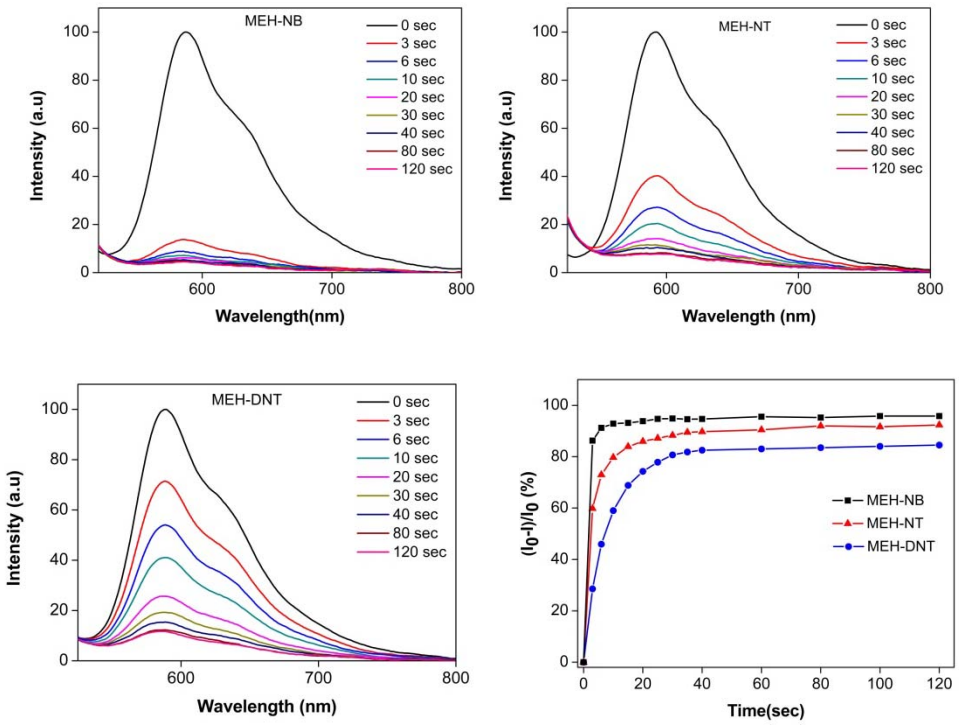

Figure 10: Time dependent fluorescence intensity of MEH PPV film upon exposure to a. NB b. NT, c. DNT vapours and d. the fluorescence quenching as a function of time

By exposure to 4-nitrotoluene, MEH PPV and 6PC showed 79% quenching (figure 10b and figure 11b), while NT quenches 89% of the fluorescence of 10PC (figure 12b). Similarly towards DNT, MEH PPV and 6PC quench 56-59% of its fluorescence (figure 10c, figure 11c). But 10PC

shows high sensitivity towards DNT and it quenches 81% fluorescence with in 10 sec (figure 12c). Comparison of the sensing experiments of 10PC with 6PC and MEH PPV, reveals that the length of the spacer has significant effect on the fluorescence quenching towards the analyte. The outstanding fluorescence quenching in 10PC towards the analytes is attributed to the large free volume and cavities inside the 10PC when compared with 6PC for trapping the analytes. The cavities facilitate charge transfer between the excited polymer backbone and the trapped analytes. The schematic representation of galleries inside the 10PC is demonstrated in figure 13.

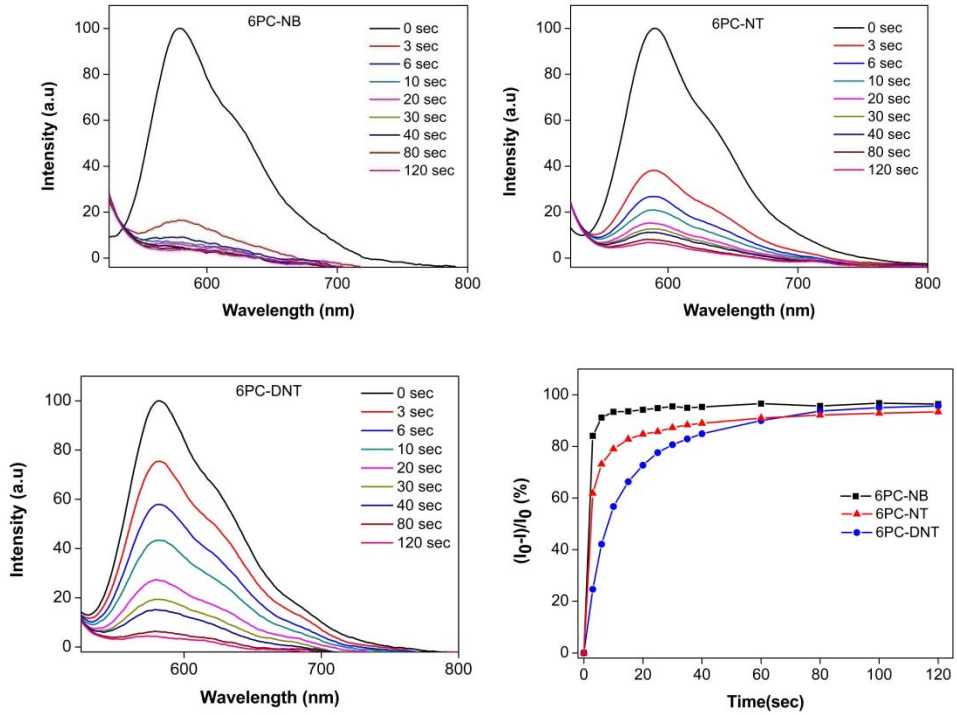

Figure 11: Time dependent fluorescence intensity of 6PC film upon exposure to a. NB, b. NT, c. DNT vapours and d. The fluorescence quenching as a function of time

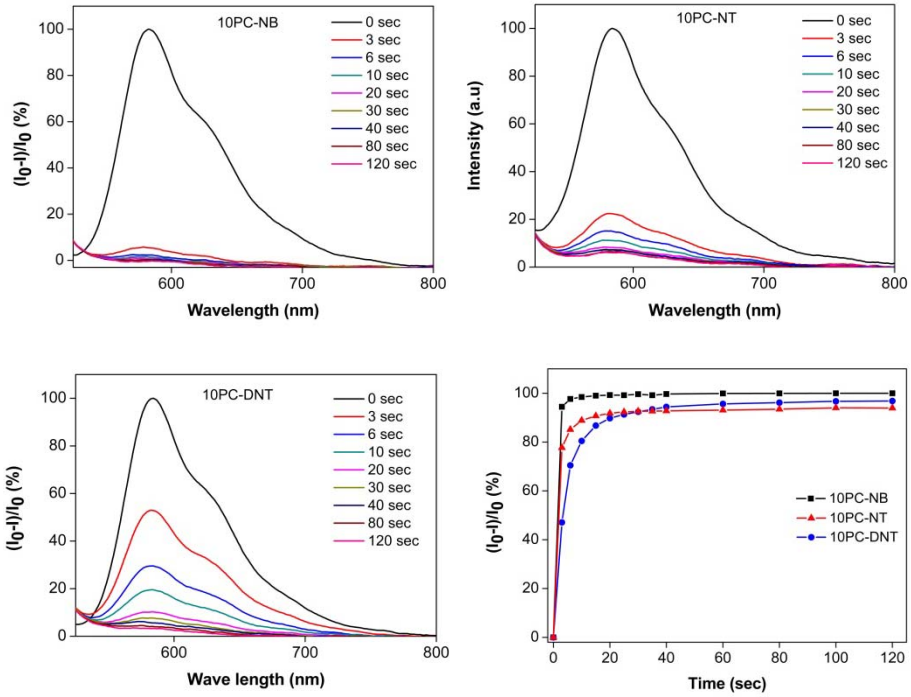

Figure 12: Time dependent fluorescence intensity of 10PC film upon exposure to a. NB, b. NT, c. DNT vapours and d. The fluorescence quenching as a function of time

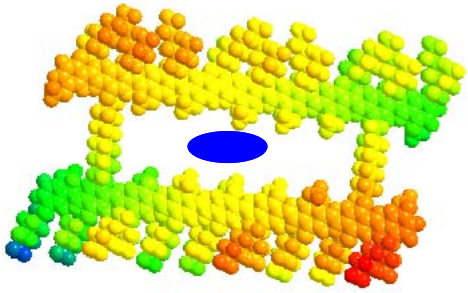

Figure 13: Schematic representation of galleries inside the 10PC

Table 4: Summary of the fluorescence quenching experiment

Polymer	Nitrobenzene		Nitrotoluene		DNT	
	After 10 sec	After 30 sec	After 10 sec	After 30 sec	After 10 sec	After 30 sec
MEH PPV	92.86%	94.86%	79.70%	88.82%	58.9%	80.68%
6PC	93.40%	95.51%	79.01%	87.27%	56.7%	80.67%
10PC	98.46%	99.61%	88.89%	92.64%	80.46%	92.38%

The sensing property of the polymers depends on certain structural and electronic factors. One factor is the electrostatic complimentarity between the analyte and the polymer. The charge density maps of the trimeric unit of MEH PPV, NB, NT, and DNT are shown in figure 14. Red regions are high and blue regions are low in electron density. This type of electrostatic binding interaction between electron-rich polymer and the electron deficient nitroaromatics plays a major role in the sensing mechanism.

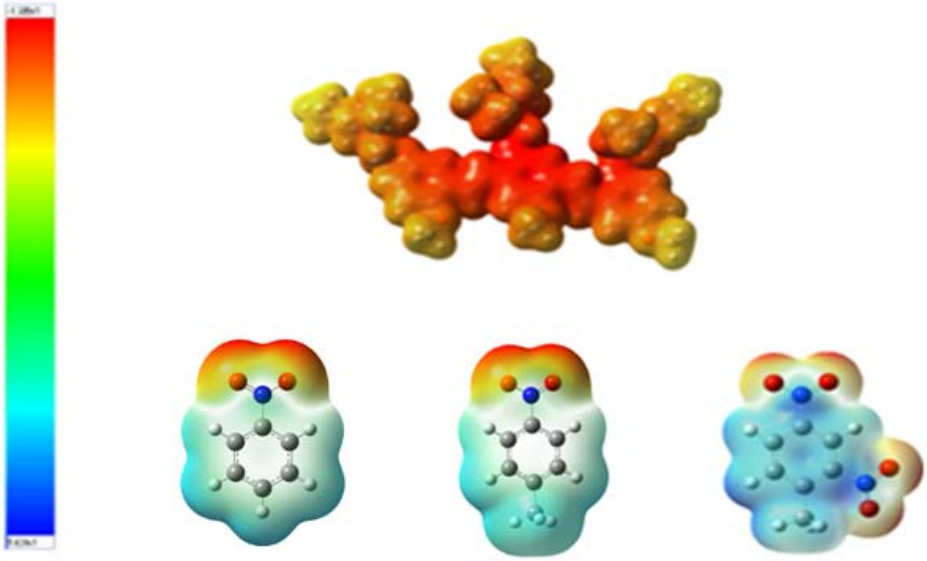

Figure 14. Electron density map of trimeric unit of PPV, NB, NT and DNT

The fluorescence quenching of conjugated polymers by nitroaromatics is achieved by an electron transfer donor-acceptor mechanism as depicted in figure 15. In this mechanism, the nitroaromatics act as electron acceptors for photoexcited electrons of the polymers.

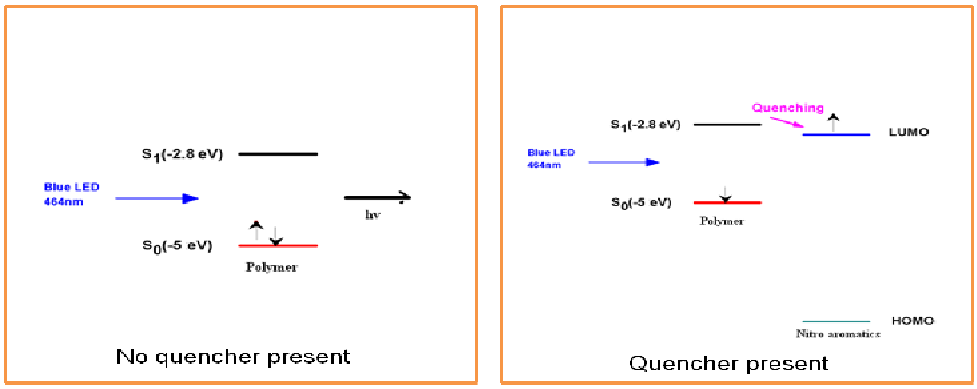

Figure 15: Electron transfer mechanism in fluorescence quenching

8.2.5. Photostability of the polymers

Crosslinking the conjugated polymer backbone is expected to prevent it from photobleaching of the polymer. This was rationalized by prolonged irradiation of the polymer with 464 nm blue LED. The change in fluorescence intensity with time is plotted in figure 16. It can be seen that for MEH PPV, fluorescence intensity was reduced by 20% on irradiation for 5 min while for crosslinked MEH PPV, fluorescence intensity was reduced by ~10%. This may be due to the prevention of the co-facial contacts of polymer backbones. It is concluded that, by crosslinking the polymer backbone, the photostability of MEH PPV has been increased.

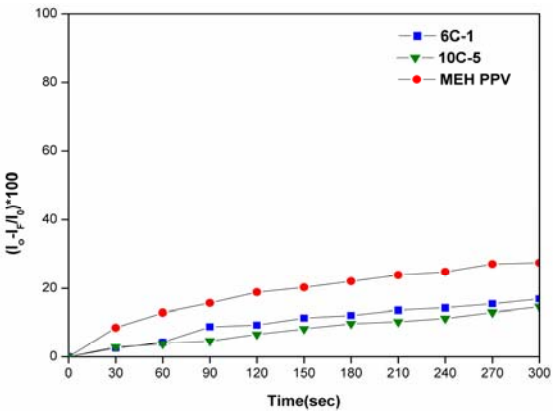

Figure 16: Photostability of MEH PPV, 6PC and 10PC films

8.2.5. Effect of interfering compounds

It is interestingly noted that there has been no significant change in fluorescence emission intensity upon exposing the film to the vapours of organic chemicals like ethanol, methanol, benzene, toluene, benzopheneone, benzaldehyde, aniline, chlorobenzene etc. Exposure of the film to phenol resulted in some decrease in the fluorescence emission of the film, but the response is weaker and slower as compared with those of nitroaromatic compounds. The change in fluorescence intensity up on exposure to suspected interfering compounds is plotted in the figure 17.

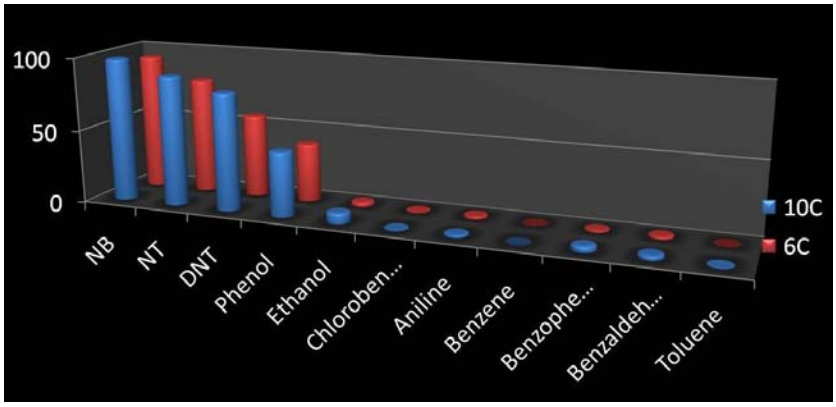

Figure 17: Effect of interfering compounds

8.2.6. Reversibility of the Quenching Process

The reversibility of the sensing process of the polymers was examined with NB, NT, DNT, as analytes. The film was first exposed to the saturated vapor of analytes at room temperature for 180-200 sec and the fluorescence emission was measured. After the measurement, hot air was blowed over the non fluorescent film for 60s for NB and 120s for DNT. The fluorescence emission of the film was measured again. It can be seen from figures 18, 19 and 20 that >75% of the fluorescence was recovered by this process. The sensing and fluorescence recovery process was repeated several times. Clearly, the sensing process is reversible.

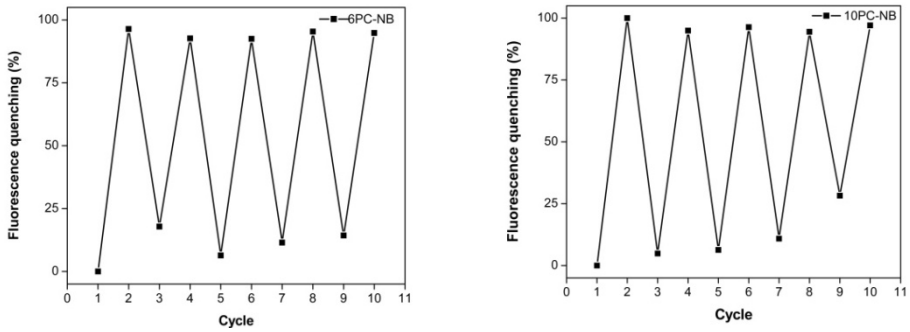

Figure 18: The fluorescence recovery cycles of 6PC and 10PC films, Cycles 3, 5, 7 and 9 are corresponding to polymer films after the desorption of analyte by air flow and cycles 2, 4, 6, 8 and 10 are corresponding to polymer films exposed to NB.

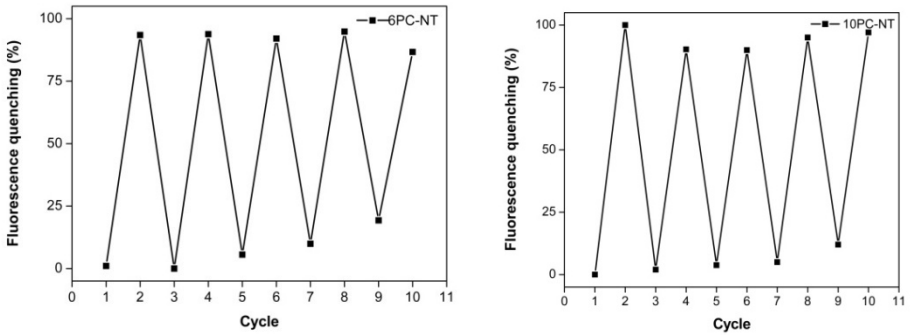

Figure 19: The fluorescence recovery cycles of 6PC and 10PC films, Cycles 3, 5, 7 and 9 are corresponding to polymer films after the desorption of analyte by air flow and cycles 2, 4, 6, 8 and 10 are corresponding to polymer films exposed to NT .

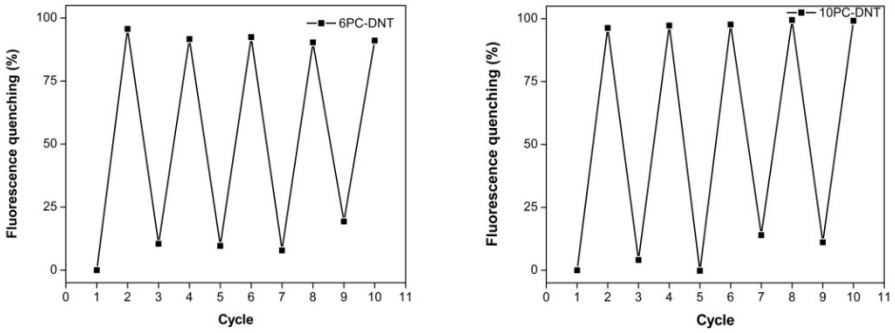

Figure 20: The fluorescence recovery cycles of 6PC and 10PC films, Cycles 3, 5, 7 and 9 are corresponding to polymer films after the desorption of analyte by air flow and cycles 2, 4, 6, 8 and 10 are corresponding to polymer films exposed to DNT

8.3.Conclusion and perspectives

We have designed two crosslinked MEH PPV with six and ten carbon spacer to reduce the photobleaching property of the MEH PPV. The polymers were synthesized through Gilch polymerization route. The photostability of the polymer was increased by crosslinking. The applicability of the polymers for the detection of nitroaromatics was tested using nitrobenzene, 4-nitrotoluene and 2,4-dinitrotoluene as analytes. The polymers with ten carbon spacer showed excellent sensitivity towards the nitroaromatics. This may due to the high pore volume of this polymer compared to six carbon spacer MEH PPV. Both the polymers showed reversible sensitivity towards the nitroaromatics. The effect of interfering compounds were also studied and phenol showed some quenching, but the response was weaker and slower. Thus, this conjugated polymer based detector provides a better method for real time monitoring of the unexploded landmines. The device can be made in to portable equipment for field use in military applications.

8.4. Experimental section

The monomer, 1-(2-ethyl hexyloxy)-2,5-bis(chloromethyl)-4-methoxybenzene and the precursor 1-(2-ethyl hexyloxy)-4-methoxybenzene were synthesized through reported procedure[27].

8.4.1. 4-(2-ethyl hexyloxy)phenol (C1)

Hydroquinone (6 g, 0.055 mol) was dissolved in a solution of KOH (3.1 g, 0.055 mol) in dry ethanol at room temperature. The solution was warmed to 60^0C under nitrogen atmosphere with constant stirring for 0.5h. 2-ethyl hexylbromide (9.6 mL, 0.055 mol) was added drop wise and the

reaction was continued by refluxing for 12h under nitrogen atmosphere. It was cooled, poured into water, extracted with dichloromethane and dried over $MgSO_4$. The solvent was evaporated to obtain the product as brown oil. The monoalkylated hydroquinone was further purified by column chromatography using hexane/dichloromethane mixture (3:1) v/v which yielded brown oil.

Yield	:	34.2% (4.1 g)
IR (cm^{-1})	:	3417, 2959, 2929, 2872, 1703, 1602, 1509, 1463, 1378, 1357, 1294, 1230, 1100, 1035, 825, 800, 770, 518
^1H NMR (400 MHz, $CDCl_3$).	:	δ 6.76 (m, 4H, Ar-H), 4.78 (s, -OH), 3.77 (dd, J_1=5.6 Hz, J_2=0.8 Hz, 2H, -OCH_2), 1.72-1.28 (m, 9H, aliphatic-H), 0.93-0.88 (m, 6H, -CH_3)

8.4.2. Synthesis of 6C2

4-(2-ethyl hexyloxy)phenol (0.75 g, 3.38 mmol) and K_2CO_3 (1.9 g, 13.76 mmol), were taken in a 50 mL flask containing distilled DMF (30 mL) and heated under nitrogen atmosphere for 0.5h. 1,6-dibromohexane (0.26 mL, 1.7 mmol) was added and heated at 80 °C for 24 h under nitrogen atmosphere. It was cooled and poured into excess water and extracted into dichloromethane. The organic layer was washed with NaOH followed by brine solution and dried over anhydrous Na_2SO_4, and the solvent was evaporated. The crude product was dissolved in minimum amount of hexane and precipitated by adding methanol. The process was repeated three times to get the pure white product.

Yield	:	70% (1.25 g)
M. P.	:	58-60^{0}C
IR (cm^{-1})	:	2953, 2929, 2862, 1563, 1508, 1468, 1394, 1377, 1285, 1230, 1112, 1034, 935, 822, 765, 731, 519
^{1}H NMR (400 MHz, $CDCl_3$,)	:	δ 6.84 (s, 8H, Ar-H), 3.93 (t, J=6.5 Hz, 4H, -OCH_2), 3.77 (dd, J_1=5.9 Hz, J_2=0.97 Hz, 4H, -OCH_2), 1.85-1.25 (m, 26H, aliphatic-H), 0.95-0.86 (m, 12H, -CH_3)
^{13}C NMR (100 MHz, $CDCl_3$,)	:	δ 153.58, 153.11, 115.43, 77.3, 77.20, 77, 76.68, 71.27, 68.55, 39.49, 30.55, 29.35, 29.09, 25.89, 23.88, 23.05, 14.06, 11.09.
MS (FAB) M^+	:	Calculated for $C_{34}H_{54}O_4$: 526.79; found: 526.85.

8.4.3. Synthesis of 6C3

Compound 6C2 (0.21 g, 0.40 mmol), was dissolved in 40 mL dioxane. The solution was cooled to 0-5^{0}C, and 0.8 mL Conc HCl and 1.6 mL 37% formalin were added. Anhydrous HCl was bubbled for 6 h. The solution was warmed up to 30^{0}C and stirred for 2 h. Another portion of 1.6 mL of formalin was added and HCl gas was bubbled for 6 h at 0-5^{0}C. The process was repeated for two times. The solution was refluxed for 4 h. It was cooled and poured into excess water and extracted into diethyl ether. The organic layer was washed with water and dried over anhydrous

$MgSO_4$, and the solvent was evaporated. The crude product was purified by recrystallisation from hexane which gave white crystalline product.

Yield	:	69% (0.202 g)
M. P.	:	102^0C
IR (cm^{-1})	:	2958, 2939, 2871,1561, 1541, 1514, 1464, 1445, 1416, 1376, 1314, 1258, 1226, 1186, 1136, 1034, 926, 866, 807, 776, 740, 707, 608
^{1}H NMR (400 MHz, $CDCl_3$)	:	δ 6.9 (d, *J*=5.24 Hz, 4H, Ar-H), 4.61 (d, *J*=4.7 Hz, 8H, -CH_2Cl), 4.0 (t, *J*=6.32 Hz, 4H, -OCH_2), 3.86 (d, *J*=5.45 Hz, 4H, -OCH_2), 2.3-1.9 (m, 26H, aliphatic-H), 0.97-0.85 (m, 12H, -CH_3)
^{13}C NMR (100MHz, $CDCl_3$)	:	δ 150.81, 150.45, 127.08, 127.03, 71.16, 68.98, 41.41, 41.35, 39.62, 30.64, 29.11, 25.79, 24.03, 23.04, 14.05, 11.21
MS (FAB) M^+	:	Calculated for $C_{38}H_{58}Cl_4O_4$: 720.68; found: 720.56.

8.4.4. Synthesis of 10C2

(2-ethyl hexyloxy)phenol (0.75 g, 3.38 mmol) and K_2CO_3 (1.9 g, 13.76 mmol), were taken in a 50 mL flask containing distilled DMF (30 mL) and heated under nitrogen atmosphere for 0.5 h. 1,10-dibromodecane (0.375 mL, 1.7 mmol) was added and heated at 80 °C for 24 h under nitrogen atmosphere. It was cooled and poured into excess water and

extracted into dichloromethane. The organic layer was washed with NaOH followed by brine solution and dried over anhydrous Na_2SO_4, and the solvent was evaporated. The crude product was dissolved in minimum amount of hexane and precipitated by adding methanol. The process was repeated three times to get the pure white product.

Yield	:	52.3% (1.03 g)
M. P.	:	57-59^{0}C
IR (cm^{-1})	:	2954, 2928, 2857, 1561, 1508, 1467, 1382, 1283, 1228, 1105, 1038, 822, 777, 523
^{1}H NMR (400MHz, $CDCl_3$)	:	δ 6.74 (s, 8H, Ar-H), 3.82 (t, J=6.6 Hz, 4H, -OCH_2), 3.71 (dd, J_1=5.7 Hz, J_2=1.12 Hz, 4H, -OCH_2), 1.69-1.2 (m, 34H, aliphatic-H), 0.88-0.8 (m, 12H, -CH_3)
^{13}C NMR (100MHz, $CDCl_3$)	:	δ 153.54, 153.17, 115.43, 71.28, 68.71, 39.49, 30.55, 29.49, 29.41, 29.39, 29.1, 26.05, 23.88, 23.06, 14.06, 11.1

8.4.5. Synthesis of 10C3

Compound 10C2 (0.234 g, 0.4 mmol), was dissolved in 40 mL dioxane. The solution was cooled to 0-5^{0}C, and 0.8 mL Conc HCl and 1.6 mL 37% formalin were added. Anhydrous HCl was bubbled for 6 h. The solution was warmed up to 30^{0}C and stirred for 2 h. Another portion of 1.6 mL of formalin was added and HCl gas was bubbled for 6 h at 0-5^{0}C. The

process was repeated for two times. The solution was refluxed for 4 h. It was cooled and poured into excess water and extracted into diethyl ether. The organic layer was washed with water and dried over anhydrous $MgSO_4$, and the solvent was evaporated. The crude product was purified by recrystallisation from hexane which gave white crystalline product.

Yield	:	84% (0.262 g)
M. P.	:	89^0C
IR(cm^{-1})	:	2954, 2937, 2856, 1561, 1541, 1514, 1458, 1445, 1416, 1402, 1314, 1259, 1225, 1186, 1039, 865, 779, 740, 707, 607
^{1}H NMR (400MHz, $CDCl_3$)	:	δ 6.83 (s, 4H, Ar-H), 4.56 (d, *J*=6.1 Hz, 8H, -CH_2Cl), 3.91 (t, *J*=6.4 Hz 4H, -OCH_2), 3.79 (d, *J*=6.4 Hz, 4H, -OCH_2), 1.9-1.2 (m, 34H, aliphatic-H), 0.9-0.79 (m, 12H, -CH_3)
^{13}C NMR (100MHz, $CDCl_3$)	:	δ 150.77, 150.49, 127.09, 126.98, 114.46, 113.94, 71.16, 69.20, 41.37, 39.62, 30.64, 29.48, 29.32, 29.11, 26.05, 24.03, 23.04, 14.05, 11.21
MS (EI) M^+	:	Calculated for $C_{42}H_{66}Cl_4O_4$: 776.78; found: 776.4

8.4.6. Synthesis of MEH PPV

To a solution of of 2,5-bis(chloromethyl)methoxy-4-(2-ethyl hexyloxy) benzene (1 g, 3 mmol) in 20 mL of anhydrous THF was added

dropwise a solution of 95% potassium tertiary butoxide (2.12 g, 18 mmol) in 80 mL of THF at 30^0C with stirring. The solution was poured into cold methanol. The precipitate was filtered and washed with methanol. The polymer was further purified by soxhlet extraction with acetone and methanol to afford a red solid.

Yield	:	45%
T_d (^{0}C)	:	395
^{1}H NMR (400MHz, $CDCl_3$)	:	δ 7.53 (s, 2H, Ar-H), 7.19 (s, 2H, -CH=CH-), 3.95 (b, -OCH_2- and -OCH_3), 1.8-0.9 (m, ~15H, aliphatic-H)
GPC	:	M_n=251917, PDI=1.73

8.4.7. Synthesis of 6PC

2,5-bis(chloromethyl)methoxy-4-(2-ethyl hexyloxy) benzene (0.25g, 0.75 mmol), and 6C3 (0.0054g, 0.0075 mmol) were dissolved in 5 mL dry THF under nitrogen atmosphere. Potassium t-butoxide (0.51 g, 4.54 mmol) in 20 mL of THF was added drop by drop. The solution was stirred for 24 h at room temperature. The solution was poured in to cold methanol. The precipitate was filtered and washed with methanol. The polymer was further purified by soxhlet extraction with acetone and methanol to afford a red solid.

Yield	:	41% (85 mg)
T_d (^{0}C)	:	396
IR (cm^{-1})	:	3432, 2962, 2929, 2861, 1572, 1422, 1375, 1320, 1110, 865
^{1}H NMR (400MHz, $CDCl_3$)	:	δ 7.53 (s, 2H, Ar-H), 7.19 (s, 2H, -CH=CH-), 3.95 (b, -OCH_2- and -

		OCH_3), 1.8-0.9 (m, ~15H, aliphatic-H)
GPC	:	M_n=427633, PDI=1.52

8.4.8. Synthesis of 10PC

2,5-bis(chloromethyl)methoxy-4-(2-ethyl hexyloxy)benzene (0.25 g, 0.75 mmol) and 10C3 (0.0058 g, 0.0075 mmol) were dissolved in 5 mL dry THF under nitrogen atmosphere. Potassium t-butoxide (0.51 g, 4.54 mmol) in 20 mL of THF was added drop by drop. The solution was stirred for 24 h at room temperature. The solution was poured in to cold methanol. The precipitate was filtered and washed with methanol. The polymer was further purified by soxhlet extraction with acetone and methanol to afford a red solid.

Yield	:	37% (77 mg)
T_d (^{0}C)	:	395
IR (cm^{-1})	:	3433, 2957, 2926, 2861, 1508, 1458, 1379, 1353, 1105, 969
^{1}H NMR (400MHz, $CDCl_3$,)	:	δ 7.54 (s, 2H, Ar-H), 7.19 (s, 2H, -CH=CH-), 3.96 (b, -OCH_2- and -OCH_3), 1.83-0.91 (m, ~15 H aliphatic-H)
GPC	:	M_n=223115, PDI=2.17

8.5. References

1. Liu, J.; Shi, Y.; Yang, Y. *Appl. Phys. Lett.* **2011**, 79, 578.
2. Dong, L. X.; Ling, S. Z.; Zheng, X.; Jun , Z. F.; Hui, Z. T.; Wei, G.; Guang, Y.; Chao, K.; Sheng, W. Y.; Rong, X. X. *Chinese Phys. B.*, **2011**, 20, 68801.

3. Rajesh Menon, M. R.; Maheshkumar, M. V.; Sreekumar, K.; Sudha Kartha, C. Vijayakumar, K. P. *physica status solidi*, **2012**, 209, 199.
4. Rajesh Menon, M. R.; Maheshkumar, M. V.; Sreekumar, K.; Sudha Kartha, C. Vijayakumar, K. P. *Solar Energy Materials and Solar Cells*, **2010**, 94, l2212.
5. Chang, C. P.; Chao, C. Y.; Huang, G. H.; Li, A. K.; Hsu, C. S.; Lin, M.S.; Hsieh, B. R.; Su, A. C. *Synthetic Metals*, **2004**, 144, 3297.
6. Ko, S. W.; Jung, B. J.; Cho, N. S.; Shim, H. K. *Bull. Korean Chem. Soc*. **2002**, 23, 1235.
7. Choo, D. J.; Talaie, A.; Lee, Y. K.; Jang, J.; Park, S. H.; Huh, G.; Yoo, K. H.; Lee, J. Y. *Thin Solid Films*, **2000**, 363, 37.
8. Ahn, T.; Ko, S. W.; Shim, H. K. *Macromolecules*, **2002**, 35, 3495.
9. Jeong, H. Y.; Lee, Y. K.; Talaie, A.; Kim, K. M.; Kwon, Y. D.; Jang, Y. R.; Yoo, K. H.; Choo, D. J.; Jang, J. *Thin Solid Films*, **2002**, 417, 171.
10. Wudl, F.; Hoger, S.; Zhang, C.; Pakbaz, K.; Heeger, A. J. *Polym. Prepr.*, **1993**, 34, 197.
11. Lee, S. H.; Jang, B. B.; Tsutsui, T. *Macromolecules*, **2002**, 35, 1356.
12. Sarker, A. M.; Ding, L.; Lahti, P. M.; Karasz, F. E. *Macromolecules*, **2002**, 35, 223.
13. Lee, N. H. S.; Chen, Z. K.; Huang, W.; Xu, Y. S.; Cao, Y. *J. Polym. Sci., Polym. Chem.*, **2004**, 42, 1647.
14. Amrutha, S. R.; Jayakannan, M. *Macromolecules*, **2007**, 40, 2380.
15. Seo, M.; Amendt, M. A.; Hillmyer, M. A. *Macromolecules*, **2011**, 44, 9310.

16. Mähr, U.; Purnama, H.; Kempin, E.; Schomäcker, R.; Reichert, K. H, *J. Membr. Sci.*, **2000**, 171, 285.

17. George,V.; Jenkins, T. F.; Leggett, D.; Cragin, J. H.; Phelan, J. *Annual International Symposium on Aerospace/Defense Sensing, Simulation, and Controls*, **1999**, 258.

18. George, V.; Jenkins, T. F.; Phelan, J. M.; Leggett, D. C.; Oxley, J. *Annual International Symposium on Aerospace/Defense Sensing, Simulation, and Controls*, **2000**, 590.

19. Leggett, D. C.; Cragin, J. H.; Jenkins, T. F.; Ranney, T. *Release of explosive-related vapors from landmines. Engineering Research and Development Center Report*, TR-01–6, Cold Regions Research and Engineering Laboratory; **2001**.

20. McQuade, D. T.; Pullen, A. E.; Swager, T. M., *Chem. Rev*., **2000**, 100, 7, 2537.

21. Thomas, S. W.; Joly, G. D.; Swager, T. M., *Chem. Rev*., **2007**, 107, 1339.

22. Swager, T. M., *Acc. Chem. Res*., **1998**, 31, 201.

23. Yang, J.; Swager, T. M., *J. Am. Chem. Soc*.,**1998**, 120, 11864.

24. Chou, H. L.; Lin, K. F.; Fan, Y. L.; Wang, D. C. *J. Polym. Sci., Polym. Phys*., **2005**, 43, 1705.

25. Padmanabhan, G.; Ramakrishnan, S. *J. Am. Chem. Soc*., **2000**, 122, 2244.

26. Egbe, D. A. M.; Tillmann, H.; Rirckner, E.; Klemm, E. *Macromol. Chem. Phys.*, **2001**, 202, 2712.

27. Huo, L.; Hou, J.; He,C.; Han, M.; Li, Y. *Synthetic Metals*, **2006**, 156, 276.

Chapter 9

SUMMARY AND OUTLOOK

We have designed sixteen polymers composed of phenothiazine, 3,4-propylenedioxythiophene, 3,4-ethylenedioxythiophene, 3,4-dimethoxythiophene (donors) and 2.1.3-benzothiadiazole, 2,1,3-benzoselenadiazole, quinoxaline, and 1,2,4-triazole (acceptors) as the core units, for photovoltaic applications by employing density functional theory in the periodic boundary condition formalism. The theoretical calculation prior to synthesis is an easy way to screen out the less effective materials before synthesis. In this work, we have calculated only the band gap and energy levels of the copolymers by PBC/DFT methods. By extending this calculation to compute the oscillator strength of the absorption by employing Time Dependent Density Functional Theory (TDDFT), it is possible to find the polymers which possess high absorption coefficient. Absorption coefficient is an important factor governing the I_{sc} of the heterojunction. If the polymers absorb large number of photons, it will be reflected in the photocurrent.

We have synthesised phenothiazine based polymers with 2,1,3-chalcogenadiazole and quinoxaline as comonomers by Suzuki polycondensation reaction. Eleven polymers were synthesized through direct arylation reaction also. The molecular weight of the polymers formed by direct arylation reaction were not sufficiently high for employing them in solar cells. Hence we got only low efficiency for the devices made from these polymers. The molecular weight could be increased by using proper solvent system like dimethyl acetamide or THF/DMF mixtures. The band gaps were determined using cyclic voltammetry and optical measurements. The experimental values along with the theoretical band gaps are given in

the table. Theoretically calculated values are in good agreement with the experimental values. Improvement in the theoretical calculation can be achieved by introducing polarization and diffuse functionals to DFT calculations. This will need more computational time.

Table: Theoretical and experimental band gap of polymers

No	Polymer	PBC/DFT band gap (eV)	Electrochemical band Gap (eV)	Optical band gap (eV)
1	PPHENO-BTZ	1.98	2.16	2.05
2	PPHENO-BSE	1.96	2.02	1.93
3	PPHENO-DDACE	2.38	2.53	2.24
4	PPHENO-DDQ	2.3	2.18	2.11
5	PPHENO-DBDP	2.0	1.95	1.92
6	PDMT-PHENO	2.52	2.7	2.24
7	PEDT-PHENO	2.45	2.64	2.26
8	PPRO-PHENO	2.48	2.7	2.1
9	PPRO-BTZ	1.8	1.85	1.52
10	PPRO-BSE	1.79	1.94	1.51
11	PPRO-DQX	1.93	2.09	1.73
12	PPRO-DDACE	1.96	2.41	1.70
13	PPRO-DDQ	1.85	2.22	1.67
14	PPRO-DBDP	1.74	2.02	1.62
15	PPRO-TD2	2.3	2.34	1.99
16	PPRO-TEH2	2.3	2.21	1.96

Bilayer heterojunction devices with device structure ITO/In_2S_3/polymer/Ag were fabricated. The devices showed low efficiency, due to the low interfacial area between the donor and acceptor materials. The efficiency of the device can be increased by optimizing the device parameters like layer thickness. A further improvement in the device can be achieved by proper designing of the bulk heterojunction device by considering the energy levels of In_2S_3 and polymers (figure 1). The conduction band edge of In_2S_3 is -3.93 eV, and LUMO level of the synthesized polymers range from -2.3.-3.1 eV. So the level of the acceptor must be between -3.5.-3.8 eV. The commonly used [6,6]-phenyl-C-61-butyric acid methyl ester (PCBM) cannot be used for this purpose because the LUMO level of PCBM is almost the same as that of In_2S_3, which will not facilitate the charge transfer. In this context, we are proposing three such acceptors for the bulk heterojunction device of device structure ITO/In_2S_3/polymer:acceptor/Ag heterojunction. The LUMO level of, ICMA[1], ICBA[1] and poly(isoindigo)[2] are -3.86, and -3.74 eV, -3.84 eV respectively (figure 2). The interfacial area between the donor and acceptor will be increased and definitely efficient charge transfer will take place. In addition to this, increasing the acceptor LUMO will increase the V_{oc}, because open circuit voltage depends on the difference between the HOMO and LUMO of donor and acceptor respectively.

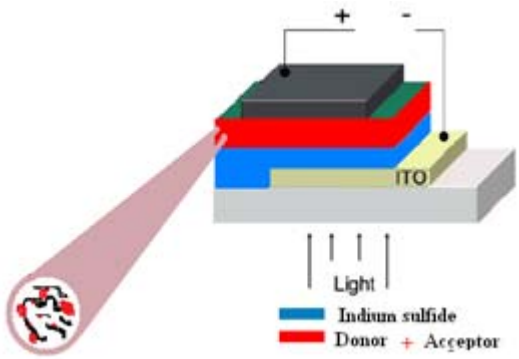

Figure 1: Structure of bulk heterojunction device

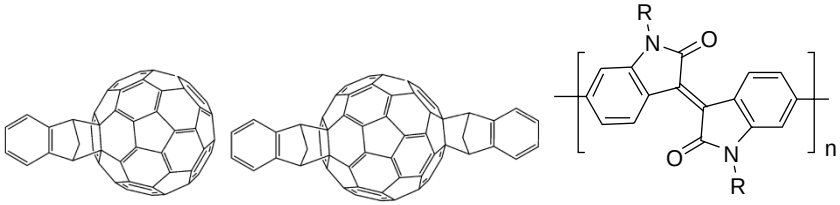

ICMA **ICBA** **Polyisoindigo**

Figure 2: Recommended acceptors for ITO/ In_2S_3/Polymer:acceptor/Ag heterojunction

In the last part of the work we had designed and synthesized two crosslinked MEH PPV with ten and six carbon spacer. The applicability of the polymers for detecting nitroaromatics was explored using nitrobenzene, 4-nitrotoluene, and 2,4-dinitrotoluene as analytes. The testing can be extended to 2,4,6-trinitrotoluene like explosives. The fabricated device can be developed into a portable device for military application.

1. He, Y.; Chen, H. Y. ; Hou, J.; Li, Y. *J. Am. Chem. Soc*., **2010**, 132, 1377.
2. Stalder, R.; Mei, J.; Subbiah, J.; Grand, C.; Estrada, L. A.; So, F.; Reynolds, J. R. *Macromolecules*, **2011**, 44, 6303.

Publications

1. Maheshkumar, M. V.; Joseph, M. J.; Sreekumar, K.; Ang, H. G, Synthesis and Characterization of Poly BAMO Suitable for Binder Application, *Chinese Journal of Energetic Materials*, 14, **2006**, 411.
2. Rajesh Menon, M. R.; Maheshkumar, M. V. ; Sreekumar, K.; Sudha, K. C.; Vijayakumar, K. P., Inverted polymer solar cells with indium sulfide electron selective layer, *Solar Energy Materials and Solar Cells*, 12, **2011**, 2212.
3. Rajesh Menon, M. R.; Maheshkumar, M. V.; Sreekumar, K.; Sudha, K. C.; Vijayakumar, K. P., Spray pyrolysed In_2S_3 thin films: A potential electron selective layer for large area inverted bulk-heterojunction solar cells, *Phys. Status Solidi A*, 209, **2012**, 199.

Oral Presentations

1. Maheshkumar, M. V.; and Sreekumar, K., Theoretical designing of conjugated polymers for optoelectronic applications, User's meeting, CMSD, University of Hyderabad, November **2008**.
2. Maheshkumar, M. V.; Sreekumar, K., Joint theoretical and experimental investigation on Phenothiazine/2,1,3-benzothiadiazole copolymer for photovoltaic Application, National seminar on computational chemistry, Mar Athanasius College, Kothamangalam, Kerala, August **2009**.

3. Maheshkumar, M. V.; Rajesh Menon, M. R.; Sreekumar, K., Combined experimental and theoretical investigation on novel phenothiazine/quinoxaline copolymers for photovoltaic application. Kerala Science Congress, Peechi, Kerala, January **2010**, p284.
4. Maheshkumar, M. V.; Rajesh Menon, M. R.; Sreekumar, K., Low band gap 3,4-Propylenedioxythiophene/2,1,3-benzoselenadiazole alternating copolymer by direct arylation reaction: Theory, synthesis and photovoltaic application, Kerala Science congress, Trivandrum, Kerala, January **2011**.
5. Maheshkumar, M. V.; Sreekumar, K., Theoretical designing of conjugated polymers for optoelectronics. User's meeting, CMSD, University of Hyderabad, February **2011**.

Conference papers

1. Maheshkumar, M. V.; Joseph, M. J.; Sreekumar, K., Experimental and theoretical studies on poly(3,4-ethyleedioxythiophene), *International conference on Materials for the Millennium*, Cochin, March **2007**.

2. Rajesh Menon, M. R.; Maheshkumar, M. V.; Joseph, M. J.; Sreekumar, K.; Sudha, K. C.; Vijayakumar, K. P., Electrical and photovoltaic properties of MEH-PPV based heterojunction; *Proceedings of the 53rd DAE Solid State Physics Symposium*, Mumbai, India; 16-20 December ***2008***, p539-540.

3. Rajesh Menon, M. R.; Maheshkumar, M. V.; Sreekumar, K.; Sudha, K. C.; Vijayakumar, K. P., Influence of polymer thickness on the photovoltaic properties of inorganic-organic heterojunction; *Proceedings of the International Conference on Advances in Polymer Technology (APT'10)*, Cochin, India; 26 & 27 February **2010**, p114.

4. Rajesh Menon, M. R.; Maheshkumar, M. V.; Sreekumar, K.; Sudha, K. C.; Vijayakumar, K. P., Temperature dependence of the photovoltaic parameters of inorganic-organic heterojunction; *Proceedings of the National Conference on Materials for Energy Storage and Conversion (NCMESC-2010)*, Tirupati, India; 23 & 24 January **2010**, p34.
5. Rajesh Menon, M. R.; Maheshkumar, M. V.; Sreekumar, K.; Sudha, K. C.; Vijayakumar, K. P., Fabrication and characterization of MEH PPV based bulk heterojunction solar cells using spray deposited indium sulfide electron selective layer, *IEEE photovoltaic specialists conference*, Austin, June **2012**.

DEPARTMENT OF APPLIED CHEMISTRY
COCHIN UNIVERSITY OF SCIENCE AND TECHNOLOGY
KOCHI-22